Fanny Marjolaine Deschepper
Mestre em Biologia-Saude

Studies of the role of sialyl Lewis X antigen and E selectin ligands in colorectal cancer

Dissertação para obtenção do Grau de Doutor em Biologia - Especialidade em Biologia Celular

Orientador: Doutora Paula Alexandra Quintela Videira, Profª. Auxiliar, Faculdade de Ciências e Tecnologia - Universidade Nova de Lisboa
Co-orientador: Doutor Fabio Dall'Olio, Professor, Dipartimento di Medicina Specialistica, Diagnostica e Sperimentale - Università di Bologna

Júri:

Presidente:	Profª. Doutora Isabel Maria Godinho de Sá Nogueira
Arguentes:	Profª. Doutora Susana Constantino Rosa Santos Invª. Doutora Salomé Soares de Pinho
Vogais:	Invª. Doutora Maria Angelina de Sá Palma Profª. Doutora Paula Alexandra Quintela Videira

FACULDADE DE CIÊNCIAS E TECNOLOGIA
UNIVERSIDADE NOVA DE LISBOA

Fevereiro 2020

Fanny Marjolaine Deschepper

Studies of the role of sialyl Lewis X antigen and E-selectin ligands in colorectal cancer

Acknowledgements

To begin, I would like to thank my supervisor Dr Paula Videira for giving me the opportunity to be part of this great project. I am grateful for the confidence and support she gave to me during this PhD project.

A special thanks goes to my co-supervisor Fabio Dall'Olio, and to my collaborators, Dr Paul Hensbergen and Dr Daniel Spencer, who welcomed me in their respective laboratories and gave me the opportunity to enlarge my knowledges and scientific skills by teaching me new techniques and analysis approaches.

I warmly thank Helen Williamson for her attentive way of listening and wise counsels.

A great thanks to the glycoimmunoly group past and present members, Mylène, Diana, Rita(s), Tiago(s) and Zelia for the good work environment and scientific discussion.

To the great former MSc students and friends Constança and Carlota, the everyday life lab would have not been the same without you.

I feel extremely lucky to have shared these PhD years with Roberta (Robi), sharing a lot of good times, joys and sometimes disappointments, thanks for the unconditional and irrevocable support.

To the adoptive Glycocan family, this team is absolutely amazing, who could imagine thirteen persons gating so much along together. I am grateful to have you in my life and to have the chance to consider you as my friends.

To the person in Leiden and Oxford I first met in labs and become friends now, I will never forget the amazing moments I have spent with you.

To my friend Yasmine, no need to write anything, she already knows because we are connected.

Finally, the best thanks go to my family, I could not imagine a better family. To my parents for your endless support and love, you always have been with me, supporting and giving me the possibility to follow my choices. I love you very much.

Resumo

As alterações da glicosilação desregulam múltiplos processos biológicos e são características do cancro, relacionadas com a tumorigénese e progressão tumoral. Este estudo foca-se na glicosilação alterada em cancro colorretal (CRC), o terceiro cancro mais comum no mundo. Um aumento da sialilação e fucosilação foram reportados em CRC e associados com características de tumores malignos. Estas alterações resultaram num incremento da expressão do antigénio sialofucosilado sialil Lewis X (sLe^X), um ligando da E-selectina endotelial, tendo potencial na formação de metástases. Assim, a sobreexpressão do antigénio sLe^X pode afectar a expressão dos ligandos da E-selectina e a capacidade de invasão de linhas celulares de CRC. Além disso, o efeito da expressão aumentada do antigénio sLe^X em estratégias imunossupressoras de células tumorais não foram claramente discutidas até à data.

Para responder a estas hipóteses, primeiro caracterizámos o impacto na biologia e no perfil de glicanos da sobreexpressão de sLe^X em células de CRC. Os resultados mostraram melhoria na migração celular e na reatividade com a E-selectina quando a expressão de sLe^X foi aumentada. Em seguida, identificámos as glicoproteínas imunoprecipitadas com E-selectina por espectrometria de massa, e os nossos resultados revelaram a molécula de adesão das células neurais L1 (L1CAM). Para além disso, mostrámos que a sobreexpressão do antigénio sLe^X nas células de CRC reduz o perfil de maturação das células dendríticas (DCs), conforme indicado pela diminuição na expressão da molécula de apresentação de antigénios, MHC-II, e a molécula co-estimuladora, CD86.

Esta tese é a primeira a relatar a capacidade de interação da L1CAM com a E-selectina. Como é conhecido que a L1CAM possui uma elevada expressão em cancro e que está associada com metástases e progressão tumoral, estes resultados devem contribuir para melhor compreender o seu mecanismo de ação. Também a redução na maturação das DCs induzida por células de CRC que expressam sLe^X pode diminuir a capacidade de iniciar adequadamente a resposta imunológica contra células tumorais. Em geral, estes resultados contribuem para elucidar o papel do antigénio sLe^X e dos ligandos de E-selectina na progressão do CRC, na formação de metástases e na estratégia tumoral de evasão do sistema imunológico, propondo novos potenciais alvos para tratamentos terapêuticos para o CRC.

Palavras-chave: Cancro colorretal, E-selectina, sialil Lewis X, metástase, imunomodulação.

Abstract

Glycosylation alterations dysregulate multiple biological processes and are a hallmark of cancer, linked to tumorigenesis and tumour progression. The present study focuses on altered glycosylation in colorectal cancer (CRC), the third most common cancer worldwide. Increased sialylation and fucosylation are reported in CRC and associated with malignant tumour features. This increase is translated by upregulation of the sialofucosylated sialyl Lewis X (sLe^X) antigen, a ligand of the endothelial E-selectin, having a potential role in metastasis. Thus, overexpressing sLe^X antigen may affect the expression of E-selectin ligands and the invasion capacity of CRC cell lines. Moreover, the effect of increased sLe^X antigen expression on tumour cells immunosuppressive strategies has not been clearly examined so far.

To address these hypotheses, we first characterised the impact on the biology and the glycan profile of sLe^X overexpression in CRC cells. The results showed improvement of cell migration and reactivity with E-selectin, upon increased sLe^X expression. Then, we identified the glycoproteins immunoprecipitated with E-selectin by mass spectrometry, and our results revealed neural cell adhesion molecule L1 (L1CAM). Furthermore, we showed that the sLe^X antigen overexpression by CRC cells reduces the maturation profile of dendritic cells (DCs), as inferred by a decreased expression of the antigen presenting molecule, MHC-II, and the co-stimulatory molecule, CD86.

This thesis is the first to report the L1CAM ability to interact with E-selectin. Since L1CAM is known to be elevated in cancer and associated with metastasis and progression, this should contribute to better understand its action mechanism. Also, the reduced DCs maturation induced by sLe^X expressing CRC cells, may diminished the capacity to appropriately engage immune response against tumour cells. Overall, these findings contribute to elucidate the role of sLe^X antigen and E-selectin ligands on CRC progression, metastasis and in the tumour immune system escape strategy, proposing potential novel targets for therapeutic treatments of CRC.

Keywords: Colorectal cancer, E-selectin, sialyl Lewis X, metastasis, immunomodulation.

Table of Contents

Illustrations index

List of Tables

List of Abbreviations

Number

5-ASA	Mesalamine
5-FU	5-Fluorouracile

A

Ab	Antibody
AJCC	American joint committee on cancer
APC	Allophycocyanin
Asn	Asparagine

B

BCA	Bicinchoninic acid assay
bFGF	Basic fibroblast growth factor
BSA	Bovine serum albumin

C

C1GalT	Core 1 β1,3 galactosyltransferase
C2GnT	Core 2 β1,6 N-acetylglucosaminyltransferase
C3GnT	Core 3 β1,3 N-acetylglucosaminyltransferase
CA-19.9	Carbohydrate Antigen 19.9
CAR-T cell	Chimeric antigen receptor-T cell
CD	Cluster of Differentiation
CDG	Congenital Disorder of Glycosylation
CEA	Carcinoembryonic antigen
CEACAM	CEA-related cell adhesion molecule
CFG	Consortium for Functional Glycomics
CHO	Chinese hamster ovary
CIMP	CpG island methylator phenotype
CLA	Cutaneous lymphocyte antigen
Cmpd	Compound
CMS	Consensus molecular subtypes
Cosmc	Core 1 beta-3-galactosyltransferase-specific molecular chaperone
CRC	Colorectal cancer
CR-CSCs/CICs	Colorectal cancer stem cells and cancer initiating cells
CRISPR-dCas9-VPR	Clustered Regularly Interspaced Short Palindromic Repeats-dead CRISPR-associated protein 9-VP64-p65-Rta
Ct	Cycle threshold
CTCs	Circulating Tumour cells
CTLs	Cytotoxic T Lymphocytes

D

DAMPS	Damage-associated molecular patterns
DC	Dendritic cell
DC-SIGN	Dendritic cell-specific intercellular adhesion molecule-3-grabbing non-integrin
DMEM	Dulbecco modified Eagle's medium
DNA	Deoxyribonucleic acid
DR5	Death Receptor-5

DTT	Dithiothreitol

E

EDTA	Ethylenediaminetetraacetic acid
EGF	Epithelial growth factor
EGFR	Epithelial growth factor receptor
E-Ig	Recombinant Human E-Selectin/CD62E Fc Chimera Protein
EMT	Epithelial-mesenchymal transition
EpCAM	Epithelial cell adhesion molecule
ER	Endoplasmic Reticulum
ERAD	Endoplasmic Reticulum Associated Degradation
Exp.	Experiment

F

FA	Formic acid
FAP	Familial adenomatous polyposis
FBS	Foetal bovine serum
FDR	False Discovery Rate
FITC	Fluorescein isothiocyanate
FOBT	Faecal occult blood testing
Fuc	Fucose
FucT	Fucosyltransferase (enzyme)
FUT	Fucosyltransferase (gene)

G

Gal	Galactose
GalT	Galactosyltransferase
GalNAc	N-acetylgalactosamine
GalNAcT	N-acetylgalactosaminyltransferase
GAPDH	Glyceraldehyde 3-phosphate dehydrogenase
GDP	Guanosine diphosphate
Glc	Glucose
GlcNAc	N-acetylglucosamine
GlcNAcT	N-acetylglucosaminyltransferase
GM-CSF	Granulocyte-macrophage colony-stimulating factor
GSLs	Glycosphingolipids
GU	Glucose unit

H

hCG	human chorionic gonadotropin
HCELL	hematopoietic cell E/L-selectin
Hex	Hexose
HexNAc	N-acetylhexosamine
HILIC-UHPLC	Hydrophilic interaction ultra-high-performance liquid chromatography
HNPCC	Hereditary non-polyposis colorectal cancer
HPLC	High-performance liquid chromatography
HRP	Horseradish peroxidase

I

IBD	Inflammatory bowel disease
ICAM-2	Intercellular adhesion molecule 2
IFN	Interferon

I

IL	Interleukin
IP	Immunoprecipitated
ITGA6	Integrin α6
ITGB1	Integrin β1

K

KD	Knock-down
KO	Knock-out

L

L-15	Leibovitz medium
L1CAM	Neural cell adhesion molecule L1
LacdiNAc	N,N-diacetyllactosamine
LacNAc	N-acetyllactosamine
LAG3	Lymphocyte activation gene 3 protein
LAMP	Lysosome-associated membrane glycoproteins
LC-ESI-MS/MS	Liquid chromatography electrospray ionisation tandem mass spectrometry
Le^A	Lewis A
Le^B	Lewis B
Le^X	Lewis X
Le^Y	Lewis Y
LGALS3BP	Lectin galactoside-binding soluble 3 binding protein
LncRNA	Long non-coding RNA
LOH	Loss of heterozygosity
LPS	Lipopolysaccharide
LSECs	Liver sinusoidal endothelial cells

M

mAb	Monoclonal antibody
Mac-2BP	Mac-2-binding protein
Man	Mannose
MAN1B1	Endoplasmic reticulum α1,2-mannosidase
MAP	MutY homolog-associated polyposis
MBP	Mannan-binding protein
MFI	Median Fluorescent Intensity
MGL	Macrophage galactose lectin
MHC-II	Major histocompatibility complex class II
miRNA/miR	microRNA
MLH1	MutL homolog 1
MMPs	Matrix-metalloproteinases
MMR	Mismatch repair
MoDC	Monocyte derived from DCs
MR	Mannose receptor
MS	Mass spectrometry

MSI	Microsatellite instability
MUC	Mucin
MW	Molecular Weight
m/z	Mass-to-charge ratio

N

N.D.	Not detectable
Neu5Ac	N-acetylneuraminic acid
NGF	Nerve Growth Factor
NK	Natural Killer
N.S.	Not significant

P

PAMPs	Pathogen-associated molecular patterns
PE	Phycoerythrin
PCLP	Podocalyxin-like protein
PBMCs	Peripheral blood mononuclear cells
PD-1	Programmed cell death 1
PHA-E	*Phaseolus vulgaris* erythroagglutinin
PIK3CA	Phosphatidylinositol-4,5-biphosphate 3-kinase catalytic subunit alpha
PMNs	Polymorphonuclear leukocytes
ppGalNAcT	polypeptide-N-acetylgalactosaminyltransferase
Pro	Proline
PRRs	Pattern recognition receptors
PTPRJ	Receptor-type tyrosine-protein phosphatase eta
PVDF	Polyvinylidene difluoride

R

RNA	Ribonucleic acid
ROI	Reactive oxygen intermediate
ROS	Reactive oxygen species
RPMI	Roswell Park Memorial Institute
rProtein	Recombinant protein
RT-qPCR	Reverse Transcription quantitative Polymerase Chain Reaction

S

SCNA	Somatic copy number alteration
SD	Standard deviation
SEM	Standard Error of Mean
SDS-PAGE	Sodium dodecyl sulphate-polyacrylamide gel electrophoresis
Ser	Serine
sLe^A	Sialyl Lewis A
sLe^X	Sialyl Lewis X
Sia	Sialic Acid
SiaT	Sialyltransferase
Siglecs	Sialic acid-binding immunoglobulin-like lectins
SIGN-R1	Specific Intercellular adhesion molecule-3-Grabbing Non-Integrin-Related 1
SR	Scavenger receptor
SRCL	Scavenger receptor with C-type lectin

sT	Sialyl Thomsen-Friedenreich
STAT3	Signal transducer and activator of transcription protein 3
ST3GalT	β-galactoside α2,3-sialyltransferase
ST6GalT	β-galactoside α2,6-sialyltransferase
ST6GalNAcT	α-N-acetylgalactosaminide α2,6-sialyltransferase
sTn	Sialyl Thomsen-nouveau

T

T	Thomsen-Friedenreich
TGF-β	Transforming growth factor β
Thr	Threonine
TIGIT	T cell immunoreceptor with Ig and ITIM domains
TIM3	T cell immunoglobulin mucin receptor 3
TIMP-1	Tissue inhibitor of metalloproteinases 1
Tn	Thomsen-nouveau
TNF-α	Tumour necrosis factor α
TNM	Tumour, nodes, metastases
TP53	Tumour protein 53
Trp	Tryptophan
Tyr	Tyrosine

U

UDP	Uridine diphosphate
UGGT	UDP-glucose glycoprotein glycosyl transferase
UMP	Uridine monophosphate

V

VLA-6	Very late antigen 6

W

WB	Western Blot

X

Xyl	Xylose

Chapter 1 – Introduction

1.1. Colorectal Cancer

Cancer is the second cause of mortality worldwide. Among the varies different types of cancer, colorectal cancer (CRC) is the deadliest one, behind lung cancer (World Health Organization 2018). In Portugal, CRC is the third and second in term of incidence and mortality, respectively (Globocan 2018). Characterisation of primary tumour or relapses and diagnosis of metastasis are key factors to reduce the incidence of CRC. Carbohydrate antigen 19.9 (CA-19.9) and carcinoembryonic antigen (CEA) are the only available serum biomarkers. However, serum CEA has low specificity since it can be found elevated in patients with other disease or cancer type. Therefore, serum CEA level is not used for diagnosis, but as prognosis factor in pre-operative condition and post-operative patient follow-up to detect persistent disease (F. Shen et al. 2019; Z. Sun et al. 2017; Thirunavukarasu et al. 2011). Serum CEA level is also used in patient undergoing chemotherapeutic treatment for metastasis (Yu et al. 2018; Duffy et al. 2014).

1.1.1. Risk factors

Age is the highest risk factor of CRC, after 50 years-old, the prevalence augments exponentially. Inflammatory Bowel Disease (IBD) such as Crohn's disease and ulcerative colitis also increases the risk of developing CRC (Johnson et al. 2013). Family history with first degree relatives affected by CRC is a risk factor too (Schoen et al. 2015). Furthermore, some familial forms of CRC exist such as Lynch syndrome (Hereditary Non-Polyposis Colorectal Cancer; HNPCC) (Boland and Troncale 1984) and familial adenomatous polyposis (FAP) (Petersen, Slack, and Nakamura 1991). More rare syndromes characterised by the development of noncancerous growths are also found associated with elevated risk of CRC, for examples Peutz-Jeghers syndrome (van Lier et al. 2010) or MutY homolog-associated polyposis (MAP) (Cleary et al. 2009). Additionally, type 2 diabetes has been identified as risk factor in CRC (Agache et al. 2018). Finally, higher incidence risk has been reported for some ethnic populations suggesting a genetic predisposition for CRC development (Lynch, Rubinstein, and Locker 2004; Alexander et al. 2007).

Lifestyle risk factors for CRC are overweight and obesity, physical inactivity (Johnson et al. 2013), diet rich in processed and red meat (Cross et al. 2007) and poor intake of fruits and vegetables consumption (van Duijnhoven et al. 2009). Moreover, smoking and regular heavy alcohol intake are linked to CRC occurrence (Cheng et al. 2015; McNabb et al. 2019).

1.1.2. Screening

Screening of CRC in regular population includes faecal occult blood testing (FOBT) addressed to over 50 years old persons, in case of negative results, the test is renewed 2 years later. Another test includes

the research of DNA markers in faeces. In case of positivity to FOBT, colonoscopy is done to search for polyps and malignant lesions. Flexible sigmoidoscopy is also a recommended screening method (Carroll, Seaman, and Halloran 2014).

1.1.3. Diagnosis

Diagnosis includes clinical exams in order to confirm CRC and to determine the location and type, and the spread of the cancer. Different types of endoscopy, proctoscopy, sigmoidoscopy, or colonoscopy, exist and allow to visualise the tumour and to collect biopsy for anatomopathological analysis. Different imagery methods can be applied to evaluate the tumour size and the presence and location of metastases. Blood analysis are done to evaluate the general health of the patient with serum CEA level dosage (Labianca et al. 2013).

1.1.4. Staging and prognosis

To establish prognosis and treatment strategies, staging of the tumour is essential. Staging is based on TNM (Tumour, Nodes, Metastases) system, which consists in T: size and invasion of local organs status of the primary tumour, N: spread level to regional lymph nodes and M: distant metastasis presence. Each category possesses sub-categories which are, for some of them, also divided in different levels, all detailed in **Table 1.1**. The tumour grade of differentiation is established from histological cancer tissue biopsy, and divided in well, moderately, poorly differentiated, and undifferentiated. Prognosis is established based on staging and grading; however, other factors are considered. For instance, the tumours can present different genetic alterations, which are chromosomal instability with loss of heterozygosity (LOH), CpG island methylator phenotype (CIMP) and microsatellites instability (MSI). LOH has the highest occurrence, can affect different gene such as *TP53*, *PIKC3A*, *APC*, *KRAS*, *BRAF*, etc., and be responsible of allelic loss of chromosome 18q (Vacante et al. 2018; Fearon et al. 1990). The CIMP is a CRC subtype characterised by the hypermethylation of CpG island on the promotor of genes such as *BRAF* or the tumour suppressor gene *MLH1* (Bae et al. 2017). MSI is characterised by genetic alteration of short tandem repeat sequences due to impair in DNA mismatch repair (MMR) system (De' Angelis et al. 2018). Besides these genetic biomarkers, CEA level is a prognosis factor used in pre-operative and follow-up for patients, high CEA level increases risk of overall mortality by approximatively 60% (Thirunavukarasu et al. 2011).

Table 1.1 TNM system and staging classification. Adapted from AJCC Cancer Staging Manual, 7th edition (American Joint Committee on Cancer 2010) including updates from 8th edition (Shida et al. 2019)

Primary Tumour (T)
TX Primary tumour cannot be assessed
T0 No evidence of primary tumour
Tis Carcinoma *in situ*: invasion of lamina propria
T1 Tumour invades submucosa
T2 Tumour invades muscularis propria
T3 Tumour invades through the muscularis propria into peri-colorectal tissues
T4a Tumour penetrates to the surface of the visceral peritoneum
T4b Tumour directly invades or is adherent to other organs or structures

Regional Lymph Nodes (N)
NX Regional lymph nodes cannot be assessed
N0 No regional lymph node metastasis
N1 Metastasis in 1–3 regional lymph nodes
N1a Metastasis in 1 regional lymph node
N1b Metastasis in 2–3 regional lymph nodes
N1c Tumour deposit(s) in the subserosa, mesentery, or non-peritonealised pericolic or perirectal tissues without regional nodal metastasis
N2 Metastasis in 4 or more regional lymph nodes
N2a Metastasis in 4–6 regional lymph nodes
N2b Metastasis in 7 or more regional lymph nodes

Distant Metastasis (M)
M0 No distant metastasis
M1 Distant metastasis
M1a Metastasis confined to one organ without peritoneal metastasis
M1b Metastases in more than one organ without peritoneal metastasis
M1c Metastasis to the peritoneum with or without another organ involvement

ANATOMIC STAGE/PROGNOSTIC GROUPS			
Stage	**T**	**N**	**M**
0	Tis	N0	M0
I	T1	N0	M0
	T2	N0	M0
IIA	T3	N0	M0
IIB	T4a	N0	M0
IIC	T4b	N0	M0
IIIA	T1–T2	N1/N1c	M0
	T1	N2a	M0
IIIB	T3–T4a	N1/N1c	M0
	T2–T3	N2a	M0
	T1–T2	N2b	M0
IIIC	T4a	N2a	M0
	T3–T4a	N2b	M0
	T4b	N1–N2	M0
IVA	Any T	Any N	M1a
IVB	Any T	Any N	M1b
IVC	Any T	Any N	M1c

A new classification strategy has been proposed based on different markers of cancer onset and progression to establish different therapeutic strategies. This classification distinguishes four consensus molecular subtypes (CMS), defined by gene mutation and expression, proteomics, immune response and immune cell infiltration, chromosomal instability, among others (Guinney et al. 2015). The different CMS are:

- CMS 1 represents 14% of tumours, named “MSI Immune”, it is defined by hypermutations, CIMP, MSI high, BRAF mutation, immune infiltration with an upregulation of immune evasion pathways.
- CMS 2 represents 37% of tumours, named “Canonical”, it is characterized by an elevated somatic copy number alteration (SCNA) and strong signalling activation of WNT and Myc pathways.

- CMS 3 represents 13% of tumours, named “Metabolic”, it shows high metabolic dysregulation and KRAS mutations.
- CMS 4 represents 23% of tumours, named “Mesenchymal”, it presents upregulation of genes involved in epithelial-mesenchymal transition (EMT) with the activation of transforming growth factor-β (TGF-β) signalling and angiogenesis.

The CMS classification defined the remaining 13% of CRC tumours as “mixed” which shows a limit to this classification system and requires further studies, for instance by including other markers.

1.1.5. Treatments

All risk factors and characterisation of the tumour (*i.e.*, stage, grade, biomarkers, CEA level) are taken into consideration to establish the treatment strategy. Surgically removal of the tumour is the main treatment. However, surgery may require adjuvant treatment, especially for patients with advanced CRC. Chemotherapy and/or radiotherapy are used to reduce the tumour size prior surgery (neoadjuvant treatment) or in post-surgery adjuvant treatment strategies. The common chemotherapeutic drugs are 5-fluorouracile (5-FU), leucovorin, oxaliplatin and capecitabine. Combination of chemotherapeutics is often used such as FOLFOX (leucovorin, 5-FU and oxaliplatin), FOLFIRI (leucovorin, 5-FU and irinotecan), CAPEOX or CAPOX (capecitabine and oxaliplatin) or FOLFOXIRI (leucovorin, 5-FU, oxaliplatin and irinotecan). Targeted therapeutic treatments are also use alone or in combination with chemotherapy. For instance, two targeted antibodies exist: Bevacizumab (Avastin) which targets vascular endothelial growth factor (VEGF) and Cetuximab (Erbitux) which targets epithelial growth factor receptor (EGFR) (Basile et al. 2017; Labianca et al. 2013).

Promising immunotherapeutic treatments are developed and are promising especially for patient with tumour resistant to chemotherapy. For instance, monoclonal antibodies have been developed against PD-1: Pembrolizumab and nivolumab are promising in patient with MMR-deficient and MSI-high metastatic CRC (André et al. 2020; Le et al. 2020; Smith and Desai 2018; Overman et al. 2017). Other T cell checkpoint molecules can be targeted, for example lymphocyte activation gene 3 protein (LAG3), T cell immunoglobulin mucin receptor 3 (TIM3) and T cell immunoreceptor with Ig and ITIM domains (TIGIT) (Anderson, Joller, and Kuchroo 2016).

1.2. N- and mucin type O-glycosylation

Protein glycosylation alteration has been shown to be a hallmark of cancer since decades. This part presents the process of protein glycosylation in humans. Section **1.3** describes the glycosylation alterations in CRC and section **1.4** discusses the involvement of Lewis antigen in CRC.

Glycosylation is a post-translational modification which concern about 70% of proteins. Its roles are multiples including protein solubility, cell interactions, protein half-lives, metabolic regulation, protein folding, etc. Minimum requirements for glycosylation are the presence of the enzyme (glycosyltransferase), a sugar-donor (nucleotide-sugar) and an acceptor (protein, lipid, glycan). Glycosylation is the association of a protein or lipid to a glycan. For glycoprotein, a chemical classification based on the nature of the atom between the glycan and the protein has been established giving three categories, O-glycosylation for oxygen, N-glycosylation for nitrogen and C-glycosylation for carbon. These three types of glycosylation can be found on the same protein. Thus, the typic structure is a monosaccharide attach to the O, N or C atom of an amino acid, followed by a core, one type of core is found in N-glycosylation and several in O-glycosylation, attached to the core there is one or several antennae finally decorated with peripheral sugars, mainly N-acetylneuraminic acid (Neu5Ac, Sia or sialic acid) and fucose (Fuc). In N-glycosylation, the linkage is between a N-acetylglucosamine (GlcNAc) and an asparagine (Asn). In very few cases, N-glycosylation can refer to the linkage between mannose (Man) on azote atom of a tryptophan (Trp). O-glycosylation is mainly mucin type, the linkage is between a N-acetylgalactosamine (GalNAc) and a serine (Ser) or a threonine (Thr). Other types of O-glycosylation exist; in collagen type, the linkage is with hydroxylysine, in glycogen type, linkage is between glucose (Glc) and tyrosine (Tyr), in proteoglycan, xylose (Xyl) is linked to Ser or Thr. Man, Fuc and GlcNAc can be linked to Ser or Thr via oxygen atom. C-glycosylation represents about 15% of glycosylated proteins and consists in the linkage between Man and Trp. N- and mucin type O-glycosylation are the most prevalent type of protein glycosylation found in humans, thus we will focus only on these two types of protein glycosylation (Corfield 2017).

1.2.1. N-glycosylation

1.2.1.1. Structure

In N-glycosylation, the GlcNAc is linked to an Asn found in a consensus sequence, this sequence is three amino acids, Asn-X-Ser/Thr, where X represents any amino acid except proline (Pro) (Bause 1983). This consensus sequence is necessary but not sufficient. The core attached to the GlcNAc is common to all N-glycoproteins (**Figure 1.1A**). Attached to the core, antennae determine the type of N-glycan, mannosidic (**Figure 1.1B**), complex (**Figure 1.1C**) or hybrid (**Figure 1.1D**). There are two main peripheral

sugars bound to the structure by sialyltransferases (SiaTs) and fucosyltransferases (FucTs). Sialylation is generally found on the galactose (Gal) in terminal position in α2,3 or α2,6 linkage. Polysialylation can occur, mainly in nervous tissues, consisting in the addition of sialic acid in α2,8 on terminal sialic acid. Fucosylation can be present on Gal or GlcNAc from the antennae, in α1,3, α1,4 or α1,2, or on GlcNAc of the core structure in α1,6 and is then referred as core-fucosylation.

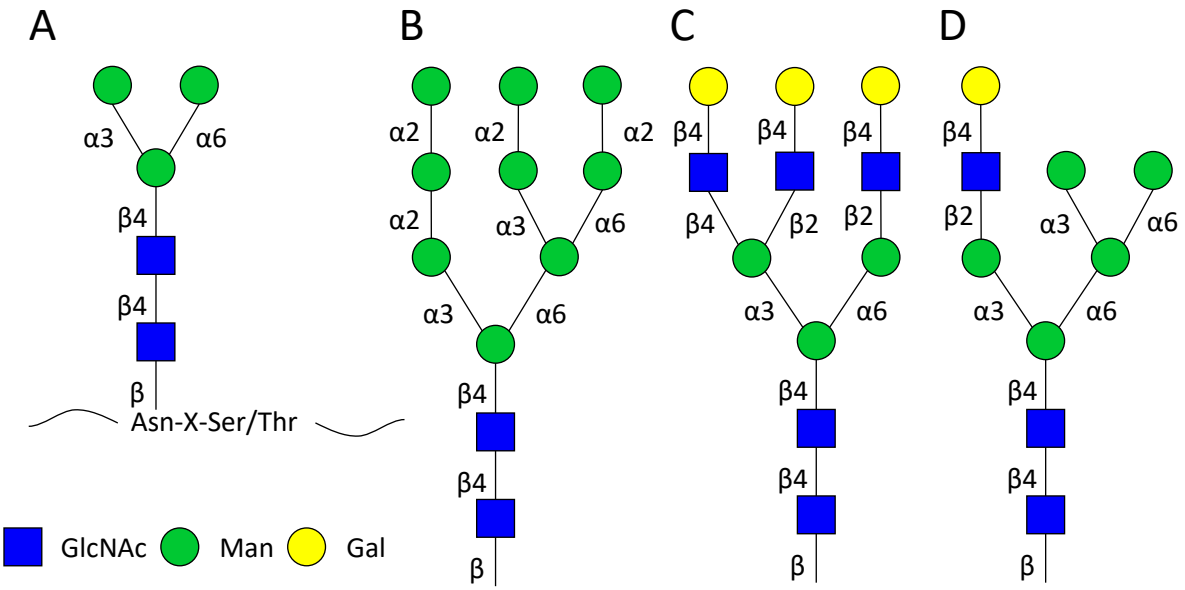

Figure 1.1 N-glycan structures. A. N-glycan core structure $Man_3GlcNAc_2$ is common to all N-glycan types. **B.** Mannosidic N-glycan type gathers structures composed of the N-glycan core and Man residues. **C.** Complex N-glycan type represents N-glycan core with one to six branches with or without peripheral sugars (Sia and/or Fuc residues). **D.** Hybrid N-glycan type is mixing the previous two types, *i.e.*, one of the terminal Man of the N-glycan core carries complex N-glycan type branch while the other terminal Man is substituted with only Man residues. Glycans are represented according to the Consortium for Functional Glycomics (CFG) Nomenclature (CFG Nomenclature).

1.2.1.2. Biosynthesis of N-glycans

N-glycan biosynthesis takes place in two organelles of the eukaryotic cell, in the endoplasmic reticulum (ER) and the Golgi apparatus. The following section details the different steps of the N-glycans biosynthesis process with their organelle localisation. Briefly, in the ER takes place the synthesis of the glycan precursor, its transfer to a nascent protein and the beginning of glycan maturation associated with the conformation step of N-glycoproteins. In the Golgi apparatus occurs the glycan maturation leading to the formation of the hybrid and complex N-glycan type structures.

1.2.1.2.1. Glycan precursor synthesis (ER)

The N-glycan precursor is composed of fourteen monosaccharides. Its synthesis is initiated in the cytoplasmic side of the ER and once the N-glycan precursor is fully synthesised, it is transferred on a nascent protein in the ER lumen (described in **Figure 1.2**). Since the transfer of the N-glycan precursor occurs while the protein did not complete its translation, the N-glycosylation modification is therefore

co-translational. In the enzymatic glycosylation reaction, the transferred sugar to an acceptor must be activated. These activated sugars, also called nucleotides-sugars (*e.g.*, UDP-GlcNAc), become the appropriate substrates of the glycosyltransferases. To penetrate the ER membrane to reach the ER lumen, the nucleotides-sugars are transferred on a lipid anchored in the ER membrane, the dolichol. The dolichol is the lipid acceptor for the precursor synthesis. This lipid comes from the same precursor than cholesterol and its use is cyclic due to the necessity to recycle it. Briefly, on the cytosolic side of the ER, phosphorylated dolichol receives the first GlcNAc, then the second, followed the addition of five Man residues. The formed dolichol-pyrophosphate-$GlcNAc_2Man_5$ complex is translocated to the ER lumen by the action of membrane transporters called "flippases". The synthesis of the N-glycan precursor ends in the ER lumen with the transfer of four extra Man and three Glc. Different glycosyltransferases are necessary to produce the glycan precursor, depending on the type of linkage, glycan donor and acceptor (Aebi 2013). Finally, the precursor is transferred *en bloc* on the Asn of a protein in synthesis by the oligosaccharide transferase (OST), a complex of several protein subunits (Shrimal, Cherepanova, and Gilmore 2015). Once the precursor is transferred, the remaining dolichol pyrophosphate undergoes the action of a pyrophosphatase, the resulting dolichol phosphate can enter once again in the synthesis of a new precursor. Therefore, this recycling process took the name of dolichol phosphate cycle.

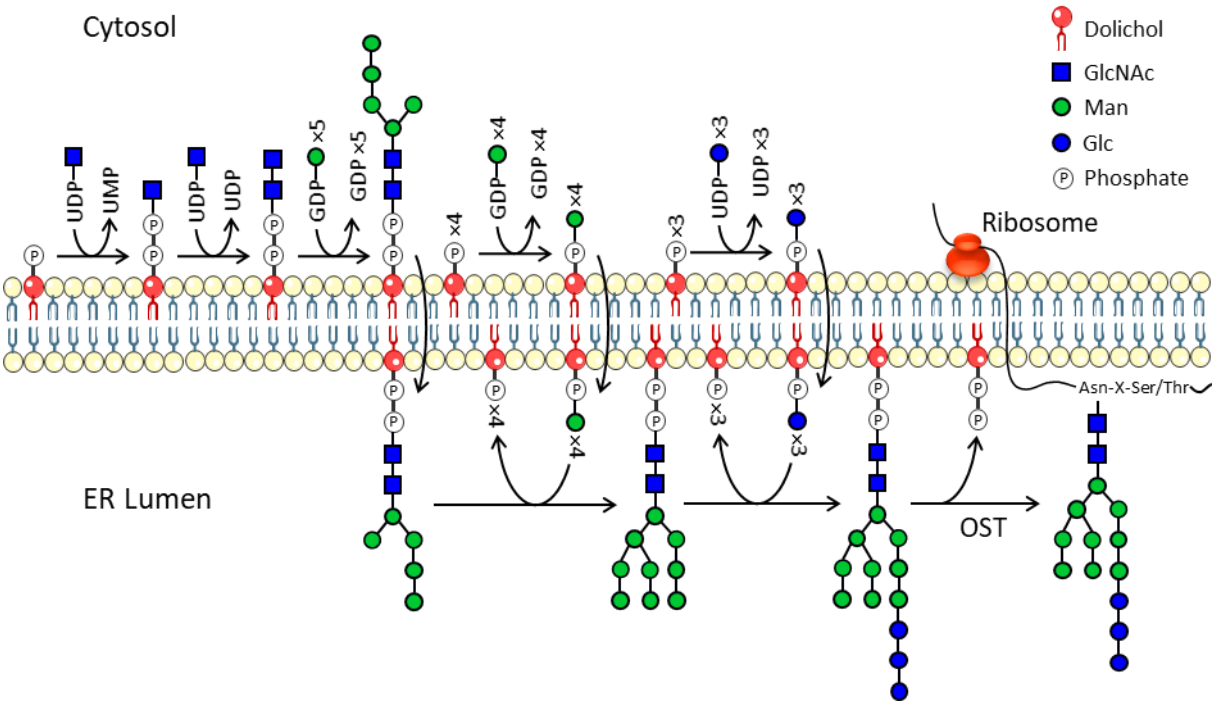

Figure 1.2 N-glycan precursor synthesis and transfer. Initiation of the N-glycan precursor synthesis occurs in the cytosolic side of the ER with the formation of the $GlcNAc_2Man_5$ structure attached to a dolichol pyrophosphate. Dolichol-pyrophosphate-$GlcNAc_2Man_5$, dolichol-phosphate-Man and dolichol-phosphate-Glc synthesised in the cytosol side of the ER are "flipped" to the lumen side where appropriate glycosyltransferases process to the complete synthesis of the N-glycan precursor. The precursor is transferred by a complex of protein, the OST, to an Asn belonging to a consensus sequence of a nascent protein peptide chain. UDP: Uridine diphosphate; UMP: Uridine monophosphate; GDP: Guanosine diphosphate.

1.2.1.2.2. ER maturation and conformation

After its transfer to the nascent protein, the precursor is subjected to the action of different glycosidases. The ER glucosidases I and II, respectively α1,2 and α1,3 glucosidases, remove the two terminal glucoses, the third one intervenes in the conformation step. Two lectins recognise the monoglucosylated precursor structure, calnexin and calreticulin. Their function is to bury the closed hydrophobic polypeptide inside the protein and their action is combined with different chaperon proteins on non-mature N-glycoproteins. The conformation change allows the action of the ER glucosidase II which removes the last glucose. If the folding of the protein is incorrect, the glucose is added again by the UDP-glucose glycoprotein glycosyl transferase (UGGT), and the protein returns to the previous step of protein conformation until it reaches the right conformation. The UGGT owns a folding sensor activity, allowing to detect immature glycoprotein. This cycle of glucosylation/deglucosylation is important and when a glycoprotein never acquires the correct conformation, it leads to its elimination to avoid the accumulation of unfolded proteins in the ER (Trombetta and Parodi 2005). This is done by the endoplasmic reticulum associated degradation (ERAD) process. As for the correctly folded glycoproteins, the ER mannosidase I (α1,2-mannosidase, *MAN1B1*) removes one mannose, giving the formation of the isomer B (**Figure 1.3** Gonzalez et al. 1999) which is sent to the Golgi apparatus where N-glycan maturation ends.

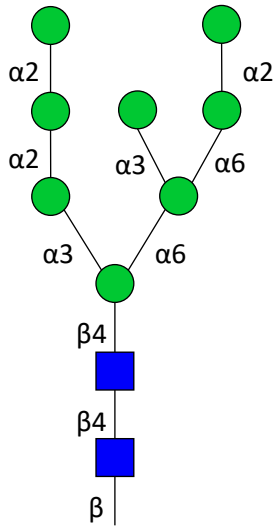

Figure 1.3 $Man_8GlcNAc_2$ isomer B.

1.2.1.2.3. Golgi maturation

In the Golgi apparatus, the N-glycan type, mannosidic, complex or hybrid, is determined by the action of two glycosidases subfamilies, the Golgi mannosidases I and II. Golgi mannosidases I remove all the remaining mannoses in α1,2 linkage (Tremblay and Herscovics 2000; Tremblay, Campbell Dyke, and Herscovics 1998; Bause et al. 1993) and without the action of these glycosidases, the N-glycan is mannosidic type. N-acetylglucosaminyltransferase I (GlcNAcT-I) can act after Golgi mannosidases I, the Golgi mannosidases II can then enter in action to remove the two last mannoses linked to the core structure (Misago et al. 1995). Without the Golgi mannosidases II action, the N-glycoprotein is hybrid type. Thus, the N-glycan mannosidic and hybrid type are due to the activity defect of Golgi mannosidases. Multiple glycosyltransferases proceed to offer the variety of glycan structure found in complex type N-glycoprotein.

1.2.1.2.3.1. Branching

The complex type N-glycans can possess up to six antennae, initiated by the transfer of a GlcNAc residue by the GlcNAcTs on the α1,6 and α1,3Man of the N-glycan core. In total, seven enzymes are found and each of them add a GlcNAc with a specific linkage/position, described in **Figure 1.4** (Stanley, Schachter, and Taniguchi 2009). Among the seven GlcNAcTs, six of them act on the terminal α1,6/3Man of the core and one on the internal β1,4Man. This later is the GlcNAcT-III, responsible of the addition of the GlcNAc called bisecting GlcNAc. Importantly, the presence of this bisecting GlcNAc prevents the action of the other GlcNAcTs.

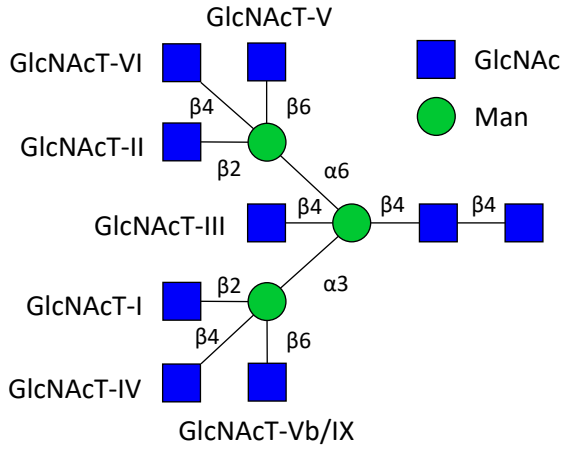

Figure 1.4 GlcNAcTs for N-glycans branching. Six GlcNAcTs, GlcNAcT-I, II, IV, V, Vb/IX and VI, can add a GlcNAc to the terminal Man residues of the N-glycan core structure, initiating the antennae of the complex N-glycans. Each one of these GlcNAcTs possesses their own substrate and linkage specificities. The GlcNAcT-III is responsible of the synthesis of the bisecting GlcNAc, added to the internal Man of the N-glycan core, which impedes the action of other GlcNAcTs.

Galactosyltransferases (GalTs) transfer Gal in β1,4 on GlcNAc residues, except on bisecting GlcNAc. This Galβ1,4GlcNAc structure is referred as type 2 N-acetyllactosamine (LacNAc), type 1 LacNAc refers to Galβ1,3GlcNAc where GalTs transfer Gal in β1,3 on GlcNAc. Repetition of type 2 LacNAc disaccharide, with the GlcNAc linked to Gal in β1,3, termed poly-N-acetyllactosamine (polyLacNAc) can be found, and sometimes ended with a type 1 LacNAc. The antennae can also be elongated with GalNAc residues instead of Gal and the linkage with the GlcNAc is in β1,4. This GalNAcβ1,4GlcNAc is called LacdiNAc for N,N-diacetyllactosamine and polyLacdiNAc sequence exists but is uncommon compared to polyLacNAc sequence (Stanley and Cummings 2009).

1.2.1.2.3.2. Peripheral sugars

N-glycans antennae can be further decorated with peripheral sugars, Sia and Fuc.

Sia is added by sialyltransferases (SiaTs), which are polygenic. There is α2,3-SiaTs, which add sialic acid on terminal Gal in α2,3 linkage; α2,6-SiaT, which add sialic acid on terminal/subterminal GlcNAc or on terminal Gal in α2,6 linkage; and α2,8-SiaT, which transfer sialic acid on sialic acid only in α2,8 linkage. Addition of sialic acid occurs in the end of the maturation process in the *trans* Golgi while branching occurs in *cis*/*median* Golgi.

Fucosylation is supported by fucosyltransferases (FucTs) coded by *FUT* and 11 *FUTs* are found. Different fucosylation arises, the core-fucosylation consists in the addition of Fuc in α1,6 on the GlcNAc linked to the Asn residues. The core-fucosylation is supported by the FucT-VIII coded by *FUT8* which is the only monogenic FucT, the others, like the SiaTs, are polygenic. The addition of Fuc on type 2 LacNAc in α1,3 leads to the Lewis X (Le^X) antigen, and if the Gal is sialylated in α2,3 the structure is therefore the sialyl Le^X (sLe^x) antigen. This fucosylation can also be in α1,4 on type 1 LacNAc leading to Lewis A (Le^A) or sialyl Le^A (sLe^A) antigen upon Gal sialylation. The fucosylation of the terminal Gal in α1,2 leads to the H antigen, only FucTs coded by *FUT1* and *FUT2* own this enzymatic activity. In presence of Fuc in α1,2, the terminal Gal can also carry a GalNAc or a Gal in α1,3 leading to, respectively, the A and B antigen. These antigens, A, B and H, found on red blood cells correspond to the antigen which determine the blood group of the ABO blood group system. When fucosylation of terminal GlcNAc and Gal occurs, two antigens are produced, Lewis Y (Le^Y) and Lewis B (Le^B) antigen (Stanley and Cummings 2009). The **Figure 1.5** resumes the different antigens mentioned above.

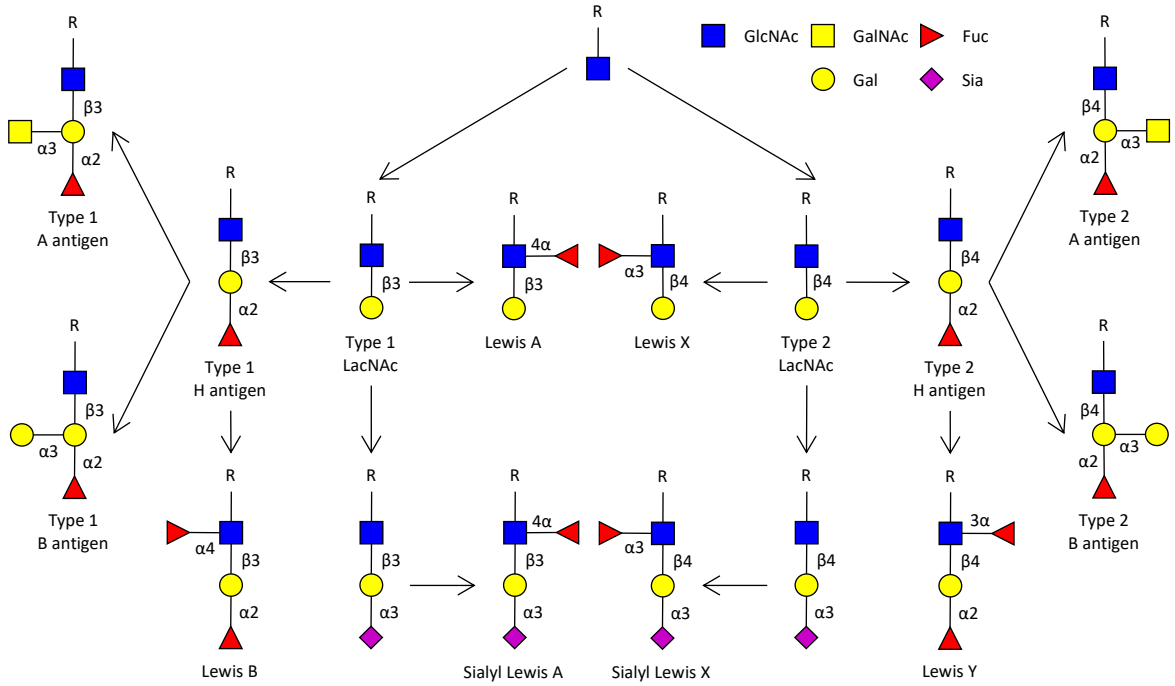

Figure 1.5 A, B and H and Lewis blood group antigens. Multiple enzymes intervene in the synthesis of glycan antigens, GalTs, GalNAcTs, SiaTs and FucTs. H, A and B blood group antigens are formed from either type 1 or 2 LacNAc structure. Le^A, sLe^A and Le^B antigens are formed from type 1 LacNAc structure, *i.e.*, Galβ1,3GlcNAc, while Le^X, sLe^X and Le^Y antigens are formed from type 2 LacNAc structure, *i.e.*, Galβ1,4GlcNAc.

1.2.2. Mucin type O-glycosylation

1.2.2.1. Structure

The basic structure of mucin type O-glycan is characterised by a GalNAc linked to a Ser or Thr residue. This GalNAc can be further modified by the action of different glycosyltransferases giving the core

structures of mucin type O-glycans. There are eight different cores which can be linked to the GalNAc, but cores 1 to 4 are the most common, cores 5 to 8 are extremely rare, thus we will describe structure and biosynthesis of core 1 to 4 only. In **Figure 1.6** (left), the structures of the four first cores are described. Two types of antenna are found: type 1 antenna with Galβ1,3GlcNAc and type 2 antenna with Galβ1,4GlcNAc. The antennae can be rearranged, been linear or branched (**Figure 1.6** right). Like in N-glycosylation, peripheral sugars are sialic acid and Fuc (Brockhausen and Stanley 2015).

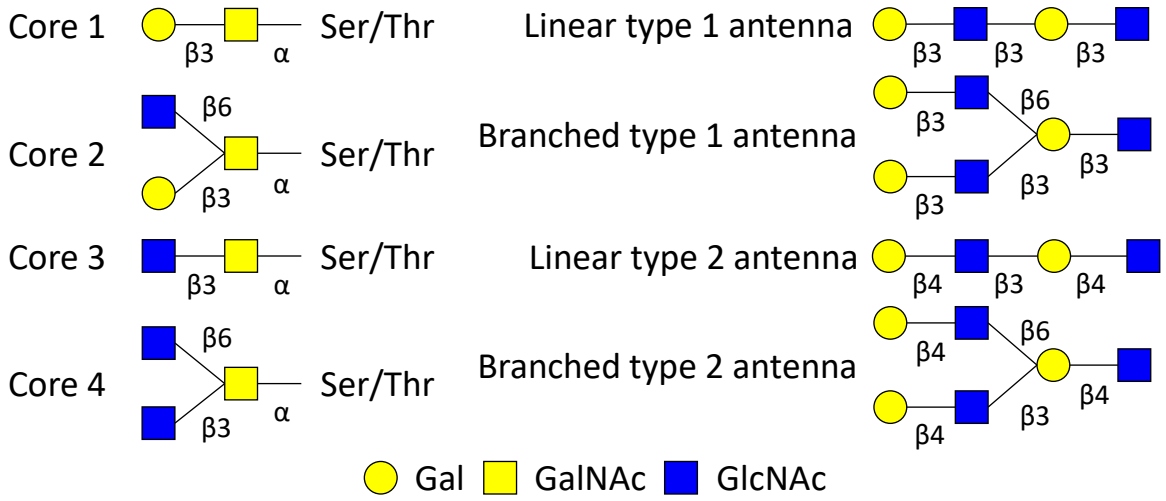

Figure 1.6 Mucin type O-glycan cores and antennae. Structures on the left are the cores. Core 1 to 4 are the most found on mucin type O-glycans, obtained with the action of GalTs and GlcNAcTs on the GalNAc linked to the Ser/Thr of the O-glycosylated protein. On the right are depicted the different antennae. Type 1 antenna consists in Galβ1,3GlcNAc repeated units and type 2 antenna in Galβ1,4GlcNAc repeated units, both via GlcNAcβ1,3Gal linkage. Type 1 or 2 LacNAc unit can be in a linear arrangement or branched via GlcNAcβ1,6Gal linkage.

1.2.2.2. Biosynthesis of mucin type O-glycans

Mucin type O-glycosylation occurs in Golgi apparatus. It starts in *cis* Golgi network in the first Golgi vesicles from the ER. In the *cis* Golgi network, the GalNAc is added. This O-glycosylation is done in a quick and sequential way. The glycosyltransferases work as those of the N-glycosylation.

1.2.2.2.1. Attach point synthesis

Contrary to N-glycosylation, no consensus sequence is found on the protein for O-glycosylation. From UDP-GalNAc, polypeptide-N-acetylgalactosaminyltransferases (ppGalNAcTs) transfer GalNAc to Ser or Thr residues. This simplest structure is named Thomsen-nouveau (Tn) antigen and is rarely found in normal mucins, but more common in mucins from cancer tissues. Tn antigen can be sialylated in α2,6 and then called sialyl Tn (sTn) antigen (**Figure 1.7**), the sTn antigen cannot be further glycosylated (Brockhausen and Stanley 2015).

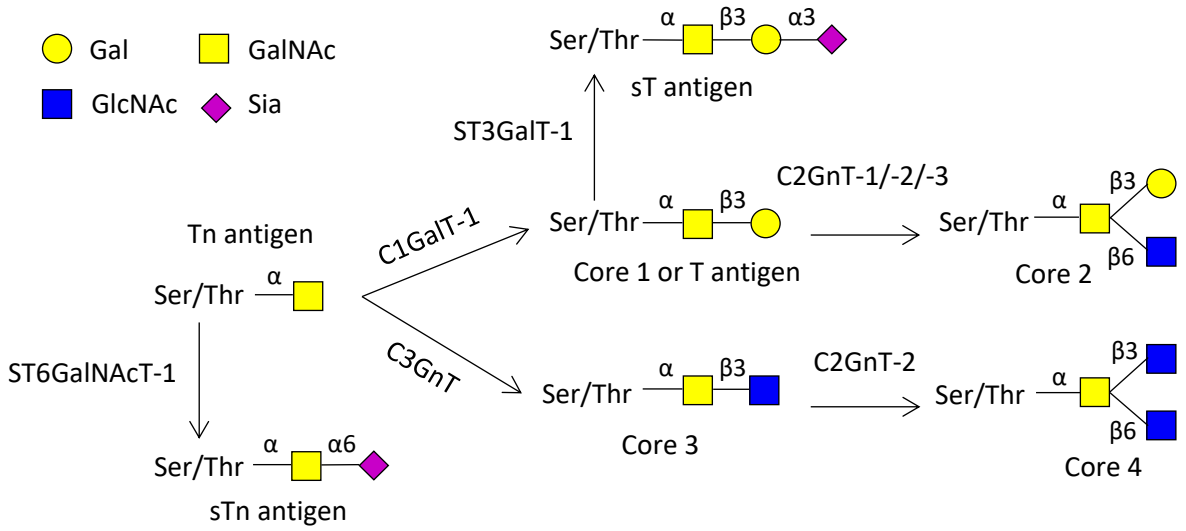

Figure 1.7 Mucin type O-glycans biosynthesis. From the GalNAc linked to the protein, several enzymes give rise to the core 1 to 4 of mucin type O-glycan or to the Tn antigen which can be sialylated. The core 1 disaccharide structure is called T antigen and, as Tn antigen, can be sialylated.

1.2.2.2.2. Cores synthesis

The core 1 is synthesised by the action of the core 1 β1,3 galactosyltransferase (C1GalT), adding a Gal residue on the first GalNAc in β1,3. This enzyme activity requires a chaperone protein, the core 1,3-Gal-T-specific molecular chaperone commonly called Cosmc (Ju and Cummings 2002). The resulting structure is called Thomsen-Friedenreich antigen or T antigen and can be sialylated in α2,3 on the Gal residue giving the sialyl T (sT) antigen. The sT antigen can only be sialylated in α2,6 on GalNAc residue and no further glycosylation is possible. The core 2 is obtained after the action of core 2 β1,6 N-acetylglucosaminyltransferase (C2GnT) on the GalNAc residue of core 1 structure. So far, three C2GnT has been identified, the C2GnT-1 and -3 are only involved in core 2 synthesis while C2GnT-2 is also involved in core 4 synthesis. Core 3 synthesis is supported by the action of core 3 β1,3-N-acetylglucosaminyltransferase (C3GnT) on the attach point GalNAc, adding a GlcNAc residue in β1,3, and, as mentioned above, C2GnT-2 action on core 3 structure results in core 4 synthesis, adding another GlcNAc on the attach point GalNAc, this time, in β1,6 linkage type (**Figure 1.7**).

1.2.2.2.3. Branching

As mentioned above, the mucin type O-glycan cores can be further elongated with two types of antenna which can be in a linear or branched arrangement. Four types of glycosyltransferases originate the antennae synthesis on mucin type O-glycans, two GlcNAcTs and two GalTs. β1,3 or β1,6GlcNAc condition the branching type, only β1,3 linkage gives linear antennae. The antenna type 1 or 2 is determined by the action of β1,3 or β1,4GalTs. As described in section **1.2.1.2.3.1**, Galβ1,3GlcNAc and Galβ1,4GlcNAc are, respectively, called type 1 and type 2 LacNAc sequence, and

LacdiNAc (GalNAcβ1,4GlcNAc) sequence can also be found. As for N-glycans, polyLacNAc with type 2 LacNAc is the most common extension found (Stanley and Cummings 2015).

1.2.2.2.4. Peripheral sugars

Sialylation and fucosylation represent the most common terminal step of mucin type O-glycosylation. Moreover, carbohydrate sulphation brings supplementary negative charges to mucins, usually on the Gal in C-3 position or on GlcNAc in C-6 position. The ABO blood group antigens and the Lewis antigens with their related sialylated forms described in **Figure 1.5** are found in terminal structures, their synthesis involves the same glycosyltransferases as in N-glycans synthesis. Unlike N-glycan, there is generally no α2,6 sialylation on terminal Gal, mostly, sialylation occurs in α2,6 on GalNAc and in α2,3 on Gal (Stanley and Cummings 2015).

1.3. Protein glycosylation alteration in colorectal cancer

Glycosylation alterations are found in all types of cancer, here, we will focus on the observed changes in CRC. Increased novel or truncated glycan structures, highly branched N-glycan, polyLacNAc, as well as enhanced sialylation and fucosylation are found in CRC. Underexpressed structures include core 3 and 4 structures on mucin type O-glycans and bisecting GlcNAc on N-glycan.

1.3.1. N-glycans

Different studies show alterations of N-glycan structures on CRC patient tissues and serum glycoproteins, and CRC cell lines. Mannosidic type N-glycan structures increase in CRC. Indeed, quantitative mass spectrometry N-glycome profiling comparing CRC tissues to adjacent normal tissues highlights an increase in high-mannose type N-glycan structure ($GlcNAc_2Man_7$ and $GlcNAc_2Man_8$) in 43 CRC patients (D. Zhang et al. 2019). Similar observations have been made in another study with five CRC patients (Sethi et al. 2015), which also shows an enhancement in paucimannose structures, *i.e.* $GlcNAc_2Man_{1-4}$. Likewise, 25 CRC cell lines N-glycome profile reveals abundant high-mannose structure, although the extent is more important when compared to tissues, probably due to enrichment of precursor structures during N-glycan extraction from cell lines (Holst et al. 2016). Comparison of rectal carcinoma versus adenoma indicates the enhancement of paucimannose structure with or without core-fucosylation in carcinomas (Kaprio et al. 2015) and also in CRC tissues compared to adjacent normal tissues (Balog et al. 2012).

Actually, core-fucosylated paucimannose structures are overexpressed at high CRC stage compared to first stage (Kaprio et al. 2015). The expression of FucT-VIII responsible for N-glycan core-fucosylation is found increased in CRC and correlates with decrease overall and disease free survival (Muinelo-

Romay et al. 2011). Moreover, *in vitro* drug resistance study shows an increase of core-fucosylated structures and an overexpression of *FUT8* mRNA level in SW620 cell line (L. Shen et al. 2018).

Lower expression of bisecting GlcNAc and increase β1,6-GlcNAc branched N-glycans are well described in CRC. The relationship between the two structures is often presented in studies due to the antagonist activity of the enzymes giving these glycan structures, GlcNAcT-III for bisecting GlcNAc and GlcNAcT-V for β1,6-GlcNAc branching. Indeed, GlcNAcT-V cannot act on N-glycan structures containing bisecting GlcNAc. GlcNAcT-III inhibits the formation of branched N-glycan structure (Sasai et al. 2002). Thus, bisecting N-glycan structures decreases in CRC tissues (D. Zhang et al. 2019; Balog et al. 2012) while β1,6-GlcNAc branched N-glycan increases (Hägerbäumer et al. 2015) as well as GlcNAcT-V enzyme (Murata et al. 2000). Enhancement of multi-antennae (tri/tetra) N-glycan structure has also been observed on serum proteins from CRC patients (de Vroome et al. 2018; Doherty et al. 2018). *In vivo*, xenograft experiments using CRC cell lines with overexpressed or silenced GlcNAcT-V shows positive regulation of tumour progression associated with high GlcNAcT-V expression and reduced tumorigenicity and proliferation with low GlcNAcT-V expression. A well-studied target of GlcNAcT-V is the tissue inhibitor of metalloproteinases-1 (TIMP-1). Kim et al. (2012) propose an original model in which increased TIMP-1 expression in early development of tumour has proliferative effect and enhances tumour growth, while, in late stage of tumour progression, aberrant glycosylation of TIMP-1 triggered by GlcNAcT-V overexpression prevents its inhibitory action on matrix-metalloproteinases (MMPs) allowing tumour progression. Inhibition of GlcNAcT-V activity and enhancement of GlcNAcT-III bisecting N-glycan product has been highlighted by the use of anti-inflammatory drug, mesalamine (5-ASA), in HT29 cell line (Khare et al. 2014). The consequence of this glycosylation modulation by 5-ASA is the maintenance of E-cadherin at the membrane which might prevents EMT in CRC progression. Surprisingly, the identification of a unique bisecting N-glycan structure in a metastatic CRC cell line, together with higher GlcNAcT-III mRNA and bisecting GlcNAc stained by PHA-E lectin levels (Sethi et al. 2014), is contradictory with published reports. For example, recent publication shows the decrease of bisecting N-glycan structures with higher stage in CRC tissues (D. Zhang et al. 2019).

As consequence of the increase of complex N-glycans with β1,6-GlcNAc branching, enhancement of (poly)LacNAc structure occurs. Synthesis of (poly)LacNAc requires β1,3-GlcNAcTs and β1,3/4-GalTs. The β1,3-GlcNAcT-VIII shows increased expression in CRC tissues and cell lines (Z. Jiang et al. 2018; Ni et al. 2014). This enzyme initiates the synthesis of polyLacNAc chains on β1,6-GlcNAc branched N-glycans (H. Ishida et al. 2005). β1,3-GlcNAcT-VIII expression has been linked to chemotherapeutic drug resistance in CRC cell line. Indeed, 5-FU treatment diminishes the expression of this enzyme in SW620 cell line sensitive to the drug, whereas resistant cell line presents the increase of polyLacNAc

structure accompanied with higher expression of β1,3GlcNAcT-VIII (L. Shen et al. 2014; Gao et al. 2014). These features have also been observed in resistance to another chemotherapeutic drug, oxaliplatin (L. Shen et al. 2018). In this study, the resistant SW620 cell line not only presents the increase of β1,3-GlcNAcT-VIII and polyLacNAc structure but also the decrease of GlcNAcT-III and bisecting GlcNAc with the increase of GlcNAcT-V and β1,6 branched structures. Others enzymes involved in polyLacNAc biosynthesis, β1,3-GalT-IV and β1,4-GalT-IV, are overexpressed which correlates with poor prognosis in CRC patients (T. Zhang et al. 2018; W.-S. Chen et al. 2005). These enzymes also provide the substrates for Lewis type antigens synthesis, β1,3-GalT for (sialyl) $Le^{A/B}$ and β1,4-GalT for (sialyl) $Le^{X/Y}$ which will be discussed in a separate section (**1.3.5**).

Increased terminal sialylation of N-glycans in tissues and serum are observed in CRC patients (de Vroome et al. 2018; Sethi et al. 2015; Gessner et al. 1993). Mediated by β-galactoside α2,6-sialyltransferase I (ST6GalT-I), radiation of CRC cells presents an increased expression of the enzyme. Consecutive overexpressed ST6GalT-I induces β1 integrin sialylation leading to adhesion and migration of CRC cells (M. Lee et al. 2010). Increased sialylation will be further discussed in separate section (**1.3.3**).

To resume, the major alterations on N-glycans in CRC are: (i) increased pauci/high-mannosidic type structures (**Figure 1.8A**), (ii) enhanced core-fucosylation (**Figure 1.8A** and **B**), (iii) decrease bisecting GlcNAc (**Figure 1.8C**) and (iv) augmentation of β1,6-GlcNAc branching (**Figure 1.8B**) (v) with higher (poly)LacNAc structures (**Figure 1.8B**), (vi) and elevated terminal α2,6 sialic acid (**Figure 1.8D**).

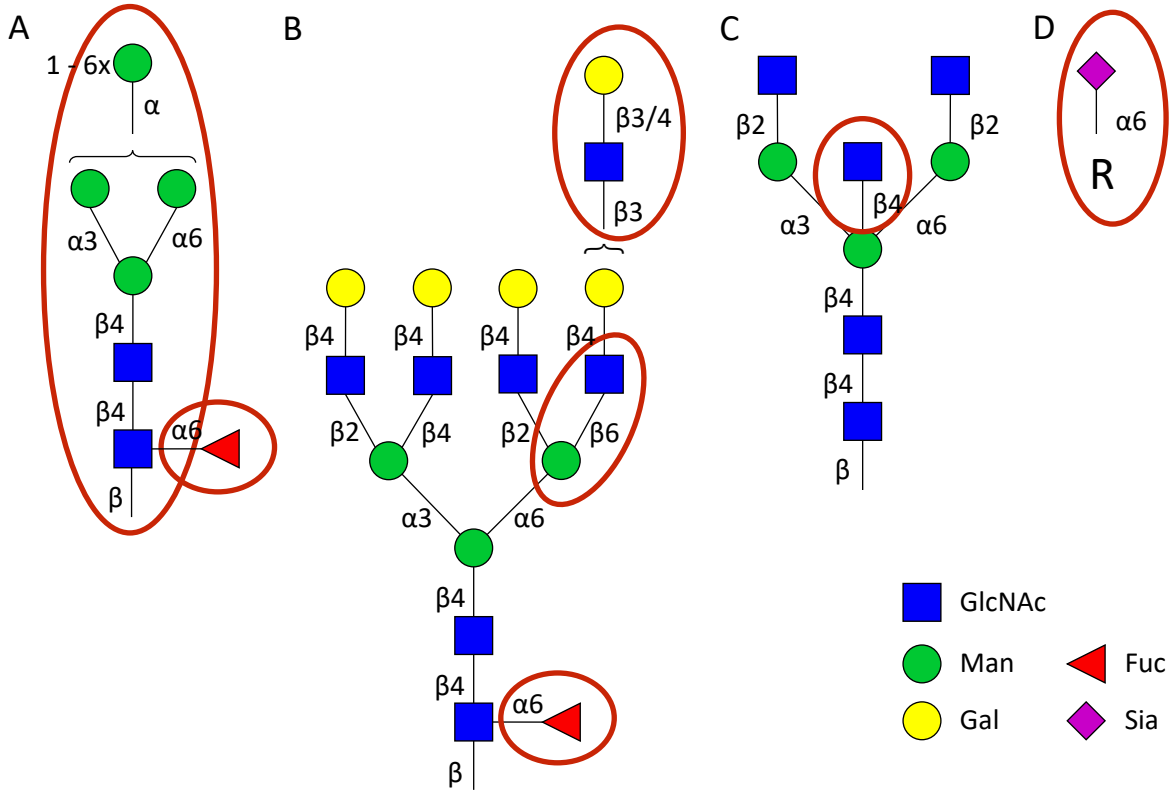

Figure 1.8 Major N-glycans alterations in colorectal cancer. A – D. Red circles emphasises altered glycans structures. **A.** Pauci/high-mannosidic type structures and core-fucosylation are increased. **B.** β1,6-GlcNAc branching, (poly)LacNAc structures and core-fucosylation are enhanced. **C.** Decrease of bisecting GlcNAc. **D.** Elevated terminal α2,6 sialic acid. R = N-glycan.

1.3.2. Mucin type O-glycans

The colonic mucus contains high level of heavily O-glycosylated mucin proteins. Observed alterations in mucin type O-glycosylation are downregulation of core 3 and 4 structures, increase of Tn, T antigens and their related sialylated forms, and, as in N-glycans, increase of sialyl Lewis antigen structures.

The glycosyltransferases which initiate the mucin type O-glycosylation by transferring a GalNAc on Ser/Thr belong to the ppGalNAcT family and count 20 enzymes. ppGalNAc-T1 and -T2 are more expressed in CRC tissues and cell lines than in adjacent normal tissue and normal colon cell lines (Kohsaki et al. 2000; Shan et al. 2018). A recent study shows, *in vitro* and *in vivo*, that long non-coding RNA (LncRNA) *SHNG7* high expression, found in CRC tissues and cell lines, promotes proliferation and metastasis, and correlates with ppGalNAc-T1 expression. The authors propose that LncRNA *SNHG7* influences the availability of microRNA (miRNA) miR-216b which target ppGalNAc-T1 gene (Shan et al. 2018). Several studies show increased expression of ppGalNAc-T3 in CRC tissues and cell lines, however, the impact on CRC malignant behaviour is controversial. Indeed, ppGalNAc-T3 and *ZEB2*, transcriptional repressor playing a role in EMT induction, have negatively correlated expression. Thus, in tissue high expression of ppGalNAc-T3 and low expression of *ZEB2* suggest less extent of EMT, disadvantaging metastasis (Balcik-Ercin et al. 2018). Furthermore, Shibao et al. (2002) associate strong

ppGalNAc-T3 expression in CRC with better outcome for patients (n=106). On the opposite, similarly to Shan et al. study on ppGalNAc-T1 gene expression, ppGalNAc-T3 expression is linked to LncRNA linc01296 expression. LncRNA linc01296 targets miRNA miR-26a which is associated with poor overall survival and prognosis, and metastasis (B. Liu et al. 2018). A study of negative prognostic factor *BRAF* mutation V600E *in vitro* demonstrates the increased expression of macrophage galactose lectin (MGL) ligand (*i.e.* sTn) via ppGalNAc-T3 (Sahasrabudhe et al. 2018). Thus, observed different outcomes in high ppGalNAc-T3 expression may be explained by the different pathways leading to this expression pattern.

ppGalNAc-T4 is a direct target of miRNA miR-4262, which has a decreased expression in CRC tissues and cell lines. *In vitro* experiments show unfavourable role of miR-4262 in apoptosis, proliferation, viability and colony formation and *in vivo* in tumour growth (Weng et al. 2018; Qu, Qu, and Zhou 2017). ppGalNAc-T4 is upregulated in CRC in a stage dependent manner, leading to establishment of a model where high expression of ppGalNAc-T4 in early stages contributes to tumorigenesis and decreased expression in later stages facilitates tumour migration and invasion (Yan et al. 2018). ppGalNAc-T5 knock-down (KD) reduces cell migration ability *in vitro* and is the target of miRNA miR-196b-5p whose expression is associated with better 5-years overall survival (Stiegelbauer et al. 2017). In patients, high ppGalNAc-T6 expression correlates with higher overall survival (Duan et al. 2018; Ubillos et al. 2018) and decreased expression is associated with poor prognosis in a subtype of CRC with MMR deficiency (Noda et al. 2018). Thus, ppGalNAc-T6 expression seems to be an interesting prognostic factor since its expression is observed in CRC patients tissues and not in adjacent normal colon tissues (Lavrsen et al. 2018; Ubillos et al. 2018).

As mentioned above, *SNHG7*/miR-216b/ppGalNAc-T1 axis is proposed as a therapeutic target for its role in proliferation and metastasis. A different study provides evidence that LncRNA *SNHG7* targets another miRNA, miR-34a, leading to the increased expression of ppGalNAc-T7 (Y. Li et al. 2018). This other axis seems to have similar influence on proliferation and metastasis *in vitro* and *in vivo*. ppGalNAc-T12 expression has been shown lower in CRC cell lines and tissues compared to normal colon, and this low expression profile influences metastases development (J.-M. Guo et al. 2004). Moreover, mutation with deleterious effect on enzyme activity is associated with higher risk of CRC susceptibility in several studies (Evans et al. 2018; Clarke et al. 2012; Guda et al. 2009).

Following ppGalNAcTs activities, different enzymes give rise to O-glycan core structures. The activity of C3GnT is reduced in tissues from CRC patients (Yang et al. 1994). Further studies observe an undetectable expression of the enzyme in tumour tissues and *in vivo* models attributing a preventive role in tumorigenesis, migration and lung metastases formation (An et al. 2007; Iwai et al. 2005). Core 3

is the substrate of core 4 structure, synthesised by C2GnT-2, which can also give core 2 structure. This enzyme is proposed for prognostic biomarker in patients due to its observed downregulation in tumour (González-Vallinas et al. 2015; Huang et al. 2006). A role in chemoresistance, *in vitro* and *in vivo* cell growth and invasion is also attributed to C2GnT-2 expression (Fernández et al. 2018; Huang et al. 2006).

When Core 1 synthase or T synthase (C1GalT) is silenced, increased expression of core 3 structure, Tn and sTn antigen are observed showing a competition between C1GalT, and C3Gnt, and α-N-acetylgalactosaminide α2,6-sialyltransferase I (ST6GalNAcT-I) (Barrow et al. 2013). C1GalT, its product T antigen, and its chaperone Cosmc are overexpressed in CRC cancer tissues and associated with lower survival rate in patients (X. Sun, Ju, and Cummings 2018; Hung et al. 2014). Although, Cosmc knock-out (KO) in two CRC cell lines results in Tn expression, leading to highest invasive, migration, and metastasis by EMT activation via H-Ras, in concordance with Cosmc/H-Ras expression level in TCGA cohort (n=438) (Z. Liu et al. 2019). Similarly, *C1GALT1* KO induces Tn expression in HCT116 colon cancer cell line, resulting in increased proliferation, adhesion, migration and invasion abilities and activation of EMT pathway (Dong et al. 2018). Tn antigen staining is positive in 86.6% of CRC patients tissues (n=186), while absent in adjacent normal tissues. Tn antigen expressing tissues present C1GalT and Cosmc expression defects (Yuliang Jiang et al. 2018). Thus, T and Tn antigen expression are closely related and, both increase malignant phenotype and poor overall survival. Their sialylated forms, sT and sTn, have similar features and will be described section below.

1.3.3. Sialylation

Increased sialylation is typically observed in CRC and associated with malignancy and poor prognosis. This hypersialylation is observed on N- and O-glycans with higher α2,6 and α2,3 terminal sialic acids and enhancement of tumour sT, sTn and $sLe^{X/A}$ antigens. Different mechanisms can lead to the observed hypersialylation, such as dysregulation of SiaT and/or neuraminidases.

Four neuraminidases *NEU1* to *4*, also called sialidases, are identified and differ by their subcellular location and targets. *NEU2* is very low expressed in healthy colon tissues and CRC cell lines (Forcella et al. 2018; Koseki et al. 2012). *NEU1* and *NEU4* are downregulated in CRC, and *in vitro* experiments show increased migration and invasion properties of KD CRC cells for both genes (Uemura et al. 2009; Yamanami et al. 2007; Forcella et al. 2018; Miyagi et al. 2008). Moreover, *in vivo* assays show marked decrease of liver metastasis upon *NEU1* overexpression (Uemura et al. 2009). *NEU4* silencing reduces apoptosis and downregulates sLe antigen expression abrogating E-selectin interaction (Yamanami et al. 2007; Shiozaki et al. 2011). On the opposite, *NEU3* is highly expressed in CRC and possesses suppressive effects on cell apoptosis (Forcella et al. 2018; Wada et al. 2007; Kakugawa et al. 2002). Its

overexpression *in vitro* facilitates cell invasion via integrin-mediated signalling through extracellular matrix interaction (Kato et al. 2006).

As mentioned above, sTn and sT are highly expressed in CRC, while these antigens are not found on normal colorectal mucosa. The sialylation of Tn antigen is mediated by ST6GalNAcT-I and sTn expression is associated with aggressiveness and poor prognosis (X. Sun, Ju, and Cummings 2018; Munkley 2016). Indeed, sTn presents strong expression on tumour, especially tumour with recurrence, accompanied by an increase of *ST6GALNAC1* mRNA level, which correlates with lower overall survival for stage III and IV *ST6GALNAC1* positive patients (Mihalache et al. 2015; Ogawa et al. 2017). The expression of *ST6GALNAC1* has been proposed as a candidate for colorectal cancer stem cells and cancer initiating cells (CR-CSCs/CICs) specific genes, silencing reveals a less extent of CR-CSCs/CICs *in vitro* and *in vivo* and overexpression enhances this characteristic phenotype of CR-CSCs/CICs *in vitro* (Ogawa et al. 2017). Several studies evaluate the potential of sTn as a therapeutic target, thus different mAb has been developed to target the disaccharide (Loureiro et al. 2018) and mAb conjugated with drug shows promising inhibiting effect on tumour growth in xenograft model using CRC cell line (Prendergast et al. 2017). Remarkably, the antigen can also be detected on circulating tumour cells (CTCs) even at early stage regardless with metastasis (Neves et al. 2019). T antigen can be mono or di-sialylated, on the Gal residue by β-galactoside α2,3-sialyltransferase I (ST3GalT-I) and on the GalNAc residue by ST6GalNAcT-II (Marcos et al. 2004), sT and di-sT antigens are more expressed on tumours and this correlates with recurrence potential (Mihalache et al. 2015). Thus, *ST3GAL1* and *ST6GALNAC2* mRNAs were highly expressed in CRC tumour tissues compared to normal tissues (Petretti et al. 2000; Schneider et al. 2001).

As mentioned in section **1.3.1**, ST6GalT-I is highly expressed in CRC tumours which results in an increase α2,6 terminal sialylation of N-glycans. Recent studies attribute to the differential expression of the enzyme a correlation with stem cell profile, tumorigenesis and chemotherapy resistance (Cui et al. 2018; S. Zhang et al. 2017; Swindall et al. 2013). Moreover, downregulation of ST6Gal-I in HT29 cell line by antisense DNA transfection reduces the cells aggressiveness and invasiveness capacities (Zhu et al. 2001). A link between α2,3 sialylation of type 2 chain, precursor of sLe^x antigen, and metastasis has been established and five-year survival rate decreases in patients presenting positive staining of this type of structure using lectin (Fukasawa et al. 2013). The sLe antigen expression in CRC will be further discussed in a separate section (**1.3.5**). In sum, increase of sialylation affect CRC aggressiveness and is related to poor prognosis for patients.

1.3.4. Fucosylation

Core fucosylation of N-glycans which is mediated by *FUT8* was discussed in section **1.3.1**. The expression of others FucTs are altered in CRC. Increased fucosylation is reported in CRC tumour tissues and serum proteins (D. Zhang et al. 2019; Takahashi et al. 2016). Inhibition of fucosylation of TGF-β reduces the invasion and migration abilities of CRC cells and EMT (Hirakawa et al. 2014). Overexpression of fucosylation in CRC patients with metastasis improves immune evasion and reduces response to cetuximab or bevacizumab drug therapy, leading to reduce overall survival (Giordano et al. 2015). FucTs involved in Lewis type antigens biosynthesis will be discussed in the section **1.3.5**.

1.3.5. Lewis antigens

Lewis blood group antigens (**Figure 1.5**) are carried in terminal position of N-/O-glycans and glycolipids. Le^A, Le^B and sLe^A are synthesised from type 1 LacNAc structure while Le^X, Le^Y and sLe^X from type 2 LacNAc structure. Several SiaTs and FucTs are involved in the synthesis of these antigens. In CRC, the increase of these antigens is observed and related to tumour progression, drug resistance, metastasis, and poor overall survival.

Type 1 or 2 LacNAc structure are obtained by the activity of β1,3- or β1,4-GalT activity, respectively. Thus, β1,3-GalT-V activity correlates with type 1 chain-derived Lewis antigens expression in CRC cell lines (Isshiki et al. 1999). Surprisingly, its transcript and protein levels, as well as enzymatic activity, are downregulated in CRC tissues (Aronica et al. 2017; Mare et al. 2013; Salvini et al. 2001), whereas the enzyme is expressed and correlates with sLe^A expression in CRC cell lines (Mare and Trinchera 2004). In CRC tissues, Isshiki et al. (2003) observe that even if the level of β1,3-GalT-V protein is lower in CRC tissues compared to normal, the sLe^A antigen is expressed. Therefore, they hypothesise that the enzyme expression level, even if downregulated in CRC tissues, remains sufficient for sLe^A synthesis and other glycosyltransferases determine the antigen expression. Indeed, for example, FucT-III is a key enzyme for type 1 chain-derived Lewis antigens expression supporting α1,4FucT activity. Together, high expression of immune checkpoint Cluster of Differentiation (CD) 276, also known as B7-H3, and β1,3GalT-IV is associated with poor overall survival in CRC patients and their expressions positively correlate in CRC cell lines (Zhang et al. 2018). Among GalTs responsible for type 2 chain structure synthesis, the increased expression of β1,4GalT-I is highlighted in CRC, with an increase of LacNAc structures (Ichikawa et al. 1999). Chen et al. (2005) show that β1,4GalT-IV expression exhibits a strong correlation with tumour metastasis and poor overall survival. No relationship between sLe^X antigen level and β1,4GalT-IV expression is found, but the study does not include other type 2 chain-derived Lewis antigens expression evaluation. On the contrary, low expression of β1,4GalT-III in CRC tissues is associated with the severity of the cancer, defined by poorly differentiated tumour grade, high tumour

stages and metastasis (Chen et al. 2014). In the same study, the authors also evaluate the impact of the β1,4GalT-III overexpression or KD in different CRC cell lines, resulting in cell migration and invasion suppression or increase, respectively.

Le^B and Le^Y antigens enhancement is due to the increased expression of α1,2 FucTs (*FUT1*, *FUT2*) in CRC tissues and cell lines (Yazawa et al. 2002; Nishihara et al. 1999; J. Sun et al. 1995). *In vitro*, overexpression of *FUT1* provides 5-FU drug resistance to CRC cells (Yazawa et al. 2002). The expressions of *FUT1* and Le^Y antigen correlate positively with adhesion, migration and angiogenesis (Sauer, Meissner, and Moehler 2015; Moehler et al. 2008). Moreover, T cells genetically engineered to target Le^Y antigen shows promising anti-tumour cells effect (Westwood et al. 2009). Le^Y antigen presents a stronger expression in stage IV tumour (Baldus et al. 2006). Nonaka et al. (2014) show that the mannan-binding protein (MBP) lectin, which recognise Le^A and Le^B antigens, stains CRC tissues and not normal mucosa, Le^B antigen is the main recognised glycan by MBP and inverse correlation is observed between MBP and sLe^A staining. MBP ligand expression depends on differentiation degree, diminishing with lower differentiation, and associates with immune cells infiltration. Thus, MBP ligand expression results in better survival for patients (Nonaka et al. 2014).

High expression of $Le^{X/A}$ antigens and their sialylated forms is found in cancer. A recent study on CRC stage II patients shows a greater disease-free survival and cancer specific survival in patients presenting low sLe^x expression than patients with high sLe^x expression on tumour. Thus, sLe^x expression correlates with poorer prognosis and higher recurrence, with liver recurrence being the most frequent one (Yamadera et al. 2018). High $sLe^{X/A}$ antigens expression is associated with metastasis and aggressiveness, translated by depth of invasion, grade and serum CEA level (Fukasawa et al. 2013; Yamadera et al. 2018). Among the FucT responsible for the Lewis antigens synthesis, FucT-III is the only characterised enzyme which possesses an α1,4FucT activity. Therefore, FucT-III can synthesise $Le^{A/B}$ and sLe^A, but this enzyme is also involved in $Le^{X/Y}$ and sLe^X expression. FucT-IV and FucT-IX are mainly responsible for non-sialylated Le^X antigen expression. In CRC, higher level of *FUT4* mRNA is found in tumour tissues compared to normal tissues (Ito et al. 1997). In a murine CRC cell line, Blanas et al. (2019) show that *FUT4* or *FUT9* transcription activation using CRISPR-dCas9-VPR system (Clustered Regularly Interspaced Short Palindromic Repeats-dead CRISPR-associated protein 9-VP64-p65-Rta) results in specific expression of Le^X antigen. FucT-III, V, VI and VII can produced sLe^X antigen, although FucT-VI and VII are more specific for its synthesis (Mondal et al. 2018). The expression of $sLe^{X/A}$ requires α2,3 sialylation prior fucosylation, ST3GalT-III transfers sialic acid on type 1 and 2 chains allowing to obtain $sLe^{X/A}$, also ST3GalT-IV and VI act on type 2 chains (Dall'Olio et al. 2014). Thus, flow cytometry staining of $sLe^{X/A}$ antigen in CRC cell lines correlates with mRNA expression of previously cited SiaTs and FucTs, together with an increase adherence to E-selectin (Carvalho et al. 2010; Majuri et al. 1995).

Indeed, $sLe^{X/A}$ are the minimal binding determinant for selectins family, involved in metastasis formation and discussed in separate section (**1.4.1**).

A recent study demonstrates the positive correlation of the LncRNA *ST3GAL6*-anti sense RNA 1 and ST3GalT-VI expression, which are downregulated in CRC tissues. Overexpression of this LncRNA reduces proliferation, tumorigenesis and metastasis *in vitro* and *in vivo* (Hu et al. 2019). Another mechanism leading to the strong expression of $sLe^{X/A}$ antigens in CRC is the downregulation of di-sLe^{A} antigen and 6-sulfo-sLe^{X} structures. Indeed, early observations present the exclusive expression of sLe^{A} antigen in tumour tissues and not in normal tissue, while Le^{A} and di-sLe^{A} antigens are found in both (Itzkowitz et al. 1988). ST6GalNAcT-VI overexpression demonstrates its involvement in di-sLe^{A} biosynthesis in CRC cell lines and leads to lower expression of sLe^{A} antigen together with the decrease of E-selectin adhesion and the increase binding to sialic acid-binding immunoglobulin-like lectin (Siglec) 7. In CRC tissues, *ST6GALNAC6* mRNA decreases compared to normal adjacent tissues, di-sLe^{A} staining occurs in non-malignant tissues while sLe^{A} staining is present in tumour tissues, and infiltration of siglec-7 expressing leucocytes decreases in CRC tissues (Tsuchida et al. 2003; Miyazaki et al. 2004).

Among FucTs, FucT-III and FucT-VI expression are involved in proliferation and tumour growth *in vitro* (Hiller et al. 2000). Interestingly, Stern et al. and Zhang et al. studies show that CRC cell lines sensitive to TRAIL-mediated apoptosis via death receptor-5 (DR5) express high *FUT3*/*6* mRNA and are sensitive to agonist drugs, dulanermin (rhApo2L/TRAIL) and drozitumab (DR5-agonist antibody). Thereby, the authors propose to assess *FUT3*/*6* expression as predictive biomarker for targeted therapy efficiency in clinical trials for these two drugs (Stern et al. 2010; B. Zhang et al. 2019). *In vitro*, different growth factor treatments-mediated EMT correlates with FucTs and SiaTs involved in $sLe^{X/A}$ antigen expression (Sakuma, Aoki, and Kannagi 2012; Hirakawa et al. 2014). Thus, epithelial growth factor (EGF)/basic fibroblast growth factor (bFGF) treatment induced *ST3GAL1*/*3*/*4* and *FUT3*/*6* increased expression and *FUT2* reduced expression, together with high $sLe^{X/A}$ and selectin ligand expression in two CRC cell lines. Furthermore, *FUT3*/*6* silencing reduces TGF-β-mediated EMT and inhibits migration and invasion.

To conclude, Lewis antigens expression in CRC are involved in different cancer progression mechanisms through, for example, newly available ligands. Specifically, selectin ligand expression takes important part in metastasis formation which will be the subject of the section below.

1.4. Role of Lewis antigens in colorectal cancer

1.4.1. Metastasis

Being the leading cause of cancer related mortality, metastases are observed in approximatively 20% of patients with CRC at first diagnostic (Siegel et al. 2017; van der Geest et al. 2015). The organs mostly affected by metastases from CRC are liver and lungs (Qiu et al. 2015).

In order to colonise a secondary site, tumour cells follow different steps of the so-called metastasis cascade (**Figure 1.9**). First, tumour cells follow EMT program and suffer downregulated expression of adhesion molecules involved in cell and matrix interactions leading to motile tumour cells (Yeung and Yang 2017). Then, degradation of extracellular environment is supported by enhanced proteolysis through principally matrix metalloproteinases. Subsequently, tumour cells intravasate, *i.e.*, enter in the lumen of lymphatic or blood vessels and initiate its circulation, being then termed CTCs. The invasion of distant organs or lymph nodes is possible only if the CTCs succeed to interact and bind to the endothelium of the vessels.

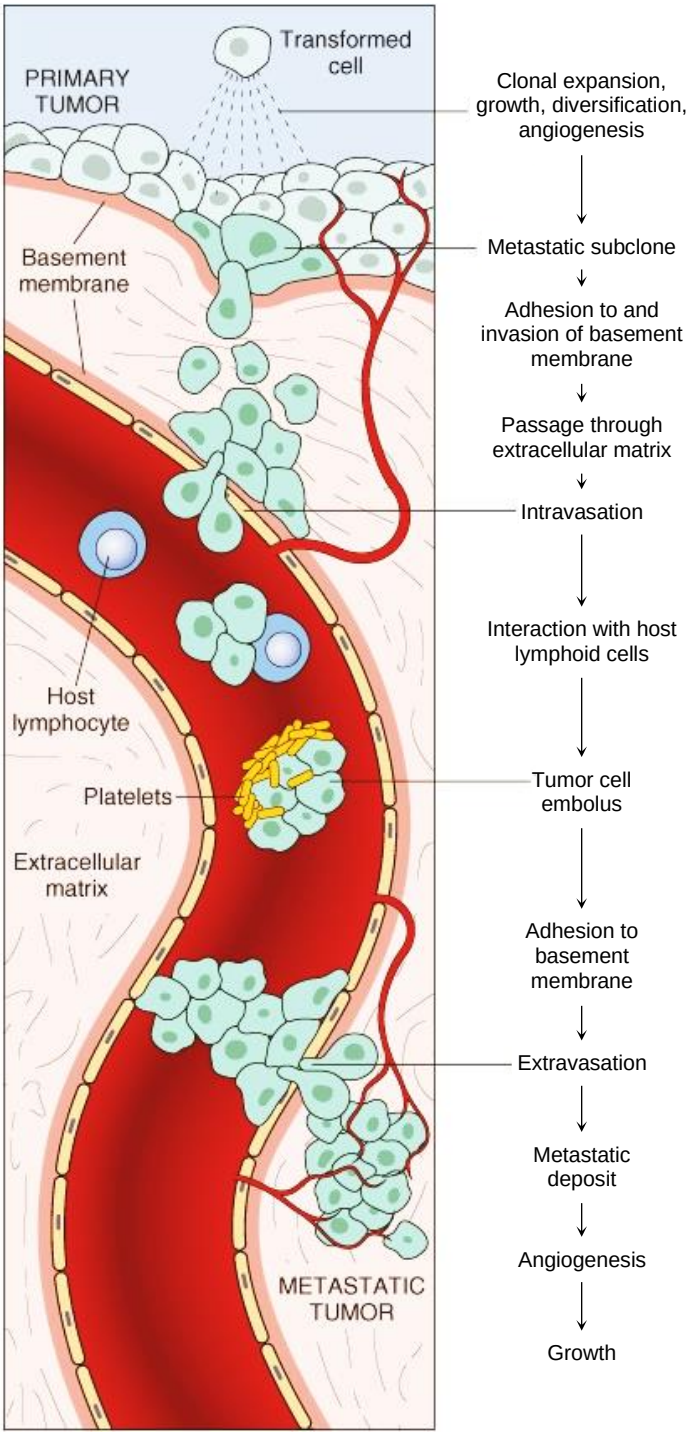

Figure 1.9 The Metastasis Cascade. Figure from "Robbins and Cotran pathologic basis of disease" (Kumar, Robbins, and Cotran 2005).

It is thought that CTCs reach distant organs by using the same mechanism as circulating leukocytes apply to extravasate from bloodstream into an inflammation site which, firstly, consists in rolling on activated endothelium through selectin-ligand interaction. This interaction is crucial since it allows cells to slow down in the stream and to receive proper stimuli, as those leading to integrin activation. The tethering and rolling steps are followed by firm adhesion via integrins allowing transendothelial

migration and, *in fine*, development of a secondary tumour, as depicted in **Figure 1.10** (Baldawa et al. 2017; Valastyan and Weinberg 2011).

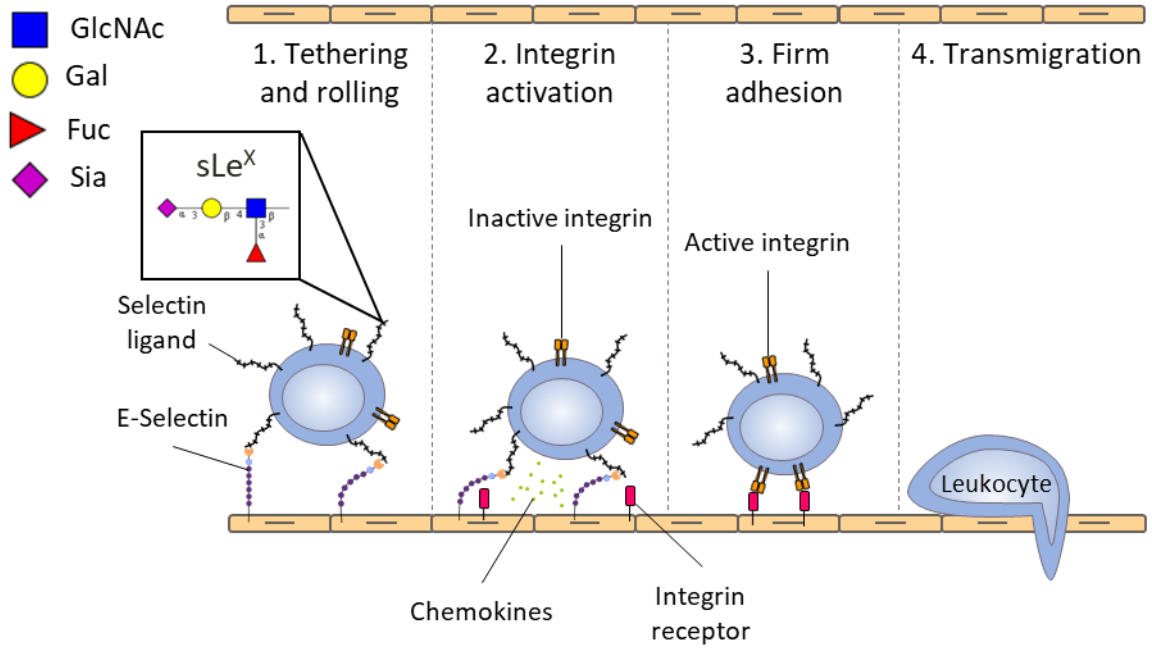

Figure 1.10 Schematic leukocyte migration. Adapted from Jacobs and Sackstein (2011). To reach inflammation site, circulating leukocytes undergo transendothelial migration. The process requires the leukocytes deceleration and rolling on endothelial surface, this step is mediated by the interaction between endothelium E-selectin and leukocytes selectin ligands. Leukocytes are then able to sense the locally expressed chemokines, resulting in integrin activation which conducts in firm adhesion to the endothelium and *in fine* transendothelial migration.

CTCs can interact with the different selectin family members by expressing sLe$^{X/A}$ antigens, as shown in **Figure 1.11**. The selectin family is composed of three transmembrane proteins called L-, E- and P-selectin. Selectins are C-type lectins expressed by leukocytes (L-selectin), platelets (P-selectin) and endothelium (E- and P-selectin). The E-selectin minimal binding tetrasaccharide is sLe^X and its isomer sLe^A. The importance of E-selectin interaction in CRC metastasis formation is shown in several studies. In fact, blocking E-selectin interaction by tumour cells prevents metastasis in CRC (Köhler et al. 2010; Kobayashi et al. 2000). *In vitro* studies show a link between metastatic potential of CRC cell lines and increased sLe$^{X/A}$ antigens expression. Thus, highly metastatic cell

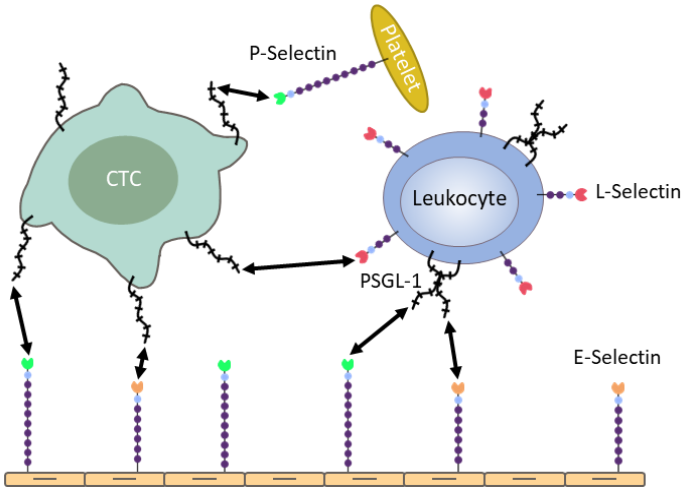

Figure 1.11 Possible interaction between CTC and selectins. Adapted from Jacobs and Sackstein (2011). Circulating tumour cells express selectin ligands allowing the interaction with the different selectins, with E- and P-selectin on activated endothelium, with L-selectin on leukocytes and with P-selectin on platelets.

lines variants express higher $sLe^{X/A}$ antigens than parental cell lines, associated with an increase of FucTs activity, rather than SiaTs (Yamada et al. 1997; Weston et al. 1999). The high $sLe^{X/A}$ antigens expression leads to increase the adhesion capacities to E-selectin and endothelial cells. In section **1.3.5**, FucT-III/VI were mentioned for their role in EMT upon growth factor treatment. Targeting E-selectin ligands in combination to epithelial cell adhesion molecule (EpCAM) allow to prevent adhesion and thereby metastasis *in vitro* (Xie et al. 2015). The protein scaffold that carries $sLe^{X/A}$ antigen also modulates E-selectin binding (Sperandio, Gleissner, and Ley 2009). In CRC cancer, several E-selectin ligands have been identified so far such as hematopoietic cell E/L-selectin (HCELL) glycoform of CD44 (Burdick et al. 2006), CEA (Thomas et al. 2008), podocalyxin-like protein (PCLP), LAMP-1 (lysosomal associated membrane glycoprotein-1) and LAMP-2 (Tomlinson et al. 2000).

During metastasis, CTCs can interact with polymorphonuclear leukocytes (PMNs) in the blood stream. This interaction CTCs-PMNs can affect the CTCs ability to metastasise. Some studies propose an anti-tumour role of the interaction CTCs-PMNs (reviewed in Di Carlo et al. 2001). However, other studies demonstrate that PMNs may promote CTCs potency to metastasise by supporting CTCs transendothelial migration *in vitro* (Wu et al. 2001; Starkey et al. 1984) and attachment to vasculature *in vivo* (Borsig et al. 2002; Ishikawa et al. 1986; Orr and Mokashi 1985). In patients with metastatic cancer from colon, breast, and pancreas, activated PMNs are found in the vascular system (Schmielau and Finn 2001). Some investigations show that PMNs interact with CRC cells via CD18 (β2) integrin receptor (Miyata et al. 1999) and via L-selectin when integrin is inactivated (Mannori et al. 1995). Nevertheless, in shear conditions, PMNs interaction with CRC cells seems to require L-selectin expression on PMNs and expression of a sialofucosylated O-glycoprotein ligand on cancer cells (Jadhav and Konstantopoulos 2002; Jadhav, Bochner, and Konstantopoulos 2001). Indeed, L-selectin binds to $sLe^{A/X}$ antigens upregulated in CRC and HCELL is the major L-selectin ligand expressed on LS174T (Burdick et al. 2006; Hanley et al. 2006; 2005). Despite the controversial role of CTCs-PMNs interaction, enhancement of $sLe^{A/X}$ antigens expression is described and associated with poor prognosis in CRC, thus interaction between $sLe^{A/X}$ antigens overexpressing CRC cells and PMNs via L-selectin could be a potential therapeutic target to inhibit metastasis development.

Like selectin-$sLe^{A/X}$ antigens interaction, other glycan-binding lectins can play essential roles in the modulation of the immune response and are further discussed below. Understanding the molecular mechanisms which govern tumour-induced immune tolerance through lectin interactions provides new insights for the development of early detection strategy and paves the way for novel therapeutic targets.

1.4.2. Immunomodulation

The cancer immunosurveillance is a process in which the immune system is able to detect and eliminate malignant cells. This concept was suggested more than one century ago by Paul Ehrlich (Ehrlich 1909) but remains controversial due to divergent experimental results, knowledges and technical limitations. Later on, tumour antigen and tumour associated antigen notions emerged, as well as immune cells infiltration within the tumour (Neville 1974; Miwa 1984). From immunosurveillance concept came the immunoediting model in which the immune system holds a dual role (Dunn et al. 2002). The elimination of malignant cells leads to the selection of tumour cells with the capability to remain hidden. Like some pathogens, these tumour cells camouflage themselves to not be spotted and eliminated. They also use the immune system for their own profit. Thus, the selective pressure of the tumour cells by the immune system brings to the survival of more aggressive tumour cells. Expression of immunomodulatory molecules allows to improve tumour evasion, for example the PD1-PDL1 interaction recently highlighted by the 2018 Nobel Prize (L. Z. Shi et al. 2016). Glycan alterations are considered as a new type of immune checkpoint molecules expressed by tumour cells to escape and modulate the immune responses. Effectively, immune cells express a large set of receptors which recognise glycan structures. These lectin-glycan interactions participate to the tumour evasion from the immune system. Sialic acid-binding immunoglobulin-like lectins (Siglecs), Dendritic Cell-Specific Intercellular adhesion molecule-3-Grabbing Non-integrin (DC-SIGN), selectins, scavenger receptors (SRs) and many other lectins interactions with their respective ligands have been studied for their evasion and immunomodulation roles (RodrÍguez, Schetters, and van Kooyk 2018; R. E. Li, van Vliet, and van Kooyk 2018).

1.4.2.1. Scavenger Receptors

Macrophages can play dual role in tumour progression according to the phenotype M1/M2, they may have a preventing or a promoting role. Macrophage displaying M2 phenotype can promote tumour growth. It has been shown that macrophages inhibit pro-inflammatory cytokines expression after phagocytosis of apoptotic cells (Fadok et al. 1998). Thus, phagocytosis of apoptotic cancer cells supports tumour growth by releasing specific anti-inflammatory mediators, such as TGF-β1, interleukine-6 (IL-6) and IL-10. Moreover, several lines of evidence point an elevated expression of IL-6 and IL-10 in patients with CRC (Galizia et al. 2002; Kamińska et al. 2000). Recognition of apoptotic cells by macrophages is supported by different receptors including SRs (Ramirez-Ortiz et al. 2013; Platt et al. 1996). SRs bind sulphatides (Yoshiizumi et al. 2002) and sulphated glycosphingolipids (GSLs) are found elevated in mucosa of CRC tumour (Siddiqui, Whitehead, and Kim 1978). One glycolipids alteration occurring in CRC affects sulphatides and is associated with lymph node metastasis

(Morichika et al. 1996). The sulphatide SM4s, expressed on apoptotic cells, enhances the clearance of these cells by macrophages in a SRs-dependent recognition manner and increases the production of TGF-β1 and IL-6 by macrophages (Popovic et al. 2007). Furthermore, mucins presenting sTn antigen mediate production of IL-6 by monocytes via SRs (Yokoigawa et al. 2005). Subsequently, IL-6 production by macrophages can bind to its receptor on CRC cells and induces production of the immunosuppressive cytokine IL-10 through the signal transducer and activator of transcription protein 3 (STAT3) signalling pathway (Herbeuval et al. 2004). Finally, Samsen et al. (2010) suggest that the interaction between scavenger receptor with C-type lectin (SRCL), expressed on subpopulations of human macrophages, and the Gal of the Le^X structure, present on CEA-related cell adhesion molecule 1 (CEACAM1) and CEACAM5, modulates the immune response during CRC.

1.4.2.2. DC-SIGN

Several studies underline the role of DC-SIGN in the association of DCs and CRC cells *in situ* through cancer-related glycans. DC-SIGN, also known as CD209b, and its homologue murine receptor Specific Intercellular adhesion molecule-3-Grabbing Non-Integrin-Related 1 (SIGN-R1), are C-type lectins whose role has been investigated in CRC. Being one of the major C-type lectin expressed on immature myeloid DCs and immature monocytes derived from DCs (moDCs), DC-SIGN is found overexpressed on these immune cells in CRC. DC-SIGN binds to "self" glycan ligands expressed on human cells and plays a role of adhesion receptor mediating binding and internalisation. Specifically, it recognises glycoconjugates containing Man, Fuc, and Le^A/Le^B antigens, which are overexpressed on tumours (Yanmei Jiang et al. 2014; Maciejewski et al. 2013). Indeed, Nonaka et al. (2011) and van Gisbergen et al. (2005) demonstrate *in vitro* with human CRC cells and with CRC patient tissues that DC-SIGN expressed on immature moDCs could interact with CEA, CEACAM1 and Mac-2-binding protein (Mac-2BP), via the recognition of Lewis epitopes carried by these glycoproteins overexpressed in CRC cells. This interaction significantly inhibits moDCs functional maturation, highlighted by the decrease of CD83 and CD86 co-stimulatory molecules expression, together with the increased levels of immunosuppressive cytokines, such as IL-6 and IL-10. These studies demonstrate that tumour cells may interact with DC-SIGN to suppress DCs functions providing a tolerogenic microenvironment to initiate a powerful anti-tumour response (Saeland et al. 2012; Samsen et al. 2010; Nonaka et al. 2008). DC-SIGN has also been taken in consideration as target molecule to eradicate tumour in preclinical animal experimentation. In the study of Melero et al. (2002), a monoclonal antibody (mAb) is used to target Intercellular adhesion molecule 2 (ICAM-2), a surface antigen glycoprotein expressed on T and B lymphocytes, leading to the modification of this molecule in a specific manner making it more prone to interact with DC-SIGN on human DCs. This interaction is important at the immunological synapse and provides an enhancement of the anti-tumour immunity. This study also shows that phagocyte

lectins could not only have a role recognising glycoconjugates on the surface of cancer cells but could also recognise glycoconjugates on the cell surface of other cell types present in the tumour microenvironment. Investigated in phase-I clinical trial in cancer patients, another study uses a recombinant glycoengineered vector directed against DC-SIGN in order to deliver antigen-encoding nucleic acids selectively to human DCs *in vivo*, leading to an enhanced CD4+ and CD8+ T-cell responses and to prophylactic protection (Odegard et al. 2015).

1.4.2.3. Siglecs

Siglecs are a family of immunomodulatory lectins either secreted into the extracellular environment or attached to the cells surface. They interact specifically with sialic acids on glycan structures and are expressed prominently on leukocytes.

1.4.2.3.1. Siglec-1

Siglec-1 (CD169, sialoadhesin) is a sialic acid receptor expressed on specific macrophages such as lymph node sinus macrophages. In a clinic pathological study, Siglec-1-expressing macrophages interact with leukosialin (CD43) expressed on CD8+ T cells suggesting that these macrophages mediate an anti-tumour immunity being correlated with a better prognosis (Ohnishi et al. 2013). In another study, the increased expression of sialylation observed on the surface of the liver membrane in response to the distal tumour acts as a ligand for macrophage receptors, such as Siglec-1, whereby it could modify cell adhesion and interaction playing a role in tumour-induced liver inflammation (Lee et al. 2011).

1.4.2.3.2. Siglec-3

Ishida et al. (2008) demonstrate *in vitro* that the mucin MUC2 secreted by CRC cells interacts with Siglec-3 (CD33) expressed by DCs through α2,6-sialic acid-containing O-glycans, including sTn antigen. The authors show also that this interaction is partially responsible for DCs apoptosis suggesting that Siglec-3 could play a role in the reduction of DCs during CRC development being therefore an attractive target for cancer immunotherapy.

1.4.2.3.3. Siglec-7 and -9

Miyazaki et al. (2004) show that in normal colonic mucosa di-sLe^A possesses binding activity to both Siglec-7 and -9, and sialyl 6-sulfo Le^X binds significantly to siglec-7. Such interactions contribute to the immunological homeostasis maintenance in normal mucosal membranes by suppressing tissue macrophage cyclooxygenase 2 (COX2) expression. During CRC, sLe$^{A/X}$ antigens replace these glycan structure ligands, and without the Siglec-7 and -9 engagements, inflammatory mediators enhance through COX2 production by mucosal macrophages providing a putative mechanism for progression

of CRC (Miyazaki et al. 2012). Moreover, Siglec-9 is described to have high affinity for heavily N-glycosylated lectin galactoside-binding soluble 3 binding protein (LGALS3BP), also called Mac-2BP, overexpressed in CRC. Interaction of LGALS3BP with Siglec-9 can inhibit spontaneous production of extracellular reactive oxygen species (ROS) formation by neutrophils, as well as lipopolysaccharide (LPS)-induced ROS production. These data suggest an immunomodulatory role of Siglec-9 on neutrophils via the inhibition of their anti-tumour activity (Läubli et al. 2014).

1.4.2.3.4. Siglec-10

Siglec-10 also binds LGALS3BP and is expressed on myeloid and B cells. Therefore, it could reasonably play a role in cancer progression. Based on a previous study that implicates soluble glycosylated CD52 to allow binding and inhibition of T cell activation via Siglec-10 (Bandala-Sanchez et al. 2013), Läubli et al. (2014) suggest that a similar mechanism could be involved in the context of Siglec-10/LGALS3BP Interaction.

1.4.2.4. Mannose Receptor

The Mannose Receptor (MR) belongs to a family of lectins which binds mannose-, N-acetylglucosamine- or fucose-terminated oligosaccharides and which is involved in the antigen uptake, processing, and presentation to T cells. Mytar et al. (2004) demonstrate that MR is involved, to different extents, in the induction of cytokines and ROI production by monocytes when stimulated with tumour cells bearing MR-glycan ligands. The MR is also the target of an *in vitro* tested vaccine for many cancers that exploits the tumour-associated antigen human chorionic gonadotropin (hCG). With this vaccine, MR expressed on DCs is targeted leading to the induction of Cytotoxic T Lymphocytes (CTLs) responses which are specific for this tumour-associated antigen, including proliferation of CD4+ and CD8+ T cells, as well as, increased cytotoxic activity of CD8+ T cells (He et al. 2004). In the context of CRC, MR has also been involved in metastatic process. Indeed, the MR expressed by liver sinusoidal endothelial cells (LSECs) leading to endocytosis and antigen presentation could, in turn, modulates the response of the adaptive immune system (Höchst et al. 2012; Arteta et al. 2010).

Chapter 2 – Rationale and aims of the thesis

Colorectal cancer (CRC) is the third most commonly occurring cancer in men and the second in women. In terms of mortality, CRC is the second leading cause of cancer death in the world, mainly due to the late diagnosis which contributes to this disastrous record. Indeed, other intestinal disorders can present symptoms similar to CRC, making its diagnostic difficult. Moreover, once the symptoms appear, CRC is often already at an advanced stage, which is also valid for other cancer types but particularly in CRC cases. Advances in CRC screening have fuelled the reduction in mortality in the developed world, even in the face of growing incidence in many nations. However, discovery of new early-stage detection system and specific targeted treatments is crucial to reduce CRC mortality.

Typically, cancer is a disease defined by the transformation of normal cells into malignant cells. This transformation deeply changes the biology of the cancerous cells which gain increased proliferation and survival properties. Several pathways and mechanisms exist to eliminate abnormal cells, *i.e.*, apoptosis, immune system recognition, etc. However, malignant cells have the capacity to avoid the cell death programs and escape the immunosurveillance. To acquire these capacities, cell biological processes changes occur including glycosylation alterations.

In CRC, glycosylation alterations include general increase of sialylation and fucosylation which are associated with malignant features and poor survival. Specific antigens increase is highlighted in CRC such as sialylated Lewis antigens ($sLe^{X/A}$), truncated O-glycans T and Tn antigens and their sialylated forms. For instance, the expression of $sLe^{X/A}$ is studied for its role in E-selectin binding and metastasis formation. Although $sLe^{X/A}$ is the minimal tetrasaccharide recognised by E-selectin, the protein carriers are as well important to appropriately engage with E-selectin.

Glycosylation alterations studies can contribute to the development of new detection and treatment strategies. For this reason, the multidisciplinary European training and research network GlyCoCan was created, with the main objective to improve the comprehension on the structure-function relationship of glycosylation in CRC allowing to discover better diagnostic and prognostic biomarkers and to pave the way for novel therapeutic targets. The present study took place in this network with the main aims to study the sialofucosylated sLe^{X} antigen function in tumour migration, E-selectin ligands expression and immunomodulation capabilities. The GlyCoCan network allowed to access to multiple techniques and methods in the different partners facilities permitting to achieve and complete the aims of the thesis.

To achieve the aims of the thesis, the first objective was to finely characterise glycoengineered CRC cell lines overexpressing sLe^{X}. Two CRC cell lines transfected with *FUT6* were used, HT29 and SW620. Immunostaining, by flow cytometry and western-blot techniques, and fucosyltransferases gene expression measurement by RT-qPCR were the techniques used to evaluate the $sLe^{X/A}$ antigens and

E-selectin ligands expression. This first task led to select SW620 cell lines overexpressing sLe^X antigen. N-glycan profiles were established for this cell line by mass spectrometry (secondment Ludger, England). To study the role of sLe^X antigen in cancer cell migration, cell growth and invasion were analysed for SW620 cell lines overexpressing sLe^X (secondment University of Bologna, Italy). **Section 4.1**

The second objective was to study the E-selectin ligand scaffolds, since the sLe^X antigen carrier is essential to appropriately engage E-selectin. Thus, E-selectin ligands expression was analysed by flow cytometry and immunoblotting. The isolation of the E-selectin ligands was performed by immunoprecipitation using E-selectin chimeras. With mass spectrometry analysis, protein scaffolds (secondment LUMC, The Netherlands) and glycans acting as selectin ligands (secondment LUD, Ludger, England, "Identification of the selectin ligand glycans") were identified. **Section 4.2**

Finally, the last objective was to determine the impact of sLe^X overexpression on immunomodulation. The maturation markers and cytokines gene expression were assessed on human dendritic cells derived from monocytes in contact with CRC cells overexpressing sLe^X antigen. **Section 4.3**

Chapter 3 – Materials and Methods

3.1. Reagents

PBS pH 7.4: 1.47 mM KH_2PO_4 (Merck), 4.29 mM Na_2HPO_4 (Merck), 137 mM NaCl (Sigma), 2.68 mM KCl (Merck), pH adjusted to 7.4 with 400 mM NaOH (Sigma) solution, diluted in sterile Milli-Q® H_2O to 1 L.

For Western Blot (WB), TBS pH 7.6: 15.4mM Tris-HCl (Sigma), 137mM NaCl, pH adjusted to 7.6 with 400mM NaOH solution, diluted in sterile Milli-Q® H_2O to 1L; wash buffer: TBS-0.1% Tween 20 (Sigma); blocking buffer: wash buffer 10% dry milk (VWR, #97063-958).

For immunoprecipitation, wash buffer: 150mM NaCl, 2mM $CaCl_2$ (Merck), 50mM Tris pH 7.4 (Sigma), 1 Complete, Mini, Ethylenediaminetetraacetic acid (EDTA)-free Protease Inhibitor Cocktail Tablet (Roche), 2% NP-40 (Sigma); blocking buffer: wash Buffer, 1% BSA (bovine serum albumin, Sigma); denaturing Buffer: wash buffer without NP-40, 0.5% SDS (Merck), 40mM DTT (Dithiothreitol, Sigma).

3.2. Cell culture

The human colon cancer cell lines, HT29Mock, HT29FUT6, SW620Mock and SW620FUT6, were kindly provided by Pr. Fabio Dall'Olio (UNIBO, University of Bologna, Italy) (Trinchera et al. 2011). In sterile condition, HT29 cell lines were grown in Dulbecco modified Eagle's medium (DMEM, Gibco™, #11960044) at 37°C with 5% CO_2 and SW620 cell lines were grown in Leibovitz (L-15) medium (Lonza, #12-700F) at 37°C without CO_2, both culture media were supplemented with 10% FBS (foetal bovine serum) (Gibco™, #10500064), 2mM L-glutamine (Gibco™, #25030081), 100U.mL^{-1} penicillin and 100µg.mL^{-1} streptomycin (Gibco™, #15140122). Cultures were passaged using 1X trypsin-EDTA (Gibco™, #15400054). Cell lines were certified authenticate and without contamination with human origin by the Microsynth AG company via their cell line authentication service. Briefly, the profiling of human cell line was done using highly-polymorphic short tandem repeat loci (STRs). STR loci were amplified using the PowerPlex® 16 HS System (Promega). Fragment analysis was done on an ABI3730xl (Life Technologies) and the resulting data were analysed with GeneMarker HID software (Softgenetics).

Monocytes were cultured and co-cultures were realised at 37°C with 5% CO_2 in Roswell Park Memorial Institute (RPMI)-1640 medium (Gibco™, #31870017), supplemented with 10% (v/v) FBS, 2mM L-glutamine, 1% (v/v) non-essential amino acid (Gibco™, #11140050), 1% sodium pyruvate (Gibco™, #11360070), 100U.mL^{-1} penicillin and 100µg.mL^{-1} streptomycin.

3.3. Monocytes isolation and differentiation to immature monocyte derived dendritic cells

In sterile conditions, peripheral blood mononuclear cells (PBMCs) were isolated by Ficoll (Biocoll, density 1.077g/.ml^{-1}, isotone, Biochrom, #L6115) gradient centrifugation, from blood buffy coats of healthy volunteers provided and ethically approved by the Portuguese Blood Institute. Monocytes

were isolated by positive selection using anti-CD14 coated magnetic microbeads (Miltenyi Biotech, #130-050-201), LS columns (Miltenyi Biotec, #130-042-401) and MidiMACS™ separator in PBS supplemented with 2mM EDTA (Merck) and 1% (v/v) FBS. To obtain immature dendritic cells derived from monocytes (moDCs), monocytes were cultured at a density of 10^6 cells per mL of complete RPMI medium (see cell culture) supplemented with 1000U.mL^{-1} of GM-CSF (R&D Systems, #215-GM-050) and 750U.mL^{-1} of IL-4 (R&D Systems, #204-IL-010) for five days, medium was changed at day 3.

3.4. SW620:moDCs co-culture conditions

In sterile condition, SW620Mock and SW620FUT6 cells were seeded 24 hours prior the co-culture in 6-wells plates at 0.3x10^6 cells per mL in 3mL of complete L-15 medium per wells and incubate at 37°C without CO_2. The moDCs were collected and resuspended in fresh RPMI medium (see cell culture). Cancer cells were washed with PBS once and moDCs were added with a ratio 1:5 (cancer cells/dendritic cells). The plates were then incubated at 37°C 5% CO_2 for the desired time. Controls consisted in unstimulated moDCs (moDCs alone, base line control), stimulated moDCs (positive control of dendritic cells activation) supplemented with 5µg.mL^{-1} LPS (Sigma-Aldrich) and cancer cells alone. After 2 hours of incubation, cells were collected for RNA extraction to proceed to further cytokines gene expression analysis by RT-qPCR. After 6 hours of incubation, cells were collected to assess maturation profile of DCs and percentage of adhering moDCs. For "LPS challenged co-culture", 1ng.mL^{-1} or 10ng.mL^{-1} of LPS were added at 6 hours of incubation to co-cultured cancer cells/moDCs as well as moDCs alone, unstimulated moDCs, stimulated moDCs supplemented with 5µg.mL^{-1} LPS and cancer cells alone were, as previously, controls. At 24 hours incubation, cells were collected to assess maturation profile of DCs and percentage of adhering moDCs.

3.5. Flow cytometry

Harvested cells were counted using Neubauer chamber, trypan blue (Merck) was used to stain dead cells. For each staining condition, 0.2x10^6 cells in suspension was used. Cells were washed with PBS.

- For E-selectin ligands staining; four conditions were necessary and cells were pre-washed once with the correct PBS: to set flow cytometer, cells alone in PBS+Ca^{2+} (2mM $CaCl_2$, Merck); to control unspecific staining, cells in PBS+Ca^{2+} with anti-human IgG (Fc Specific)-Fluorescein isothiocyanate (FITC) (Sigma, #F9512); as negative control, cells in PBS+EDTA (2mM, Merck) with recombinant Human E-Selectin/CD62E Fc Chimera Protein (R&D, 724-ES), here called E-Ig chimera, plus anti-human IgG (Fc Specific)-FITC; to evaluate E-selectin ligands staining, cells in PBS+Ca^{2+} with recombinant E-Ig chimera plus anti-human IgG (Fc Specific)-FITC. Cells were

incubated at 4°C for one hour, then washed and resuspended in 1mL using correct PBS for each condition.

- For HECA-452, CD15s, CA19-9, L1CAM, PTPRJ, integrin α-6 and integrin β-1 staining; three conditions were used: to set flow cytometer, cells alone in PBS; to control unspecific staining, cells in PBS with secondary antibody goat anti-rat Ig allophycocyanin (APC) (BD Pharmingem™, #551019), or goat anti-mouse Ig FITC (Dako, #F0479), or secondary antibody goat anti-mouse IgG FITC (Southern Biotech, #1030-02); to evaluate proteins staining, cells in PBS with primary monoclonal antibody (mAb) rat anti-human Cutaneous Lymphocyte Antigen (CLA) clone HECA-452 (BioLegend, # 321302), or primary mAb mouse anti-human CD15s clone CSLEX1 (BD Pharmingem™, #551344), or primary mAb mouse anti-human CA19-9 clone CA19-9-203 (Abcam, #ab116024), or primary mAb mouse anti-human L1CAM clone UJ127.11 (Santa Cruz, #sc-53386), or primary mAb mouse anti-human PTPRJ clone F-12 (Santa Cruz, #sc-376794), or primary mAb mouse anti-human integrin α-6 clone BQ16 (Santa Cruz, #sc-13542), or primary mAb mouse anti-human integrin β-1 clone JB1B (Santa Cruz, #sc-59829), plus appropriate secondary antibody. Cells were incubated at room temperature for 30 minutes (min) with primary antibody, then washed with PBS, incubated 15 min with secondary antibody, washed and resuspended in 1mL of PBS.
- For co-cultures; cells from co-cultures were harvested, washed, and stained with FITC-labelled monoclonal antibody (mAb) mouse anti-human CD86 clone BU63 (Immunotools, #21480863), phycoerythrin (PE)-labelled mAb mouse anti-human CD45 clone MEM-28 (Immunotools, #21270454) and APC-labelled mAb mouse anti-human HLA-DR clone GRB-1 (Immunostep, #HLADRA-100T). Negative controls were unstained and corresponding isotype control stained cells. Cells were incubated at 4°C for 30 min, then washed with PBS and resuspended in 1mL of PBS.

Cells were read with flow cytometer Attune™ Acoustic Focusing Cytometer (Applied Biosystems®). To analyse the results and for the figures, FlowJo software was used. Median fluorescent intensities (MFI) ratios were determined by the MFI values of stained *FUT6* transfected cell lines divided by MFI values of stained Mock transfected cell lines values and used for statistical analysis for E-Ig chimera, HECA-452, CD15s and CA19-9 staining. MFI values were used for statistical analysis for L1CAM, PTPRJ, integrin α-6 and integrin β-1 staining. For co-cultures, MFI fold changes were determined by (MFI values of stained stimulated moDCs or moDCs+SW620FUT6 transfected cell lines minus MFI values of unstimulated moDCs or stained moDCs+SW620Mock transfected cell lines values) divided by MFI values of unstimulated moDCs or stained moDCs+SW620Mock transfected cell lines values, respectively, and used for statistical analysis.

3.6. Membrane protein extraction

Membrane proteins from SW620Mock and SW620FUT6 cells were obtained using Mem-PER™ Plus Membrane Protein Extraction Kit (Thermo Scientific™, #89842) following the manufacturer's instruction. Protease inhibitor (Roche, #11836170001) was added to extracted membrane and membrane-associated proteins. Protein concentrations were evaluated using Pierce™ BCA (Bicinchoninic acid assay) Protein Assay Kit (Thermo Scientific™, #23225).

3.7. Immunoprecipitation

Two tubes with the recombinant Protein (rProtein) G Agarose (Invitrogen, #15920010) beads for each protein extracts were used, one for clearing (80µL) and one for immunoprecipitation (60µL). Beads were washed three times with wash buffer (see **3.1**), blocked with blocking buffer (see **3.1**) for an hour at 4°C with rotation and washed again three times. Then, 100µg of membrane extracted proteins was cleared with rProtein G-agarose ('clearing' tube), incubation was made at 4°C for two hours with agitation. Cleared samples were saved and rProtein G agarose beads ('immunoprecipitation' tube) were incubated with 3 or 2µg of antibody (E-Ig chimera or mAb mouse anti-human L1CAM, respectively) overnight at 4°C with agitation. Cleared proteins were added to the rProtein G agarose ('immunoprecipitation' tube) with antibody for six to eight hours at 4°C with agitation. After three washes, immunoprecipitated (IP) proteins were obtained by boiling the rProtein G-agarose with denaturing buffer (see **3.1**) for ten minutes. Supernatant containing IP proteins were conserved at -80°C.

3.8. Mass spectrometry

3.8.1. E-selectin ligands identification

3.8.1.1. Mass Spectrometry

IP proteins with E-Ig chimera were subjected to SDS-PAGE short run (NuPAGE™ 4-12% Bis-Tris Protein Gels, Invitrogen™). Proteins were in-gel digested with trypsin after reduction (dithiothreitol) and alkylation (iodoacetamide) using Proteineer DP digestion robot (Bruker Daltonics). Tryptic peptides were then extracted from the gel slices, lyophilized, dissolved in solvent A (water/0.1 formic acid (FA) v/v), and subsequently analysed by online C18 nano-HPLC MS/MS with a system consisting of an Easy nLC 1200 gradient HPLC system (Thermo, Bremen, Germany) and a LUMOS mass spectrometer (Thermo). Fractions were injected onto a homemade pre-column (100µm × 15mm; Reprosil-Pur C18-AQ 3µm, Dr. Maisch, Ammerbuch, Germany) and eluted via a homemade analytical nano-HPLC column (20cm × 75µm; Reprosil-Pur C18-AQ 3µm) using a gradient from 10 to 40% solvent B (20/80/0.1

water/acetonitrile/FA v/v/v) in 20 min. The nano-HPLC column was drawn to a tip of ~5µm and acted as the electrospray needle of the MS source. The LUMOS mass spectrometer was operated in data-dependent MS/MS mode (cycle time 3 seconds) with a normalised collision energy of 32 and recording of the MS2 spectrum in the Orbitrap. In the master scan (MS1) the resolution was 120 000, and the scan range was from m/z 400–1500 at an AGC target of 400 000 with maximum fill time of 50ms. Dynamic exclusion after n=1 with exclusion duration of 10s was applied. Charge states 2–5 were included for MS2. For this, precursors were isolated with the quadrupole with an isolation width of 1.2Da. The MS2 scan resolution was 30 000 with an AGC target of 50 000 with maximum fill time of 60ms.

3.8.1.2. Data analysis

MS/MS data were searched against a human protein database (UniProt, 67915 entries) using the Mascot search algorithm (Matrix Science, London, UK; version 2.2.04). Trypsin was selected as enzyme (up to two missed cleavages were allowed) and the MS and MS/MS tolerance were 10p.p.m. and 0.02Da, respectively. Carbamidomethylation of cysteine was set as a fixed modification and oxidation of methionine was specified as a variable modification. Scaffold (version Scaffold_4.8.4, Proteome Software Inc., Portland, OR) was used to validate MS/MS based peptide and protein identifications applying an FDR (False Discovery Rate) of 1% at minimum two unique peptides identified with a 95% peptide threshold identification.

3.8.2. Glycoanalysis

3.8.2.1. *N*-glycan release

IP proteins with L1CAM mAb, L1CAM mAb and membrane proteins extracted from SW620Mock and SW620FUT6 cells were dried down. Reagents used for N-glycan released were obtained from the LudgerZyme™ PNGase F Release Kit (LZ-rPNGaseF-kit, Ludger). Samples were resuspended in water and denatured at 100°C for 10 min with denaturation buffer (5% SDS 400mM DTT). Following the denaturation, after the samples cool down to room temperature, samples were incubated with PNGase F in reaction buffer (500mM sodium phosphate, pH 7.5 at 1X dilution) and NP-40 at 37°C overnight. Released N-glycans were dried with vacuum centrifugation and then converted to aldoses by incubating with 1% formic acid solution at room temperature for 45 min. Remaining proteins and enzymes were removed using a LudgerClean™ Protein Binding Membrane Plate (LC-PBM-96, Ludger). Finally, eluted N-glycans were dried using vacuum centrifugation prior to labelling.

3.8.2.2. Glycans labelling

Glycans were labelled with procainamide using a LudgerTag™ Procainamide Glycan Labelling Kit with sodium cyanoborohydride (LT-KPROC-24, Ludger; Kozak et al. 2015). The procainamide dye solution (DMSO, acetic acid, procainamide, sodium cyanoborohydride, water) was prepared following the manufacturer's protocol and added to the samples. Labelling was done at 65°C for one hour and labelled samples were then cleaned-up.

3.8.2.3. *N*-glycan clean-up

Clean up of samples and removal of excess dye was performed using a Ludger Clean plate (LC-PROC-96, Ludger) following the manufacturer's protocol. Briefly, samples were added to the plate in acetonitrile, washed 3 times with acetonitrile (200µL) and eluted in water (2 x 100µL). Purified labelled N-glycans were stored at 4°C until they could be processed. For longer term storage -20°C was used.

3.8.2.4. HILIC-UHPLC analysis on a Dionex Ultimate 3000 with inline MS

Samples and standards were analysed by liquid chromatography electrospray ionisation tandem mass spectrometry (LC-ESI-MS/MS). Procainamide labelled glycans were dried using vacuum centrifugation. Samples were resuspended in pure water. Samples were injected in 25% aqueous/75% acetonitrile; injection volume 25 µL. Samples made up as follows: IP, 12.5µL plus 3.57µL acetonitrile; mAb, 12.5µL plus 37.5µL acetonitrile; membrane proteins, 12.5µL plus 37.5µL acetonitrile; standards, 25µL plus 75µL acetonitrile.

Samples were analysed by HILIC-LC on an Ultimate 3000 UHPLC using a BEH-Glycan 1.7µm, 2.1 x 150mm column (Waters) at 40°C with a fluorescence detector (λ_{ex} = 310nm, λ_{em} = 370nm), controlled by Bruker HyStar 3.2 and Chromeleon data software version 7.2. Buffer A was 50mM ammonium formate made from LudgerSep N Buffer stock solution, pH4.4 [LS-N-BUFFX40]; Buffer B was acetonitrile (acetonitrile 190 far UV/gradient quality; Romil #H049). Gradient conditions were: 0 to 53.5min, 24 to 49.0% A (0.4mL.min^{-1}); 53.5 to 55.5min, 49.0 to 0% A (0.4 to 0.2mL.min^{-1}); 55.5 to 57.5min, 100% A (0.2mL.min^{-1}); 57.5 to 59.5min, 100 to 24% A (0.2mL.min^{-1}); 59.5 to 65.5min, 24% A (0.2mL.min^{-1}); 65.5 to 66.5min 24% A (0.2 to 0.4mL.min^{-1}); 66.5 to 70min, 24% A (0.4mL.min^{-1}). Sensitivity S5 was used for the standards and membrane protein samples. Sensitivity S8 was used for the IP and mAb samples. Chromeleon data software version 7.2 with a cubic spline fit was used to allocate glucose unit (GU) values to peaks. Procainamide labelled glucose homopolymer was used as a system suitability standard as well as an external calibration standard for GU allocation for the system (Guile et al. 1996).

Analysis was performed using a Bruker amaZon Speed ETD electrospray mass spectrometer which was coupled directly after the UHPLC FD without splitting. The instrument scanned samples in maximum resolution mode, positive ion setting, MS scan + three MS/MS scans, nebulizer pressure 14.5 psi, nitrogen flow 10L.min^{-1}, capillary voltage 4500 Volts. MS/MS was performed on three ions in each scan sweep with a mixing time of 40ms. Mass spectrometry data were analysed using the Bruker Compass DataAnalysis 4.1 software. LC-ESI-MS/MS chromatogram analysis was performed using Bruker Compass DataAnalysis 4.4 and GlycoWorkbench software. Structures were identified by comparing LC, MS, and MS/MS data.

3.9. RT-qPCR

RNA extraction was made using GenElute™ Mammalian Total RNA Miniprep Kit (Sigma-Aldrich) following the manufacturer's instruction. On-Column DNase I Digestion Set (Sigma-Aldrich) was used to eliminate genomic DNA from RNA extracts. RNA was converted to cDNA using High-Capacity cDNA Reverse Transcription Kit (Applied Biosystems™, #4368814) following the manufacturer's instruction. qPCR assays were performed in Rotor-Gene 6000 system (Corbett Research) using TaqMan™ Fast Universal PCR Master Mix (2X), no AmpErase™ UNG (Applied Biosystems™, #4366073), TaqMan™ Gene Expression Assay primers and probe with the following ID: Hs00356857_m1 (*FUT3*, #4331182), Hs01106466_s1 (*FUT4*, #4331182), Hs00704908_s1 (*FUT5*, #4331182), Hs03026676_s1 (*FUT6*, #4331182), Hs00237083_m1 (*FUT7*, #4331182), Hs00276003_m1 (*FUT9*, #4331182), Hs00327091_m1 (*FUT10*, #4331182), Hs00543033_m1 (*FUT11*, #4331182), Hs00174097_m1 (*IL-1β*, #4331182), Hs00174131_m1 (*IL-6*, #4331182), Hs00174086_m1 (*IL-10*, #4331182), Hs00168405_m1 (*IL-12A*, #4331182), Hs00233688_m1 (*IL-12B*, #4331182), Hs00171257_m1 (*TGF-β1*, #4331182) and Hs00174128_m1 (Tumor Necrosis Factor α, *TNF-α*, #4331182). The relative mRNA levels were normalised against the mean of the β-actin (Hs99999903_m1, #4352935E) and *GAPDH* (Hs99999905_m1, #4333764F) expression and calculated by adapted formula $2^{-\Delta Ct}\times1000$ which infers the number of mRNA molecules of the gene of interest per 1000 molecules of the endogenous controls (Videira et al. 2009). ΔCt stands for the cycle threshold difference between the target gene and the endogenous control genes. Cycle thresholds were obtained by analysing the qPCR results with Rotor Gene 6000 software.

3.10. SDS-PAGE and Western-Blot

Protein concentrations were evaluated using Pierce™ BCA Protein Assay Kit (Thermo Scientific™, #23225). 20µg of proteins obtained from total cell lysates, 10µg of membrane extracted proteins, 20µL of cleared proteins from immunoprecipitation or 10µL of IP proteins were diluted with SDS-PAGE sample buffer (Alfa Aesar™, #J61337) and electrophoresed through 6% (v/v) polyacrylamide SDS-PAGE

gels. Pre-stained protein ladder (Abcam, #ab116028) was included in adjacent lanes in all experiments. Separated proteins were transferred to polyvinylidene difluoride (PVDF, GE Healthcare Life Science, #10600021) membranes. PVDF membranes were blocked for one hour at room temperature, then stained with E-Ig chimera (in this case, all buffers were supplemented with 2mM $CaCl_2$), or mAb mouse anti-human L1CAM clone UJ127.11 (Santa Cruz, #sc-53386), or rat anti-human Cutaneous Lymphocyte Antigen (CLA) mAb clone HECA-452 (BioLegend, # 321302), overnight at 4°C. After three washes, for E-Ig chimera staining only, incubations with rat anti-mouse CD62E mAb (BD Pharmingen™, #553749) for an hour at room temperature were done and membrane was washed three times. After washes, membranes were incubated with appropriate Horseradish peroxidase (HRP)-conjugated secondary antibodies at room temperature for one hour, for L1CAM, with goat anti-mouse Ig HRP (BD Pharmingen™, #554002), for E-Ig chimera, with goat anti-rat IgG (H+L) HRP (Southern Biotech, #3050-05), and for HECA-452, with goat anti-rat IgM HRP (Southern Biotech, #3020-05). Lumi-light western blotting substrate (Roche, #12015200001) was used as developing reagent on washed PVDF membrane. To obtain the results, PVDF membranes were exposed to Hyperfilm™ ECL™ (GE Healthcare Life Science, #28906837) and to develop the films, developer (Sigma, #P7042) and fixer (Sigma, #P7167) solutions were employed. β tubulin protein expression level was analysed as loading control using mAb mouse anti-human β tubulin clone D-10 (Santa Cruz, #sc-5274) with appropriate HRP-conjugated secondary antibody.

3.11. Wound healing assay

The Ibidi Culture-Inserts 2 Wells (#80209) were used according to the manufacturer's instructions to perform wound healing assay. For SW620Mock and SW620FUT6 cell lines, to obtain confluent layer after 24 hours, cell suspension concentration was 7.5×10^5cells.mL^{-1}. Culture conditions were identical as in “Cell culture”. To assess the migration capability, microscope with a digital camera was used to take pictures of the wound each day. Then, the pictures were analysed using ImageJ software to measure the area of the wound free of cells.

3.12. Statistical analysis

Statistical analysis was performed using GraphPad Prism 6 (GraphPad Software, Inc). Data were analysed using D'Agostino and Pearson omnibus normality test to determine normal distribution, then unpaired Student’s *t*-test for parametric data or Mann-Whitney test for non-parametric data were applied. Differences were considered statistically significant when $p < 0.05$ (*), $p < 0.01$ (**), $p < 0.005$ (***) and $p<0.0001$ (****).

Chapter 4 – Results

4.1. Characterisation of sialyl Lewis X expressing cell lines

4.1.1. Characterisation of colon cancer cell lines overexpressing *FUT6*

In order to characterise the glycoengineered CRC cell lines overexpressing sialyl Lewis X (sLe^X), we confirmed the *FUT6* overexpression and determine the effect of the transfection on others *FUTs* expression by RT-qPCR. Immunostaining, by flow cytometry and western-blot techniques, were used to evaluate the expression of $sLe^{X/A}$ antigens and E-selectin ligands. SW620 and HT29 colon cancer cell lines were transfected with *FUT6* gene (Trinchera et al. 2011). The **Table 4.1** resumes the known information on these two cell lines. Presenting different grade, SW620 cell line was obtained from lymph node metastatic site while HT29 cell line from primary tumour site. The two cell lines differ also in term of differentiation profile, poorly differentiated for SW620 cells whereas HT29 cells are well differentiated, involving different aggressiveness properties.

Table 4.1 Cell lines information. Colon cancer cell lines used in this study and their characteristics. Information obtained from ATCC and additionally stated literature. **†** Leibovitz et al. 1976, **§** Fogh and Trempe 1975, **‡** Blottière et al. 1993.

Cancer cell line	Patient's Age and Gender	Tissue	Histologic type	Clinical stage	Tumour site	Grade‡	Differen-tiation‡
SW620†	51, Male	Colon; derived from metastatic site: lymph node	Duke's type C colon adenocarcinoma	3	Lymph node metastasis	IV	Poorly
HT29§	44, Female	Colon	Duke's type B colon adenocarcinoma	3	Primary	I	Well

FUT6 overexpression was confirmed by RT-qPCR (**Figure 4.1**). As expected, *FUT6* transfected cell lines presented significant higher level of *FUT6* mRNA level compared to Mock transfected cell lines in both SW620 and HT29 cells. Among others α1,3/4-fucosyltransferases (*FUTs*), *FUT5* mRNA expression was found decreased in *FUT6* transfected cells in both cell lines and, only in SW620 cell lines, *FUT3* mRNA expression was lower in *FUT6* transfected cell lines. However, the expression values were extremely low, especially for *FUT3* gene. Others *FUTs* mRNA expression levels were not significantly affected by *FUT6* transfection. *FUT9* was not expressed or at an undetectable level by the experimental procedure.

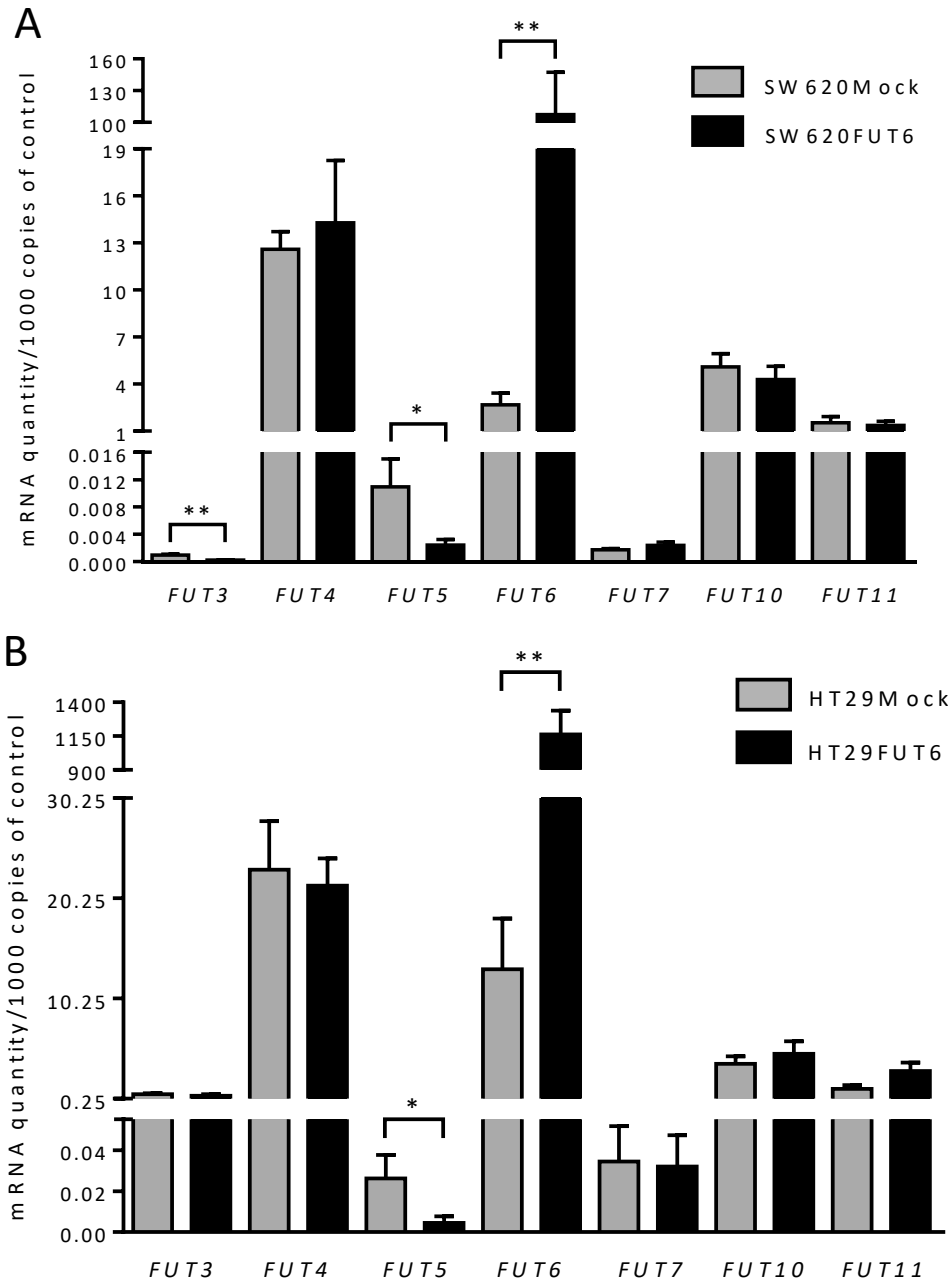

Figure 4.1 α1,3/4 fucosyltransferases (*FUTs*) gene expression in SW620 and HT29 cell lines by RT qPCR. A – B. Values represented in mean ± SEM (Standard Error of Mean) are the number of mRNA molecules of the gene of interest per 1000 molecules of the endogenous controls (section **3.9**), p value obtained with Mann-Whitney test, n=5, p=0.0317 (*), p=0.0079 (**). *FUT9* was not detectable.

FUT6 gene expression has been shown to impact sLe^X antigen expression in these cell lines (Trinchera et al. 2011), thus to confirm that *FUT6*-overexpressing cell lines show increase of sLe^X expression, we extracted proteins from Mock and *FUT6* transfected cell lines and stained with HECA-452 mAb by WB. This mAb reacts with both sialyl Lewis A (sLe^A) and sLe^X antigens (Berg, Robinson, et al. 1991; Berg, Yoshino, et al. 1991). **Figure 4.2A** shows no staining of proteins from SW620Mock cells while proteins from SW620FUT6 cells present different bands between 75 and 245 kDa. In **Figure 4.2B**, proteins from

HT29 cells transfected with *FUT6* also present multiple different bands with a wider range of weight compared to SW620FUT6 cells. However, contrary to extracted proteins from SW620Mock cells, HT29Mock proteins shows reactivity with HECA-452. Expression levels of $sLe^{X/A}$ highlighted by WB stained with HECA-452 mAb is high in both SW620 and HT29 cell lines transfected with *FUT6*, null in SW620Mock cells but not in HT29Mock cells.

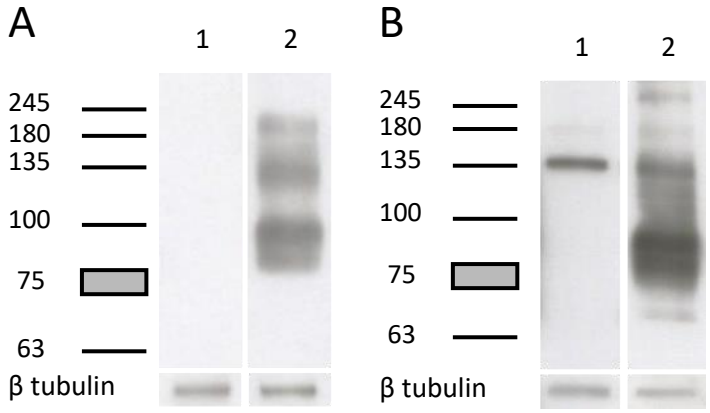

Figure 4.2 Expression levels of $sLe^{X/A}$ antigens in Mock and *FUT6* transfected SW620 and HT29 cell lines. Whole cell lysates were resolved by SDS-page and immunoblotted. **A.** Protein extracted from SW620Mock (lane 1) and SW620FUT6 cells (lane 2) and **B.** protein extracted from HT29Mock (lane 1) and HT29FUT6 cells (lane 2) were stained with rat anti-human HECA-452 mAb plus goat anti-rat IgM HRP by WB. β tubulin protein expression level was analysed as loading control.

Further analysis by flow cytometry allowed to precise the expression pattern of the two cell lines, Mock or *FUT6* transfected, for sLe^X antigen, sLe^A antigen and E-selectin ligands (**Figure 4.3**). For this purpose, we used HECA-452 mAb for $sLe^{X/A}$ antigens, anti-CD15s for sLe^x antigen, anti-CA19-9 for sLe^A antigen and E-selectin chimera (E-Ig) for E-selectin ligands, which can carry sLe^A and/or sLe^X antigens. **Figure 4.3A** shows increased and strong staining of *FUT6* transfected cells for $sLe^{X/A}$ antigens (HECA-452), sLe^x antigen (anti-CD15s) and E-selectin ligands (E-Ig) compared to SW620Mock cells, which, unlike WB staining suggested it, are not null in term of $sLe^{X/A}$ antigens expression. For sLe^A antigen (anti-CA19-9), expression levels are low in SW620 cells, even more in *FUT6* transfected cells compared to Mock. Statistical analysis confirmed the significant differences between SW620FUT6 and Mock cells regarding $sLe^{X/A}$ antigen and E-selectin ligands expression. Thus, **Figure 4.3C** showed the MFI ratios comparing *FUT6* vs. Mock SW620 transfected cells, sLe^X antigen and E-selectin ligands are overexpressed and sLe^A antigen expression is decreased in SW620FUT6 compared to SW620Mock. Regarding HT29 cell lines staining with same mAbs by flow cytometry was inconclusive. Indeed, while proteins from HT29 cells WB staining suggested strong difference of $sLe^{X/A}$ antigens expression in favour of HT29 cells transfected with *FUT6*, flow cytometry indicates opposite results with anti-CD15s and anti-CA19-9 but not with HECA-452 mAb and E-selectin ligands staining (**Figure 4.3B**). According to statistical analysis, no significant differences are observed for $sLe^{X/A}$ antigens (HECA-452) and E-selectin ligands staining, while HT29Mock cells shows higher staining for sLe^X (anti-CD15s) and sLe^A antigens (anti-CA19-9) compared to HT29FUT6 with significance (**Figure 4.3D**). WB and flow cytometry results of HT29 cell lines do not allow to make conclusions in term of $sLe^{X/A}$ antigens and E-selectin ligands expression regarding *FUT6* overexpression. For this reason, we focus further experiments only on SW620 cell lines.

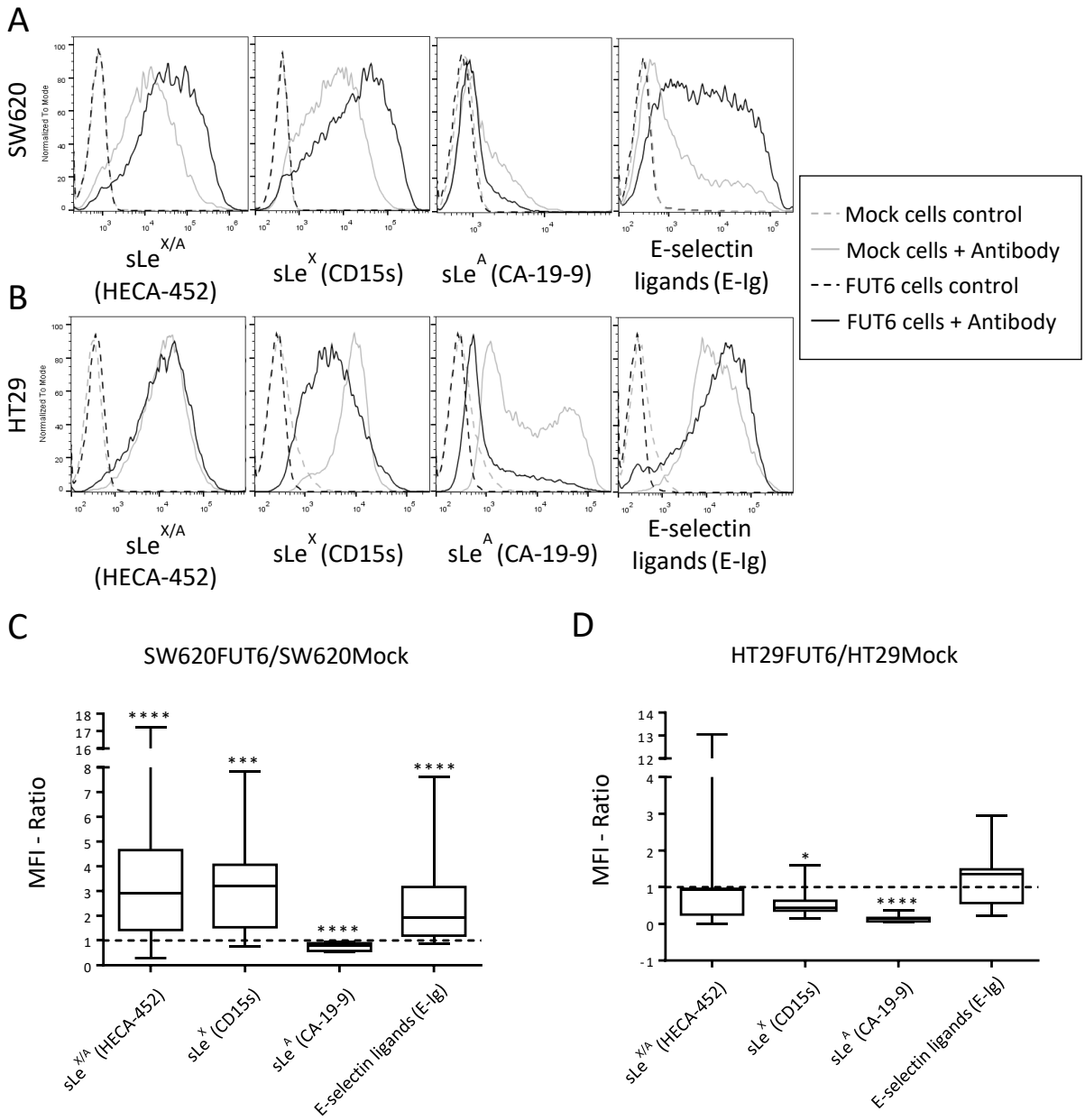

Figure 4.3 Comparison of sialyl Lewis X/A and E-selectin ligand expression on Mock and *FUT6* transfected cell line. A. SW620Mock cells (grey) and SW620FUT6 transfected cells (black) were stained with primary antibody (see below histograms) plus fluorescent secondary antibody in PBS, supplemented with Ca^{2+} for E-selectin chimera staining. SW620Mock and SW620FUT6 transfected cells controls (dashed lane) were stained with secondary antibody only, or in PBS with EDTA for E-selectin chimera staining. **B.** Same as A with HT29Mock and HT29FUT6 transfected cell lines. **C.** MFI ratios for each independent staining experiment were determined by the MFI values of stained SW620FUT6 transfected cell lines divided by MFI values of stained SW620Mock transfected cell lines; for $sLe^{X/A}$ (HECA-452) staining n=17 p<0.0001 (****); for sLe^{X} (CD15s) staining n=17 p=0.0001 (***); for sLe^{A} (CA-19-9) staining n=12 p<0.0001 (****); for E-selectin ligands (E-Ig) staining n=14 p<0.0001 (****). **D.** Same as C with HT29Mock and HT29FUT6 transfected cell lines; for $sLe^{X/A}$ (HECA-452) staining n=7 p=0.4514; for sLe^{X} (CD15s) staining n=7 p=0.0169 (*); for sLe^{A} (CA-19-9) staining n=7 p<0.0001 (****); for E-selectin ligands (E-Ig) staining n=7 p=0.49 (N.S.).

4.1.2. N-glycan profiles of Mock vs. *FUT6* transfected SW620 cells

To obtain more information on the glycosylated structures of SW620 cells transfected with *FUT6* compared to Mock, we extracted membrane proteins from both cell lines and released N-glycans using PNGase F enzyme. N-glycan profiles of SW620 cell lines were obtained by HILIC-UHPLC-MS/MS. The profiles of N-glycans from SW620Mock and SW620FUT6 cell lines ranged from m/z 960 and 3910. The ions were singly to quadruply charged. In the **Figure 4.4**, each identified structure is represented with its attributed peak ID reported on supplementary **Table S4.1** and **Table S4.2** for SW620Mock and SW620FUT6 cells, respectively. The composition of the N-glycans has been confirmed by MS^n fragmentation analysis. Thus, the identified Y- and B-ion fragments for each structure are shown in supplementary **Table S4.1** and **Table S4.2**. In total, 69 and 78 N-glycans were identified in SW620Mock and SW620FUT6 cells, respectively. Among them, it appeared some isomeric structures, for example N-glycans #50 in SW620Mock and #53 in SW620FUT6 have same m/z^{3+} value of 815.35, the two structures differentiate by the position of the antennary fucose, in Mock the Fuc residue is on the non-sialylated antennae while in *FUT6* it is on the sialylated antennae, giving, respectively, Le and sLe antigen structures. This difference was identified in the B-ion fragments, indeed, characteristic B-ions of sLe structure 803.34 (H1N1F1S1), 1289.63 (H4N1S1F1) and 1330.38 (H3N2S1F1) were identified in SW620FUT6 #53 N-glycan when absent in SW620Mock #50 N-glycan. Such differences appeared on other structures, such as N-glycan #65 and #68 from Mock compared to #76 from *FUT6*, here the difference concerned the core position of the Fuc residue in Mock versus sLe antigen structure in *FUT6* established by ion fragments intensities comparison. Similar differences were attributed to the following N-glycan structures from Mock compared to *FUT6*: #38 compared to #34, #45 compared to #48, #55 compared to #59, #67 compare to #73 and #74. All these differences are consistent with the increase of sLe structures due to the transfection of *FUT6* in SW620 cells. Other structure differences were identified for isomeric structures, the #18 and #22 from Mock cells compared to the #21 and #25 from *FUT6* cells, in these cases, bisecting GlcNAc for mono-galactosylated N-glycan (#18) was identified in Mock and not in *FUT6* (#21) and inversely bisecting GlcNAc for bi-galactosylated N-glycan (#25) was identified in *FUT6* and not in Mock cells (#22). Other neutral N-glycans were identified only in Mock or *FUT6* cells, comprising hybrid and complex N-glycan structures. Furthermore, N-glycan structures with four sialylated antennae were identified only in SW620FUT6 cells.

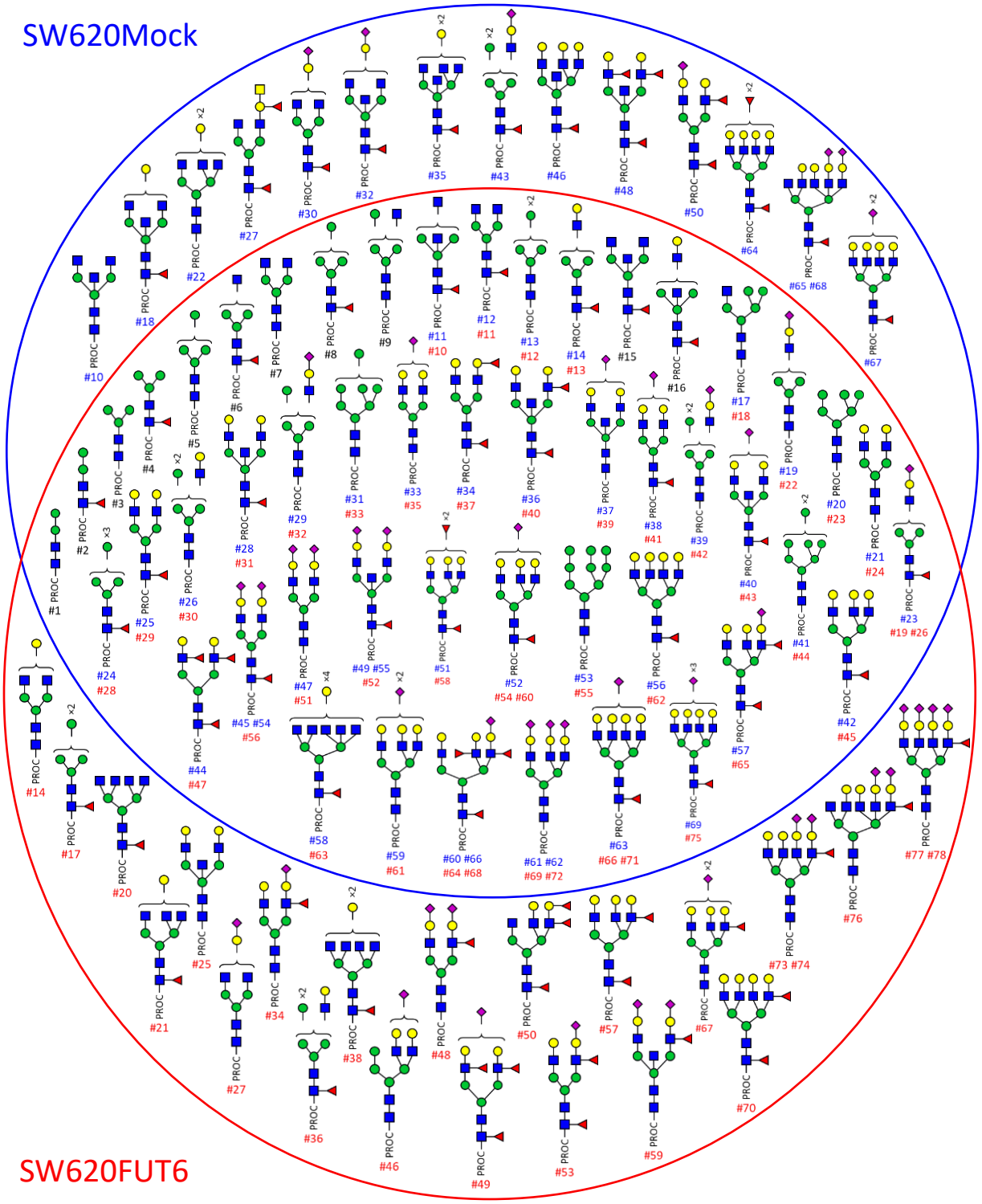

Figure 4.4 N-glycans identified by HILIC-UHPLC-MS from membrane proteins of SW620Mock and FUT6 cells. Schematic representation of the N-glycans released from SW620Mock cells (inside the blue circle) and from SW620FUT6 cells (inside the red circle) membrane proteins. Structures identified in both cell lines are in the two circles overlap. 69 N-glycan structures were identified for SW620Mock membrane proteins and 78 for SW620FUT6 membrane proteins. Y- and B-ion fragments identification, which allowed N-glycan composition determination, is depicted in supplementary **Table S4.1** and **Table S4.2** for SW620Mock and SW620FUT6 cells membrane proteins, respectively. In the supplementary **Table S4.1** and **Table S4.2**, peak ID has been attributed to each structure which correspond to the #number under each N-glycans (in blue for N-glycans from SW620Mock proteins, in red for N-glycans from SW620FUT6 proteins, in black for identical peak ID number attributed to N-glycans from both SW620Mock and FUT6 protein).

4.1.3. *FUT6* overexpression increases migration ability in SW620 cells

Cells migration capacity was evaluated using scratch wound healing assay. Therefore, Ibidi culture inserts were used with SW620Mock and SW620FUT6 cells and wound healing monitored for seven days. In **Figure 4.5A**, qualitative observation of pictures at day 4 indicated that wound with SW620FUT6 cells healed better than with SW620Mock cells and, at day 6, healed completely while some area for wound with SW620Mock cells were still free of cells. Quantitative measurements, plotted in **Figure 4.5B**, allowed to significantly confirm the higher faculty of SW620FUT6 cells to heal the wound more rapidly than SW620Mock. Thus, cells transfected with *FUT6*, with increased expression of sLe^x antigen and E-selectin ligands, possess improved migration ability compared to Mock transfected cells.

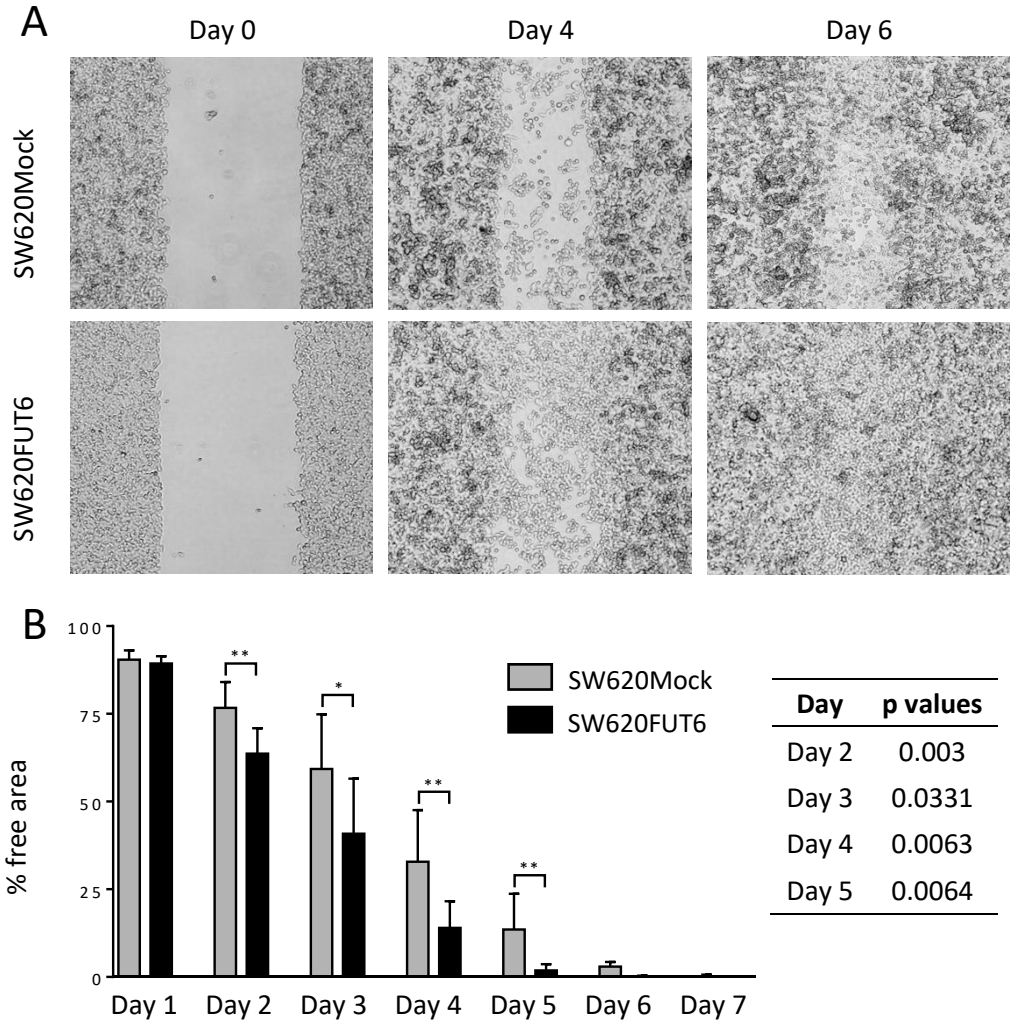

Day	p values
Day 2	0.003
Day 3	0.0331
Day 4	0.0063
Day 5	0.0064

Figure 4.5 *FUT6* overexpression in SW620 cells lead to increased cell migration faculty. A. Pictures of one of the scratch wound healing assays, performed using Ibidi culture inserts, from day 0 (left), day 4 (middle) and day 6 (right) with SW620Mock cells (upper) and SW620FUT6 cells (lower) obtained with an inverted microscope. **B.** Percentage means with standard deviation of free area for 8 independent experiments are represented, free areas were determined from pictures using ImageJ and converted into percentage values. At day 2, 3, 4 and 5, statistical analysis using unpaired Student's *t*-test demonstrated significant higher migration ability for SW620FUT6 cells compared to SW620Mock cells.

4.2. E-selectin ligands

4.2.1. SW620FUT6 cell line presents high expression of E-selectin ligands

The expression of E-selectin ligands has been observed on SW620Mock and SW620FUT6 cell lines by flow cytometry and WB. Using E-Ig chimera, flow cytometry analysis of the two cell lines highlighted a clear higher expression of E-selectin ligands on SW620FUT6 cells compared to SW620Mock cells (**Figure 4.6A**). Since E-selectin ligands can interact with E-selectin only if expressed on cell surface, membrane proteins from SW620Mock and SW620FUT6 cells were extracted. Analysis of these membrane proteins with E-Ig chimera by WB confirmed the flow cytometry results. Indeed, SW620Mock cells membrane proteins did not show stained bands whereas SW620FUT6 presented E-selectin ligands with high molecular weight. Three main bands were identified at ~100kDa, between 135kDa and 180kDa and ~245kDa (**Figure 4.6B**). E-selectin ligands were then immunoprecipitated (IP) from membrane protein of SW620FUT6 cells. The E-selectin ligands were successfully isolated as the E-Ig staining showed it (**Figure 4.6C**).

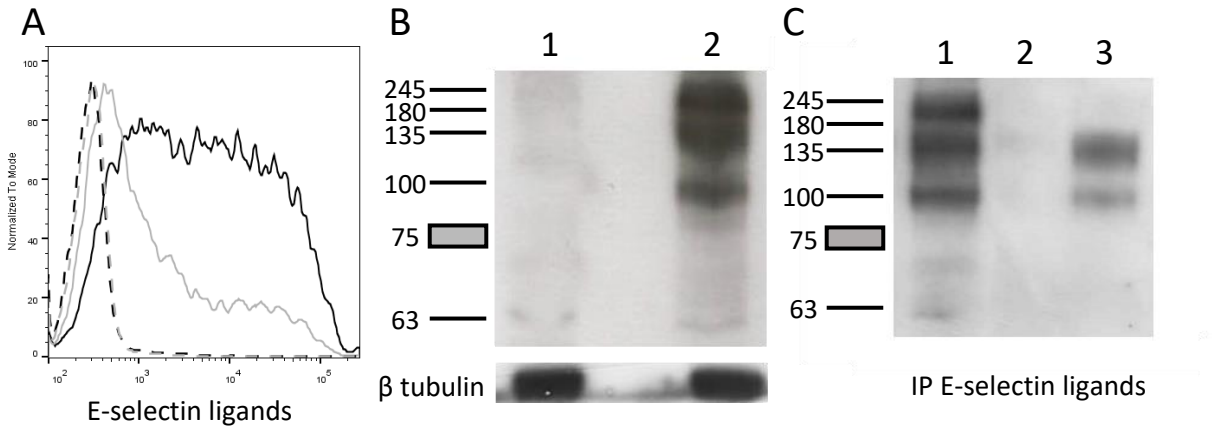

Figure 4.6 SW620FUT6 cells expresses E-selectin ligands. A. E-selectin ligands were stained with E-Ig chimera plus anti-human IgG (Fc Specific) -FITC on SW620Mock (grey filled lane) and SW620FUT6 (black filled lane) cells in PBS with Ca^{2+} and analysed by flow cytometry. SW620Mock and SW620FUT6 negative controls (grey and dark dashed lane, respectively) were stained similarly in PBS with EDTA. **B.** Membrane proteins from SW620Mock (lane 1) and SW620FUT6 cells (lane 2) were stained with E-Ig chimera plus anti-mouse CD62E plus anti-rat IgG (H+L) HRP in PBS with Ca^{2+} by WB. β tubulin protein expression level was analyzed as loading control. **C.** Membrane protein (lane 1), cleared membrane protein from immunoprecipitated (IP) E-selectin ligands (lane 2) and IP E-selectin ligands (lane 3) from SW620FUT6 cells were stained with E-Ig chimera plus anti-mouse CD62E plus anti-rat IgG (H+L) HRP in PBS with Ca^{2+} by WB.

4.2.2. E-selectin ligands from SW620FUT6 identification

To identify the E-selectin ligands, immunoprecipitations using E-Ig chimera were made on membrane proteins from SW620Mock and SW620FUT6 cells. IP E-selectin ligands were denatured and run in SDS-PAGE (short run). Six bands were cut on the gel, digested by trypsin, and analysed by LC-MS/MS. Four independent immunoprecipitations were performed and analysed, resulting in the identification

of 1066 proteins (data not shown). Among these proteins, 434 were present in at least two immunoprecipitations (data not shown). Since E-selectin ligands are glycosylated protein, the list was reduced to 57 glycoproteins, according to UniProtKB database annotations (supplementary **Table S4.3**). 13 glycoproteins of this list were only identified in IP E-selectin ligands from SW620FUT6 membrane proteins, the others being identified in IP E-selectin ligands from both SW620Mock and SW620FUT6 membrane proteins. The final list of 13 E-selectin ligands is mainly containing plasma membrane protein (**Table 4.2**). The four first E-selectin ligands from the list had the highest number of identified unique peptide by LC-MS/MS and were plasma membrane proteins presenting high molecular weight. Thus, we decided to continue this work with these proteins: neural cell adhesion molecule L1 (L1CAM), integrin α-6, receptor-type tyrosine-protein phosphatase eta (PTPRJ) and integrin β-1.

Table 4.2 List of identified E-selectin ligands in SW620FUT6 cells by mass spectrometry†. † From SW620Mock and SW620FUT6 cells extracted membrane protein, four immunoprecipitations with E-Ig chimera were performed and analysed by LC-MS/MS. The present list shows the glycosylated‡ immunoprecipitated E-selectin ligands only identified in SW620FUT6 cells (supplementary **Table S4.3** for glycosylated‡ IP E-selectin ligands identified in both cell lines). **§** Proteins identified are described with the number of unique peptides for each experiment and the sum of the total spectrum count from the four experiments. **‡** Protein information on glycosylation status and subcellular location were extracted from UniProtKB database.
Abbreviation: MW, Molecular Weight; Exp., Experiment.

Protein Name	Gene Name	MW (kDa)	UniProtKB entry	Exclusive Unique Peptide Count§				Total spectrum count (sum)§	Subcellular location‡
				Exp. 1	Exp. 2	Exp. 3	Exp. 4		
Neural cell adhesion molecule L1	L1CAM	140	P32004 (L1CAM_HUMAN)	31	20	30	27	118	Plasma membrane
Integrin alpha 6	ITGA6	127	P23229 (ITA6_HUMAN)	11	31	12	10	91	Plasma membrane
Receptor-type tyrosine-protein phosphatase eta	PTPRJ	146	Q12913 (PTPRJ_HUMAN)	21	9	18	11	58	Plasma membrane
Integrin beta 1	ITGB1	88	P05556 (ITB1_HUMAN)	6	11	7	5	39	Plasma membrane, recycling endosome
Cation-independent mannose-6-phosphate receptor	IGF2R	274	P11717 (MPRI_HUMAN)	16	3	16	7	39	Lysosome membrane
Receptor-type tyrosine-protein phosphatase alpha	PTPRA	91	P18433 (PTPRA_HUMAN)	10	3	4	5	22	Membrane
Leucyl-cystinyl aminopeptidase	LNPEP	117	Q9UIQ6 (LCAP_HUMAN)	7	9	6	5	22	Plasma membrane, secreted
Carboxypeptidase D	CPD	153	O75976 (CBPD_HUMAN)	2	0	6	6	13	Plasma membrane
Lysosome-associated membrane glycoprotein 2	LAMP2	45	P13473 (LAMP2_HUMAN)	3	3	3	3	12	Lysosome/endosome/ plasma membrane
CD109 antigen	CD109	162	Q6YHK3 (CD109_HUMAN)	3	2	2	4	12	Plasma membrane
Golgi membrane protein 1	GOLM1	45	Q8NBJ4 (GOLM1_HUMAN)	2	2	2	4	10	Golgi apparatus membrane
Plexin-D1	PLXND1	212	Q9Y4D7 (PLXD1_HUMAN)	2	0	1	4	7	Plasma membrane
Zymogen granule protein 16 homolog B	ZG16B	23	Q96DA0 (ZG16B_HUMAN)	0	2	0	2	4	Secreted

4.2.3. L1CAM, integrin α-6 and integrin β-1 are expressed on SW620Mock and SW620FUT6 cells surface

E-selectin ligands being expressed on cell surface, the expression of the selected identified E-selectin ligands on cell surface was assessed by flow cytometry on SW620Mock and SW620FUT6 cells. Unfortunately, PTPRJ was presenting almost no staining in both cell lines (**Figure 4.7**).

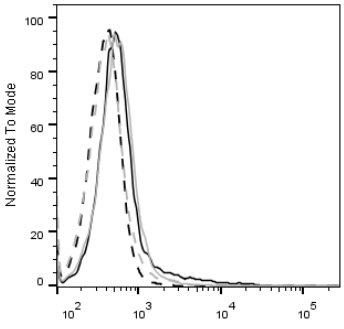

Figure 4.7 PTRJ is not present in SW620 cell surface. PTPRJ was stained with corresponding mAb plus anti-mouse IgG FITC on SW620Mock (grey filled lane) and SW620FUT6 (black filled lane) cells in PBS and analysed by flow cytometry. SW620Mock and SW620FUT6 negative control (grey and dark dashed lane, respectively) were stained with secondary antibody only (anti-mouse IgG FITC).

However, L1CAM, integrin α-6 and integrin β-1 were successfully stained by flow cytometry (**Figure 4.8A** and **B**). Interestingly, L1CAM presented a higher expression level on SW620FUT6 cells when compared to SW620Mock cells (**Figure 4.8B**). This higher expression was also emphasised by WB staining assay (**Figure 4.8C**). The expression level of integrin α-6 and integrin β-1 was similar between SW620Mock and SW620FUT6 cells (**Figure 4.8B**).

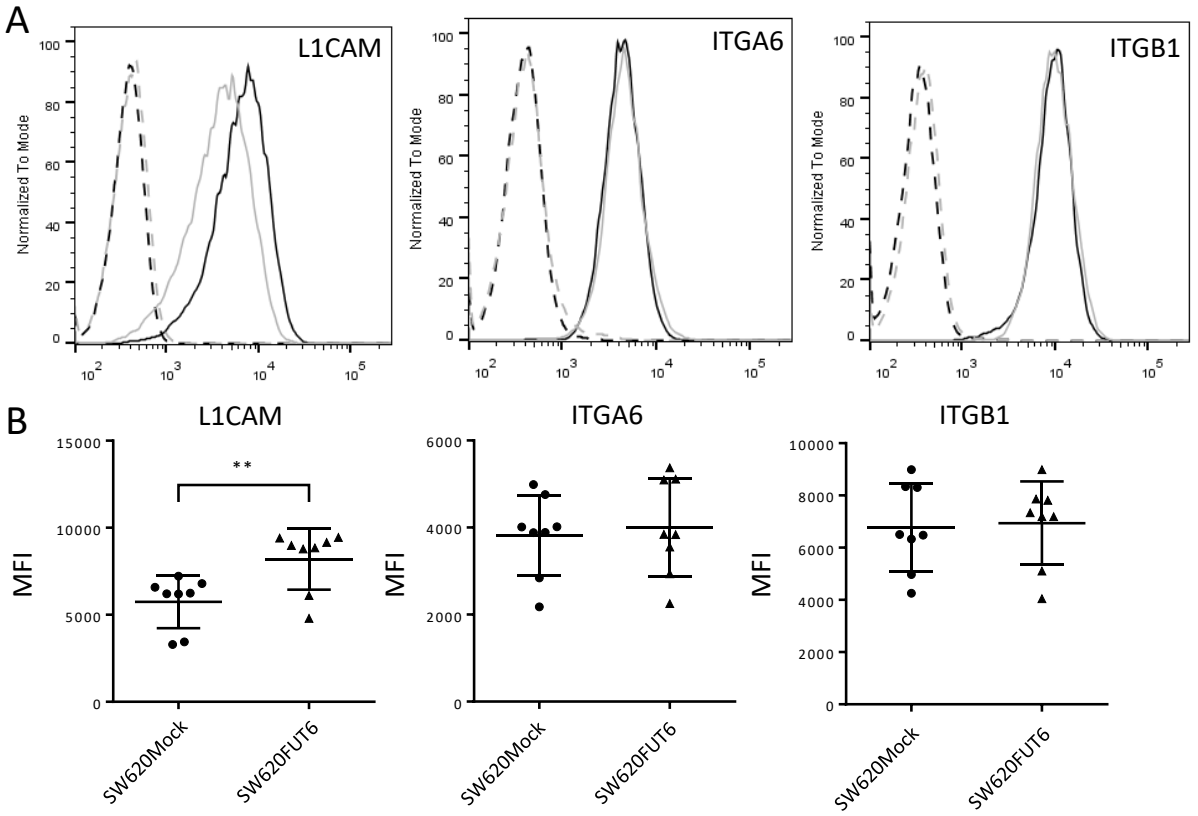

Figure 4.8 E-selectin ligands expression in SW620 cell lines. A. L1CAM, ITGA6 (integrin α6) and ITGB1 (integrin β1) were stained with corresponding mAb plus anti-mouse IgG FITC on SW620Mock (grey filled lane) and SW620FUT6 (black filled lane) cells in PBS and analysed by flow cytometry. SW620Mock and SW620FUT6 negative control (grey and dark dashed lane, respectively) were stained with secondary antibody only (anti-mouse IgG FITC). **B.** Median Fluorescent Intensity (MFI) values (filled circles and tringles) of 8 biological independent experiments of anti-L1CAM, anti-ITGA6 and anti-ITGB1 mAb plus anti-mouse IgG FITC staining obtained by flow cytometry. The data are represented in scatter plot with mean ± SD. L1CAM expression was significantly higher in SW620FUT6 cells compared to SW620Mock cells, ** p=0.0096 (unpaired Student's *t*-test). **C.** Membrane proteins from SW620Mock (lane 1) and SW620FUT6 cells (lane 2) were stained with anti-L1CAM mAb plus anti-mouse Ig HRP in PBS by WB. β tubulin protein expression level was analysed as loading control.

4.2.4. L1CAM is an E-selectin ligand in SW620FUT6 cells

Further analysis showed that L1CAM is an E-selectin ligand only in SW620FUT6 cells. Indeed, immunoprecipitation of L1CAM has been done on SW620Mock and SW620FUT6 membrane proteins

and subjected to L1CAM staining by WB, as well as IP E-selectin ligands. From SW620Mock membrane and IP proteins, L1CAM was only identified in total membrane protein and IP L1CAM, not in IP E-selectin ligands. On the opposite, IP L1CAM and IP E-selectin ligands presented a band at the same size when stained with mAb against L1CAM in SW620FUT6 (**Figure 4.9A**). IP L1CAM and IP E-selectin ligands from SW620FUT6 membrane protein were then stained with HECA-452 ($sLe^{X/A}$ antigens) and E-Ig chimera. The same band as in L1CAM staining appeared with $sLe^{X/A}$ antigen and E-selectin ligands staining in both IP L1CAM and IP E-selectin ligands (**Figure 4.9B**). Together, these results show that L1CAM is an E-selectin ligand in SW620FUT6 cells.

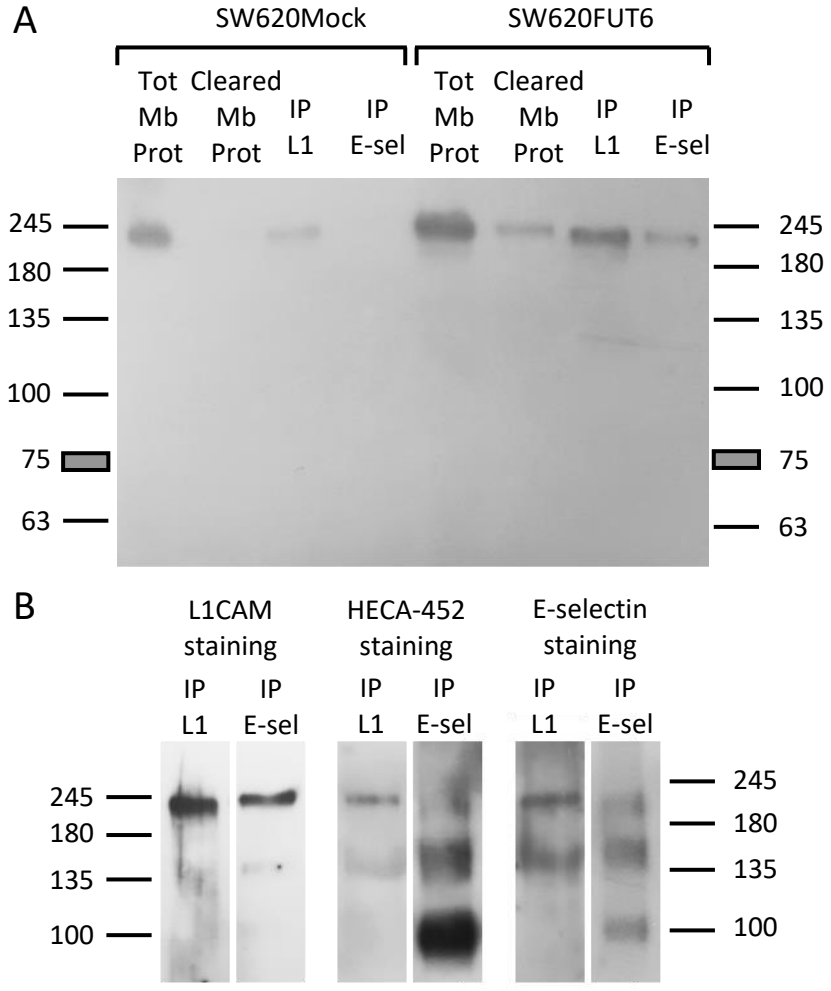

Figure 4.9 Identification of L1CAM as an E-selectin ligand in SW620FUT6 cells. A. L1CAM and E-selectin ligands immunoprecipitations from SW620Mock and FUT6 cells membrane proteins, as well as cleared membrane protein from IP L1CAM, were stained with anti-L1CAM mAb plus anti-mouse Ig HRP in PBS by WB. IP E-selectin ligands from SW620FUT6 cells showed a stained band corresponding to L1CAM protein suggesting that L1CAM is an E-selectin ligand, in contrast to IP E-selectin ligands from SW620Mock cells. **B.** IP L1CAM and IP E-selectin ligands from SW620FUT6 membrane proteins were stained with anti-human L1CAM mAb plus anti-mouse Ig HRP in PBS (left), with HECA-452 (anti-human CLA mAb) plus anti-rat IgM HRP in PBS (middle) and with E-Ig chimera plus anti-mouse CD62E plus anti-rat IgG (H+L) HRP in PBS with Ca^{2+} (right) by WB.
Tot: total, Mb Prot: membrane proteins, IP: immunoprecipitated, L1: L1CAM, E-sel: E-selectin ligands.

4.2.5. L1CAM N-glycan analysis

To determine the N-glycan structures of L1CAM from SW620FUT6 cells, immunoprecipitations of L1CAM were performed on membrane proteins. To make immunoprecipitations L1CAM mAb is used and can be a source of contamination in the MS analysis since the mAb is N-glycosylated. Thereby, N-glycan structures from mAb were analysed like N-glycan structures from IP L1CAM to exclude N-glycan structures from the mAb to the N-glycan analysis of IP L1CAM. N-glycans from IP L1CAM and L1CAM mAb were released with PNGase F treatment, labelled with procainamide, and analysed by HILIC-UHPLC-MS. The profiles of N-glycans from L1CAM mAb and IP L1CAM ranged from m/z 1110 and 3100. The ions were singly to triply charged. The composition of the N-glycans has been confirmed by MS^n fragmentation analysis. Thus, the identified Y- and B-ion fragments for each structure are shown in supplementary **Table S4.4** and **Table S4.5** for L1CAM mAb and IP L1CAM, respectively. The N-glycan structures from mAb and IP were compared, once common structures excluded, remaining structures were annotated on the chromatogram in **Figure 4.10** with their attributed peak ID reported on supplementary **Table S4.5**. Unfortunately, sLe^X structure was not identified on N-glycans, but we cannot exclude the possibility of the presence of this structure on O-glycans.

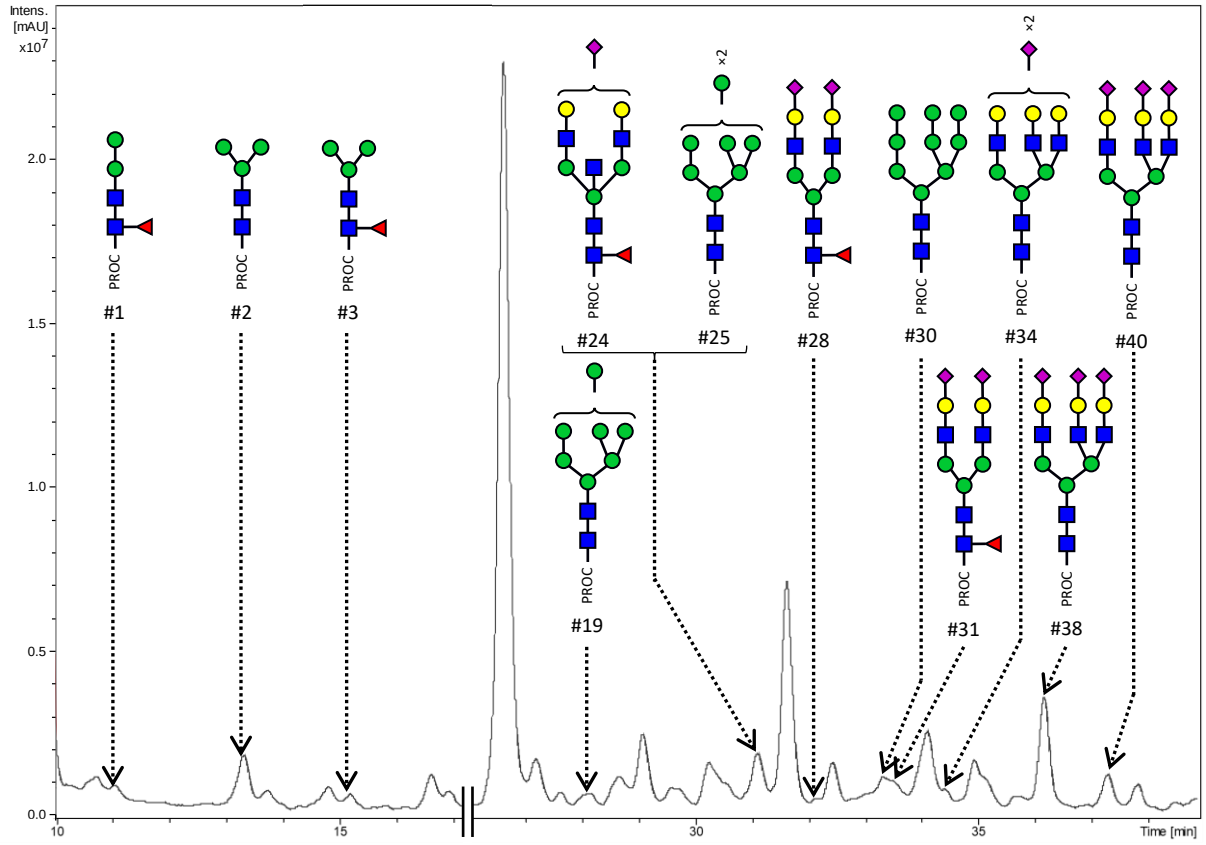

Figure 4.10 HPLC profile of N-glycans released from IP L1CAM. N-glycans from IP L1CAM and anti-L1CAM mAb were released by PNGase F treatment, reduced, and labelled with procainamide. N-glycans were analysed by LC-ESI-MS/MS in positive mode. Structures only identified in IP L1CAM samples are represented with their peak ID number (supplementary **Table S4.5**). PROC: procainamide; blue square: N-acetylglucosamine; green circle: Mannose; yellow circle: Galactose; red triangle: Fucose; purple diamond: N-acetylneuraminic acid.

4.3. Immunomodulation

4.3.1. MoDCs adherence to SW620 cells and maturation profile are affected by *FUT6* overexpression

In vitro co-cultures were established to study the influence of sLe^X/selectin ligand overexpressing CRC cells interaction on moDCs. Thus, SW620 cells transfected with *FUT6* overexpress sLe^X and E-selectin ligands compare to Mock transfected SW620 cells, as shown previously. The two cell lines were co-cultured with moDCs. The adherence of moDCs to cancer cells was significantly higher in the co-cultures with *FUT6* transfected cells than Mock (**Figure 4.11**), suggesting a role of sLe^X in moDCs interaction.

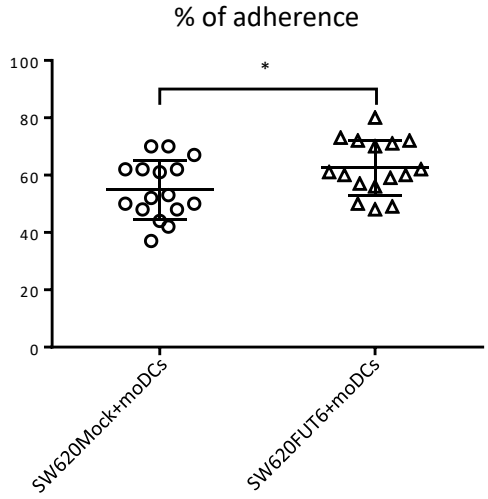

Figure 4.11 MoDCs adhere more to *FUT6* transfected SW620 than Mock cells. MoDCs were co-cultured with SW620 cell lines and after 6 hours incubation, non-adherent moDCs were washed and the percentages of adhering moDCs to cancer cells were determined by flow cytometry using the expression of CD45 marker to differentiate moDCs from tumour cells. Data were collected for 16 independent experiments and adhering moDCs percentages were significantly higher in the co-cultures with SW620FUT6 than SW620Mock cells with p=0.0369 (*, unpaired Student's *t*-test).

Then, we assess the maturation phenotype of the moDCs which interacted with the colon cancer cells. For this purpose, the expression patterns on moDCs of major histocompatibility complex class II (MHC-II), an antigen presenting protein, and CD86, a co-stimulatory protein, were measured by flow cytometry. The gating strategy presented in **Figure 4.12A** demonstrates how the moDCs and the colon cancer cells populations were distinguished. Firstly, the singlets population was selected using forward scatter height versus area, secondly, living cells selection was done using side versus forward scatter height. Thirdly, the CRC cells alone control allowed to confirm the absence of CD45 and CD86 expression which was thus used to establish the distinction between moDCs and CRC cells. The staining comparison of stimulated moDCs with LPS and unstimulated moDCs permitted to confirm that the moDCs were susceptible to maturation. Indeed, upon LPS stimulation moDCs showed higher mature profile with 2.5 and 2.2-fold change in MHC-II and CD86 expression, respectively (**Figure 4.12B**). Cancer cells alone and in the co-cultures did not show MHC-II or CD86 staining (data not shown). In the co-cultures, the moDCs incubated with SW620FUT6 cells presented a lower expression of MHC-II and CD86 than the moDCs incubated with SW620Mock cells (**Figure 4.12B**). Taken together, these results

suggest an influence of sLe^X antigen/selectin ligands expression by CRC cells on immune cells maturation.

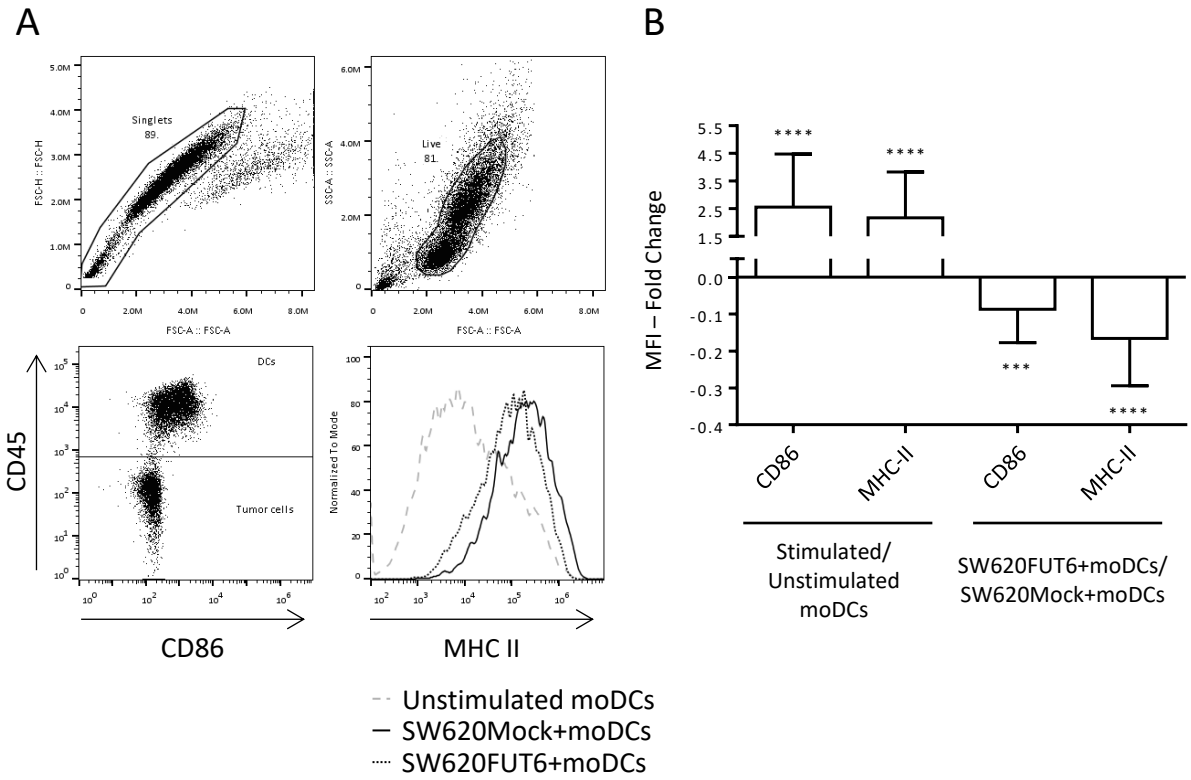

Figure 4.12 MoDCs are less mature when co-cultured with SW620FUT6 cells compared to Mock. A. Gating strategy to differentiate tumour cells and moDCs in co-cultures, singlets selection (upper left) using forward scatter height/area, living cells selection (upper right) using side/forward scatter height, distinction of moDCs and tumour cells (lower left) using CD45/CD86 staining, and MHC-II staining histogram (lower right) with unstimulated moDCs (dashed grey lane), moDCs populations from co-culture with SW620Mock cells (dotted black lane) and SW620FUT6 cells (black lane). **B.** MoDCs were co-cultured with SW620 cell lines and after 6 hours incubation, non-adherent moDCs were washed and co-cultured cells were harvested to assess MHC-II and CD86 expression by flow cytometry. MFI fold changes for 16 independent experiments were determined as described in materials and methods, for both CD86 and MHC-II $p<0.0001$ (****) for stimulated/unstimulated moDCs, for CD86 $p=0.0006$ (***) and MHC-II $p<0.0001$ (****) for moDCs with SW620FUT6 cells/moDCs with SW620Mock cells.

4.3.2. No effect of *FUT6* expression in SW620 cells to moDCs cytokines gene expression

To further investigate the role of sLe^X antigen/selectin ligands expression by CRC cells on the moDCs maturation profile, the expression levels of different cytokines genes were determined. Thus, the expression of *IL-1β*, *IL-6*, *IL-10*, *IL-12B*, *TGF-β1* and *TNFα* was analysed by RT-qPCR on extracted RNA from co-cultures after two hours of incubation (**Figure 4.13**). Regarding immune cells controls, moDCs stimulated by LPS expressed higher levels of pro-inflammatory cytokines *IL-1β*, *IL-6*, *IL-12B* (subunit of IL-12 and IL-23 cytokines) and *TNFα* (respectively **Figure 4.13A**, **B**, **D** and **F**). Controls with tumour cells alone showed undetectable expression levels for these pro-inflammatory cytokines, however, anti-inflammatory cytokines *IL-10* and *TGF-β1* (respectively **Figure 4.13C** and **E**) were both expressed by CRC cells and *IL-10* was significantly more expressed by SW620Mock cells than SW620FUT6 cells.

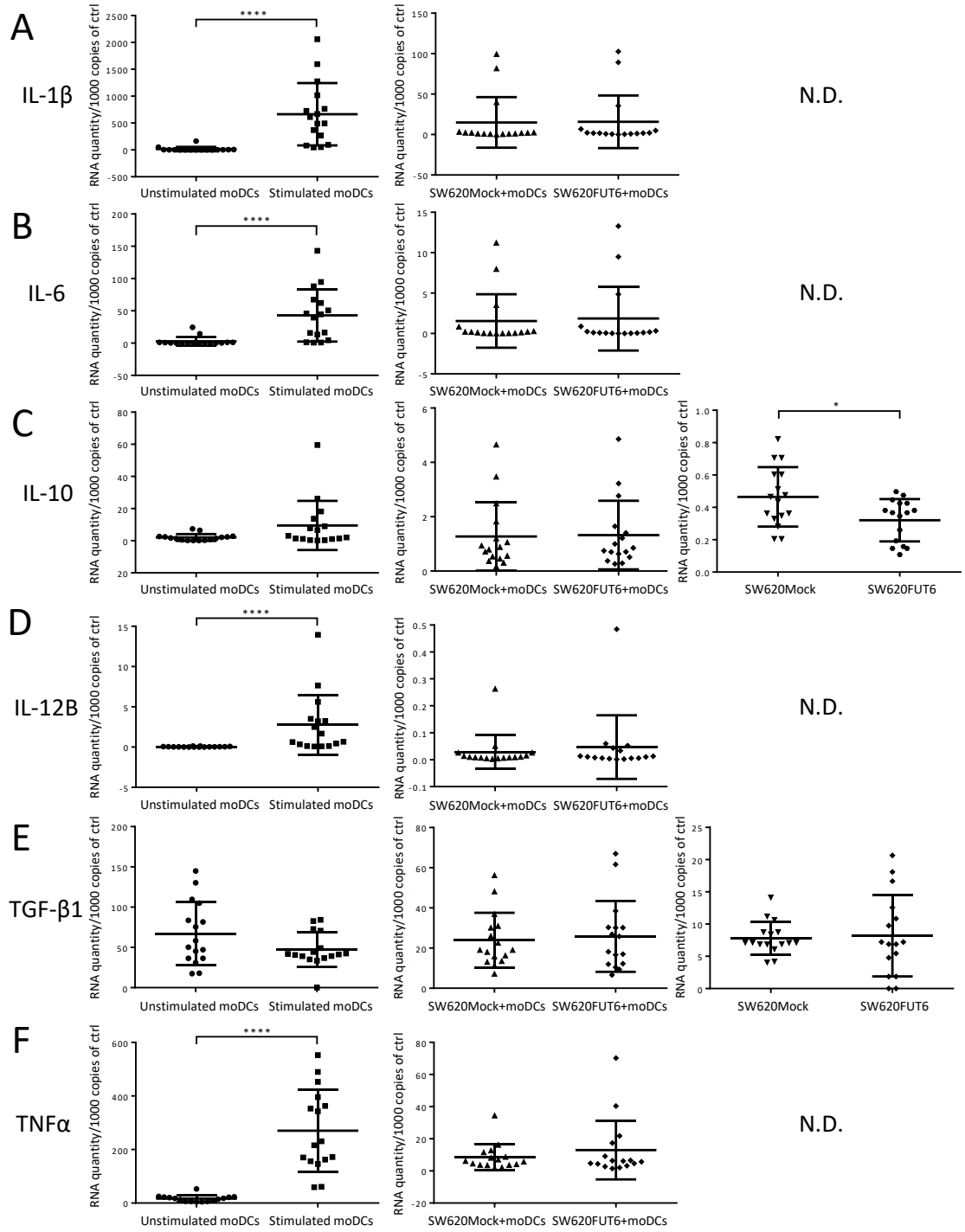

Figure 4.13 Co-cultures with SW620FUT6 cell line do not affect cytokines gene expression. **A – F.** Values represented in mean ± SD (Standard Deviation) are the number of mRNA molecules of the gene of interest per 1000 molecules of the endogenous controls (section **3.9**), left column scatter plots show gene expression for immune cells controls, middle column scatter plots show gene expression for co-cultures, left column scatter plots show gene expression for tumour cells controls, n=16. **A.** *IL-1β* expression is increased in stimulated moDCs compared to unstimulated p<0.0001 (****, Mann-Whitney test), **B.** *IL-6* expression is increased in stimulated moDCs compared to unstimulated p<0.0001 (****, Mann-Whitney test), **C.** *IL-10* expression is increased in SW620Mock compared SW620FUT6 p=0.0156 (*, unpaired Student's *t*-test), **D.** *IL-12B* expression is increased in stimulated moDCs compared to unstimulated p<0.0001 (****, Mann-Whitney test), **E.** *TGF-β1* expression, **F.** *TNFα* expression is increased in stimulated moDCs compared to unstimulated p<0.0001 (****, Mann-Whitney test). N.D.: not detectable.

Unfortunately, no differences were observed for cytokines gene expression levels in the co-cultures with CRC cells and moDCs. Thus, sLe^X antigen/selectin ligands expression by tumour cells does not influence the expression of pro- or anti-inflammatory cytokines by moDCs.

4.3.3. MoDCs maturation profile is affected by *FUT6* overexpression after stimulation

Subsequently, we evaluated the effect of sLe^X antigen/selectin ligands overexpressing tumour cells on the maturation profile of moDCs challenged with LPS. Therefore, LPS has been added at 6 hours of incubation to co-cultures and maturation profile of DCs and percentages of adhering moDCs were assessed after 24 hours of incubation. Unlike previous observation, no significant differences were observed in the adherence of moDCs to Mock or *FUT6* transfected SW620 cells with or without LPS challenges (**Figure 4.14**).

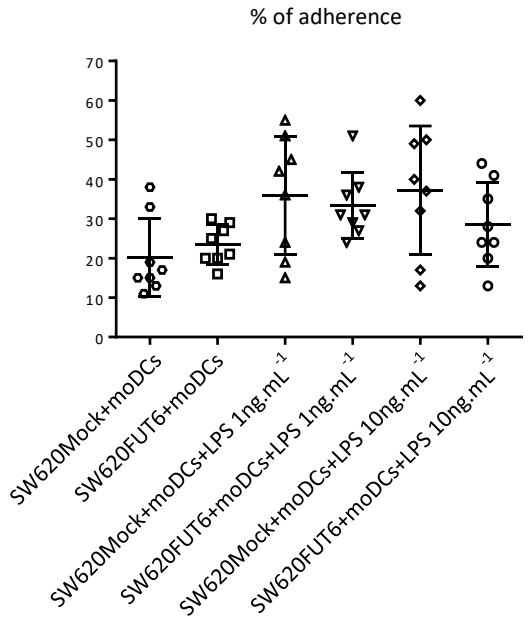

Figure 4.14 MoDCs adherence in co-cultures challenged with LPS. MoDCs were co-cultured with SW620 cell lines, supplemented or not at 6 hours with LPS 1ng.mL^{-1} or 10ng.mL^{-1}, and after 24 hours incubation, non-adherent moDCs were washed and the percentages of adhering moDCs to cancer cells were determined by flow cytometry using the expression of CD45 marker to differentiate moDCs from tumour cells. Data were collected for 8 independent experiments and no significant difference has been observed for the adhering moDCs percentages comparing the co-cultures with SW620FUT6 and SW620Mock cells without or with 1 or 10ng.mL^{-1} of LPS.

As previously, the expression patterns on moDCs of MHC-II, antigen presenting protein, and CD86, co-stimulatory protein, were measured by flow cytometry using the same gating strategy presented in **Figure 4.12A**. The staining comparison of stimulated moDCs with LPS, challenged with LPS 1 or 10ng.mL^{-1} and unstimulated moDCs confirmed the moDCs susceptibility to maturate: for CD86 expression 40.7, 23.7 and 40.4-fold changes and for MHC-II expression 2.9, 2.4 and 2.9-fold changes were observed, respectively (**Figure 4.15A** and **B**). In addition, the comparison of LPS 10ng.mL^{-1} challenged moDCs with LPS 1ng.mL^{-1} challenged moDCs showed a positive correlation between the LPS-dose and the expression extent of CD86 and MHC-II ($p<0.0001$ **Figure S4.** and $p=0.0009$ **Figure S4.17**, respectively). Cancer cells alone and in the co-cultures, challenged with 1 or 10ng.mL^{-1} of LPS, did not show CD86 or MHC-II staining (data not shown).

As observed with moDCs controls, the expression extent of maturation markers was LPS-dose dependant in both SW620Mock and SW620FUT6 co-cultured with moDCs (**Figure S4.** and for CD86 expression and **Figure S4.17** for MHC-II expression). As shown previously at 6 hours of incubation (**Figure 4.12B**), the moDCs incubated with SW620FUT6 cells presented a lower expression of CD86 and MHC-II than the moDCs incubated with SW620Mock cells, also observed with LPS challenges (respectively **Figure 4.15A** and **B**). Thus, the greater resistance to maturate was incontestable when moDCs were incubated with SW620FUT6 cells, as compared with SW620Mock cells, with or without LPS. These results reinforce the influence potential of sLe^X antigen/selectin ligands expression by CRC cells on immune cells maturation.

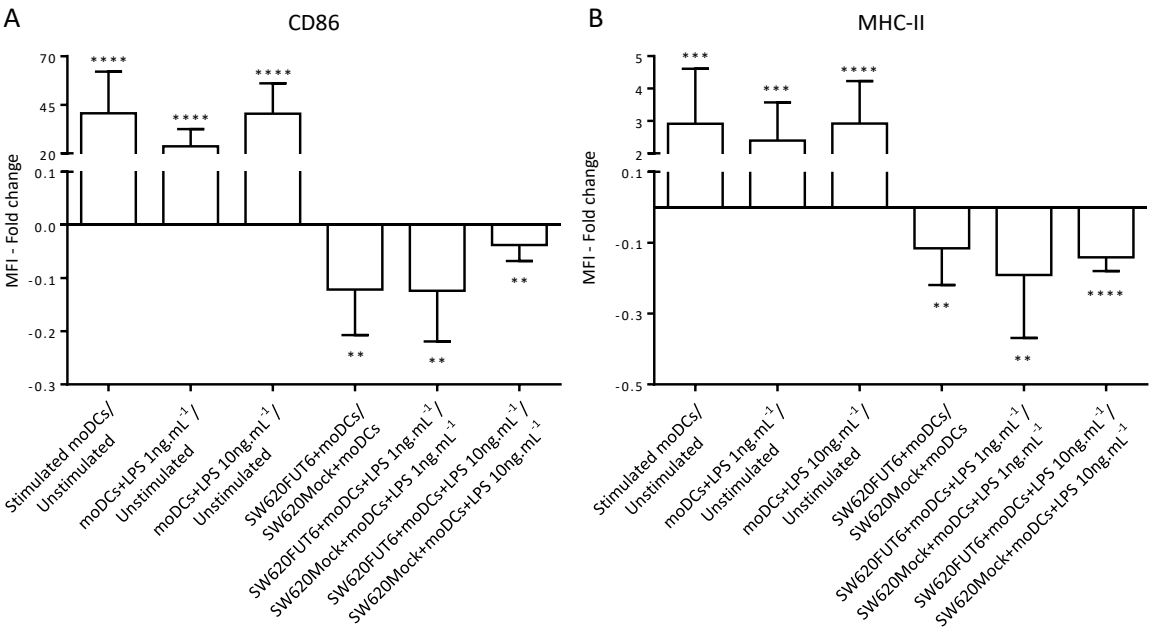

Figure 4.15 Increased resistance to maturation of moDCs when incubated with *FUT6* transfected cancer cell line. A – B. MoDCs were co-cultured with SW620 cell lines, supplemented or not at 6 hours with LPS 1ng.mL^{-1} or 10ng.mL^{-1}, and after 24 hours incubation, non-adherent moDCs were washed and co-cultured cells were harvested to assess MHC-II and CD86 expression by flow cytometry. MFI fold changes for 8 independent experiments were determined as described in materials and methods, **A.** MFI fold changes for CD86 co-stimulatory protein, p<0.0001 (****) for stimulated/unstimulated moDCs, moDCs with LPS 1ng.mL^{-1}/unstimulated moDCs and moDCs with LPS 10ng.mL^{-1}/unstimulated moDCs, p=0.0013 (**) for moDCs with SW620FUT6 cells/moDCs with SW620Mock cells, p=0.0025 (**) for moDCs with SW620FUT6 cells/moDCs with SW620Mock cells both challenged with LPS 1ng.mL^{-1}, p=0.0033 (**) for moDCs with SW620FUT6 cells/moDCs with SW620Mock cells both challenged with LPS 10ng.mL^{-1}. **B.** MFI fold changes for MHC-II antigen presenting protein, p=0.0003 (***) for stimulated/unstimulated moDCs, p=0.0002 (***) moDCs with LPS 1ng.mL^{-1}/unstimulated moDCs, p<0.0001 (****) moDCs with LPS 10ng.mL^{-1}/unstimulated moDCs, p=0.0073 (**) for moDCs with SW620FUT6 cells/moDCs with SW620Mock cells, p=0.0087 (**) for moDCs with SW620FUT6 cells/moDCs with SW620Mock cells both challenged with LPS 1ng.mL^{-1}, p<0.0001 (****) for moDCs with SW620FUT6 cells/moDCs with SW620Mock cells both challenged with LPS 10ng.mL^{-1}.

4.4. Supplementary Data

Table S4.1 Membrane proteins N-glycans composition of SW620Mock cells identified by MS^n fragmentation analysis with identified Y- and B-ion fragments. Membrane proteins N-glycans from SW620Mock cells were released, labelled, and analysed by LC-ESI-MS/MS. Mass spectrometry data were analysed using the Bruker Compass DataAnalysis 4.1 software. LC-ESI-MS/MS chromatogram analysis was performed using Bruker Compass DataAnalysis 4.4 and GlycoWorkbench software. Structures were identified by comparing LC, MS, and MS/MS data. Structures for N-glycans are depicted with the following notation: PROC: procainamide; blue square: N-acetylglucosamine; green circle: Mannose; yellow circle: Galactose; red triangle: Fucose; purple diamond: N-acetylneuraminic acid. Identified Y- and B-ion fragments, noted respectively in black and blue, are given in terms of the number of hexose (H), N-acetylhexosamine (N), deoxyhexose (F) and N-acetylneuraminic acid (S). Abbreviations: LC-ESI-MS/MS, liquid chromatography electrospray ionisation tandem mass spectrometry; Hex, hexose; HexNAc, N-acetylhexosamine; Fuc, Fucose; Neu5Ac, N-acetylneuraminic acid; Cmpd, compound; n.d., not detectable.

Peak ID	Retention time (min)	Structure	Composition				LC-ESI-MS									
			Hex (H)	HexNAc (N)	Fuc (F)	Neu5Ac (S)	$[M/Z]^+$ calculated	$[M/Z]^{2+}$ calculated	$[M/Z]^{3+}$ calculated	$[M/Z]^+$ registered	$[M/Z]^{2+}$ registered	$[M/Z]^{3+}$ registered	[M/Z] characteristic fragment ions (composition)					
1	8.5 (Cmpd 524)	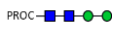	2	2	0	0	968.45	484.73	323.49	968.46	484.73	n.d.	441.27 (N1-PROC)	528.18 (H2N1)				
													644.33 (N2-PROC)					
													806.42 (H1N2-PROC)					
													325.14 (H2)					
													366.12 (H1N1)					
2	10.4 (Cmpd 645)	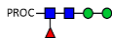	2	2	1	0	1114.51	557.76	372.18	1114.50	557.76	n.d.	441.30 (N1-PROC)	952.46 (H1N2F1-PROC)				
													587.33 (N1F1-PROC)	968.50 (H2N2-PROC)				
													644.33 (N2-PROC)	325.16 (H2)				
													790.45 (N2F1-PROC)	366.17 (H1N1)				
													806.43 (H1N2-PROC)	528.21 (H2N1)				
3	12.5 (Cmpd 779)	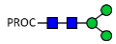	3	2	0	0	1130.51	565.76	377.51	1130.51	565.77	n.d.	441.28 (N1-PROC)	203.96 (N1)	690.21 (H3N1)			
													644.35 (N2-PROC)	325.18 (H2)				
													806.50 (H1N2-PROC)	366.12 (H1N1)				
													968.50 (H2N2-PROC)	487.14 (H3)				
													162.98 (H1)	528.16 (H2N1)				
4	14.5 (Cmpd 901)	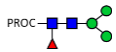	3	2	1	0	1276.57	638.79	426.19	1276.58	638.83	n.d.	441.29 (N1-PROC)	968.50 (H2N2-PROC)	528.15 (H2N1)			
													587.34 (N1F1-PROC)	203.95 (N1)	690.21 (H3N1)			
													644.41 (N2-PROC)	325.06 (H2)				
													790.37 (N2F1-PROC)	366.10 (H1N1)				
													806.35 (H1N2-PROC)	487.13 (H3)				
5	16.5 (Cmpd 1020)	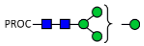	4	2	0	0	1292.56	646.78	431.53	1292.58	646.80	n.d.	441.27 (N1-PROC)	366.08 (H1N1)				
													806.30 (H1N2-PROC)	487.00 (H3)				
													968.44 (H2N2-PROC)	528.14 (H2N1)				
													203.94 (N1)	690.19 (H3N1)				
													325.10 (H2)	852.31 (H4N1)				
6	17.0 (Cmpd 1050)	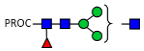	3	3	1	0	1479.65	740.33	493.89	n.d.	740.35	n.d.	441.30 (N1-PROC)	952.42 (H1N2F1-PROC)	204.03 (N1)	690.32 (H3N1)		
													587.33 (N1F1-PROC)	968.48 (H2N2-PROC)	325.20 (H2)	731.36 (H2N2)		
													644.41 (N2-PROC)	1114.58 (H2N2F1-PROC)	366.09 (H1N1)	893.35 (H3N2)		
													790.47 (N2F1-PROC)	1130.57 (H3N2-PROC)	528.14 (H2N1)			
													806.47 (H1N2-PROC)	1276.63 (H3N2F1-PROC)	569.25 (H1N2)			
7	17.3 (Cmpd 1069)		3	4	0	0	1536.67	768.84	512.89	n.d.	768.85	n.d.	441.22 (N1-PROC)	1171.61 (H2N3-PROC)	893.19 (H3N2)			
													644.41 (N2-PROC)	1333.62 (H3N3-PROC)	1096.48 (H3N3)			
													806.38 (H1N2-PROC)	325.00 (H2)				
													968.28 (H2N2-PROC)	366.16 (H1N1)				
													1130.51 (H3N2-PROC)	731.08 (H2N2)				
8	18.0 (Cmpd 1114)	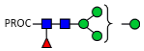	4	2	1	0	1438.62	719.81	480.21	1438.60	719.81	n.d.	441.28 (N1-PROC)	952.50 (H1N2F1-PROC)	487.25 (H3)			
													587.33 (N1F1-PROC)	968.50 (H2N2-PROC)	528.13 (H2N1)			
													644.37 (N2-PROC)	203.98 (N1)	690.20 (H3N1)			
													790.40 (N2F1-PROC)	325.16 (H2)	852.29 (H4N1)			
													806.29 (H1N2-PROC)	366.07 (H1N1)				
9	18.8 (Cmpd 1161)	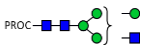	4	3	0	0	1495.64	748.32	499.22	1495.64	748.33	499.24	441.28 (N1-PROC)	1171.63 (H2N3-PROC)	649.00 (H4)			
													644.51 (N2-PROC)	1292.63 (H4N2-PROC)	690.39 (H3N1)			
													806.32 (H1N2-PROC)	325.18 (H2)	731.18 (H2N2)			
													968.47 (H2N2-PROC)	366.08 (H1N1)	893.28 (H3N2)			
													1130.54 (H3N2-PROC)	528.20 (H2N1)	1055.42 (H4N2)			
10	19.0 (Cmpd 1174)	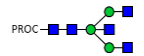	3	5	0	0	1739.75	870.38	580.59	n.d.	870.44	580.64	441.30 (N1-PROC)	1171.63 (H2N3-PROC)	689.99 (H3N1)	1299.55 (H3N4)		
													644.63 (N2-PROC)	1333.64 (H3N3-PROC)	731.00 (H2N2)			
													806.34 (H1N2-PROC)	1374.65 (H2N4-PROC)	893.38 (H3N2)			
													1009.38 (H2N3-PROC)	1536.69 (H3N4-PROC)	934.25 (H2N3)			
													1130.63 (H3N2-PROC)	366.13 (H1N1)	1096.46 (H3N3)			
11	19.2 (Cmpd 1181)	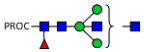	3	4	1	0	1682.72	841.87	561.58	1682.71	841.88	561.58	441.20 (N1-PROC)	952.50 (H1N2F1-PROC)	1155.38 (H2N3F1-PROC)	1479.70 (H3N3F1-PROC)	569.24 (H1N2)	1096.41 (H3N3)
													587.27 (N1F1-PROC)	968.58 (H2N2-PROC)	1171.65 (H2N3-PROC)	325.17 (H2)	690.13 (H3N1)	
													644.38 (N2-PROC)	1009.50 (H2N3-PROC)	1276.58 (H3N2F1-PROC)	366.15 (H1N1)	731.32 (H2N2)	
													790.41 (N2F1-PROC)	1114.54 (H2N2F1-PROC)	1317.65 (H2N3F1-PROC)	487.38 (H3)	893.30 (H3N2)	
													806.12 (H1N2-PROC)	1130.63 (H3N2-PROC)	1333.68 (H3N3-PROC)	528.18 (H2N1)	934.25 (H2N3)	

Table S4.1 (continued)

Peak ID	Retention time (min)	Structure	Composition				LC-ESI-MS						[M/Z] characteristic fragment ions (composition)					
			Hex (H)	HexNAc (N)	Fuc (F)	Neu5Ac (S)	$[M/Z]^{+}$ calculated	$[M/Z]^{2+}$ calculated	$[M/Z]^{3+}$ calculated	$[M/Z]^{+}$ registered	$[M/Z]^{2+}$ registered	$[M/Z]^{3+}$ registered						
12	20.1 (Cmpd 1239)	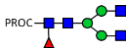	3	4	1	0	1682.72	841.87	561.58	n.d.	841.87	561.59	441.38 (N1-PROC)	1114.13 (H2N2F1-PROC)	487.18 (H3)			
													587.37 (N1F1-PROC)	1276.56 (H3N2F1-PROC)	690.22 (H3N1)			
													644.25 (N2-PROC)	1317.63 (H2N3F1-PROC)	731.30 (H2N2)			
													790.38 (N2F1-PROC)	1479.71 (H3N3F1-PROC)	893.35 (H3N2)			
													806.63 (H1N2-PROC)	325.13 (H2)	1096.50 (H3N3)			
13	20.4 (Cmpd 1256)	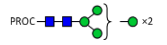	5	2	0	0	1454.61	727.81	485.54	1454.60	727.82	n.d.	441.27 (N1-PROC)	325.09 (H2)	852.35 (H4N1)			
													644.36 (N2-PROC)	366.17 (H1N1)	1014.38 (H5N1)			
													806.48 (H1N2-PROC)	487.13 (H3)				
													968.38 (H2N2-PROC)	528.19 (H2N1)				
													203.08 (N1)	690.18 (H3N1)				
14	20.3 (Cmpd 1258)		4	3	1	0	1641.70	821.35	547.90	n.d.	821.34	547.83	441.28 (N1-PROC)	952.45 (H1N2F1-PROC)	325.13 (H2)	731.22 (H2N2)		
													587.31 (N1F1-PROC)	968.39 (H2N2-PROC)	366.13 (H1N1)	852.13 (H4N1)		
													644.38 (N2-PROC)	1114.63 (H2N2F1-PROC)	487.50 (H3)	893.49 (H3N2)		
													790.48 (N2F1-PROC)	1130.56 (H3N2-PROC)	528.19 (H2N1)	1055.43 (H4N2)		
													805.76 (H1N2-PROC)	1276.61 (H3N2F1-PROC)	690.25 (H3N1)			
15	20.7 (Cmpd 1273)	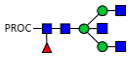	3	5	1	0	1885.80	943.41	629.27	n.d.	943.40	629.27	441.20 (N1-PROC)	1009.63 (H2N3-PROC)	1333.54 (H3N3-PROC)	325.06 (H2)	1299.50 (H3N4)	
													587.34 (N1F1-PROC)	1155.54 (H2N3F1-PROC)	1479.73 (H3N3F1-PROC)	366.06 (H1N1)		
													644.38 (N2-PROC)	1171.71 (H2N3-PROC)	1520.71 (H2N4F1-PROC)	569.14 (H1N2)		
													790.63 (N2F1-PROC)	1276.63 (H3N2F1-PROC)	1536.61 (H3N4-PROC)	731.35 (H2N2)		
													952.63 (H1N2F1-PROC)	1317.64 (H2N3F1-PROC)	1682.75 (H3N4F1-PROC)	1096.51 (H3N3)		
16	21.9 (Cmpd 1351)	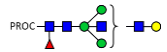	4	4	1	0	1844.78	922.89	615.60	n.d.	922.88	615.56	441.01 (N1-PROC)	952.13 (H1N2F1-PROC)	1155.63 (H2N3F1-PROC)	1374.75 (H2N4-PROC)	569.38 (H1N2)	1258.47 (H4N3)
													587.30 (N1F1-PROC)	968.38 (H2N2-PROC)	1171.60 (H2N3-PROC)	1479.67 (H3N3F1-PROC)	731.25 (H2N2)	
													644.25 (N2-PROC)	1009.50 (H2N3-PROC)	1276.44 (H3N2F1-PROC)	1641.71 (H4N3F1-PROC)	852.89 (H4N1)	
													790.00 (N2F1-PROC)	1114.50 (H2N2F1-PROC)	1317.62 (H2N3F1-PROC)	366.11 (H1N1)	893.26 (H3N2)	
													806.25 (H1N2-PROC)	1130.75 (H3N2-PROC)	1333.61 (H3N3-PROC)	528.15 (H2N1)	1096.39 (H3N3)	
17	22.4 (Cmpd 1377)		5	3	0	0	1657.69	829.35	553.24	n.d.	829.36	n.d.	441.27 (N1-PROC)	1454.70 (H5N2-PROC)	731.28 (H2N2)	1217.50 (H5N2)		
													644.34 (N2-PROC)	325.01 (H2)	811.69 (H5)			
													968.34 (H2N2-PROC)	366.08 (H1N1)	852.38 (H4N1)			
													1130.55 (H3N2-PROC)	528.51 (H2N1)	893.37 (H3N2)			
													1292.63 (H4N2-PROC)	690.25 (H3N1)	1055.14 (H4N2)			
18	23.4 (Cmpd 1437)	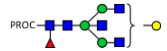	4	5	1	0	2047.86	1024.43	683.29	n.d.	1024.45	683.30	441.19 (N1-PROC)	968.43 (H2N2-PROC)	1317.65 (H2N3F1-PROC)	366.10 (H1N1)	934.50 (H2N3)	
													587.39 (N1F1-PROC)	1009.56 (H2N3-PROC)	1333.64 (H3N3-PROC)	528.21 (H2N1)	1096.46 (H3N3)	
													644.32 (N2-PROC)	1155.50 (H2N3F1-PROC)	1479.66 (H3N3F1-PROC)	569.01 (H1N2)	1258.48 (H4N3)	
													790.38 (N2F1-PROC)	1171.66 (H2N3-PROC)	1641.74 (H4N3F1-PROC)	731.21 (H2N2)		
													806.75 (H1N2-PROC)	1276.63 (H3N2F1-PROC)	203.90 (N1)	893.01 (H3N2)		
19	23.7 (Cmpd 1455)	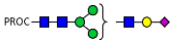	4	3	0	1	1786.74	893.87	596.25	n.d.	893.89	596.29	441.30 (N1-PROC)	1333.63 (H3N3-PROC)	657.25 (H1N1S1)	1143.63 (H4N1S1)		
													644.38 (N2-PROC)	1495.55 (H4N3-PROC)	690.38 (H3N1)	1184.45 (H3N2S1)		
													806.34 (H1N2-PROC)	325.23 (H2)	819.11 (H2N1S1)	1346.18 (H4N2S1)		
													968.49 (H2N2-PROC)	366.11 (H1N1)	981.51 (H3N1S1)			
													1130.54 (H3N2-PROC)	528.18 (H2N1)	1055.41 (H4N2)			
20	23.9 (Cmpd 1466)	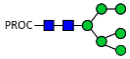	6	2	0	0	1616.67	808.84	539.56	n.d.	808.86	n.d.	441.29 (N1-PROC)	366.14 (H1N1)	852.29 (H4N1)			
													644.33 (N2-PROC)	487.76 (H3)	1014.36 (H5N1)			
													968.66 (H2N2-PROC)	528.15 (H2N1)	1176.44 (H6N1)			
													1130.38 (H3N2-PROC)	649.24 (H4)				
													325.10 (H2)	690.21 (H3N1)				
21	24.5 (Cmpd 1506)		5	4	0	0	1860.77	930.89	620.93	n.d.	930.90	620.96	644.50 (N2-PROC)	1495.67 (H4N3-PROC)	893.18 (H3N2)			
													968.13 (H2N2-PROC)	366.11 (H1N1)	1258.50 (H4N3)			
													1130.47 (H3N2-PROC)	528.13 (H2N1)	1420.38 (H5N3)			
													1171.88 (H2N3-PROC)	690.25 (H3N1)				
													1333.74 (H3N3-PROC)	731.14 (H2N2)				
22	25.2 (Cmpd 1549)		5	5	0	0	2063.85	1032.43	688.62	n.d.	1032.42	688.63	441.20 (N1-PROC)	1495.58 (H4N3-PROC)	1420.63 (H5N3)			
													968.49 (H2N2-PROC)	204.03 (N1)	1623.77 (H5N4)			
													1130.58 (H3N2-PROC)	366.11 (H1N1)				
													1171.47 (H2N3-PROC)	528.05 (H2N1)				
													1333.65 (H3N3-PROC)	1258.55 (H4N3)				
23	25.3 (Cmpd 1550)		4	3	1	1	1932.79	966.90	644.94	n.d.	966.91	644.95	441.25 (N1-PROC)	952.50 (H1N2F1-PROC)	1333.68 (H3N3-PROC)	325.08 (H2)	690.25 (H3N1)	1055.26 (H4N2)
													587.31 (N1F1-PROC)	1114.55 (H2N2F1-PROC)	1479.69 (H3N3F1-PROC)	366.14 (H1N1)	731.22 (H2N2)	1143.36 (H4N1S1)
													644.29 (N2-PROC)	1130.58 (H3N2-PROC)	1495.61 (H4N3-PROC)	454.13 (H1S1)	819.28 (H2N1S1)	1184.34 (H3N2S1)
													790.41 (N2F1-PROC)	1276.63 (H3N2F1-PROC)	1641.73 (H4N3F1-PROC)	528.19 (H2N1)	852.25 (H4N1)	1346.51 (H4N2S1)
													806.49 (H1N2-PROC)	1317.50 (H3N2F1-PROC)	292.05 (S1)	657.25 (H1N1S1)	893.90 (H3N2)	
24	25.6 (Cmpd 1568)	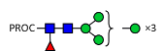	6	2	1	0	1762.72	881.87	588.25	n.d.	881.87	n.d.	441.29 (N1-PROC)	952.51 (H1N2F1-PROC)	528.10 (H2N1)	1014.34 (H5N1)		
													587.33 (N1F1-PROC)	968.38 (H2N2-PROC)	649.25 (H4)	1176.44 (H6N1)		
													644.29 (N2-PROC)	1130.13 (H3N2-PROC)	690.18 (H3N1)			
													790.41 (N2F1-PROC)	325.19 (H2)	811.07 (H5)			
													806.45 (H1N2-PROC)	366.13 (H1N1)	852.34 (H4N1)			
25	25.8 (Cmpd 1583)	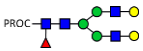	5	4	1	0	2006.83	1003.92	669.61	n.d.	1003.93	669.62	441.21 (N1-PROC)	952.72 (H1N2F1-PROC)	203.95 (N1)	893.29 (H3N2)		
													587.32 (N1F1-PROC)	968.49 (H2N2-PROC)	325.08 (H2)	1055.43 (H4N2)		
													644.19 (N2-PROC)	1114.53 (H2N2F1-PROC)	366.14 (H1N1)			
													790.38 (N2F1-PROC)	1130.62 (H3N2-PROC)	528.09 (H2N1)			
													806.36 (H1N2-PROC)	1276.63 (H3N2F1-PROC)	690.13 (H3N1)			
26	25.8 (Cmpd 1585)		6	3	0	0	1819.75	910.38	607.25	n.d.	910.38	607.28	441.23 (N1-PROC)	1333.38 (H3N3-PROC)	649.22 (H4)	1014.38 (H5N1)		
													644.25 (N2-PROC)	1454.66 (H5N2-PROC)	690.25 (H3N1)	1055.59 (H4N2)		
													968.01 (H2N2-PROC)	325.13 (H2)	811.71 (H5)	1379.48 (H6N2)		
													1130.55 (H3N2-PROC)	366.12 (H1N1)	852.13 (H4N1)			
													1292.52 (H4N2-PROC)	528.18 (H2N1)	893.00 (H3N2)			

Table S4.1 (continued)

Peak ID	Retention time (min)	Structure	Composition				LC-ESI-MS						[M/Z] characteristic fragment ions (composition)					
			Hex (H)	HexNAc (N)	Fuc (F)	Neu5Ac (S)	$[M/Z]^{+}$ calculated	$[M/Z]^{2+}$ calculated	$[M/Z]^{3+}$ calculated	$[M/Z]^{+}$ registered	$[M/Z]^{2+}$ registered	$[M/Z]^{3+}$ registered						
27	26.1 (Cmpd 1603)	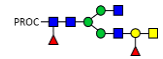	4	5	2	0	2193.91	1097.46	731.98	n.d.	1097.46	732.01	441.25 (N1-PROC)	968.63 (H2N2-PROC)	1317.68 (H2N3F1-PROC)	1787.67 (H4N3F2-PROC)	528.06 (H2N1)	1096.40 (H3N3)
													587.31 (N1F1-PROC)	1114.51 (H2N2F1-PROC)	1333.61 (H3N3-PROC)	204.01 (N1)	674.20 (H2N1F1)	1242.43 (H3N3F1)
													644.37 (N2-PROC)	1130.57 (H3N2-PROC)	1479.61 (H3N3F1-PROC)	325.14 (H2)	690.51 (H3N1)	1258.57 (H4N3)
													790.50 (N2F1-PROC)	1171.35 (H2N3-PROC)	1625.71 (H3N3F2-PROC)	366.08 (H1N1)	715.26 (H1N2F1)	1404.54 (H4N3F1)
													806.40 (H1N2-PROC)	1276.71 (H3N2F1-PROC)	1641.75 (H4N3F1-PROC)	512.15 (H1N1F1)	1039.38 (H3N2F1)	
28	26.4 (Cmpd 1619)	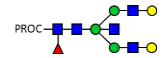	5	5	1	0	2209.91	1105.46	737.31	n.d.	1105.47	737.32	441.27 (N1-PROC)	1009.51 (H2N3-PROC)	1276.60 (H3N2F1-PROC)	1641.82 (H4N3F1-PROC)	569.28 (H1N2)	1217.63 (H5N2)
													587.33 (N1F1-PROC)	1114.42 (H2N2F1-PROC)	1317.70 (H2N3F1-PROC)	204.10 (N1)	690.25 (H3N1)	1258.46 (H4N3)
													644.17 (N2-PROC)	1130.63 (H3N2-PROC)	1333.67 (H3N3-PROC)	325.38 (H2)	893.62 (H3N2)	
													790.55 (N2F1-PROC)	1155.55 (H1N3F1-PROC)	1479.76 (H3N3F1-PROC)	366.11 (H1N1)	1055.38 (H4N2)	
													952.63 (H1N2F1-PROC)	1171.56 (H2N3-PROC)	1495.61 (H4N3-PROC)	528.07 (H2N1)	1096.38 (H3N3)	
29	26.6 (Cmpd 1630)		5	3	0	1	1948.79	974.90	650.27	n.d.	974.90	650.27	441.28 (N1-PROC)	1292.64 (H4N2-PROC)	454.00 (H1S1)	819.25 (H2N1S1)	1055.48 (H4N2)	
													644.34 (N2-PROC)	203.91 (N1)	528.18 (H2N1)	852.25 (H4N1)	1143.44 (H4N1S1)	
													806.50 (H1N2-PROC)	291.98 (S1)	657.21 (H1N1S1)	893.30 (H3N2)	1217.35 (H5N2)	
													968.55 (H2N2-PROC)	325.04 (H2)	690.16 (H3N1)	981.25 (H3N1S1)		
													1130.56 (H3N2-PROC)	366.10 (H1N1)	731.25 (H2N2)	1014.38 (H5N1)		
30	26.8 (Cmpd 1642)	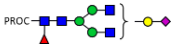	4	4	1	1	2135.87	1068.44	712.63	n.d.	1068.45	712.64	441.29 (N1-PROC)	952.50 (H1N2F1-PROC)	1276.62 (H3N2F1-PROC)	203.91 (N1)	528.19 (H2N1)	893.36 (H3N2)
													587.28 (N1F1-PROC)	968.52 (H2N2-PROC)	1333.59 (H3N3-PROC)	292.08 (S1)	657.20 (H1N1S1)	1055.33 (H4N2)
													644.19 (N2-PROC)	1114.56 (H2N2F1-PROC)	1479.70 (H3N3F1-PROC)	325.07 (H2)	690.29 (H3N1)	1184.45 (H3N2S1)
													790.26 (N2F1-PROC)	1130.52 (H3N2-PROC)	1495.81 (H4N3-PROC)	366.13 (H1N1)	731.32 (H2N2)	1346.27 (H4N2S1)
													806.37 (H1N2-PROC)	1171.68 (H2N3-PROC)	1641.78 (H4N3F1-PROC)	454.13 (H1S1)	819.06 (H2N1S1)	
31	27.3 (Cmpd 1672)		7	2	0	0	1778.72	889.86	593.58	n.d.	889.87	593.40	441.28 (N1-PROC)	325.06 (H2)	690.21 (H3N1)	1176.45 (H6N1)		
													644.38 (N2-PROC)	366.14 (H1N1)	811.19 (H5)	1338.47 (H7N1)		
													806.36 (H1N2-PROC)	487.09 (H3)	852.29 (H4N1)			
													968.47 (H2N2-PROC)	528.16 (H2N1)	973.15 (H6)			
													1130.59 (H3N2-PROC)	649.10 (H4)	1014.31 (H5N1)			
32	27.9 (Cmpd 1707)	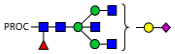	4	5	1	1	2338.95	1169.98	780.32	n.d.	1170.96	780.32	441.29 (N1-PROC)	968.52 (H2N2-PROC)	1171.62 (H2N3-PROC)	1536.75 (H3N4-PROC)	366.10 (H1N1)	731.35 (H2N2)
													587.25 (N1F1-PROC)	1009.63 (H2N3-PROC)	1276.68 (H3N2F1-PROC)	1641.63 (H4N3F1-PROC)	528.05 (H2N1)	819.18 (H2N1S1)
													644.43 (N2-PROC)	1114.74 (H2N2F1-PROC)	1317.62 (H2N3F1-PROC)	1682.89 (H3N4F1-PROC)	569.37 (H1N2)	1096.41 (H3N3)
													790.38 (N2F1-PROC)	1130.58 (H3N2-PROC)	1333.55 (H3N3-PROC)	1770.88 (H3N3F1S1-PROC)	690.35 (H3N1)	1184.51 (H3N2S1)
													806.40 (H1N2-PROC)	1155.63 (H1N3F1-PROC)	1479.66 (H3N3F1-PROC)	292.00 (S1)	657.21 (H1N1S1)	1258.38 (H4N3)
33	28.1 (Cmpd 1723)	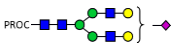	5	4	0	1	2151.87	1076.44	717.96	n.d.	1076.44	717.97	441.25 (N1-PROC)	1333.51 (H3N3-PROC)	366.13 (H1N1)	731.32 (H2N2)	1184.53 (H3N2S1)	
													644.20 (N2-PROC)	1495.65 (H4N3-PROC)	454.20 (H1S1)	819.30 (H2N1S1)	1258.47 (H4N3)	
													806.48 (H1N2-PROC)	204.03 (N1)	528.19 (H2N1)	981.43 (H3N1S1)	1346.49 (H4N2S1)	
													968.46 (H2N2-PROC)	292.04 (S1)	657.21 (H1N1S1)	1055.34 (H4N2)	1420.55 (H5N3)	
													1130.56 (H3N2-PROC)	325.03 (H2)	690.24 (H3N1)	1096.00 (H3N3)		
34	28.7 (Cmpd 1758)	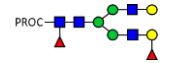	5	4	2	0	2152.89	1076.95	718.30	n.d.	1076.94	718.28	441.17 (N1-PROC)	968.26 (H2N2-PROC)	309.24 (H1F1)	690.25 (H3N1)	1363.25 (H5N2F1)	
													587.38 (N1F1-PROC)	1114.51 (H2N2F1-PROC)	325.13 (H2)	893.48 (H3N2)		
													644.38 (N2-PROC)	1130.51 (H3N2-PROC)	366.08 (H1N1)	1014.13 (H5N1)		
													806.38 (H1N2-PROC)	1276.64 (H3N2F1-PROC)	512.19 (H1N1F1)	1201.44 (H4N2F1)		
													952.39 (H1N2F1-PROC)	203.76 (N1)	528.13 (H2N1)	1242.75 (H3N3F1)		
35	28.8 (Cmpd 1764)	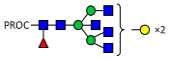	5	6	1	0	2412.99	1207.00	805.00	n.d.	n.d.	805.01	441.35 (N1-PROC)	1155.50 (H1N3F1-PROC)	1698.75 (H4N4-PROC)	1137.63 (H2N4)		
													587.29 (N1F1-PROC)	1171.55 (H2N3-PROC)	1844.75 (H4N4F1-PROC)	1461.5 (H4N4)		
													790.38 (N2F1-PROC)	1479.69 (H3N3F1-PROC)	366.09 (H1N1)	1623.63 (H5N4)		
													952.38 (H1N2F1-PROC)	1536.79 (H3N4-PROC)	731.32 (H2N2)			
													1114.13 (H2N2F1-PROC)	1682.90 (H3N4F1-PROC)	893.76 (H3N2)			
36	29.0 (Cmpd 1776)	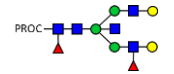	5	5	2	0	2355.97	1178.49	785.99	n.d.	1178.43	785.99	441.23 (N1-PROC)	1130.50 (H3N2-PROC)	1463.71 (H2N3F2-PROC)	1787.75 (H4N3F2-PROC)	690.37 (H3N1)	1096.51 (H3N3)
													587.27 (N1F1-PROC)	1155.68 (H1N3F1-PROC)	1479.66 (H3N3F1-PROC)	366.12 (H1N1)	731.38 (H2N2)	1242.25 (H3N3F1)
													644.30 (N2-PROC)	1171.58 (H2N3-PROC)	1495.5 (H4N3-PROC)	487.01 (H3)	836.33 (H3N1F1)	1258.51 (H4N3)
													806.37 (H1N2-PROC)	1276.49 (H3N2F1-PROC)	1625.71 (H3N3F2-PROC)	512.18 (H1N1F1)	877.38 (H2N2F1)	1404.46 (H4N3F1)
													952.50 (H1N2F1-PROC)	1317.54 (H2N3F1-PROC)	1641.51 (H4N3F1-PROC)	569.38 (H1N2)	1039.5 (H3N2F1)	1420.38 (H5N3)
													968.63 (H2N2-PROC)	1333.63 (H3N3-PROC)	1698.63 (H4N4-PROC)	674.43 (H2N1F1)	1055.36 (H4N2)	1623.55 (H5N4)
37	29.1 (Cmpd 1779)	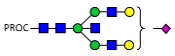	5	5	0	1	2354.95	1177.98	785.65	n.d.	1177.92	785.66	441.30 (N1-PROC)	1171.48 (H2N3-PROC)	1786.76 (H4N3S1-PROC)	657.20 (H1N1S1)	981.00 (H3N1S1)	1623.63 (H5N4)
													644.41 (N2-PROC)	1333.66 (H3N3-PROC)	325.10 (H2)	731.26 (H2N2)	1096.38 (H3N3)	1711.63 (H5N3S1)
													968.61 (H2N2-PROC)	1495.79 (H4N3-PROC)	366.15 (H1N1)	819.49 (H2N1S1)	1184.38 (H3N2S1)	
													1009.13 (H2N3-PROC)	1624.73 (H3N3S1-PROC)	528.18 (H2N1)	852.25 (H4N1)	1258.52 (H4N3)	
													1130.47 (H3N2-PROC)	1698.72 (H4N4-PROC)	569.16 (H1N2)	934.88 (H2N3)	1346.63 (H4N2S1)	
38	29.4 (Cmpd 1797)	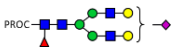	5	4	1	1	2297.93	1149.47	766.65	n.d.	1149.49	766.66	441.25 (N1-PROC)	952.42 (H1N2F1-PROC)	1317.51 (H2N3F1-PROC)	292.03 (S1)	657.22 (H1N1S1)	981.38 (H3N1S1)
													587.29 (N1F1-PROC)	968.45 (H2N2-PROC)	1333.58 (H3N3-PROC)	325.10 (H2)	690.25 (H3N1)	1055.43 (H4N2)
													644.44 (N2-PROC)	1114.57 (H2N2F1-PROC)	1479.67 (H3N3F1-PROC)	366.11 (H1N1)	731.30 (H2N2)	1096.64 (H3N3)
													790.23 (N2F1-PROC)	1130.52 (H3N2-PROC)	1495.71 (H4N3-PROC)	453.98 (H1S1)	819.23 (H2N1S1)	1143.55 (H4N1S1)
													806.47 (H1N2-PROC)	1276.60 (H3N2F1-PROC)	1641.73 (H4N3F1-PROC)	528.14 (H2N1)	893.28 (H3N2)	1184.51 (H3N2S1)
39	29.6 (Cmpd 1810)	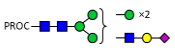	6	3	0	1	2110.84	1055.92	704.28	n.d.	1056.36	703.30	441.28 (N1-PROC)	1292.55 (H4N2-PROC)	366.08 (H1N1)	690.19 (H3N1)	1055.33 (H4N2)	
													644.34 (N2-PROC)	1454.71 (H5N2-PROC)	454.08 (H1S1)	819.25 (H2N1S1)	1143.50 (H4N1S1)	
													806.31 (H1N2-PROC)	203.93 (N1)	487.25 (H3)	852.28 (H4N1)	1217.32 (H5N2)	
													968.51 (H2N2-PROC)	291.99 (S1)	528.21 (H2N1)	981.44 (H3N1S1)	1305.01 (H5N1S1)	
													1130.64 (H3N2-PROC)	325.02 (H2)	657.20 (H1N1S1)	1014.32 (H5N1)	1379.43 (H6N2)	
40	30.2 (Cmpd 1846)	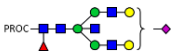	5	5	1	1	2501.01	1251.01	834.34	n.d.	1250.98	834.36	441.32 (N1-PROC)	1009.50 (H2N3-PROC)	1333.59 (H3N3-PROC)	1844.89 (H4N4F1-PROC)	528.15 (H2N1)	893.75 (H3N2)
													587.22 (N1F1-PROC)	1130.41 (H3N2-PROC)	1479.57 (H3N3F1-PROC)	1932.75 (H4N3F1S1-PROC)	569.23 (H1N2)	934.38 (H2N3)
													644.39 (N2-PROC)	1155.88 (H1N3F1-PROC)	1495.63 (H4N3-PROC)	292.13 (S1)	657.19 (H1N1S1)	981.13 (H3N1S1)
													790.25 (N2F1-PROC)	1171.51 (H2N3-PROC)	1641.50 (H4N3F1-PROC)	325.08 (H2)	731.13 (H2N2)	1055.38 (H4N2)
													952.50 (H1N2F1-PROC)	1276.64 (H3N2F1-PROC)	1682.50 (H3N4F1-PROC)	366.13 (H1N1)	819.25 (H2N1S1)	1096.50 (H3N3)
													968.54 (H2N2-PROC)	1317.69 (H3N2F1-PROC)	1698.88 (H4N4-PROC)	454.10 (H1S1)	852.38 (H4N1)	1184.88 (H3N2S1)
41	30.3 (Cmpd 1851)	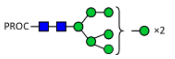	8	2	0	0	1940.77	970.89	647.60	n.d.	970.88	n.d.	441.28 (N1-PROC)	1454.63 (H5N2-PROC)	649.15 (H4)	1176.42 (H6N1)		
													644.32 (N2-PROC)	325.10 (H2)	690.18 (H3N1)	1297.88 (H8)		
													806.42 (H1N2-PROC)	366.09 (H1N1)	811.16 (H5)	1338.46 (H7N1)		
													1130.57 (H3N2-PROC)	487.18 (H3)	852.30 (H4N1)	1500.59 (H8N1)		
													1292.64 (H4N2-PROC)	528.22 (H2N1)	1014.39 (H5N1)			

Table S4.1 (continued)

Peak ID	Retention time (min)	Structure	Composition				LC-ESI-MS						[M/Z] characteristic fragment ions (composition)					
			Hex (H)	HexNAc (N)	Fuc (F)	Neu5Ac (S)	$[M/Z]^{+}$ calculated	$[M/Z]^{2+}$ calculated	$[M/Z]^{3+}$ calculated	$[M/Z]^{+}$ registered	$[M/Z]^{2+}$ registered	$[M/Z]^{3+}$ registered						
42	30.7 (Cmpd 1879)		6	5	1	0	2371.96	1186.48	791.33	n.d.	n.d.	791.34	441.15 (N1-PROC)	1479.76 (H3N3F1-PROC)	569.26 (H1N2)	1420.51 (H5N3)		
													587.32 (N1F1-PROC)	1495.72 (H4N3-PROC)	731.27 (H2N2)			
													1276.63 (H3N2F1-PROC)	1641.77 (H4N3F1-PROC)	852.25 (H4N1)			
													1317.50 (H2N3F1-PROC)	366.09 (H1N1)	893.30 (H3N2)			
													1333.72 (H3N3-PROC)	528.16 (H2N1)	1055.38 (H4N2)			
43	30.8 (Cmpd 1883)	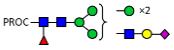	6	3	1	1	2256.90	1128.95	752.97	n.d.	1128.93	752.98	441.28 (N1-PROC)	952.53 (H1N2F1-PROC)	1438.67 (H4N2F1-PROC)	366.11 (H1N1)	731.38 (H2N2)	1014.44 (H5N1)
													587.30 (N1F1-PROC)	968.45 (H2N2-PROC)	1454.45 (H5N2-PROC)	487.25 (H3)	811.38 (H5)	1055.33 (H4N2)
													644.37 (N2-PROC)	1130.56 (H3N2-PROC)	1600.61 (H5N2F1-PROC)	528.13 (H2N1)	819.21 (H2N1S1)	1379.39 (H6N2)
													790.50 (N2F1-PROC)	1276.61 (H3N2F1-PROC)	292.00 (S1)	657.20 (H1N1S1)	852.32 (H4N1)	
													806.51 (H1N2-PROC)	1292.43 (H4N2-PROC)	325.10 (H2)	690.31 (H3N1)	893.80 (H3N2)	
44	31.2 (Cmpd 1905)	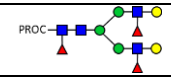	5	5	3	0	2298.95	1149.98	766.99	n.d.	1149.96	766.99	441.20 (N1-PROC)	952.39 (H1N2F1-PROC)	1641.63 (H4N3F1-PROC)	512.20 (H1N1F1)	893.38 (H3N2)	1201.47 (H4N2F1)
													587.38 (N1F1-PROC)	968.41 (H2N2-PROC)	325.25 (H2)	528.17 (H2N1)	998.13 (H4N1F1)	1258.75 (H4N3)
													644.33 (N2-PROC)	1114.50 (H2N2F1-PROC)	350.04 (N1F1)	674.08 (H2N1F1)	1039.55 (H3N2F1)	1347.62 (H4N2F2)
													790.41 (N2F1-PROC)	1130.52 (H3N2-PROC)	366.09 (H1N1)	690.25 (H3N1)	1055.50 (H4N2)	1404.63 (H4N3F1)
													806.38 (H1N2-PROC)	1276.61 (H3N2F1-PROC)	487.00 (H3)	731.13 (H2N2)	1185.76 (H3N2F2)	1420.51 (H5N3)
45	31.4 (Cmpd 1917)		5	4	1	2	2589.02	1295.01	863.68	n.d.	1295.03	863.68	441.33 (N1-PROC)	952.56 (H1N2F1-PROC)	1276.59 (H3N2F1-PROC)	1624.00 (H4N3S1-PROC)	325.25 (H2)	690.25 (H3N1)
													587.33 (N1F1-PROC)	968.42 (H2N2-PROC)	1317.63 (H2N3F1-PROC)	1641.70 (H4N3F1-PROC)	366.14 (H1N1)	731.43 (H2N2)
													644.44 (N2-PROC)	1114.52 (H2N2F1-PROC)	1333.66 (H3N3-PROC)	1786.75 (H4N3S1-PROC)	454.10 (H1S1)	819.30 (H2N1S1)
													790.44 (N2F1-PROC)	1130.61 (H3N2-PROC)	1479.76 (H3N3F1-PROC)	1932.72 (H4N3F1S1-PROC)	528.24 (H2N1)	852.47 (H4N1)
													806.38 (H1N2-PROC)	1171.38 (H2N3-PROC)	1495.66 (H4N3-PROC)	292.09 (S1)	657.21 (H1N1S1)	893.88 (H3N2)
46	31.4 (Cmpd 1918)	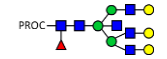	6	6	1	0	2575.04	1288.02	859.02	n.d.	n.d.	859.03	587.25 (N1F1-PROC)	1009.76 (H1N3-PROC)	1844.75 (H4N4F1-PROC)	893.22 (H3N2)		
													644.25 (N2-PROC)	1479.50 (H3N3F1-PROC)	2006.96 (H5N4F1-PROC)	934.50 (H2N3)		
													790.38 (N2F1-PROC)	1536.88 (H3N4-PROC)	325.13 (H2)	1258.38 (H4N3)		
													952.63 (H1N2F1-PROC)	1641.85 (H4N3F1-PROC)	366.10 (H1N1)	1623.52 (H5N4)		
													968.47 (H2N2-PROC)	1682.68 (H3N4F1-PROC)	528.00 (H2N1)			
47	31.6 (Cmpd 1929)	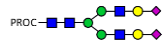	5	4	0	2	2442.96	1221.99	814.99	n.d.	1221.95	815.00	441.31 (N1-PROC)	1495.65 (H4N3-PROC)	366.13 (H1N1)	731.75 (H2N2)	1143.50 (H4N1S1)	
													644.33 (N2-PROC)	1624.63 (H4N3S1-PROC)	454.12 (H1S1)	852.75 (H4N1)	1184.51 (H3N2S1)	
													968.49 (H2N2-PROC)	1786.51 (H4N3S1-PROC)	528.15 (H2N1)	893.13 (H3N2)	1346.53 (H4N2S1)	
													1130.58 (H3N2-PROC)	292.06 (S1)	657.22 (H1N1S1)	1055.30 (H4N2)	1420.38 (H5N3)	
													1333.67 (H3N3-PROC)	325.21 (H2)	690.20 (H3N1)	1096.38 (H3N3)	1508.49 (H5N2S1)	
48	31.6 (Cmpd 1930)	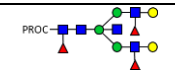	5	5	3	0	2502.03	1251.52	834.68	n.d.	1251.45	834.69	441.27 (N1-PROC)	1114.13 (H2N2F1-PROC)	1463.50 (H2N3F2-PROC)	350.00 (N1F1)	731.25 (H2N2)	1217.38 (H5N2)
													587.26 (N1F1-PROC)	1155.63 (H1N3F1-PROC)	1479.67 (H3N3F1-PROC)	366.10 (H1N1)	852.26 (H4N1)	1550.25 (H4N3F2)
													790.38 (N2F1-PROC)	1171.62 (H2N3-PROC)	1625.70 (H4N3F2-PROC)	487.88 (H3)	877.36 (H2N2F1)	
													806.24 (H1N2-PROC)	1276.63 (H3N2F1-PROC)	1641.88 (H4N3F1-PROC)	512.15 (H1N1F1)	893.50 (H3N2)	
													1009.13 (H1N3-PROC)	1333.60 (H3N3-PROC)	325.04 (H2)	528.25 (H2N1)	1201.38 (H4N2F1)	
49	31.6 (Cmpd 1932)	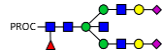	5	5	1	2	2792.10	1396.55	931.37	n.d.	n.d.	931.37	441.38 (N1-PROC)	1130.49 (H3N2-PROC)	1479.73 (H3N3F1-PROC)	1698.81 (H4N4-PROC)	325.03 (H2)	819.24 (H2N1S1)
													587.30 (N1F1-PROC)	1155.38 (H1N3F1-PROC)	1495.63 (H4N3-PROC)	1770.66 (H3N3F1S1-PROC)	366.10 (H1N1)	893.79 (H3N2)
													644.31 (N2-PROC)	1171.55 (H2N3-PROC)	1520.63 (H2N4F1-PROC)	1844.74 (H4N4F1-PROC)	454.14 (H1S1)	1055.25 (H4N2)
													790.43 (N2F1-PROC)	1276.50 (H3N2F1-PROC)	1536.50 (H3N4-PROC)	1932.81 (H4N3F1S1-PROC)	569.13 (H1N2)	1096.41 (H3N3)
													968.42 (H2N2-PROC)	1317.70 (H3N3F1-PROC)	1641.53 (H4N3F1-PROC)	2135.94 (H4N4F1S1-PROC)	657.21 (H1N1S1)	1184.38 (H3N2S1)
													1114.62 (H2N2F1-PROC)	1333.70 (H3N3-PROC)	1682.69 (H3N4F1-PROC)	292.07 (S1)	731.13 (H2N2)	1346.50 (H4N2S1)
50	32.0 (Cmpd 1953)	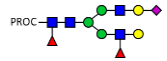	5	4	2	1	2443.98	1222.50	815.33	n.d.	1222.45	815.35	441.30 (N1-PROC)	968.38 (H2N2-PROC)	1495.64 (H4N3-PROC)	366.12 (H1N1)	690.25 (H3N1)	1039.21 (H3N2F1)
													587.36 (N1F1-PROC)	1114.52 (H2N2F1-PROC)	1641.82 (H4N3F1-PROC)	453.89 (H1S1)	731.75 (H2N2)	1055.38 (H4N2)
													644.33 (N2-PROC)	1130.55 (H3N2-PROC)	1786.88 (H4N3S1-PROC)	512.24 (H1N1F1)	836.50 (H3N1F1)	1143.63 (H4N1S1)
													790.39 (N2F1-PROC)	1171.51 (H2N3-PROC)	292.07 (S1)	528.20 (H2N1)	877.38 (H2N2F1)	1184.23 (H3N2S1)
													806.15 (H1N2-PROC)	1276.60 (H3N2F1-PROC)	325.00 (H2)	657.21 (H1N1S1)	893.25 (H3N2)	1201.45 (H4N2F1)
													952.56 (H1N2F1-PROC)	1479.86 (H3N3F1-PROC)	350.06 (N1F1)	674.22 (H2N1F1)	981.36 (H3N1S1)	1258.70 (H4N3)
51	32.1 (Cmpd 1964)	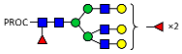	6	5	3	0	2664.08	1332.54	888.70	n.d.	n.d.	888.71	441.30 (N1-PROC)	968.39 (H2N2-PROC)	1495.58 (H4N3-PROC)	512.03 (H1N1F1)		
													587.35 (N1F1-PROC)	1276.63 (H3N2F1-PROC)	1641.74 (H4N3F1-PROC)	1055.38 (H4N2)		
													644.01 (N2-PROC)	1317.63 (H2N3F1-PROC)	1787.98 (H4N3F2-PROC)	1217.38 (H5N2)		
													790.13 (N2F1-PROC)	1333.44 (H3N3-PROC)	2006.76 (H5N4F1-PROC)	1420.50 (H5N3)		
													952.63 (H1N2F1-PROC)	1479.75 (H3N3F1-PROC)	366.10 (H1N1)	1712.60 (H5N3F2)		
52	32.2 (Cmpd 1966)	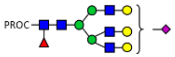	6	5	1	1	2663.06	1332.03	888.36	n.d.	n.d.	888.37	587.36 (N1F1-PROC)	1171.38 (H2N3-PROC)	1495.62 (H4N3-PROC)	292.00 (S1)	852.25 (H4N1)	
													644.13 (N2-PROC)	1276.38 (H2N2F1-PROC)	1641.74 (H4N3F1-PROC)	366.08 (H1N1)	1022.51 (H2N2S1)	
													790.17 (N2F1-PROC)	1317.63 (H2N3F1-PROC)	1844.75 (H4N4F1-PROC)	528.38 (H2N1)	1420.49 (H5N3)	
													952.50 (H1N2F1-PROC)	1333.57 (H3N3-PROC)	1932.90 (H4N3F1S1-PROC)	657.21 (H1N1S1)	1711.63 (H5N3S1)	
													1114.63 (H2N2F1-PROC)	1479.64 (H3N3F1-PROC)	2006.89 (H5N4F1-PROC)	731.23 (H2N2)		
53	32.5 (Cmpd 1983)		9	2	0	0	2102.82	1051.92	701.61	n.d.	1051.90	701.70	441.30 (N1-PROC)	1292.70 (H4N2-PROC)	528.25 (H2N1)	973.29 (H6)	1500.54 (H8N1)	
													644.37 (N2-PROC)	1454.66 (H5N2-PROC)	649.19 (H4)	1014.35 (H5N1)	1662.58 (H9N1)	
													806.41 (H1N2-PROC)	325.07 (H2)	690.25 (H3N1)	1135.38 (H7)		
													968.55 (H2N2-PROC)	366.17 (H1N1)	811.41 (H5)	1176.39 (H6N1)		
													1130.67 (H3N2-PROC)	487.09 (H3)	852.31 (H4N1)	1338.51 (H7N1)		
54	32.7 (Cmpd 2000)		5	4	1	2	2589.02	1295.01	863.68	n.d.	n.d.	863.69	441.43 (N1-PROC)	952.55 (H1N2F1-PROC)	1276.57 (H3N2F1-PROC)	1786.78 (H4N3S1-PROC)	528.16 (H2N1)	893.00 (H3N2)
													587.31 (N1F1-PROC)	968.42 (H2N2-PROC)	1333.72 (H3N3-PROC)	1932.90 (H4N3F1S1-PROC)	657.24 (H1N1S1)	981.38 (H3N1S1)
													644.33 (N2-PROC)	1114.55 (H2N2F1-PROC)	1479.64 (H3N3F1-PROC)	292.10 (S1)	690.76 (H3N1)	1055.36 (H4N2)
													790.39 (N2F1-PROC)	1130.56 (H3N2-PROC)	1495.75 (H4N3-PROC)	325.13 (H2)	819.20 (H2N1S1)	1184.43 (H3N2S1)
													806.42 (H1N2-PROC)	1171.58 (H2N3-PROC)	1641.70 (H4N3F1-PROC)	366.12 (H1N1)	852.63 (H4N1)	1346.52 (H4N2S1)
55	33.1 (Cmpd 2022)	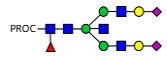	5	5	1	2	2792.10	1396.55	931.37	n.d.	n.d.	931.38	441.29 (N1-PROC)	1114.50 (H2N2F1-PROC)	1479.68 (H3N3F1-PROC)	1932.75 (H4N3F1S1-PROC)	528.14 (H2N1)	1184.63 (H3N2S1)
													587.30 (N1F1-PROC)	1130.50 (H3N2-PROC)	1495.75 (H4N3-PROC)	1973.63 (H3N4F1S1-PROC)	569.25 (H1N2)	1217.50 (H5N2)
													644.39 (N2-PROC)	1155.42 (H1N3F1-PROC)	1520.88 (H2N4F1-PROC)	1989.90 (H4N4S1-PROC)	657.22 (H1N1S1)	1258.57 (H4N3)
													790.50 (N2F1-PROC)	1171.56 (H2N3-PROC)	1698.70 (H4N4-PROC)	2135.97 (H4N4F1S1-PROC)	731.50 (H2N2)	1346.57 (H4N2S1)
													806.38 (H1N2-PROC)	1276.71 (H3N2F1-PROC)	1770.80 (H3N3F1S1-PROC)	292.00 (S1)	819.36 (H2N1S1)	1387.63 (H3N3S1)
													968.53 (H2N2-PROC)	1317.59 (H2N3F1-PROC)	1786.88 (H4N3S1-PROC)	325.00 (H2)	893.83 (H3N2)	1420.63 (H5N3)
													1009.68 (H1N3-PROC)	1333.66 (H3N3-PROC)	1844.74 (H4N4F1-PROC)	366.11 (H1N1)	981.38 (H3N1S1)	1549.64 (H4N3S1)

Table S4.1 (continued)

Peak ID	Retention time (min)	Structure	Composition				LC-ESI-MS						[M/Z] characteristic fragment ions (composition)					
			Hex (H)	HexNAc (N)	Fuc (F)	Neu5Ac (S)	$[M/Z]^{+}$ calculated	$[M/Z]^{2+}$ calculated	$[M/Z]^{3+}$ calculated	$[M/Z]^{+}$ registered	$[M/Z]^{2+}$ registered	$[M/Z]^{3+}$ registered						
56	34.1 (Cmpd 2079)	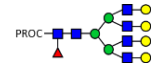	7	6	1	0	2737.09	1369.05	913.04	n.d.	n.d.	913.03	441.38 (N1-PROC)	1114.54 (H2N2F1-PROC)	1641.63 (H4N3F1-PROC)	569.38 (H1N2)	1420.38 (H5N3)		
													587.50 (N1F1-PROC)	1276.50 (H3N2F1-PROC)	1844.87 (H4N4F1-PROC)	731.23 (H2N2)	1785.63 (H6N4)		
													644.38 (N2-PROC)	1333.22 (H3N3-PROC)	1860.63 (H5N4-PROC)	852.75 (H4N1)			
													952.50 (H1N2F1-PROC)	1479.67 (H3N3F1-PROC)	2006.89 (H5N4F1-PROC)	893.43 (H3N2)			
													968.87 (H2N2-PROC)	1495.78 (H4N3-PROC)	366.14 (H1N1)	934.38 (H2N3)			
57	34.3 (Cmpd 2095)	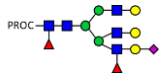	6	5	2	1	2809.12	1405.06	937.04	n.d.	n.d.	937.04	441.39 (N1-PROC)	1171.63 (H2N3-PROC)	1641.67 (H4N3F1-PROC)	2078.63 (H4N3S1F2-PROC)	569.13 (H1N2)	877.38 (H2N2F1)	1330.75 (H3N2S1F1)
													587.32 (N1F1-PROC)	1317.54 (H2N3F1-PROC)	1786.74 (H4N3S1-PROC)	2135.78 (H4N4F1S1-PROC)	657.25 (H1N1S1)	965.27 (H2N1S1F1)	1404.56 (H4N3F1)
													790.00 (N2F1-PROC)	1333.75 (H3N3-PROC)	1787.81 (H4N3F2-PROC)	2153.06 (H5N4F2-PROC)	674.13 (H2N1F1)	1080.39 (H2N3F1)	1420.42 (H5N3)
													806.00 (H1N2-PROC)	1479.69 (H3N3F1-PROC)	1844.90 (H4N4F1-PROC)	366.10 (H1N1)	731.13 (H2N2)	1168.38 (H2N2S1F1)	1508.50 (H5N2S1)
													968.44 (H2N2-PROC)	1495.68 (H4N3-PROC)	1932.97 (H4N3F1S1-PROC)	512.27 (H1N1F1)	803.14 (H1N1S1F1)	1201.38 (H4N2F1)	1711.51 (H5N3S1)
													1114.50 (H2N2F1-PROC)	1520.88 (H2N4F1-PROC)	1991.00 (H4N4F2-PROC)	528.25 (H2N1)	819.30 (H2N1S1)	1242.25 (H3N3F1)	1857.85 (H5N3F1S1)
58	34.4 (Cmpd 2100)	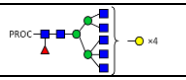	7	7	1	0	2940.17	1470.59	980.73	n.d.	n.d.	980.70	790.51 (N2F1-PROC)	1317.63 (H2N3F1-PROC)	366.11 (H1N1)	1055.41 (H4N2)			
													806.50 (H1N2-PROC)	1682.66 (H3N4F1-PROC)	528.25 (H2N1)	1096.50 (H3N3)			
													952.13 (H1N2F1-PROC)	2063.92 (H5N5-PROC)	852.63 (H4N1)	1137.5 (H2N4)			
													1114.50 (H2N2F1-PROC)	2209.95 (H5N5F1-PROC)	893.20 (H3N2)	1785.25 (H6N4)			
													1171.39 (H2N3-PROC)	2372.06 (H6N5F1-PROC)	934.88 (H2N3)	1988.75 (H6N5)			
59	34.7 (Cmpd 2118)	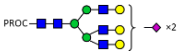	6	5	0	2	2808.10	1404.55	936.70	n.d.	n.d.	936.68	441.38 (N1-PROC)	1495.85 (H4N3-PROC)	657.24 (H1N1S1)	1022.63 (H2N2S1)			
													644.63 (N2-PROC)	1786.74 (H4N3S1-PROC)	819.14 (H2N1S1)	1055.50 (H4N2)			
													806.40 (H1N2-PROC)	366.08 (H1N1)	852.63 (H4N1)	1785.63 (H6N4)			
													968.50 (H2N2-PROC)	528.13 (H2N1)	893.38 (H3N2)	1873.40 (H6N3S1)			
													1333.55 (H3N3-PROC)	569.88 (H1N2)	981.00 (H3N1S1)	2002.50 (H5N3S2)			
60	35.2 (Cmpd 2146)	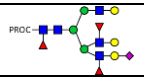	6	5	3	1	2955.17	1478.10	985.73	n.d.	n.d.	985.71	441.50 (N1-PROC)	1641.63 (H4N3F1-PROC)	657.16 (H1N1S1)	934.75 (H2N3)	1258.75 (H4N3)		
													968.50 (H2N2-PROC)	1786.75 (H4N3S1-PROC)	803.38 (H1N1S1F1)	965.79 (H2N1F1S1)	1314.38 (H2N2S1F2)		
													1114.50 (H2N2F1-PROC)	1932.76 (H4N3F1S1-PROC)	836.88 (H3N1F1)	1022.38 (H2N2S1)			
													1171.01 (H2N3-PROC)	366.10 (H1N1)	852.63 (H4N1)	1023.25 (H2N2F2)			
													1276.63 (H3N2F1-PROC)	512.25 (H1N1F1)	893.75 (H3N2)	1143.00 (H4N1S1)			
61	35.2 (Cmpd 2148)	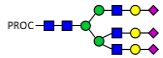	6	5	0	3	3099.19	1550.10	1033.74	n.d.	n.d.	1033.70	441.16 (N1-PROC)	1171.50 (H2N3-PROC)	1860.75 (H5N4-PROC)	366.14 (H1N1)	934.63 (H2N3)	1549.50 (H4N3S1)	
													644.25 (N2-PROC)	1333.65 (H3N3-PROC)	2151.75 (H5N4S1-PROC)	528.19 (H2N1)	1022.50 (H2N2S1)	1711.41 (H5N3S1)	
													806.57 (H1N2-PROC)	1495.72 (H4N3-PROC)	291.89 (S1)	657.20 (H1N1S1)	1184.63 (H3N2S1)		
													968.66 (H2N2-PROC)	1624.85 (H4N3S1-PROC)	325.13 (H2)	690.29 (H3N1)	1299.75 (H3N4)		
													1130.44 (H3N2-PROC)	1786.72 (H4N3S1-PROC)	454.13 (H1S1)	819.30 (H2N1S1)	1475.74 (H3N2S2)		
62	36.4 (Cmpd 2217)	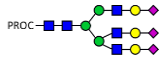	6	5	0	3	3099.19	1550.10	1033.74	n.d.	n.d.	1033.73	441.41 (N1-PROC)	1333.68 (H3N3-PROC)	1827.88 (H3N4F2-PROC)	292.01 (S1)	657.21 (H1N1S1)	1022.38 (H2N2S1)	2205.64 (H5N4S2)
													644.25 (N2-PROC)	1495.67 (H4N3-PROC)	1860.76 (H5N4-PROC)	325.13 (H2)	731.3 (H2N2)	1184.62 (H3N2S1)	
													806.34 (H1N2-PROC)	1536.75 (H3N4-PROC)	1989.88 (H4N4S1-PROC)	454.25 (H1S1)	819.42 (H2N1S1)	1475.48 (H3N2S2)	
													968.44 (H2N2-PROC)	1624.88 (H4N3S1-PROC)	2151.79 (H5N4S1-PROC)	366.10 (H1N1)	852.00 (H4N1)	1799.88 (H5N2S2)	
													1130.32 (H3N2-PROC)	1786.81 (H4N3S1-PROC)	2442.81 (H5N4S2-PROC)	528.38 (H2N1)	934.59 (H2N3)	2002.86 (H5N3S2)	
63	36.4 (Cmpd 2218)	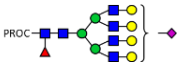	7	6	1	1	3028.19	1514.60	1010.07	n.d.	n.d.	1010.06	587.38 (N1F1-PROC)	1770.75 (H3N3F1S1-PROC)	731.25 (H2N2)	1184.38 (H3N2S1)			
													790.00 (N2F1-PROC)	2006.85 (H5N4F1-PROC)	981.38 (H3N1S1)	2076.75 (H6N4S1)			
													1114.52 (H2N2F1-PROC)	2297.90 (H5N4F1S1-PROC)	1022.50 (H2N2S1)				
													1479.71 (H3N3F1-PROC)	366.17 (H1N1)	1096.00 (H3N3)				
													1641.63 (H4N3F1-PROC)	657.10 (H1N1S1)	1143.26 (H4N1S1)				
64	36.5 (Cmpd 2228)	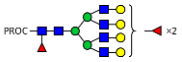	7	6	3	0	3029.21	1515.11	1010.41	n.d.	n.d.	1010.38	441.04 (N1-PROC)	1495.63 (H4N3-PROC)	569.25 (H1N2)	998.50 (H4N1F1)			
													1130.88 (H3N2-PROC)	1641.63 (H4N3F1-PROC)	731.50 (H2N2)	1023.13 (H2N2F2)			
													1171.50 (H2N3-PROC)	2006.85 (H5N4F1-PROC)	852.13 (H4N1)	1055.00 (H4N2)			
													1333.01 (H3N3-PROC)	2298.97 (H5N4F3-PROC)	861.75 (H1N2F2)	1347.63 (H4N2F2)			
													1479.72 (H3N3F1-PROC)	366.08 (H1N1)	893.25 (H3N2)	2296.91 (H7N5F1)			
65	36.8 (Cmpd 2243)	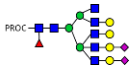	7	7	1	2	3522.36	1761.69	1174.79	n.d.	n.d.	1174.63	952.63 (H1N2F1-PROC)	1990.01 (H4N4S1-PROC)	366.18 (H1N1)	981.38 (H3N1S1)			
													967.75 (H2N2-PROC)	2135.63 (H4N4F1S1-PROC)	569.50 (H1N2)	1022.63 (H2N2S1)			
													1479.75 (H3N3F1-PROC)	2209.88 (H5N5F1-PROC)	656.95 (H1N1S1)	1055.50 (H4N2)			
													1844.78 (H4N4F1-PROC)	2501 (H5N5F1S1-PROC)	731.38 (H2N2)				
													1860.76 (H5N4-PROC)	292.00 (S1)	819.50 (H2N1S1)				
66	36.8 (Cmpd 2244)	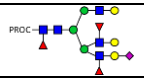	6	5	3	1	2955.17	1478.10	985.73	n.d.	n.d.	985.70	441.38 (N1-PROC)	1479.63 (H3N3F1-PROC)	350.13 (N1F1)	674.13 (H2N1F1)	1184.38 (H3N2S1)	1566.75 (H5N3F1)	
													587.34 (N1F1-PROC)	1641.73 (H4N3F1-PROC)	366.04 (H1N1)	803.16 (H1N1F1S1)	1258.38 (H4N3)	1638.63 (H4N2F2S1)	
													790.13 (N2F1-PROC)	1787.52 (H4N3F2-PROC)	512.17 (H1N1F1)	819.38 (H2N1S1)	1289.75 (H4N1F1S1)	1712.63 (H5N3F2)	
													952.25 (H1N2F1-PROC)	1932.83 (H4N3F1S1-PROC)	528.25 (H2N1)	965.52 (H2N1F1S1)	1330.63 (H3N2F1S1)	1785.75 (H6N4)	
													1114.51 (H2N2F1-PROC)	2226.13 (H6N5-PROC)	657.15 (H1N1S1)	1039.88 (H3N2F1)	1404.50 (H4N3F1)		
67	37.6 (Cmpd 2294)	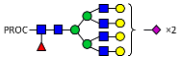	7	6	1	2	3319.29	1660.15	1107.10	n.d.	n.d.	1107.08	587.25 (N1F1-PROC)	1860.79 (H5N4-PROC)	454.75 (H1S1)	1475.50 (H3N2S2)			
													790.38 (N2F1-PROC)	2006.88 (H5N4F1-PROC)	569.25 (H1N2)				
													1171.38 (H2N3-PROC)	2151.84 (H5N4S1-PROC)	657.07 (H1N1S1)				
													1333.13 (H3N3-PROC)	2297.94 (H5N4F1S1-PROC)	819.25 (H2N1S1)				
													1479.66 (H3N3F1-PROC)	366.12 (H1N1)	1184.47 (H3N2S1)				
68	38.1 (Cmpd 2320)	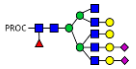	7	7	1	2	3522.36	1761.69	1174.79	n.d.	n.d.	1174.77	441.25 (N1-PROC)	1844.75 (H4N4F1-PROC)	2354.88 (H5NS1-PROC)	657.29 (H1N1S1)	1508.50 (H5N2S1)		
													587.41 (N1F1-PROC)	1990.05 (H4N4S1-PROC)	2500.88 (H5N5F1S1-PROC)	819.62 (H2N1S1)	1711.88 (H5N3S1)		
													952.26 (H1N2F1-PROC)	2136.01 (H4N4F1S1-PROC)	292.00 (S1)	893.39 (H3N2)			
													968.50 (H2N2-PROC)	2151.88 (H5N4S1-PROC)	366.15 (H1N1)	1022.63 (H2N2S1)			
													1479.64 (H3N3F1-PROC)	2210.01 (H5N5F1-PROC)	454.06 (H1S1)	1137.00 (H2N4)			
69	38.8 (Cmpd 2363)	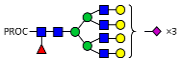	7	6	1	3	3610.38	1805.69	1204.13	n.d.	n.d.	1204.74	587.30 (N1F1-PROC)	1317.76 (H2N3F1-PROC)	1932.76 (H4N3F1S1-PROC)	454 (H1S1)	1022.38 (H2N2S1)		
													806.38 (H1N2-PROC)	1333 (H3N3-PROC)	2226.01 (H6N5-PROC)	528.25 (H2N1)	1184.30 (H3N2S1)		
													952.63 (H1N2F1-PROC)	1495.75 (H4N3-PROC)	2297.75 (H5N4F1S1-PROC)	657.25 (H1N1S1)	1475.38 (H3N2S2)		
													968.38 (H2N2-PROC)	1641.86 (H4N3F1-PROC)	292.02 (S1)	852.25 (H4N1)	1711.63 (H5N3S1)		
													1114.5 (H2N2F1-PROC)	1770.88 (H3N3F1S1-PROC)	366.1 (H1N1)	981.66 (H3N1S1)			

Table S4.2 Membrane proteins N-glycans composition of SW620FUT6 cells identified by MS^n fragmentation analysis with identified Y- and B-ion fragments.
Membrane proteins N-glycans from SW620FUT6 cells were released, labelled, and analysed by LC-ESI-MS/MS. Mass spectrometry data were analysed using the Bruker Compass DataAnalysis 4.1 software. LC-ESI-MS/MS chromatogram analysis was performed using Bruker Compass DataAnalysis 4.4 and GlycoWorkbench software. Structures were identified by comparing LC, MS, and MS/MS data. Structures for N-glycans are depicted with the following notation: PROC: procainamide; blue square: N-acetylglucosamine; green circle: Mannose; yellow circle: Galactose; red triangle: Fucose; purple diamond: N-acetylneuraminic acid. Identified Y- and B-ion fragments, noted respectively in black and blue, are given in terms of the number of hexose (H), N-acetylhexosamine (N), deoxyhexose (F) and N-acetylneuraminic acid (S). Abbreviations: LC-ESI-MS/MS, liquid chromatography electrospray ionisation tandem mass spectrometry; Hex, hexose; HexNAc, N-acetylhexosamine; Fuc, Fucose; Neu5Ac, N-acetylneuraminic acid; Cmpd, compound; n.d., not detectable.

Peak ID	Retention time (min)	Structure	Composition				LC-ESI-MS									
			Hex (H)	HexNAc (N)	Fuc (F)	Neu5Ac (S)	$[M/Z]^+$ calculated	$[M/Z]^{2+}$ calculated	$[M/Z]^{3+}$ calculated	$[M/Z]^+$ registered	$[M/Z]^{2+}$ registered	$[M/Z]^{3+}$ registered	[M/Z] characteristic fragment ions (composition)				
1	8.6 (Cmpd 522)		2	2	0	0	968.45	484.73	323.49	967.44	484.73	n.d.	441.32 (N1-PROC)	528.24 (H2N1)			
													644.34 (N2-PROC)				
													806.44 (H1N2-PROC)				
													325.15 (H2)				
													366.10 (H1N1)				
2	10.4 (Cmpd 638)	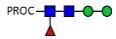	2	2	1	0	1114.51	557.76	372.18	1114.54	557.77	n.d.	441.30 (N1-PROC)	952.52 (H1N2F1-PROC)			
													587.34 (N1F1-PROC)	968.48 (H2N2-PROC)			
													644.34 (N2-PROC)	325.13 (H2)			
													790.43 (N2F1-PROC)	366.17 (H1N1)			
													806.41 (H1N2-PROC)	528.33 (H2N1)			
3	12.5 (Cmpd 776)	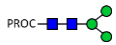	3	2	0	0	1130.51	565.76	377.51	1130.52	565.77	n.d.	441.31 (N1-PROC)	366.14 (H1N1)			
													644.34 (N2-PROC)	487.63 (H3)			
													162.98 (H1)	528.19 (H2N1)			
													203.98 (N1)	690.22 (H3N1)			
													325.22 (H2)				
4	14.4 (Cmpd 891)	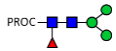	3	2	1	0	1276.57	638.79	426.19	1276.58	638.79	n.d.	441.28 (N1-PROC)	325.18 (H2)			
													587.32 (N1F1-PROC)	366.16 (H1N1)			
													644.26 (N2-PROC)	528.20 (H2N1)			
													806.31 (H1N2-PROC)	690.20 (H3N1)			
													203.97 (N1)				
5	16.4 (Cmpd 1008)		4	2	0	0	1292.56	646.78	431.53	1292.58	646.79	n.d.	441.30 (N1-PROC)	366.14 (H1N1)			
													806.41 (H1N2-PROC)	486.99 (H3)			
													968.61 (H2N2-PROC)	528.17 (H2N1)			
													203.94 (N1)	690.23 (H3N1)			
													325.13 (H2)	852.31 (H4N1)			
6	16.9 (Cmpd 1038)	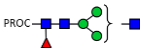	3	3	1	0	1479.65	740.33	493.89	n.d.	740.35	n.d.	441.29 (N1-PROC)	952.53 (H1N2F1-PROC)	203.97 (N1)	690.25 (H3N1)	
													587.32 (N1F1-PROC)	968.48 (H2N2-PROC)	325.19 (H2)	731.33 (H2N2)	
													644.32 (N2-PROC)	1114.61 (H2N2F1-PROC)	366.09 (H1N1)	893.25 (H3N2)	
													790.47 (N2F1-PROC)	1130.59 (H3N2-PROC)	487.25 (H3)		
													806.47 (H1N2-PROC)	1276.65 (H3N2F1-PROC)	528.16 (H2N1)		
7	17.3 (Cmpd 1059)	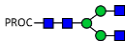	3	4	0	0	1536.67	768.84	512.89	n.d.	768.87	n.d.	441.34 (N1-PROC)	1171.56 (H2N3-PROC)	893.38 (H3N2)		
													644.32 (N2-PROC)	1333.64 (H3N3-PROC)	1096.40 (H3N3)		
													806.45 (H1N2-PROC)	366.18 (H1N1)			
													968.43 (H2N2-PROC)	528.25 (H2N1)			
													1130.50 (H3N2-PROC)	731.16 (H2N2)			
8	17.9 (Cmpd 1100)	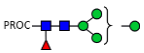	4	2	1	0	1438.62	719.81	480.21	n.d.	719.84	n.d.	441.29 (N1-PROC)	952.50 (H1N2F1-PROC)	528.20 (H2N1)		
													587.34 (N1F1-PROC)	1130.50 (H3N2-PROC)	690.23 (H3N1)		
													644.28 (N2-PROC)	203.93 (N1)	852.29 (H4N1)		
													790.43 (N2F1-PROC)	325.10 (H2)			
													806.57 (H1N2-PROC)	366.14 (H1N1)			
9	18.7 (Cmpd 1149)	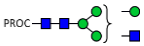	4	3	0	0	1495.64	748.32	499.22	n.d.	748.32	n.d.	441.29 (N1-PROC)	1292.62 (H4N2-PROC)	690.08 (H3N1)		
													644.38 (N2-PROC)	325.09 (H2)	731.37 (H2N2)		
													806.33 (H1N2-PROC)	366.09 (H1N1)	852.38 (H4N1)		
													968.49 (H2N2-PROC)	528.16 (H2N1)	893.22 (H3N2)		
													1130.58 (H3N2-PROC)	649.01 (H4)	1055.45 (H4N2)		
10	19.1 (Cmpd 1172)	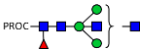	3	4	1	0	1682.72	841.87	561.58	n.d.	841.88	n.d.	441.30 (N1-PROC)	968.57 (H2N2-PROC)	1276.60 (H3N2F1-PROC)	366.07 (H1N1)	1096.41 (H3N3)
													587.41 (N1F1-PROC)	1009.13 (H1N3-PROC)	1317.62 (H2N3F1-PROC)	528.25 (H2N1)	
													644.74 (N2-PROC)	1114.56 (H2N2F1-PROC)	1333.59 (H3N3-PROC)	569.48 (H1N2)	
													790.26 (N2F1-PROC)	1130.68 (H3N2-PROC)	1479.74 (H3N3F1-PROC)	690.36 (H3N1)	
													806.88 (H1N2-PROC)	1171.66 (H2N3-PROC)	325.00 (H2)	893.22 (H3N2)	
11	20.0 (Cmpd 1225)	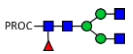	3	4	1	0	1682.72	841.87	561.58	n.d.	841.87	n.d.	441.42 (N1-PROC)	1114.50 (H2N2F1-PROC)	1479.71 (H3N3F1-PROC)	1096.33 (H3N3)	
													587.26 (N1F1-PROC)	1130.57 (H3N2-PROC)	366.13 (H1N1)		
													644.13 (N2-PROC)	1276.54 (H3N2F1-PROC)	690.63 (H3N1)		
													806.01 (H1N2-PROC)	1317.68 (H2N3F1-PROC)	731.19 (H2N2)		
													968.38 (H2N2-PROC)	1333.57 (H3N3-PROC)	893.35 (H3N2)		
12	20.3 (Cmpd 1247)		5	2	0	0	1454.61	727.81	485.54	1454.59	727.83	n.d.	441.29 (N1-PROC)	325.11 (H2)	690.21 (H3N1)		
													644.37 (N2-PROC)	366.15 (H1N1)	852.28 (H4N1)		
													806.41 (H1N2-PROC)	487.25 (H3)	1014.39 (H5N1)		
													968.42 (H2N2-PROC)	528.20 (H2N1)			
													203.97 (N1)	649.17 (H4)			

Table S4.2 (continued)

Peak ID	Retention time (min)	Structure	Composition				LC-ESI-MS					
			Hex (H)	HexNAc (N)	Fuc (F)	Neu5Ac (S)	$[M/Z]^{+}$ calculated	$[M/Z]^{2+}$ calculated	$[M/Z]^{3+}$ calculated	$[M/Z]^{+}$ registered	$[M/Z]^{2+}$ registered	$[M/Z]^{3+}$ registered
			[M/Z] characteristic fragment ions (composition)									
13	20.4 (Cmpd 1249)		4	3	1	0	1641.70	821.35	547.90	n.d.	821.35	n.d.
			441.28 (N1-PROC)	952.58 (H1N2F1-PROC)	325.13 (H2)	852.38 (H4N1)						
			587.26 (N1F1-PROC)	968.49 (H2N2-PROC)	366.11 (H1N1)	893.46 (H3N2)						
			644.49 (N2-PROC)	1114.55 (H2N2F1-PROC)	528.20 (H2N1)	1055.42 (H4N2)						
			790.48 (N2F1-PROC)	1130.59 (H3N2-PROC)	690.31 (H3N1)							
			806.35 (H1N2-PROC)	1276.64 (H3N2F1-PROC)	731.25 (H2N2)							
14	21.2 (Cmpd 1302)	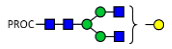	4	4	0	0	1698.72	849.86	566.91	n.d.	849.85	n.d.
			441.38 (N1-PROC)	1495.74 (H4N3-PROC)	1096.49 (H3N3)							
			806.26 (H1N2-PROC)	366.07 (H1N1)								
			968.43 (H2N2-PROC)	528.25 (H2N1)								
			1130.63 (H3N2-PROC)	690.25 (H3N1)								
			1333.65 (H3N3-PROC)	731.38 (H2N2)								
15	21.9 (Cmpd 1340)	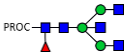	3	5	1	0	1885.80	943.41	629.27	n.d.	943.42	n.d.
			441.25 (N1-PROC)	1114.57 (H2N2F1-PROC)	1333.71 (H3N3-PROC)	366.38 (H1N1)	893.00 (H3N2)					
			587.34 (N1F1-PROC)	1130.38 (H3N2-PROC)	1479.67 (H3N3F1-PROC)	487.15 (H3)	934.38 (H2N3)					
			644.25 (N2-PROC)	1171.63 (H2N3-PROC)	1520.75 (H2N4F1-PROC)	528.21 (H2N1)	1096.35 (H3N3)					
			968.50 (H2N2-PROC)	1276.66 (H3N2F1-PROC)	1536.73 (H3N4-PROC)	569.75 (H1N2)	1299.41 (H3N4)					
			1009.50 (H1N3-PROC)	1317.62 (H2N3F1-PROC)	1682.79 (H3N4F1-PROC)	690.25 (H3N1)						
16	21.9 (Cmpd 1345)	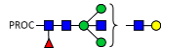	4	4	1	0	1844.78	922.89	615.60	n.d.	922.89	615.56
			441.30 (N1-PROC)	1155.46 (H1N3F1-PROC)	1641.78 (H4N3F1-PROC)	852.38 (H4N1)						
			587.28 (N1F1-PROC)	1276.59 (H3N2F1-PROC)	325.13 (H2)	893.68 (H3N2)						
			790.42 (N2F1-PROC)	1317.60 (H2N3F1-PROC)	366.13 (H1N1)	1096.38 (H3N3)						
			806.00 (H1N2-PROC)	1333.51 (H3N3-PROC)	528.50 (H2N1)	1258.53 (H4N3)						
			1114.63 (H2N2F1-PROC)	1479.69 (H3N3F1-PROC)	690.75 (H3N1)							
17	22.0 (Cmpd 1346)		5	2	1	0	1600.67	800.84	534.23	n.d.	800.85	n.d.
			441.31 (N1-PROC)	325.17 (H2)	690.21 (H3N1)							
			587.34 (N1F1-PROC)	366.09 (H1N1)	852.30 (H4N1)							
			644.32 (N2-PROC)	487.11 (H3)	1014.36 (H5N1)							
			790.47 (N2F1-PROC)	528.19 (H2N1)								
			968.39 (H2N2-PROC)	649.25 (H4)								
18	22.3 (Cmpd 1367)		5	3	0	0	1657.69	829.35	553.24	n.d.	829.36	n.d.
			441.37 (N1-PROC)	1292.65 (H4N2-PROC)	731.09 (H2N2)							
			644.44 (N2-PROC)	1454.57 (H5N2-PROC)	811.38 (H5)							
			806.30 (H1N2-PROC)	366.13 (H1N1)	852.75 (H4N1)							
			968.49 (H2N2-PROC)	528.11 (H2N1)	1055.40 (H4N2)							
			1130.54 (H3N2-PROC)	690.13 (H3N1)	1217.42 (H5N2)							
19	22.9 (Cmpd 1400)		4	3	1	1	1932.79	966.90	644.94	n.d.	966.91	644.94
			441.25 (N1-PROC)	1114.57 (H2N2F1-PROC)	1641.88 (H4N3F1-PROC)	528.24 (H2N1)	1055.41 (H4N2)					
			587.41 (N1F1-PROC)	1130.62 (H3N2-PROC)	1786.75 (H4N3S1-PROC)	657.22 (H1N1S1)	1346.43 (H4N2S1)					
			790.44 (N2F1-PROC)	1276.61 (H3N2F1-PROC)	292.05 (S1)	819.35 (H2N1S1)						
			806.45 (H1N2-PROC)	1317.63 (H2N3F1-PROC)	366.14 (H1N1)	852.25 (H4N1)						
			952.50 (H1N2F1-PROC)	1479.75 (H3N3F1-PROC)	454.07 (H1S1)	893.51 (H3N2)						
20	23.3 (Cmpd 1425)	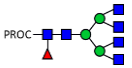	3	6	1	0	2088.88	1044.95	696.97	n.d.	1044.95	696.96
			441.24 (N1-PROC)	1276.51 (H3N2F1-PROC)	1536.76 (H3N4-PROC)	934.38 (H2N3)						
			587.24 (N1F1-PROC)	1317.64 (H2N3F1-PROC)	1682.69 (H3N4F1-PROC)	1096.46 (H3N3)						
			644.50 (N2-PROC)	1333.60 (H3N3-PROC)	203.96 (N1)	1299.40 (H3N4)						
			1114.57 (H2N2F1-PROC)	1479.69 (H3N3F1-PROC)	528.14 (H2N1)	1502.63 (H3N5)						
			1171.63 (H2N3-PROC)	1520.75 (H2N4F1-PROC)	569.19 (H1N2)							
21	23.3 (Cmpd 1428)		4	5	1	0	2047.86	1024.43	683.29	n.d.	1024.46	683.30
			587.27 (N1F1-PROC)	1317.66 (H2N3F1-PROC)	1682.78 (H3N4F1-PROC)	1258.38 (H4N3)						
			644.50 (N2-PROC)	1374.76 (H2N4-PROC)	1844.83 (H4N4F1-PROC)							
			790.50 (N2F1-PROC)	1479.71 (H3N3F1-PROC)	366.13 (H1N1)							
			1114.76 (H2N2F1-PROC)	1520.88 (H2N4F1-PROC)	528.20 (H2N1)							
			1171.50 (H2N3-PROC)	1536.50 (H3N4-PROC)	893.02 (H3N2)							
22	23.6 (Cmpd 1443)		4	3	0	1	1786.74	893.87	596.25	n.d.	893.88	n.d.
			441.34 (N1-PROC)	1333.50 (H3N3-PROC)	454.23 (H1S1)	819.28 (H2N1S1)						
			644.31 (N2-PROC)	1495.63 (H4N3-PROC)	528.06 (H2N1)	981.00 (H3N1S1)						
			806.44 (H1N2-PROC)	292.00 (S1)	657.21 (H1N1S1)	1184.38 (H3N2S1)						
			968.50 (H2N2-PROC)	324.99 (H2)	690.13 (H3N1)	1346.46 (H4N2S1)						
			1130.56 (H3N2-PROC)	366.16 (H1N1)	731.21 (H2N2)							
23	23.8 (Cmpd 1457)	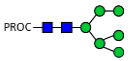	6	2	0	0	1616.67	808.84	539.56	1616.63	808.86	n.d.
			441.29 (N1-PROC)	366.11 (H1N1)	852.33 (H4N1)							
			644.34 (N2-PROC)	487.09 (H3)	1014.46 (H5N1)							
			968.48 (H2N2-PROC)	528.13 (H2N1)	1176.44 (H6N1)							
			1292.62 (H4N2-PROC)	649.63 (H4)								
			325.14 (H2)	690.21 (H3N1)								
24	24.3 (Cmpd 1490)	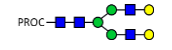	5	4	0	0	1860.77	930.89	620.93	n.d.	930.89	620.94
			441.34 (N1-PROC)	1495.69 (H4N3-PROC)	690.25 (H3N1)	1217.51 (H5N2)						
			644.38 (N2-PROC)	325.29 (H2)	731.20 (H2N2)	1420.56 (H5N3)						
			968.13 (H2N2-PROC)	366.13 (H1N1)	893.25 (H3N2)							
			1130.47 (H3N2-PROC)	528.11 (H2N1)	934.76 (H2N3)							
			1333.66 (H3N3-PROC)	569.13 (H1N2)	1055.27 (H4N2)							
25	25.0 (Cmpd 1529)	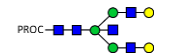	5	5	0	0	2063.85	1032.43	688.62	n.d.	1032.45	688.64
			441.32 (N1-PROC)	1171.59 (H2N3-PROC)	366.10 (H1N1)	1096.62 (H3N3)						
			644.25 (N2-PROC)	1333.64 (H3N3-PROC)	528.25 (H2N1)	1258.46 (H4N3)						
			806.46 (H1N2-PROC)	1495.59 (H4N3-PROC)	731.28 (H2N2)	1420.57 (H5N3)						
			968.38 (H2N2-PROC)	203.94 (N1)	893.25 (H3N2)							
			1009.64 (H1N3-PROC)	325.08 (H2)	1055.33 (H4N2)							
26	25.2 (Cmpd 1540)	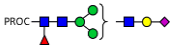	4	3	1	1	1932.79	966.90	644.94	n.d.	966.92	644.95
			441.24 (N1-PROC)	952.47 (H1N2F1-PROC)	1479.53 (H3N3F1-PROC)	366.13 (H1N1)	731.75 (H2N2)	1143.43 (H4N1S1)				
			587.37 (N1F1-PROC)	1114.52 (H2N2F1-PROC)	1495.51 (H4N3-PROC)	454.21 (H1S1)	819.25 (H2N1S1)	1184.62 (H3N2S1)				
			644.35 (N2-PROC)	1130.54 (H3N2-PROC)	1641.96 (H4N3F1-PROC)	528.10 (H2N1)	893.90 (H3N2)	1346.54 (H4N2S1)				
			790.42 (N2F1-PROC)	1276.62 (H3N2F1-PROC)	292.00 (S1)	657.22 (H1N1S1)	981.28 (H3N1S1)					
			806.37 (H1N2-PROC)	1333.65 (H3N3-PROC)	325.12 (H2)	690.13 (H3N1)	1055.52 (H4N2)					
27	25.4 (Cmpd 1551)	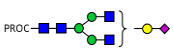	4	4	0	1	1989.81	995.41	663.94	n.d.	995.43	n.d.
			441.50 (N1-PROC)	1171.55 (H2N3-PROC)	366.00 (H1N1)	981.50 (H3N1S1)						
			644.25 (N2-PROC)	1333.65 (H3N3-PROC)	528.13 (H2N1)	1055.63 (H4N2)						
			806.63 (H1N2-PROC)	1495.51 (H4N3-PROC)	657.25 (H1N1S1)	1258.77 (H4N3)						
			968.70 (H2N2-PROC)	1624.77 (H3N3S1-PROC)	819.04 (H2N1S1)	1549.51 (H4N3S1)						
			1130.43 (H3N2-PROC)	292.00 (S1)	893.83 (H3N2)							

Table S4.2 (continued)

Peak ID	Retention time (min)	Structure	Composition				LC-ESI-MS						[M/Z] characteristic fragment ions (composition)					
			Hex (H)	HexNAc (N)	Fuc (F)	Neu5Ac (S)	$[M/Z]^+$ calculated	$[M/Z]^{2+}$ calculated	$[M/Z]^{3+}$ calculated	$[M/Z]^+$ registered	$[M/Z]^{2+}$ registered	$[M/Z]^{3+}$ registered						
28	25.6 (Cmpd 1562)	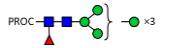	6	2	1	0	1762.72	881.87	588.25	n.d.	881.85	n.d.	441.29 (N1-PROC)	366.14 (H1N1)	811.25 (H5)			
													644.38 (N2-PROC)	487.37 (H3)	852.26 (H4N1)			
													806.75 (H1N2-PROC)	528.09 (H2N1)	973.00 (H6)			
													968.64 (H2N2-PROC)	649.13 (H4)	1014.31 (H5N1)			
													325.08 (H2)	690.34 (H3N1)	1176.56 (H6N1)			
29	25.7 (Cmpd 1571)	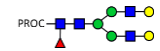	5	4	1	0	2006.83	1003.92	669.61	n.d.	1003.94	669.63	441.28 (N1-PROC)	952.42 (H1N2F1-PROC)	1333.71 (H3N3-PROC)	528.16 (H2N1)	1055.40 (H4N2)	1258.50 (H4N3)
													587.34 (N1F1-PROC)	968.51 (H2N2-PROC)	1495.50 (H4N3-PROC)	690.19 (H3N1)		
													644.36 (N2-PROC)	1114.59 (H2N2F1-PROC)	203.98 (N1)	731.26 (H2N2)		
													790.35 (N2F1-PROC)	1130.56 (H3N2-PROC)	325.14 (H2)	852.25 (H4N1)		
													806.35 (H1N2-PROC)	1276.59 (H3N2F1-PROC)	366.11 (H1N1)	893.27 (H3N2)		
30	25.7 (Cmpd 1572)	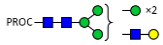	6	3	0	0	1819.75	910.38	607.25	n.d.	910.39	n.d.	441.20 (N1-PROC)	1292.57 (H4N2-PROC)	690.32 (H3N1)	1217.63 (H5N2)		
													644.38 (N2-PROC)	1454.69 (H5N2-PROC)	811.71 (H5)	1379.58 (H6N2)		
													806.58 (H1N2-PROC)	325.01 (H2)	852.26 (H4N1)			
													968.52 (H2N2-PROC)	366.12 (H1N1)	893.41 (H3N2)			
													1130.57 (H3N2-PROC)	528.17 (H2N1)	1014.02 (H5N1)			
31	26.3 (Cmpd 1606)	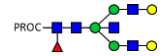	5	5	1	0	2209.91	1105.46	737.31	n.d.	1105.47	737.32	441.24 (N1-PROC)	968.63 (H2N2-PROC)	1171.68 (H2N3-PROC)	1495.52 (H4N3-PROC)	569.18 (H1N2)	1217.51 (H5N2)
													587.34 (N1F1-PROC)	1009.64 (H1N3-PROC)	1276.60 (H3N2F1-PROC)	1641.68 (H4N3F1-PROC)	690.13 (H3N1)	1258.49 (H4N3)
													644.33 (N2-PROC)	1114.55 (H2N2F1-PROC)	1317.67 (H2N3F1-PROC)	203.96 (N1)	893.42 (H3N2)	
													790.33 (N2F1-PROC)	1130.63 (H3N2-PROC)	1333.61 (H3N3-PROC)	366.12 (H1N1)	1055.25 (H4N2)	
													952.33 (H2N2-PROC)	1155.50 (H1N3F1-PROC)	1479.72 (H3N3F1-PROC)	528.20 (H2N1)	1096.51 (H3N3)	
32	26.5 (Cmpd 1619)	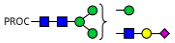	5	3	0	1	1948.79	974.90	650.27	n.d.	974.91	650.28	441.34 (N1-PROC)	1292.61 (H4N2-PROC)	366.12 (H1N1)	1055.37 (H4N2)	1346.58 (H4N2S1)	
													644.38 (N2-PROC)	1333.88 (H3N3-PROC)	657.20 (H1N1S1)	1143.50 (H4N1S1)	1508.47 (H5N2S1)	
													806.42 (H1N2-PROC)	1495.69 (H4N3-PROC)	731.37 (H2N2)	1184.60 (H3N2S1)		
													968.42 (H2N2-PROC)	1657.88 (H5N3-PROC)	819.33 (H2N1S1)	1217.48 (H5N2)		
													1130.59 (H3N2-PROC)	325.07 (H2)	893.85 (H3N2)	1305.38 (H5N1S1)		
33	27.2 (Cmpd 1663)		7	2	0	0	1778.72	889.86	593.58	n.d.	889.86	n.d.	441.27 (N1-PROC)	1292.75 (H4N2-PROC)	649.11 (H4)	1014.39 (H5N1)		
													644.35 (N2-PROC)	325.11 (H2)	690.23 (H3N1)	1135.38 (H7)		
													806.42 (H1N2-PROC)	366.17 (H1N1)	811.09 (H5)	1176.44 (H6N1)		
													968.52 (H2N2-PROC)	486.90 (H3)	852.29 (H4N1)	1338.51 (H7N1)		
													1130.52 (H3N2-PROC)	528.17 (H2N1)	973.18 (H6)			
34	27.7 (Cmpd 1691)		5	4	1	1	2297.93	1149.47	766.65	n.d.	1149.48	766.64	441.34 (N1-PROC)	1317.76 (H2N3F1-PROC)	325.13 (H2)	528.09 (H2N1)	819.45 (H2N1S1)	
													644.13 (N2-PROC)	1333.75 (H3N3-PROC)	350.0 (N1F1)	657.21 (H1N1S1)	852.41 (H4N1)	
													806.45 (H1N2-PROC)	1479.88 (H3N3F1-PROC)	366.12 (H1N1)	690.38 (H3N1)	893.25 (H3N2)	
													968.42 (H2N2-PROC)	1641.70 (H4N3F1-PROC)	454.10 (H1S1)	731.13 (H2N2)	1055.29 (H4N2)	
													1130.64 (H3N2-PROC)	292.07 (S1)	512.18 (H1N1F1)	803.47 (H1N1S1F1)	1346.50 (H4N2S1)	
35	28.0 (Cmpd 1711)	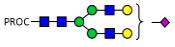	5	4	0	1	2151.87	1076.44	717.96	n.d.	1076.42	717.98	441.30 (N1-PROC)	1171.43 (H2N3-PROC)	325.17 (H2)	731.38 (H2N2)	1143.50 (H4N1S1)	1508.25 (H5N2S1)
													644.34 (N2-PROC)	1333.60 (H3N3-PROC)	366.14 (H1N1)	819.31 (H2N1S1)	1184.47 (H3N2S1)	
													806.43 (H1N2-PROC)	1495.70 (H4N3-PROC)	528.17 (H2N1)	893.36 (H3N2)	1217.50 (H5N2)	
													968.45 (H2N2-PROC)	203.98 (N1)	657.22 (H1N1S1)	981.27 (H3N1S1)	1346.46 (H4N2S1)	
													1130.57 (H3N2-PROC)	292.08 (S1)	690.19 (H3N1)	1055.38 (H4N2)	1420.57 (H5N3)	
36	28.4 (Cmpd 1737)		6	3	1	0	1965.80	983.41	655.94	n.d.	983.42	655.97	441.30 (N1-PROC)	1292.67 (H4N2-PROC)	528.31 (H2N1)			
													952.26 (H1N2F1-PROC)	1438.75 (H4N2F1-PROC)	811.88 (H5)			
													968.54 (H2N2-PROC)	1454.60 (H5N2-PROC)	893.38 (H3N2)			
													1130.60 (H3N2-PROC)	1600.77 (H5N2F1-PROC)				
													1171.13 (H2N3-PROC)	366.08 (H1N1)				
37	28.6 (Cmpd 1738)	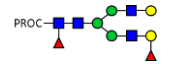	5	4	2	0	2152.89	1076.95	718.30	n.d.	1076.96	718.31	441.29 (N1-PROC)	968.67 (H2N2-PROC)	1625.63 (H3N3F2-PROC)	512.15 (H1N1F1)	836.25 (H3N1F1)	1258.75 (H4N3)
													587.32 (N1F1-PROC)	1114.57 (H2N2F1-PROC)	1641.75 (H4N3F1-PROC)	528.22 (H2N1)	893.19 (H3N2)	1347.60 (H4N2F2)
													790.38 (N2F1-PROC)	1130.60 (H3N2-PROC)	203.90 (N1)	674.34 (H2N1F1)	1039.59 (H3N2F1)	1363.38 (H5N2F1)
													806.51 (H1N2-PROC)	1276.61 (H3N2F1-PROC)	309.35 (H1F1)	690.28 (H3N1)	1055.42 (H4N2)	1420.63 (H5N3)
													952.53 (H1N2F1-PROC)	1333.75 (H3N3-PROC)	366.12 (H1N1)	731.36 (H2N2)	1201.45 (H4N2F1)	
38	28.7 (Cmpd 1755)	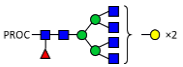	5	6	1	0	2412.99	1207.00	805.00	n.d.	n.d.	805.02	441.13 (N1-PROC)	1536.76 (H3N4-PROC)	487.50 (H3)			
													587.40 (N1F1-PROC)	1682.78 (H3N4F1-PROC)	731.25 (H2N2)			
													1130.63 (H3N2-PROC)	1698.76 (H4N4-PROC)	1096.63 (H3N3)			
													1317.53 (H2N3F1-PROC)	1844.73 (H4N4F1-PROC)	1461.56 (H4N4)			
													1479.70 (H3N3F1-PROC)	366.19 (H1N1)				
39	29.0 (Cmpd 1768)	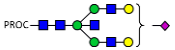	5	5	0	1	2354.95	1177.98	785.65	n.d.	1177.96	785.66	441.24 (N1-PROC)	1171.59 (H2N3-PROC)	1698.68 (H4N4-PROC)	569.75 (H1N2)	852.50 (H4N1)	
													644.17 (N2-PROC)	1333.70 (H3N3-PROC)	291.94 (S1)	657.16 (H1N1S1)	893.00 (H3N2)	
													806.32 (H1N2-PROC)	1495.62 (H4N3-PROC)	325.09 (H2)	690.22 (H3N1)	1258.46 (H4N3)	
													968.50 (H2N2-PROC)	1536.75 (H3N4-PROC)	366.11 (H1N1)	731.88 (H2N2)	1549.59 (H4N3S1)	
													1130.63 (H3N2-PROC)	1624.71 (H3N3S1-PROC)	528.07 (H2N1)	819.55 (H2N1S1)	1711.63 (H3N3S1)	
40	29.1 (Cmpd 1777)	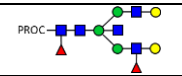	5	5	2	0	2355.97	1178.49	785.99	n.d.	1178.42	786.00	441.38 (N1-PROC)	1171.70 (H2N3-PROC)	1495.51 (H4N3-PROC)	512.14 (H1N1F1)	836.26 (H3N1F1)	1242.38 (H3N3F1)
													587.51 (N1F1-PROC)	1276.63 (H3N2F1-PROC)	1625.69 (H3N3F2-PROC)	528.09 (H2N1)	852.25 (H4N1)	1258.25 (H4N3)
													644.33 (N2-PROC)	1317.50 (H2N3F1-PROC)	1641.89 (H4N3F1-PROC)	569.38 (H1N2)	1055.88 (H4N2)	
													806.00 (H1N2-PROC)	1333.68 (H3N3-PROC)	1787.75 (H4N3F2-PROC)	690.13 (H3N1)	1096.50 (H3N3)	
													1009.88 (H1N3-PROC)	1479.70 (H3N3F1-PROC)	366.06 (H1N1)	731.08 (H2N2)	1217.51 (H5N2)	
41	29.3 (Cmpd 1786)	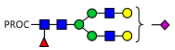	5	4	1	1	2297.93	1149.47	766.65	n.d.	1149.48	766.64	441.20 (N1-PROC)	952.42 (H1N2F1-PROC)	1276.65 (H3N2F1-PROC)	1641.70 (H4N3F1-PROC)	528.24 (H2N1)	852.38 (H4N1)	1346.45 (H4N2S1)
													587.30 (N1F1-PROC)	968.45 (H2N2-PROC)	1317.50 (H2N3F1-PROC)	292.07 (S1)	657.26 (H1N1S1)	893.19 (H3N2)	1420.67 (H5N3)
													644.40 (N2-PROC)	1114.56 (H2N2F1-PROC)	1333.55 (H3N3-PROC)	325.11 (H2)	690.63 (H3N1)	981.35 (H3N1S1)	1508.50 (H5N2S1)
													790.32 (N2F1-PROC)	1130.58 (H3N2-PROC)	1479.42 (H3N3F1-PROC)	366.11 (H1N1)	731.25 (H2N2)	1055.36 (H4N2)	
													806.45 (H1N2-PROC)	1171.63 (H2N3-PROC)	1495.65 (H4N3-PROC)	454.13 (H1S1)	819.33 (H2N1S1)	1184.38 (H3N2S1)	
42	29.5 (Cmpd 1799)	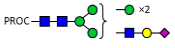	6	3	0	1	2110.84	1055.92	704.28	n.d.	1055.88	704.30	441.25 (N1-PROC)	1292.65 (H4N2-PROC)	366.14 (H1N1)	657.23 (H1N1S1)	981.29 (H3N1S1)	1379.56 (H6N2)
													644.19 (N2-PROC)	1454.63 (H5N2-PROC)	454.13 (H1S1)	690.20 (H3N1)	1014.32 (H5N1)	
													806.34 (H1N2-PROC)	203.97 (N1)	487.27 (H3)	819.31 (H2N1S1)	1143.46 (H4N1S1)	
													968.51 (H2N2-PROC)	291.96 (S1)	528.17 (H2N1)	852.30 (H4N1)	1217.40 (H5N2)	
													1130.57 (H3N2-PROC)	325.10 (H2)	649.15 (H4)	893.28 (H3N2)	1305.55 (H5N1S1)	

Table S4.2 (continued)

Peak ID	Retention time (min)	Structure	Composition				LC-ESI-MS											
			Hex (H)	HexNAc (N)	Fuc (F)	Neu5Ac (S)	$[M/Z]^{+}$ calculated	$[M/Z]^{2+}$ calculated	$[M/Z]^{3+}$ calculated	$[M/Z]^{+}$ registered	$[M/Z]^{2+}$ registered	$[M/Z]^{3+}$ registered	[M/Z] characteristic fragment ions (composition)							
43	30.0 (Cmpd 1832)	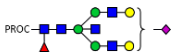	5	5	1	1	2501.01	1251.01	834.34	n.d.	1250.98	834.35	441.26 (N1-PROC)	1114.48 (H2N2F1-PROC)	1479.70 (H3N3F1-PROC)	292.04 (S1)	657.27 (H1N1S1)	1096.52 (H3N3)		
													587.33 (N1F1-PROC)	1155.51 (H1N3F1-PROC)	1536.88 (H3N4-PROC)	325.10 (H2)	731.34 (H2N2)	1184.47 (H3N2S1)		
													644.40 (N2-PROC)	1171.60 (H2N3-PROC)	1641.77 (H4N3F1-PROC)	366.13 (H1N1)	819.19 (H2N1S1)	1258.45 (H4N3)		
													806.26 (H1N2-PROC)	1276.74 (H3N2F1-PROC)	1770.88 (H3N3S1F1-PROC)	454.00 (H1S1)	893.28 (H3N2)	1346.50 (H4N2S1)		
													968.53 (H2N2-PROC)	1317.69 (H2N3F1-PROC)	1844.83 (H4N4F1-PROC)	528.24 (H2N1)	934.28 (H2N3)	1549.53 (H4N3S1)		
													1009.70 (H1N3-PROC)	1333.61 (H3N3-PROC)	1932.67 (H4N3S1F1-PROC)	569.13 (H1N2)	1055.75 (H4N2)	1623.54 (H5N4)		
44	30.2 (Cmpd 1840)	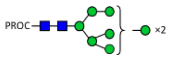	8	2	0	0	1940.77	970.89	647.60	n.d.	970.88	647.61	441.28 (N1-PROC)	325.09 (H2)	690.22 (H3N1)	1338.49 (H7N1)				
													644.36 (N2-PROC)	366.17 (H1N1)	811.25 (H5)	1500.53 (H8N1)				
													806.41 (H1N2-PROC)	486.94 (H3)	852.32 (H4N1)					
													1130.59 (H3N2-PROC)	528.13 (H2N1)	1014.38 (H5N1)					
													1292.62 (H4N2-PROC)	649.20 (H4)	1176.43 (H6N1)					
45	30.5 (Cmpd 1852)	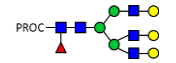	6	3	1	0	2371.96	1186.48	791.33	n.d.	n.d.	791.32	441.36 (N1-PROC)	1276.38 (H3N2F1-PROC)	366.12 (H1N1)	893.29 (H3N2)				
													587.37 (N1F1-PROC)	1333.63 (H3N3-PROC)	528.17 (H2N1)	1055.38 (H4N2)				
													644.38 (N2-PROC)	1479.64 (H3N3F1-PROC)	690.38 (H3N1)	1420.54 (H5N3)				
													806.38 (H1N2-PROC)	1495.86 (H4N3-PROC)	731.13 (H2N2)					
													1114.59 (H2N2F1-PROC)	1641.75 (H4N3F1-PROC)	852.25 (H4N1)					
46	30.7 (Cmpd 1875)	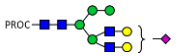	6	4	0	1	2313.92	1157.46	771.98	n.d.	n.d.	771.98	441.21 (N1-PROC)	1495.67 (H4N3-PROC)	657.16 (H1N1S1)	1055.41 (H4N2)				
													806.40 (H1N2-PROC)	292.07 (S1)	731.26 (H2N2)					
													968.41 (H2N2-PROC)	325.25 (H2)	819.14 (H2N1S1)					
													1130.58 (H3N2-PROC)	366.11 (H1N1)	893.26 (H3N2)					
													1333.63 (H3N3-PROC)	528.22 (H2N1)	981.46 (H3N1S1)					
47	31.0 (Cmpd 1891)	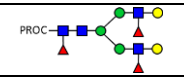	5	4	3	0	2298.95	1149.98	766.99	n.d.	1149.95	766.99	441.34 (N1-PROC)	968.50 (H2N2-PROC)	1495.50 (H4N3-PROC)	674.27 (H2N1F1)	1055.41 (H4N2)	1420.51 (H5N3)		
													587.35 (N1F1-PROC)	1114.56 (H2N2F1-PROC)	350.21 (N1F1)	690.50 (H3N1)	1185.63 (H3N2F2)	1509.50 (H5N2F2)		
													644.29 (N2-PROC)	1130.64 (H3N2-PROC)	366.11 (H1N1)	731.31 (H2N2)	1201.46 (H4N2F1)			
													806.75 (H1N2-PROC)	1276.63 (H3N2F1-PROC)	512.18 (H1N1F1)	893.56 (H3N2)	1258.64 (H4N3)			
													952.42 (H1N2F1-PROC)	1479.55 (H3N3F1-PROC)	528.16 (H2N1)	1039.40 (H3N2F1)	1347.60 (H4N2F2)			
48	31.1 (Cmpd 1898)	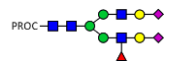	5	4	1	2	2589.02	1295.01	863.68	n.d.	1295.01	863.69	441.36 (N1-PROC)	1317.63 (H2N3F1-PROC)	1786.76 (H4N3S1-PROC)	528.17 (H2N1)	819.18 (H2N1S1)	1096.75 (H3N3)		
													644.31 (N2-PROC)	1333.67 (H3N3-PROC)	1932.86 (H4N3S1F1-PROC)	657.23 (H1N1S1)	836.38 (H3N1F1)	1184.63 (H3N2S1)		
													806.25 (H1N2-PROC)	1479.69 (H3N3F1-PROC)	292.07 (S1)	674.63 (H2N1F1)	893.85 (H3N2)	1201.38 (H4N2F1)		
													968.44 (H2N2-PROC)	1495.65 (H4N3-PROC)	366.10 (H1N1)	690.26 (H3N1)	965.34 (H2N1S1F1)	1346.45 (H4N2S1)		
													1130.55 (H3N2-PROC)	1536.75 (H3N4-PROC)	454.16 (H1S1)	731.38 (H2N2)	981.35 (H3N1S1)	1492.57 (H4N2S1F1)		
													1171.63 (H2N3-PROC)	1641.74 (H4N3F1-PROC)	512.04 (H1N1F1)	803.25 (H1N1S1F1)	1055.00 (H4N2)	1549.50 (H4N3S1)		
49	31.2 (Cmpd 1901)	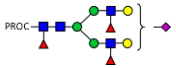	5	4	3	1	2590.04	1295.52	864.02	n.d.	1295.44	864.04	441.23 (N1-PROC)	968.44 (H2N2-PROC)	1479.81 (H3N3F1-PROC)	292.06 (S1)	657.23 (H1N1S1)	965.48 (H2N1S1F1)	1346.51 (H4N2S1)	
													587.33 (N1F1-PROC)	1114.52 (H2N2F1-PROC)	1495.60 (H4N3-PROC)	325.09 (H2)	690.50 (H3N1)	981.26 (H3N1S1)	1347.48 (H4N2F2)	
													644.27 (N2-PROC)	1130.58 (H3N2-PROC)	1624.63 (H3N3S1-PROC)	366.10 (H1N1)	731.25 (H2N2)	1039.38 (H3N2F1)	1492.65 (H4N2S1F1)	
													790.45 (N2F1-PROC)	1276.65 (H3N2F1-PROC)	1641.69 (H4N3F1-PROC)	454.11 (H1S1)	803.33 (H1N1S1F1)	1055.36 (H4N2)	1566.63 (H5N3F1)	
													806.29 (H1N2-PROC)	1317.53 (H2N3F1-PROC)	1787.88 (H4N3F2-PROC)	512.21 (H1N1F1)	819.25 (H2N1S1)	1184.40 (H3N2S1)	1654.63 (H5N2S1F1)	
													952.47 (H1N2F1-PROC)	1333.71 (H3N3-PROC)	1932.81 (H4N3S1F1-PROC)	528.21 (H2N1)	893.32 (H3N2)	1201.59 (H4N2F1)		
50	31.4 (Cmpd 1914)	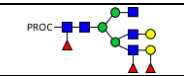	5	5	3	0	2502.03	1251.52	834.68	n.d.	n.d.	834.70	441.37 (N1-PROC)	1317.56 (H2N3F1-PROC)	1771.84 (H3N3F3-PROC)	487.00 (H3)	674.25 (H2N1F1)	1388.88 (H3N3F2)		
													587.35 (N1F1-PROC)	1333.73 (H3N3-PROC)	1787.74 (H4N3F2-PROC)	512.18 (H1N1F1)	715.75 (H1N2F1)	1550.61 (H4N3F2)		
													806.25 (H1N2-PROC)	1479.69 (H3N3F1-PROC)	309.25 (H1F1)	528.01 (H2N1)	731.36 (H2N2)			
													1130.63 (H3N2-PROC)	1625.68 (H3N3F2-PROC)	325.24 (H2)	569.13 (H1N2)	820.38 (H2N1F2)			
													1276.75 (H3N2F1-PROC)	1641.63 (H4N3F1-PROC)	366.14 (H1N1)	658.19 (H1N1F2)	1185.38 (H3N2F2)			
51	31.5 (Cmpd 1921)		5	4	0	2	2442.96	1221.99	814.99	n.d.	1221.98	815.00	441.22 (N1-PROC)	1333.68 (H3N3-PROC)	366.17 (H1N1)	731.25 (H2N2)	1184.49 (H3N2S1)			
													644.34 (N2-PROC)	1495.65 (H4N3-PROC)	454.24 (H1S1)	893.26 (H3N2)	1346.42 (H4N2S1)			
													806.46 (H1N2-PROC)	1786.78 (H4N3S1-PROC)	528.17 (H2N1)	981.13 (H3N1S1)	1420.50 (H5N3)			
													968.47 (H2N2-PROC)	292.21 (S1)	657.20 (H1N1S1)	1055.38 (H4N2)	1508.63 (H5N2S1)			
													1130.55 (H3N2-PROC)	325.13 (H2)	690.13 (H3N1)	1143.38 (H4N1S1)	1711.38 (H5N3S1)			
52	31.6 (Cmpd 1928)	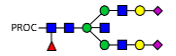	5	5	1	2	2792.10	1396.55	931.37	n.d.	n.d.	931.36	441.31 (N1-PROC)	1130.65 (H3N2-PROC)	1333.64 (H3N3-PROC)	292.03 (S1)	690.19 (H3N1)	1387.56 (H3N3S1)		
													587.32 (N1F1-PROC)	1155.49 (H1N3F1-PROC)	1479.64 (H3N3F1-PROC)	366.18 (H1N1)	819.20 (H2N1S1)	1420.50 (H5N3)		
													644.35 (N2-PROC)	1171.60 (H2N3-PROC)	1495.75 (H4N3-PROC)	454.17 (H1S1)	1096.39 (H3N3)	1549.26 (H4N3S1)		
													806.36 (H1N2-PROC)	1276.80 (H3N2F1-PROC)	1520.89 (H2N4F1-PROC)	528.17 (H2N1)	1184.38 (H3N2S1)			
													968.55 (H2N2-PROC)	1317.66 (H2N3F1-PROC)	1770.72 (H3N3S1F1-PROC)	657.19 (H1N1S1)	1258.38 (H4N3)			
53	31.8 (Cmpd 1939)		5	4	2	1	2443.98	1222.50	815.33	n.d.	1222.44	815.35	441.30 (N1-PROC)	1114.59 (H2N2F1-PROC)	1641.56 (H4N3F1-PROC)	512.19 (H1N1F1)	803.34 (H1N1S1F1)	1039.91 (H3N2F1)	1346.44 (H4N2S1)	
													587.31 (N1F1-PROC)	1130.54 (H3N2-PROC)	1787.82 (H4N3F2-PROC)	528.12 (H2N1)	836.28 (H3N1F1)	1055.40 (H4N2)	1420.56 (H5N3)	
													644.41 (N2-PROC)	1276.61 (H3N2F1-PROC)	292.13 (S1)	657.22 (H1N1S1)	852.25 (H4N1)	1184.63 (H3N2S1)	1492.74 (H4N2S1F1)	
													806.21 (H1N2-PROC)	1333.55 (H3N3-PROC)	350.25 (N1F1)	674.04 (H2N1F1)	877.38 (H2N2F1)	1201.38 (H4N2F1)	1654.38 (H5N2S1F1)	
													952.54 (H1N2F1-PROC)	1479.75 (H3N3F1-PROC)	366.11 (H1N1)	690.18 (H3N1)	893.87 (H3N2)	1289.63 (H4N1S1F1)		
													968.40 (H2N2-PROC)	1495.62 (H4N3-PROC)	454.17 (H1S1)	731.13 (H2N2)	981.25 (H3N1S1)	1330.38 (H3N2S1F1)		
54	32.0 (Cmpd 1950)	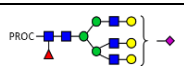	6	5	1	1	2663.06	1332.03	888.36	n.d.	n.d.	888.37	441.19 (N1-PROC)	1114.63 (H2N2F1-PROC)	1495.63 (H4N3-PROC)	2006.90 (H5N4F1-PROC)	657.21 (H1N1S1)	1022.50 (H2N2S1)		
													587.25 (N1F1-PROC)	1171.75 (H2N3-PROC)	1641.74 (H4N3F1-PROC)	291.89 (S1)	731.01 (H2N2)	1096.26 (H3N3)		
													644.15 (N2-PROC)	1276.52 (H3N2F1-PROC)	1770.63 (H3N3S1F1-PROC)	366.09 (H1N1)	819.36 (H2N1S1)	1184.78 (H3N2S1)		
													790.51 (N2F1-PROC)	1333.50 (H3N3-PROC)	1844.64 (H4N4F1-PROC)	454.17 (H1S1)	851.94 (H4N1)	1258.63 (H4N3)		
													806.13 (H1N2-PROC)	1479.66 (H3N3F1-PROC)	1932.89 (H4N3S1F1-PROC)	528.13 (H2N1)	981.26 (H3N1S1)	1420.58 (H5N3)		
55	32.4 (Cmpd 1972)	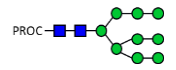	9	2	0	0	2102.82	1051.92	701.61	n.d.	1051.91	701.62	441.30 (N1-PROC)	1292.56 (H4N2-PROC)	486.80 (H3)	852.30 (H4N1)	1338.53 (H7N1)			
													644.33 (N2-PROC)	1454.68 (H5N2-PROC)	527.98 (H2N1)	973.35 (H6)	1500.49 (H8N1)			
													806.45 (H1N2-PROC)	1616.75 (H6N2-PROC)	649.10 (H4)	1014.35 (H5N1)	1662.58 (H9N1)			
													968.45 (H2N2-PROC)	325.09 (H2)	690.28 (H3N1)	1135.39 (H7)				
													1130.57 (H3N2-PROC)	366.07 (H1N1)	811.42 (H5)	1176.44 (H6N1)				
56	32.6 (Cmpd 1989)	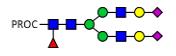	5	4	1	2	2589.02	1295.01	863.68	n.d.	n.d.	863.70	441.22 (N1-PROC)	952.41 (H1N2F1-PROC)	1276.58 (H3N2F1-PROC)	1786.63 (H4N3S1-PROC)	690.26 (H3N1)	1055.49 (H4N2)		
													587.28 (N1F1-PROC)	968.43 (H2N2-PROC)	1479.63 (H3N3F1-PROC)	1932.88 (H4N3S1F1-PROC)	731.25 (H2N2)	1096.00 (H3N3)		
													644.46 (N2-PROC)	1114.62 (H2N2F1-PROC)	1495.38 (H4N3-PROC)	366.13 (H1N1)	819.30 (H2N1S1)	1184.25 (H3N2S1)		
													790.50 (N2F1-PROC)	1130.53 (H3N2-PROC)	1641.90 (H4N3F1-PROC)	528.09 (H2N1)	893.40 (H3N2)	1346.30 (H4N2S1)		
													806.42 (H1N2-PROC)	1171.75 (H2N3-PROC)	1770.51 (H3N3S1F1-PROC)	657.20 (H1N1S1)	981.38 (H3N1S1)	1420.75 (H5N3)		

Table S4.2 (continued)

Peak ID	Retention time (min)	Structure	Composition				[M/Z]$^{+}$ calculated	[M/Z]$^{2+}$ calculated	[M/Z]$^{3+}$ calculated	[M/Z]$^{+}$ registered	[M/Z]$^{2+}$ registered	[M/Z]$^{3+}$ registered	LC-ESI-MS [M/Z] characteristic fragment ions (composition)						
			Hex (H)	HexNAc (N)	Fuc (F)	Neu5Ac (S)													
57	32.9 (Cmpd 2002)	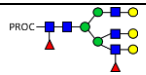	6	5	2	0	2518.02	1259.51	840.01	n.d.	n.d.	840.04	587.43 (N1F1-PROC)	1479.45 (H3N3F1-PROC)	1828.75 (H3N4F2-PROC)	674.38 (H2N1F1)	1258.50 (H4N3)		
													790.75 (N2F1-PROC)	1495.75 (H4N3-PROC)	325.14 (H2)	877.38 (H2N2F1)	1363.63 (H5N2F1)		
													952.50 (H1N2F1-PROC)	1625.75 (H3N3F2-PROC)	366.10 (H1N1)	893.13 (H3N2)			
													1114.61 (H2N2F1-PROC)	1641.71 (H4N3F1-PROC)	512.21 (H1N1F1)	1055.38 (H4N2)			
													1317.02 (H2N3F1-PROC)	1787.78 (H4N3F2-PROC)	528.14 (H2N1)	1217.42 (H5N2)			
58	32.9 (Cmpd 2006)	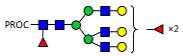	6	5	3	0	2664.08	1332.54	888.70	n.d.	n.d.	888.70	441.13 (N1-PROC)	1114.66 (H2N2F1-PROC)	1641.82 (H4N3F1-PROC)	512.16 (H1N1F1)	1039.25 (H3N2F1)		
													644.25 (N2-PROC)	1130.45 (H3N2-PROC)	1682.75 (H3N4F1-PROC)	569.26 (H1N2)	1096.88 (H3N3)		
													790.02 (N2F1-PROC)	1276.45 (H3N2F1-PROC)	1787.63 (H4N3F2-PROC)	731.35 (H2N2)	1217.51 (H5N2)		
													806.00 (H1N2-PROC)	1479.66 (H3N3F1-PROC)	2007.13 (H5N4F1-PROC)	852.50 (H4N1)	1347.39 (H4N2F2)		
													968.38 (H2N2-PROC)	1495.64 (H4N3-PROC)	366.16 (H1N1)	877.13 (H2N2F1)	1420.39 (H5N3)		
59	33.0 (Cmpd 2008)	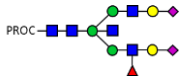	5	5	1	2	2792.10	1396.55	931.37	n.d.	n.d.	931.39	441.32 (N1-PROC)	1171.59 (H2N3-PROC)	1641.84 (H4N3F1-PROC)	2135.86 (H4N4S1F1-PROC)	569.13 (H1N2)	836.38 (H3N1F1)	1695.62 (H4N3S1F1)
													644.35 (N2-PROC)	1317.70 (H2N3F1-PROC)	1682.81 (H3N4F1-PROC)	292.02 (S1)	657.22 (H1N1S1)	852.88 (H4N1)	1914.63 (H5N4S1)
													806.41 (H1N2-PROC)	1333.70 (H3N3-PROC)	1786.75 (H4N3S1-PROC)	325.10 (H2)	674.15 (H2N1F1)	877.09 (H2N2F1)	
													968.50 (H2N2-PROC)	1479.80 (H3N3F1-PROC)	1844.92 (H4N4F1-PROC)	366.10 (H1N1)	690.38 (H3N1)	893.73 (H3N2)	
													1009.55 (H1N3-PROC)	1495.72 (H4N3-PROC)	1932.65 (H4N3S1F1-PROC)	512.10 (H1N1F1)	803.20 (H1N1S1F1)	965.54 (H2N1S1F1)	
													1130.50 (H3N2-PROC)	1624.63 (H3N3S1-PROC)	1989.70 (H4N4S1-PROC)	528.38 (H2N1)	819.60 (H2N1S1)	1549.75 (H4N3S1)	
60	33.4 (Cmpd 2032)	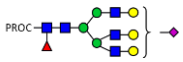	6	4	1	1	2663.06	1332.03	888.36	n.d.	n.d.	888.37	441.25 (N1-PROC)	1114.41 (H2N2F1-PROC)	1495.65 (H4N3-PROC)	366.10 (H1N1)	731.15 (H2N2)		
													587.24 (N1F1-PROC)	1130.88 (H3N2-PROC)	1641.57 (H4N3F1-PROC)	454.13 (H1S1)	852.26 (H4N1)		
													790.00 (N2F1-PROC)	1276.38 (H3N2F1-PROC)	1786.93 (H4N3S1-PROC)	528.20 (H2N1)	934.60 (H2N3)		
													952.54 (H1N2F1-PROC)	1333.63 (H3N3-PROC)	1932.88 (H4N3S1F1-PROC)	569.12 (H1N2)	1096.00 (H3N3)		
													968.38 (H2N2-PROC)	1479.50 (H3N3F1-PROC)	2006.51 (H5N4F1-PROC)	657.16 (H1N1S1)	1184.38 (H3N2S1)		
61	33.5 (Cmpd 2042)	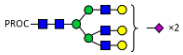	6	5	0	2	2808.10	1404.55	936.70	n.d.	n.d.	936.69	441.39 (N1-PROC)	1698.75 (H4N4-PROC)	366.09 (H1N1)	819.26 (H2N1S1)	1420.25 (H5N3)		
													806.38 (H1N2-PROC)	1786.78 (H4N3S1-PROC)	454.00 (H1S1)	893.29 (H3N2)	1475.63 (H3N2S1)		
													968.47 (H2N2-PROC)	1989.88 (H4N4S1-PROC)	528.14 (H2N1)	1022.50 (H2N2S1)	1711.59 (H5N3S1)		
													1333.69 (H3N3-PROC)	2151.96 (H5N4S1-PROC)	657.17 (H1N1S1)	1184.38 (H3N2S1)	1752.13 (H4N4S1)		
													1495.72 (H4N3-PROC)	325.25 (H2)	690.38 (H3N1)	1346.38 (H4N2S1)			
62	33.9 (Cmpd 2062)	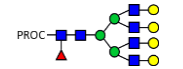	7	6	1	0	2737.09	1369.05	913.04	n.d.	1368.91	913.04	587.41 (N1F1-PROC)	1130.13 (H3N2-PROC)	1844.87 (H4N4F1-PROC)	731.25 (H2N2)			
													790.42 (N2F1-PROC)	1317.50 (H2N3F1-PROC)	1860.75 (H5N4-PROC)	893.13 (H3N2)			
													952.38 (H1N2F1-PROC)	1333.50 (H3N3-PROC)	2006.91 (H5N4F1-PROC)	934.63 (H2N3)			
													968.51 (H2N2-PROC)	1479.67 (H3N3F1-PROC)	366.10 (H1N1)	1785.51 (H6N4)			
													1114.74 (H2N2F1-PROC)	1641.77 (H4N3F1-PROC)	528.28 (H2N1)				
63	34.2 (Cmpd 2084)		7	7	1	0	2940.17	1470.59	980.73	n.d.	n.d.	980.72	441.25 (N1-PROC)	1682.89 (H3N4F1-PROC)	2063.97 (H5N5-PROC)	893.40 (H3N2)	1988.74 (H6N5)		
													587.25 (N1F1-PROC)	1698.63 (H4N4-PROC)	2209.93 (H5N5F1-PROC)	1096.26 (H3N3)			
													644.38 (N2-PROC)	1844.76 (H4N4F1-PROC)	325.25 (H2)	1420.50 (H5N3)			
													790.42 (N2F1-PROC)	2006.88 (H5N4F1-PROC)	366.14 (H1N1)	1623.72 (H5N4)			
													806.41 (H1N2-PROC)	2047.97 (H4N5F1-PROC)	528.06 (H2N1)	1664.13 (H4N5)			
64	34.6 (Cmpd 2104)	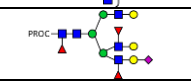	6	5	3	1	2955.17	1478.10	985.73	n.d.	n.d.	985.70	441.28 (N1-PROC)	1114.38 (H2N2F1-PROC)	1641.73 (H4N3F1-PROC)	1932.75 (H4N3S1F1-PROC)	657.21 (H1N1S1)	1055.50 (H4N2)	1508.75 (H5N2S1)
													587.14 (N1F1-PROC)	1276.50 (H3N2F1-PROC)	1682.63 (H3N4F1-PROC)	292.06 (S1)	803.26 (H1N1S1F1)	1080.00 (H2N3F1)	1654.50 (H5N2S1F1)
													790.50 (N2F1-PROC)	1333.51 (H3N3-PROC)	1770.63 (H3N3S1F1-PROC)	366.03 (H1N1)	998.13 (H4N1F1)	1185.50 (H3N2F2)	1711.64 (H5N3S1)
													952.63 (H1N2F1-PROC)	1479.70 (H3N3F1-PROC)	1786.75 (H4N3S1-PROC)	454.00 (H1S1)	1022.00 (H2N2S1)	1258.63 (H4N3)	1931.76 (H6N4F1)
													968.38 (H2N2-PROC)	1495.75 (H4N3-PROC)	1787.75 (H4N3F2-PROC)	512.16 (H1N1F1)	1023.38 (H2N2F2)	1492.88 (H4N2S1F1)	
65	34.9 (Cmpd 2127)	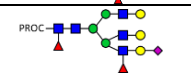	6	5	2	1	2809.12	1405.06	937.04	n.d.	n.d.	937.10	441.25 (N1-PROC)	1114.50 (H2N2F1-PROC)	1787.82 (H4N3F2-PROC)	487.50 (H3)	803.39 (H1N1S1F1)		
													587.44 (N1F1-PROC)	1479.65 (H3N3F1-PROC)	1932.72 (H4N3S1F1-PROC)	512.06 (H1N1F1)	819.25 (H2N1S1)		
													790.63 (N2F1-PROC)	1495.72 (H4N3-PROC)	2006.63 (H5N4F1-PROC)	657.19 (H1N1S1)	852.00 (H4N1)		
													952.51 (H1N2F1-PROC)	1626.00 (H3N3F2-PROC)	2079.11 (H4N3S1F2-PROC)	674.13 (H2N1F1)	1022.38 (H2N2S1)		
													968.25 (H2N2-PROC)	1641.68 (H4N3F1-PROC)	366.11 (H1N1)	731.38 (H2N2)	1785.63 (H6N4)		
66	35.0 (Cmpd 2131)	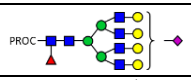	7	6	1	1	3028.19	1514.60	1010.07	n.d.	n.d.	1010.04	587.38 (N1F1-PROC)	1495.51 (H4N3-PROC)	2135.75 (H4N4S1F1-PROC)	454.12 (H1S1)	893.17 (H3N2)		
													790.51 (N2F1-PROC)	1641.63 (H4N3F1-PROC)	2209.88 (H5N5F1-PROC)	528.00 (H2N1)	934.50 (H2N3)		
													1114.75 (H2N2F1-PROC)	1844.88 (H4N4F1-PROC)	2297.91 (H5N4S1F1-PROC)	657.19 (H1N1S1)	1022.26 (H2N2S1)		
													1333.88 (H3N3-PROC)	1860.89 (H5N4-PROC)	2371.95 (H6N3F1-PROC)	819.88 (H2N1S1)	1184.51 (H3N2S1)		
													1479.82 (H3N3F1-PROC)	2006.84 (H5N4F1-PROC)	366.06 (H1N1)	852.50 (H4N1)	1549.38 (H4N3S1)		
67	35.0 (Cmpd 2132)	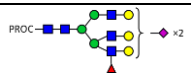	6	5	1	2	2954.15	1477.58	985.39	n.d.	n.d.	985.36	441.50 (N1-PROC)	1479.76 (H3N3F1-PROC)	2297.83 (H5N4S1F1-PROC)	528.13 (H2N1)	1022.50 (H2N2S1)	1711.88 (H5N3S1)	
													968.13 (H2N2-PROC)	1641.71 (H4N3F1-PROC)	2792.26 (H5N5S2F1-PROC)	657.15 (H1N1S1)	1039.50 (H3N2F1)	1785.75 (H6N4)	
													1130.88 (H3N2-PROC)	1770.75 (H3N3S1F1-PROC)	292.08 (S1)	731.38 (H2N2)	1080.00 (H2N3F1)	1931.13 (H6N4F1)	
													1317.50 (H2N3F1-PROC)	1844.78 (H4N4F1-PROC)	366.07 (H1N1)	836.76 (H3N1F1)	1363.64 (H5N2F1)		
													1333.63 (H3N3-PROC)	1932.85 (H4N3S1F1-PROC)	512.25 (H1N1F1)	965.72 (H2N1S1F1)	1475.63 (H3N2S1)		
68	35.1 (Cmpd 2135)	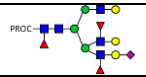	6	5	3	1	2955.17	1478.10	985.73	n.d.	n.d.	985.71	441.25 (N1-PROC)	1130.64 (H3N2-PROC)	1770.75 (H3N3S1F1-PROC)	2226.01 (H6N5-PROC)	803.37 (H1N1S1F1)	1168.63 (H2N2S1F1)	1711.88 (H5N3S1)
													587.43 (N1F1-PROC)	1276.63 (H3N2F1-PROC)	1786.88 (H4N3S1-PROC)	366.12 (H1N1)	819.38 (H2N1S1)	1201.50 (H4N2F1)	1931.75 (H6N4F1)
													644.25 (N2-PROC)	1479.75 (H3N3F1-PROC)	1787.77 (H4N3F2-PROC)	512.00 (H1N1F1)	1022.53 (H2N2S1)	1404.75 (H4N3F1)	2165.88 (H6N3S1F2)
													806.62 (H1N2-PROC)	1495.68 (H4N3-PROC)	1932.90 (H4N3S1F1-PROC)	657.27 (H1N1S1)	1080.13 (H2N3F1)	1420.75 (H5N3)	
													1114.63 (H2N2F1-PROC)	1641.76 (H4N3F1-PROC)	2006.75 (H5N4F1-PROC)	731.25 (H2N2)	1096.25 (H3N3)	1476.63 (H3N2S1F2)	
69	35.1 (Cmpd 2138)	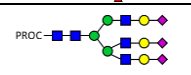	6	5	0	3	3099.19	1550.10	1033.74	n.d.	n.d.	1033.72	441.20 (N1-PROC)	1333.76 (H3N3-PROC)	2151.73 (H5N4S1-PROC)	528.25 (H2N1)	893.38 (H3N2)	1346.38 (H4N2S1)	
													644.63 (N2-PROC)	1495.68 (H4N3-PROC)	292.07 (S1)	657.24 (H1N1S1)	934.00 (H2N3)	1475.49 (H3N2S1)	
													806.47 (H1N2-PROC)	1624.79 (H3N3S1-PROC)	325.13 (H2)	731.50 (H2N2)	1055.51 (H4N2)	2002.83 (H5N3S2)	
													968.56 (H2N2-PROC)	1786.79 (H4N3S1-PROC)	366.08 (H1N1)	819.28 (H2N1S1)	1096.13 (H3N3)		
													1130.54 (H3N2-PROC)	1989.88 (H4N4S1-PROC)	454.03 (H1S1)	852.25 (H4N1)	1184.41 (H3N2S1)		
70	36.0 (Cmpd 2186)	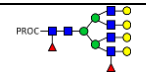	7	6	2	0	2883.15	1442.08	961.72	n.d.	n.d.	961.73	441.25 (N1-PROC)	1333.62 (H3N3-PROC)	1990.75 (H4N4F2-PROC)	731.25 (H2N2)	1931.79 (H6N4F1)		
													644.38 (N2-PROC)	1479.63 (H3N3F1-PROC)	2006.86 (H5N4F1-PROC)	877.38 (H2N2F1)			
													790.38 (N2F1-PROC)	1495.70 (H4N3-PROC)	2152.91 (H5N4F2-PROC)	934.75 (H2N3)			
													952.00 (H1N2F1-PROC)	1625.75 (H3N3F2-PROC)	366.09 (H1N1)	1039.25 (H3N2F1)			
													1114.12 (H2N2F1-PROC)	1641.87 (H4N3F1-PROC)	512.25 (H1N1F1)	1201.88 (H4N2F1)			
71	36.2 (Cmpd 2203)	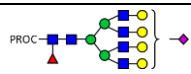	7	6	1	1	3028.19	1514.60	1010.07	n.d.	n.d.	1010.06	587.36 (N1F1-PROC)	1641.68 (H4N3F1-PROC)	325.13 (H2)	852.50 (H4N1)	1387.50 (H3N3S1)		
													790.50 (N2F1-PROC)	1932.88 (H4N3S1F1-PROC)	366.17 (H1N1)	934.38 (H2N3)	1420.63 (H5N3)		
													1276.75 (H3N2F1-PROC)	2006.72 (H5N4F1-PROC)	528.13 (H2N1)	981.25 (H3N1S1)	1785.50 (H6N4)		
													1333.63 (H3N3-PROC)	2047.88 (H4N5F1-PROC)	657.21 (H1N1S1)	1022.47 (H2N2S1)			
													1479.66 (H3N3F1-PROC)	2297.98 (H5N4S1F1-PROC)	819.25 (H2N1S1)	1184.00 (H3N2S1)			

Table S4.2 (continued)

Peak ID	Retention time (min)	Structure	Composition				LC-ESI-MS											
			Hex (H)	HexNAc (N)	Fuc (F)	Neu5Ac (S)	$[M/Z]^{+}$ calculated	$[M/Z]^{2+}$ calculated	$[M/Z]^{3+}$ calculated	$[M/Z]^{+}$ registered	$[M/Z]^{2+}$ registered	$[M/Z]^{3+}$ registered	[M/Z] characteristic fragment ions (composition)						
72	36.3 (Cmpd 2209)	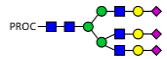	6	5	0	3	3099.19	1550.10	1033.74	n.d.	n.d.	1033.72	441.19 (N1-PROC)	1333.75 (H3N3-PROC)	291.88 (S1)	657.23 (H1N1S1)	1055.37 (H4N2)	1711.60 (H5N3S1)	
													644.38 (N2-PROC)	1495.66 (H4N3-PROC)	325.09 (H2)	690.75 (H3N1)	1096.45 (H3N3)	2002.69 (H5N3S2)	
													806.39 (H1N2-PROC)	1624.63 (H3N3S1-PROC)	366.12 (H1N1)	819.35 (H2N1S1)	1184.44 (H3N2S1)		
													968.53 (H2N2-PROC)	1786.74 (H4N3S1-PROC)	454.00 (H1S1)	893.13 (H3N2)	1475.51 (H3N2S1)		
													1130.66 (H3N2-PROC)	2151.88 (H5N4S1-PROC)	528.05 (H2N1)	934.58 (H2N3)	1508.38 (H5N2S1)		
73	36.5 (Cmpd 2216)	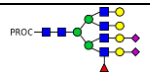	7	6	1	2	3319.29	1660.15	1107.10	n.d.	n.d.	1107.09	441.25 (N1-PROC)	1786.88 (H3N3S1-PROC)	325.13 (H2)	690.38 (H3N1)	1258.50 (H4N3)		
													806.00 (H1N2-PROC)	1844.63 (H4N4F1-PROC)	366.08 (H1N1)	715.97 (H1N2F1)			
													1333.57 (H3N3-PROC)	1932.50 (H4N3S1F1-PROC)	512.27 (H1N1F1)	731.84 (H2N2)			
													1479.71 (H3N3F1-PROC)	2006.77 (H5N4F1-PROC)	657.22 (H1N1S1)	877.99 (H2N2F1)			
													1641.75 (H4N3F1-PROC)	291.88 (S1)	674.88 (H2N1F1)	1184.63 (H3N2S1)			
74	37.5 (Cmpd 2276)	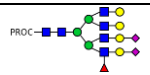	7	6	1	2	3319.29	1660.15	1107.10	n.d.	n.d.	1107.10	968.63 (H2N2-PROC)	1932.88 (H4N3S1F1-PROC)	690.25 (H3N1)	1022.38 (H2N2S1)	1931.89 (H6N4F1)		
													1130.44 (H3N2-PROC)	2298.13 (H5N4S1F1-PROC)	715.01 (H1N2F1)	1201.25 (H4N2F1)			
													1333.50 (H3N3-PROC)	366.10 (H1N1)	731.21 (H2N2)	1420.51 (H5N3)			
													1495.75 (H4N3-PROC)	512.13 (H1N1F1)	803.25 (H1N1S1F1)	1475.52 (H3N2S1)			
													1624.63 (H3N3S1-PROC)	657.26 (H1N1S1)	852.25 (H4N1)	1840.77 (H4N3S2)			
75	37.7 (Cmpd 2287)	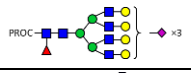	7	6	1	3	3610.38	1805.69	1204.13	n.d.	n.d.	1204.11	587.37 (N1F1-PROC)	1333.06 (H3N3-PROC)	1932.79 (H4N3S1F1-PROC)	366.08 (H1N1)	934.38 (H2N3)	2002.75 (H5N3S2)	
													952.63 (H1N2F1-PROC)	1479.70 (H3N3F1-PROC)	1989.76 (H4N4S1-PROC)	454.00 (H1S1)	1055.25 (H4N2)	2367.75 (H6N4S2)	
													968.50 (H2N2-PROC)	1641.72 (H4N3F1-PROC)	2006.95 (H5N4F1-PROC)	528.26 (H2N1)	1096.63 (H3N3)		
													1114.75 (H2N2F1-PROC)	1770.75 (H3N3S1F1-PROC)	2297.88 (H5N4S1F1-PROC)	657.16 (H1N1S1)	1475.75 (H3N2S1)		
													1276.38 (H3N2F1-PROC)	1860.75 (H5N4-PROC)	292.13 (S1)	731.50 (H2N2)	1752.63 (H4N4S1)		
76	38.1 (Cmpd 2314)	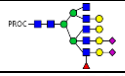	7	7	1	2	3522.36	1761.69	1174.79	n.d.	n.d.	1174.82	441.13 (N1-PROC)	2006.75 (H5N4F1-PROC)	657.27 (H1N1S1)	1127.38 (H3N1S1F1)			
													1641.63 (H4N3F1-PROC)	2209.88 (H5N5F1-PROC)	772.63 (H1N3)				
													1682.63 (H3N4F1-PROC)	2501.13 (H5N5S1F1-PROC)	803.25 (H1N1S1F1)				
													1698.75 (H4N4-PROC)	292.08 (S1)	819.80 (H2N1S1)				
													1989.88 (H4N4S1-PROC)	366.27 (H1N1)	852.75 (H4N1)				
77	39.1 (Cmpd 2371)	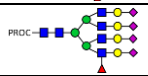	7	6	1	4	3901.48	1951.24	1301.16	n.d.	n.d.	n.d.	441.36 (N1-PROC)	1641.71 (H4N3F1-PROC)	2135.75 (H4N4S1F1-PROC)	366.12 (H1N1)	836.40 (H3N1F1)	1184.63 (H3N2S1)	1914.94 (H5N4S1)
													806.38 (H1N2-PROC)	1770.63 (H3N3S1F1-PROC)	2297.94 (H5N4S1F1-PROC)	657.21 (H1N1S1)	852.38 (H4N1)	1217.38 (H5N2)	
													1333.63 (H3N3-PROC)	1786.74 (H4N3S1-PROC)	2372.00 (H6N3F1-PROC)	715.50 (H1N2F1)	877.25 (H2N2F1)	1475.40 (H3N2S1)	
													1479.85 (H3N3F1-PROC)	1932.79 (H4N3S1F1-PROC)	2591.13 (H7N6-PROC)	803.35 (H1N1S1F1)	893.25 (H3N2)	1623.25 (H5N4)	
													1495.63 (H4N3-PROC)	2006.88 (H5N4F1-PROC)	292.00 (S1)	819.25 (H2N1S1)	1022.38 (H2N2S1)	1728.75 (H6N3F1)	
78	40.0 (Cmpd 2427)	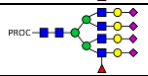	7	6	1	4	3901.48	1951.24	1301.16	n.d.	n.d.	n.d.	441.13 (N1-PROC)	1932.86 (H4N3S1F1-PROC)	291.91 (S1)	819.38 (H2N1S1)	1387.51 (H3N3S1)		
													806.13 (H1N2-PROC)	2006.75 (H5N4F1-PROC)	365.96 (H1N1)	877.13 (H2N2F1)	1475.38 (H3N2S1)		
													1479.77 (H3N3F1-PROC)	2297.86 (H5N4S1F1-PROC)	454.13 (H1S1)	893.38 (H3N2)	1623.59 (H5N4)		
													1641.63 (H4N3F1-PROC)	2589.13 (H5N4S2F1-PROC)	512.13 (H1N1F1)	965.50 (H2N1S1F1)	2002.63 (H5N3S2)		
													1770.88 (H3N3S1F1-PROC)	2590.97 (H7N6-PROC)	657.18 (H1N1S1)	1096.38 (H3N3)			

Table S4.3 57 immunoprecipitated glycoproteins with E-selectin chimera in SW620 cell lines identified by mass spectrometry†. † From SW620Mock and SW620FUT6 cells extracted membrane proteins, four immunoprecipitations with E-Ig chimera were performed and analysed by HPLC-MS/MS. The present list shows the glycosylated‡ immunoprecipitated proteins with E-selectin chimera identified in SW620 cell lines. **§** Proteins identified are described with the number of unique peptides for each experiment and the sum of the total spectrum count from the four experiments. **‡** Protein information on glycosylation status and subcellular location were obtained from UniProtKB database. Abbreviation: MW, Molecular Weight; Exp., Experiment.

Protein Name	Gene Name	UniProtKB entry	MW (kDa)	Exclusive Unique Peptide Count§								Total spectrum count (sum)§		Subcellular location‡
				E-selectin ligand from SW620Mock				E-selectin ligand from SW620FUT6				E-selectin ligand from SW620Mock	E-selectin ligand from SW620FUT6	
				Exp. 1	Exp. 2	Exp. 3	Exp. 4	Exp. 1	Exp. 2	Exp. 3	Exp. 4			
Ig gamma-3 chain C region (Fragment)	IGHG3	P01860 (IGHG3_HUMAN)	41	4	4	3	4	4	5	3	3	840	831	Cell membrane, secreted
Keratin, type II cytoskeletal 8	KRT8	P05787 (K2C8_HUMAN)	54	59	62	60	64	48	40	41	43	884	469	Cytoplasm, nucleus
Golgi apparatus protein 1	GLG1	Q92896 (GSLG1_HUMAN)	135	31	44	43	37	78	58	77	67	284	697	Golgi apparatus membrane
Ig gamma-2 chain C region	IGHG2	P01859 (IGHG2_HUMAN)	36	4	3	1	3	4	4	3	2	600	551	Cell membrane, secreted
Ig gamma-4 chain C region	IGHG4	P01861 (IGHG4_HUMAN)	36	3	3	4	5	3	3	4	3	434	424	Cell membrane, secreted
Keratin, type I cytoskeletal 18	KRT18	P05783 (K1C18_HUMAN)	48	46	49	43	51	30	29	21	22	485	145	Nucleus
Galectin-3-binding protein	LGALS3BP	Q08380 (LG3BP_HUMAN)	65	26	28	28	24	35	30	28	29	285	452	Secreted, extracellular matrix
Serum albumin	ALB	P02768 (ALBU_HUMAN)	69	8	7	15	33	10	40	13	15	235	216	Secreted
Vimentin	VIM	P08670 (VIME_HUMAN)	54	32	32	24	28	31	15	19	25	162	110	Cytoplasm, Cytoskeleton, Nucleus
Sortilin-related receptor	SORL1	Q92673 (SORL_HUMAN)	248	32	19	15	33	35	17	41	21	100	130	Endosome, Golgi apparatus, Membrane, Secreted
Sulfhydryl oxidase 2	QSOX2	Q6ZRP7 (QSOX2_HUMAN)	78	11	8	17	8	28	11	27	25	78	150	Cell/nucleus membrane, secreted
Integrin beta 4	ITGB4	P16144 (ITB4_HUMAN)	202	7	8	1	5	20	42	21	26	20	163	Cell membrane
Neutral amino acid transporter B(0)	SLC1A5	Q15758 (AAAT_HUMAN)	57	3	5	5	4	5	17	6	6	21	113	Cell membrane
Heat shock protein HSP 90-beta	HSP90AB1	P08238 (HS90B_HUMAN)	83	34	37	15	17	39	9	18	21	110	92	Cell membrane, Cytoplasm, Nucleus, Secreted

Table S4.3 (continued)

Protein Name	Gene Name	UniProtKB entry	MW (kDa)	Exclusive Unique Peptide Count§								Total spectrum count (sum)§		Subcellular location‡
				E-selectin ligand from SW620Mock				E-selectin ligand from SW620FUT6				E-selectin ligand from SW620Mock	E-selectin ligand from SW620FUT6	
				Exp. 1	Exp. 2	Exp. 3	Exp. 4	Exp. 1	Exp. 2	Exp. 3	Exp. 4			
Heterogeneous nuclear ribonucleoprotein K	HNRNPK	P61978 (HNRPK_HUMAN)	51	21	18	15	16	19	2	14	21	102	78	Cytoplasm, nucleus
Neural cell adhesion molecule L1	L1CAM	P32004 (L1CAM_HUMAN)	140	0	0	0	0	31	20	30	27	0	118	Plasma membrane
Transferrin receptor protein 1	TFRC	P02786 (TFR1_HUMAN)	85	13	18	8	2	24	32	12	13	35	98	Cell membrane, secreted
4F2 cell-surface antigen heavy chain	SLC3A2	P08195 (4F2_HUMAN)	68	1	2	1	1	11	22	13	14	5	94	Cell membrane
Junction plakoglobin	JUP	P14923 (PLAK_HUMAN)	82	8	15	10	30	9	14	9	16	91	63	Cytoskeleton
Integrin alpha 6	ITGA6	P23229 (ITA6_HUMAN)	127	0	0	0	0	11	31	12	10	0	91	Plasma membrane
ATP synthase subunit beta, mitochondrial	ATP5F1B	P06576 (ATPB_HUMAN)	57	14	14	14	16	16	10	17	15	81	75	Mitochondrion membrane
ATP synthase subunit alpha, mitochondrial	ATP5F1A	P25705 (ATPA_HUMAN)	60	25	20	16	15	26	6	20	17	78	72	Cell/mitochondrion membrane
Desmoglein-1	DSG1	Q02413 (DSG1_HUMAN)	114	7	6	6	20	5	5	5	8	58	29	Cell membrane
Receptor-type tyrosine-protein phosphatase eta	PTPRJ	Q12913 (PTPRJ_HUMAN)	146	0	0	0	0	21	9	18	11	0	58	Plasma membrane
RNA-binding motif protein, X chromosome	RBMX	P38159 (RBMX_HUMAN)	42	7	29	5	12	9	8	3	3	48	22	Nucleus
Alpha-1,6-mannosyl-glycoprotein 6-beta-N-acetylglucosaminyl-transferase A	MGAT5	Q09328 (MGT5A_HUMAN)	85	3	3	1	2	14	11	6	5	5	42	Golgi apparatus membrane/secreted
DnaJ homolog subfamily C member 10	DNAJC10	Q8IXB1 (DJC10_HUMAN)	91	10	14	10	10	9	2	12	14	40	33	Endoplasmic reticulum lumen
Dipeptidase 1	DPEP1	P16444 (DPEP1_HUMAN)	46	10	9	5	6	8	2	6	7	40	27	Cell membrane
Integrin beta-1	ITGB1	P05556 (ITB1_HUMAN)	88	0	0	0	0	6	11	7	5	0	39	Plasma membrane, recycling endosome
UPF0378 protein KIAA0100	KIAA0100	Q14667 (K0100_HUMAN)	254	2	2	2	2	2	2	2	2	38	38	Secreted

Table S4.3 (continued)

Protein Name	Gene Name	UniProtKB entry	MW (kDa)	Exclusive Unique Peptide Count§								Total spectrum count (sum)§		Subcellular location‡
				E-selectin ligand from SW620Mock				E-selectin ligand from SW620FUT6				E-selectin ligand from SW620Mock	E-selectin ligand from SW620FUT6	
				Exp. 1	Exp. 2	Exp. 3	Exp. 4	Exp. 1	Exp. 2	Exp. 3	Exp. 4			
Cation-independent mannose-6-phosphate receptor	IGF2R	P11717 (MPRI_HUMAN)	274	0	0	0	0	16	3	16	7	0	39	Lysosome membrane
N-acetylglucosamine-1-phosphotransferase subunits alpha/beta	GNPTAB	Q3T906 (GNPTA_HUMAN)	144	12	8	6	10	5	1	3	6	31	12	Golgi apparatus membrane
Polypeptide N-acetylgalactosaminyl-transferase 5	GALNT5	Q7Z7M9 (GALT5_HUMAN)	106	9	8	6	9	5	3	6	8	29	22	Golgi apparatus membrane
ATP-binding cassette sub-family D member 3	ABCD3	P28288 (ABCD3_HUMAN)	75	9	4	0	1	14	12	1	2	12	28	Peroxisome membrane
Endoplasmin	HSP90B1	P14625 (ENPL_HUMAN)	92	0	2	4	0	9	0	5	8	10	28	Endoplasmic reticulum lumen
Lysosome-associated membrane glycoprotein 1	LAMP1	P11279 (LAMP1_HUMAN)	45	0	0	0	1	4	6	6	5	1	28	Lysosome/endosome/cell membrane
Receptor-type tyrosine-protein phosphatase alpha	PTPRA	P18433 (PTPRA_HUMAN)	91	0	0	0	0	10	3	4	5	0	22	Membrane
Leucyl-cystinyl aminopeptidase	LNPEP	Q9UIQ6 (LCAP_HUMAN)	117	0	0	0	0	7	9	6	5	0	22	Plasma membrane/secreted
HLA class I histocompatibility antigen, A-23 alpha chain	HLA-A	P30447 (1A23_HUMAN)	41	2	3	1	1	7	4	5	4	7	21	Membrane
Prolactin-inducible protein	PIP	P12273 (PIP_HUMAN)	17	3	3	5	3	3	5	1	1	17	18	Secreted
Syndecan-1	SDC1	P18827 (SDC1_HUMAN)	32	1	0	1	2	2	2	4	5	3	18	Secreted, exosome, membrane
DNA replication licensing factor MCM7	MCM7	P33993 (MCM7_HUMAN)	81	6	8	2	2	2	0	0	4	17	4	Nucleus
Keratinocyte-associated transmembrane protein 2	KCT2	Q8NC54 (KCT2_HUMAN)	29	2	3	3	3	0	0	2	1	15	3	Membrane
Podocalyxin	PODXL	O00592 (PODXL_HUMAN)	59	3	2	0	0	4	4	4	3	5	13	Cell membrane
Ig gamma-1 chain C region	IGHA1	P01876 (IGHA1_HUMAN)	38	0	0	0	5	0	9	0	0	4	13	Cell membrane, secreted

Table S4.3 (continued)

Protein Name	Gene Name	UniProtKB entry	MW (kDa)	Exclusive Unique Peptide Count§								Total spectrum count (sum)§		Subcellular location‡
				E-selectin ligand from SW620Mock				E-selectin ligand from SW620FUT6				E-selectin ligand from SW620Mock	E-selectin ligand from SW620FUT6	
				Exp. 1	Exp. 2	Exp. 3	Exp. 4	Exp. 1	Exp. 2	Exp. 3	Exp. 4			
Carboxypeptidase D	CPD	O75976 (CBPD_HUMAN)	153	0	0	0	0	2	0	6	6	0	13	Plasma membrane
Leukosialin	SPN	P16150 (LEUK_HUMAN)	40	1	0	1	1	2	2	2	2	2	12	Membrane, nucleus
Lysosome-associated membrane glycoprotein 2	LAMP2	P13473 (LAMP2_HUMAN)	45	0	0	0	0	3	3	3	3	0	12	Lysosome/endosome/plasma membrane
Serpin H1	SERPINH1	P50454 (SERPH_HUMAN)	46	3	4	1	3	2	2	1	1	10	6	Endoplasmic reticulum lumen
Cathepsin D	CTSD	P07339 (CATD_HUMAN)	45	2	0	1	6	0	0	1	0	8	0	Lysosome, secreted
CD109 antigen	CD109	Q6YHK3 (CD109_HUMAN)	162	0	0	0	0	3	2	2	4	0	8	Plasma membrane
Zinc-alpha-2-glycoprotein	AZGP1	P25311 (ZA2G_HUMAN)	34	3	0	1	2	1	3	2	1	7	7	Secreted
Golgi membrane protein 1	GOLM1	Q8NBJ4 (GOLM1_HUMAN)	45	0	0	0	0	2	2	2	4	0	7	Golgi apparatus membrane
Procollagen-lysine,2-oxoglutarate 5-dioxygenase 3	PLOD3	O60568 (PLOD3_HUMAN)	85	2	4	1	0	1	0	1	3	5	5	ER lumen/membrane, RER, Secreted
Heparan sulphate 2-O-sulfotransferase 1	HS2ST1	Q7LGA3 (HS2ST_HUMAN)	42	1	0	0	2	1	3	0	0	2	2	Golgi apparatus membrane
Plexin-D1	PLXND1	Q9Y4D7 (PLXD1_HUMAN)	212	0	0	0	0	2	0	1	4	0	4	Plasma membrane
Zymogen granule protein 16 homolog B	ZG16B	Q96DA0 (ZG16B_HUMAN)	23	0	0	0	0	0	2	0	2	0	4	Secreted

Table S4.4 N-glycans composition of L1CAM monoclonal antibody identified by MS^n fragmentation analysis with identified Y- and B-ion fragments. N-glycans from L1CAM mAb were released, labelled, and analysed by LC-ESI-MS/MS. Mass spectrometry data were analysed using the Bruker Compass DataAnalysis 4.1 software. LC-ESI-MS/MS chromatogram analysis was performed using Bruker Compass DataAnalysis 4.4 and GlycoWorkbench software. Structures were identified by comparing LC, MS, and MS/MS data. Structures for N-glycans are depicted with the following notation: PROC: procainamide; blue square: N-acetylglucosamine; green circle: Mannose; yellow circle: Galactose; red triangle: Fucose; purple diamond: N-acetylneuraminic acid; white diamond: N-glycolylneuraminic acid. Identified Y- and B-ion fragments, noted respectively in black and blue, are given in terms of the number of hexose (H), N-acetylhexosamine (N), deoxyhexose (F), N-acetylneuraminic acid (S) and N-glycolylneuraminic acid (G). Abbreviations: LC-ESI-MS/MS, liquid chromatography electrospray ionisation tandem mass spectrometry; Hex, hexose; HexNAc, N-acetylhexosamine; Fuc, Fucose; Neu5Ac, N-acetylneuraminic acid; Neu5Gc, N-glycolylneuraminic acid; Cmpd, compound; n.d., not detectable.

Peak ID	Retention time (min)	Structure	Composition					LC-ESI-MS						[M/Z] characteristic fragment ions (composition)					
			Hex (H)	HexNAc (N)	Fuc (F)	Neu5Ac (S)	Neu5Gc (G)	$[M/Z]^+$ calculated	$[M/Z]^{2+}$ calculated	$[M/Z]^{3+}$ calculated	$[M/Z]^+$ registered	$[M/Z]^{2+}$ registered	$[M/Z]^{3+}$ registered						
1	17.5 (Cmpd 1010)	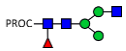	3	3	1	0	0	1479.65	740.33	493.89	1479.62	740.35	493.85	441.26 (N1-PROC)	952.49 (H1N2F1-PROC)	1276.62 (H3N2F1-PROC)	690.20 (H3N1)		
														587.27 (N1F1-PROC)	968.54 (H2N2-PROC)	203.99 (N1)	731.27 (H2N2)		
														644.37 (N2-PROC)	1114.53 (H2N2F1-PROC)	325.13 (H2)	893.31 (H3N2)		
														790.32 (N2F1-PROC)	1130.57 (H3N2-PROC)	366.00 (H1N1)			
														806.44 (H1N2-PROC)	1171.38 (H2N3-PROC)	528.17 (H2N1)			
2	18.2 (Cmpd 1048)		3	4	0	0	0	1536.67	768.84	512.89	1536.67	768.86	512.87	441.32 (N1-PROC)	1171.65 (H2N3-PROC)	528.16 (H2N1)			
														644.35 (N2-PROC)	1333.68 (H3N3-PROC)	690.13 (H3N1)			
														806.49 (H1N2-PROC)	325.19 (H2)	731.25 (H2N2)			
														968.46 (H2N2-PROC)	366.06 (H1N1)	893.37 (H3N2)			
														1130.53 (H3N2-PROC)	487.53 (H3)	1096.43 (H3N3)			
3	19.7 (Cmpd 1140)	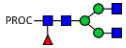	3	4	1	0	0	1682.72	841.87	561.58	1682.72	841.90	561.61	441.45 (N1-PROC)	952.63 (H1N2F1-PROC)	1276.65 (H3N2F1-PROC)	366.12 (H1N1)	1096.46 (H3N3)	
														587.34 (N1F1-PROC)	968.49 (H2N2-PROC)	1317.58 (H2N3F1-PROC)	528.09 (H2N1)		
														644.32 (N2-PROC)	1114.65 (H2N2F1-PROC)	1333.67 (H3N3-PROC)	690.23 (H3N1)		
														790.68 (N2F1-PROC)	1130.75 (H3N2-PROC)	1479.75 (H3N3F1-PROC)	731.50 (H2N2)		
														806.38 (H1N2-PROC)	1171.59 (H2N3-PRPC)	325.13 (H2)	893.23 (H3N2)		
4	20.0 (Cmpd 1160)	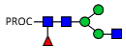	3	3	1	0	0	1479.65	740.33	493.89	1479.64	740.33	n.d.	441.26 (N1-PROC)	952.49 (H1N2F1-PROC)	203.91 (N1)	731.18 (H2N2)		
														587.39 (N1F1-PROC)	968.53 (H2N2-PROC)	325.03 (H2)	893.35 (H3N2)		
														644.36 (N2-PROC)	1114.54 (H2N2F1-PROC)	366.18 (H1N1)			
														790.63 (N2F1-PROC)	1130.48 (H3N2-PROC)	528.23 (H2N1)			
														806.41 (H1N2-PROC)	1276.60 (H3N2F1-PROC)	690.18 (H3N1)			
5	21.1 (Cmpd 1227)	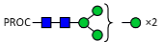	5	2	0	0	0	1454.61	727.81	485.54	1454.64	727.85	485.96	441.29 (N1-PROC)	325.09 (H2)	690.17 (H3N1)			
														644.39 (N2-PROC)	366.12 (H1N1)	811.56 (H5)			
														806.35 (H1N2-PROC)	487.23 (H3)	852.30 (H4N1)			
														968.55 (H2N2-PROC)	528.18 (H2N1)	1014.39 (H5N1)			
														203.95 (N1)	649.13 (H4)				
6	21.2 (Cmpd 1232)	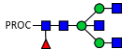	3	5	1	0	0	1885.80	943.41	629.27	n.d.	943.89	629.29	441.19 (N1-PROC)	952.50 (H1N2F1-PROC)	1171.60 (H2N3-PROC)	1479.67 (H3N3F1-PROC)	366.09 (H1N1)	893.21 (H3N2)
														587.32 (N1F1-PROC)	968.46 (H2N2-PROC)	1276.54 (H3N2F1-PROC)	1520.80 (H2N4F1-PROC)	528.07 (H2N1)	934.57 (H2N3)
														644.35 (N2-PROC)	1114.38 (H2N2F1-PROC)	1317.69 (H2N3F1-PROC)	1536.60 (H3N4-PROC)	569.17 (H1N2)	1096.48 (H3N3)
														790.52 (N2F1-PROC)	1130.50 (H3N2-PROC)	1333.61 (H3N3-PROC)	1682.83 (H3N4F1-PROC)	690.25 (H3N1)	1299.54 (H3N4)
														806.50 (H1N2-PROC)	1155.60 (H1N3F1-PROC)	1374.64 (H2N4-PROC)	325.13 (H2)	731.37 (H2N2)	
7	21.5 (Cmpd 1248)	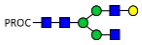	4	4	0	0	0	1698.72	849.86	566.91	1698.72	849.87	n.d.	441.28 (N1-PROC)	1171.56 (H2N3-PROC)	528.24 (H2N1)	1258.50 (H4N3)		
														644.32 (N2-PROC)	1333.65 (H3N3-PROC)	690.05 (H3N1)			
														806.39 (H1N2-PROC)	1495.73 (H4N3-PROC)	731.29 (H2N2)			
														968.50 (H2N2-PROC)	366.12 (H1N1)	893.38 (H3N2)			
														1130.56 (H3N2-PROC)	487.13 (H3)	1055.35 (H4N2)			
8	22.0 (Cmpd 1281)		4	4	0	0	0	1698.72	849.86	566.91	n.d.	849.88	566.93	441.25 (N1-PROC)	1171.59 (H2N3-PROC)	690.25 (H3N1)	1258.49 (H4N3)		
														644.38 (N2-PROC)	1333.64 (H3N3-PROC)	731.25 (H2N2)			
														806.23 (H1N2-PROC)	1495.73 (H4N3-PROC)	893.50 (H3N2)			
														968.43 (H2N2-PROC)	366.08 (H1N1)	1055.58 (H4N2)			
														1130.69 (H3N2-PROC)	528.17 (H2N1)	1096.25 (H3N3)			
9	22.9 (Cmpd 1332)	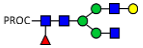	4	4	1	0	0	1844.78	922.89	615.60	n.d.	922.90	615.61	441.30 (N1-PROC)	952.50 (H1N2F1-PROC)	1276.65 (H3N2F1-PROC)	1641.73 (H4N3F1-PROC)	731.25 (H2N2)	
														587.32 (N1F1-PROC)	968.54 (H2N2-PROC)	1317.67 (H2N3F1-PROC)	325.00 (H2)	852.25 (H4N1)	
														644.26 (N2-PROC)	1114.54 (H2N2F1-PROC)	1333.70 (H3N3-PROC)	366.12 (H1N1)	893.26 (H3N2)	
														790.38 (N2F1-PROC)	1130.50 (H3N2-PROC)	1479.72 (H3N3F1-PROC)	528.23 (H2N1)	1055.46 (H4N2)	
														806.59 (H1N2-PROC)	1171.53 (H2N3-PROC)	1495.56 (H4N3-PROC)	690.16 (H3N1)	1258.52 (H4N3)	
10	23.6 (Cmpd 1380)	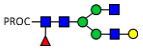	4	4	1	0	0	1844.78	922.89	615.60	n.d.	922.91	615.61	441.13 (N1-PROC)	968.46 (H2N2-PROC)	1317.69 (H2N3F1-PROC)	325.13 (H2)	852.75 (H4N1)	
														587.37 (N1F1-PROC)	1114.58 (H2N2F1-PROC)	1333.74 (H3N3-PROC)	366.07 (H1N1)	893.75 (H3N2)	
														790.52 (N2F1-PROC)	1130.61 (H3N2-PROC)	1479.72 (H3N3F1-PROC)	528.25 (H2N1)	1055.33 (H4N2)	
														806.37 (H1N2-PROC)	1171.50 (H2N3-PROC)	1495.69 (H4N3-PROC)	690.17 (H3N1)	1096.62 (H3N3)	
														952.52 (H1N2F1-PROC)	1276.64 (H3N2F1-PROC)	1641.72 (H4N3F1-PROC)	731.26 (H2N2)	1258.45 (H4N3)	
11	24.0 (Cmpd 1404)	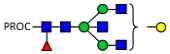	4	5	1	0	0	2047.86	1024.43	683.29	n.d.	1024.46	683.31	441.37 (N1-PROC)	968.38 (H2N2-PROC)	1333.51 (H3N3-PROC)	1641.68 (H4N3F1-PROC)	528.38 (H2N1)	1299.50 (H3N4)
														587.33 (N1F1-PROC)	1114.63 (H2N2F1-PROC)	1479.69 (H3N3F1-PROC)	1682.78 (H3N4F1-PROC)	893.36 (H3N2)	1461.63 (H4N4)
														644.38 (N2-PROC)	1155.75 (H1N3F1-PROC)	1495.63 (H4N3-PROC)	1844.83 (H4N4F1-PROC)	934.38 (H2N3)	
														790.49 (N2F1-PROC)	1171.66 (H2N3-PROC)	1520.88 (H2N4F1-PROC)	325.25 (H2)	1055.26 (H4N2)	
														806.50 (H1N2-PROC)	1317.58 (H2N3F1-PROC)	1536.69 (H3N4-PROC)	366.11 (H1N1)	1258.13 (H4N3)	
12	24.6 (Cmpd 1442)		6	2	0	0	0	1616.67	808.84	539.56	n.d.	808.84	n.d.	441.29 (N1-PROC)	366.01 (H1N1)	852.30 (H4N1)			
														644.39 (N2-PROC)	487.25 (H3)	973.38 (H6)			
														968.72 (H2N2-PROC)	528.10 (H2N1)	1014.36 (H5N1)			
														1130.63 (H3N2-PROC)	649.13 (H4)	1176.48 (H6N1)			
														325.05 (H2)	690.26 (H3N1)				

Table S4.4 (continued)

Peak ID	Retention time (min)	Structure	Composition					LC-ESI-MS									
			Hex (H)	HexNAc (N)	Fuc (F)	Neu5Ac (S)	Neu5Gc (G)	$[M/Z]^{+}$ calculated	$[M/Z]^{2+}$ calculated	$[M/Z]^{3+}$ calculated	$[M/Z]^{+}$ registered	$[M/Z]^{2+}$ registered	$[M/Z]^{3+}$ registered	[M/Z] characteristic fragment ions (composition)						
13	25.1 (Cmpd 1473)		5	4	0	0	0	1860.77	930.89	620.93	n.d.	930.91	620.95	441.20 (N1-PROC)	1333.62 (H3N3-PROC)	731.13 (H2N2)	1420.53 (H5N3)			
														644.36 (N2-PROC)	1495.69 (H4N3-PROC)	852.20 (H4N1)				
														968.55 (H2N2-PROC)	366.12 (H1N1)	893.63 (H3N2)				
														1130.53 (H3N2-PROC)	528.17 (H2N1)	1055.39 (H4N2)				
														1171.0 (H2N3-PROC)	690.39 (H3N1)	1258.39 (H4N3)				
14	26.3 (Cmpd 1546)	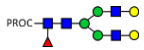	5	4	1	0	0	2006.83	1003.92	669.62	n.d.	1003.96	669.63	441.29 (N1-PROC)	968.63 (H2N2-PROC)	1333.55 (H3N3-PROC)	366.09 (H1N1)	1055.29 (H4N2)		
														587.34 (N1F1-PROC)	1114.63 (H2N2F1-PROC)	1479.71 (H3N3F1-PROC)	528.21 (H2N1)	1096.50 (H3N3)		
														644.39 (N2-PROC)	1130.50 (H3N2-PROC)	1495.67 (H4N3-PROC)	690.16 (H3N1)	1217.75 (H5N2)		
														790.38 (N2F1-PROC	1171.00 (H2N3-PROC)	1641.75 (H4N3F1-PROC)	731.38 (H2N2)	1258.59 (H4N3)		
														952.51 (H1N2F1-PROC)	1276.68 (H3N2F1-PROC)	325.35 (H2)	893.38 (H3N2)	1420.52 (H5N3)		
15	27.0 (Cmpd 1590)	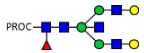	5	5	1	0	0	2209.91	1105.46	737.31	n.d.	1105.44	737.32	441.25 (N1-PROC)	952.25 (H1N2F1-PROC)	1155.63 (H1N3F1-PROC)	1479.68 (H3N3F1-PROC)	366.11 (H1N1)	1055.15 (H4N2)	
														587.34 (N1F1-PROC)	968.44 (H2N2-PROC)	1276.79 (H3N2F1-PROC)	1495.70 (H4N3-PROC)	528.16 (H2N1)	1096.38 (H3N3)	
														644.50 (N2-PROC)	1009.75 (H1N3-PROC)	1171.58 (H2N3-PROC)	1641.63 (H4N3F1-PROC)	569.25 (H1N2)	1258.54 (H4N3)	
														790.47 (N2F1-PROC)	1114.63 (H2N2F1-PROC)	1317.63 (H2N3F1-PROC)	203.95 (N1)	690.25 (H3N1)		
														806.75 (H1N2-PROC)	1130.00 (H3N2-PROC)	1333.61 (H3N3-PROC)	325.25 (H2)	893.17 (H3N2)		
16	27.5 (Cmpd 1617)	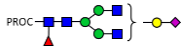	4	4	1	1	0	2135.87	1068.44	712.63	n.d.	1068.46	712.66	441.31 (N1-PROC)	968.48 (H2N2-PROC)	1333.71 (H3N3-PROC)	366.19 (H1N1)	893.78 (H3N2)		
														587.31 (N1F1-PROC)	1114.58 (H2N2F1-PROC)	1438.38 (H4N2F1-PROC)	528.04 (H2N1)	981.38 (H3N1S1)		
														644.43 (N2-PROC)	1130.62 (H3N2-PROC)	1479.69 (H3N3F1-PROC)	657.20 (H1N1S1)	1055.50 (H4N2)		
														806.51 (H1N2-PROC)	1276.59 (H3N2F1-PROC)	1495.75 (H4N3-PROC)	690.22 (H3N1)	1184.38 (H3N2S1)		
														952.41 (H1N2F1-PROC)	1317.53 (H2N3F1-PROC)	1641.79 (H4N3F1-PROC)	819.38 (H2N1S1)	1258.25 (H4N3)		
17	28.8 (Cmpd 1700)	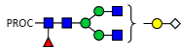	5	4	0	1	1	2151.87	1076.44	717.96	n.d.	1076.47	717.98	441.19 (N1-PROC)	952.45 (H1N2F1-PROC)	1276.60 (H3N2F1-PROC)	1641.85 (H4N3F1-PROC)	366.08 (H1N1)	835.25 (H2N1G1)	1362.48 (H4N2G1)
														587.29 (N1F1-PROC)	968.33 (H2N2-PROC)	1317.58 (H2N3F1-PROC)	1786.82 (H3N3G1F1-PROC)	528.12 (H2N1)	893.88 (H3N2)	1565.60 (H4N3G1)
														644.39 (N2-PROC)	1114.53 (H2N2F1-PROC)	1333.59 (H3N3-PROC)	1802.79 (H4N3G1-PROC)	673.20 (H1N1G1)	997.13 (H3N1G1)	
														790.39 (N2F1-PROC)	1130.55 (H3N2-PROC)	1479.69 (H3N3F1-PROC)	1948.82 (H4N3G1F1-PROC)	690.13 (H3N1)	1159.47 (H4N1G1)	
														806.44 (H1N2-PROC)	1171.66 (H2N3-PROC)	1495.61 (H4N3-PROC)	308.26 (G1)	731.25 (H2N2)	1200.50 (H3N2G1)	
18	29.4 (Cmpd 1734)	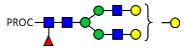	6	4	1	0	0	2168.88	1084.95	723.63	n.d.	1084.97	723.65	441.27 (N1-PROC)	952.52 (H1N2F1-PROC)	1495.75 (H4N3-PROC)	690.22 (H3N1)	1096.38 (H3N3)		
														587.31 (N1F1-PROC)	968.43 (H2N2-PROC)	203.95 (N1)	731.88 (H2N2)	1217.45 (H5N2)		
														644.07 (N2-PROC)	1114.59 (H2N2F1-PROC)	325.10 (H2)	852.34 (H4N1)			
														790.46 (N2F1-PROC)	1130.55 (H3N2-PROC)	366.10 (H1N1)	893.28 (H3N2)			
														806.33 (H1N2-PROC)	1276.61 (H3N2F1-PROC)	528.17 (H2N1)	1055.52 (H4N2)			
19	30.0 (Cmpd 1770)	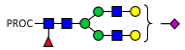	5	4	1	1	0	2297.93	1149.47	766.65	n.d.	1149.44	766.68	441.33 (N1-PROC)	968.52 (H2N2-PROC)	1479.79 (H3N3F1-PROC)	366.09 (H1N1)	819.29 (H2N1S1)	1184.56 (H3N2S1)	
														587.29 (N1F1-PROC)	1114.56 (H2N2F1-PROC)	1495.67 (H4N3-PROC)	528.09 (H2N1)	852.13 (H4N1)	1217.63 (H5N2)	
														644.20 (N2-PROC)	1130.52 (H3N2-PROC)	1641.84 (H4N3F1-PROC)	657.17 (H1N1S1)	893.38 (H3N2)	1346.53 (H4N2S1)	
														806.11 (H1N2-PROC)	1276.62 (H3N2F1-PROC)	292.05 (S1)	690.75 (H3N1)	981.01 (H3N1S1)		
														952.53 (H1N2F1-PROC)	1333.63 (H3N3-PROC)	325.13 (H2)	731.39 (H2N2)	1055.42 (H4N2)		
20	30.9 (Cmpd 1824)	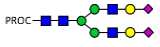	5	4	0	2	0	2442.96	1221.99	814.99	n.d.	n.d.	814.67	441.34 (N1-PROC)	1333.54 (H3N3-PROC)	325.18 (H2)	731.88 (H2N2)			
														644.50 (N2-PROC)	1495.65 (H4N3-PROC)	366.16 (H1N1)	893.85 (H3N2)			
														806.41 (H1N2-PROC)	1624.88 (H3N3S1-PROC)	454.02 (H1S1)	1055.38 (H4N2)			
														968.50 (H2N2-PROC)	1786.97 (H4N3S1-PROC)	657.22 (H1N1S1)	1143.64 (H4N1S1)			
														1130.56 (H3N2-PROC)	292.03 (S1)	690.25 (H3N1)	1184.63 (H3N2S1)			
21	31.6 (Cmpd 1866)	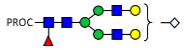	5	4	1	0	1	2313.92	1157.46	771.98	n.d.	1157.94	771.99	441.24 (N1-PROC)	952.48 (H1N2F1-PROC)	1276.64 (H3N2F1-PROC)	1802.54 (H4N3G1-PROC)	528.16 (H2N1)	893.27 (H3N2)	1217.50 (H5N2)
														587.26 (N1F1-PROC)	968.54 (H2N2-PROC)	1333.76 (H3N3-PROC)	308.05 (G1)	673.16 (H1N1G1)	997.50 (H3N1G1)	1362.63 (H4N2G1)
														644.37 (N2-PROC)	1114.54 (H2N2F1-PROC)	1479.63 (H3N3F1-PROC)	325.14 (H2)	690.16 (H3N1)	1055.35 (H4N2)	1420.50 (H5N3)
														790.26 (N2F1-PROC)	1130.52 (H3N2-PROC)	1495.64 (H4N3-PROC)	366.11 (H1N1)	731.13 (H2N2)	1159.38 (H4N1G1)	1524.51 (H5N2G1)
														806.51 (H1N2-PROC)	1171.50 (H2N3-PROC)	1641.88 (H4N3F1-PROC)	470.02 (H1G1)	835.33 (H2N1G1)	1200.76 (H3N2G1)	
22	33.9 (Cmpd 2004)	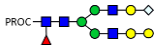	6	4	1	0	1	2475.97	1238.49	826.00	n.d.	1238.97	826.02	441.23 (N1-PROC)	952.43 (H1N2F1-PROC)	1479.75 (H3N3F1-PROC)	307.99 (G1)	673.20 (H1N1G1)	893.82 (H3N2)	1200.50 (H3N2G1)
														587.38 (N1F1-PROC)	968.48 (H2N2-PROC)	1495.67 (H4N3-PROC)	325.13 (H2)	690.35 (H3N1)	997.45 (H3N1G1)	1217.71 (H5N2)
														644.51 (N2-PROC)	1114.59 (H2N2F1-PROC)	1641.65 (H4N3F1-PROC)	366.10 (H1N1)	731.13 (H2N2)	1014.50 (H5N1)	1362.53 (H4N2G1)
														790.60 (N2F1-PROC)	1130.55 (H3N2-PROC)	1657.75 (H5N3-PROC)	470.08 (H1G1)	835.28 (H2N1G1)	1055.33 (H4N2)	1420.50 (H5N3)
														806.58 (H1N2-PROC)	1276.62 (H3N2F1-PROC)	1803.92 (H5N3F1-PROC)	528.19 (H2N1)	852.63 (H4N1)	1159.50 (H4N1G1-PROC)	1582.50 (H6N3)
23	34.7 (Cmpd 2052)	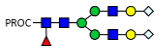	5	4	1	0	2	2621.01	1311.01	874.34	n.d.	n.d.	874.36	441.12 (N1-PROC)	952.13 (H1N2F1-PROC)	1317.75 (H2N3F1-PROC)	1641.74 (H4N3F1-PROC)	527.92 (H2N1)	1055.25 (H4N2)	1362.38 (H4N2G1)
														587.33 (N1F1-PROC)	968.46 (H2N2-PROC)	1333.63 (H3N3-PROC)	1948.62 (H4N3F1G1-PROC)	673.24 (H1N1G1)	1096.25 (H3N3)	1524.62 (H5N2G1)
														644.49 (N2-PROC)	1114.56 (H2N2F1-PROC)	1479.70 (H3N3F1-PROC)	308.05 (G1)	835.63 (H2N1G1)	1159.63 (H4N1G1)	1565.50 (H4N3G1)
														790.51 (N2F1-PROC)	1130.56 (H3N2-PROC)	1495.60 (H4N3-PROC)	366.20 (H1N1)	893.37 (H3N2)	1200.38 (H3N2G1)	
														806.38 (H1N2-PROC)	1276.64 (H3N2F1-PROC)	1640.76 (H3N3G1-PROC)	470.63 (H1G1)	997.51 (H3N1G1)	1258.38 (H4N3)	
24	36.0 (Cmpd 2127)	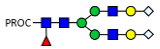	5	4	1	0	2	2621.01	1311.01	874.34	n.d.	n.d.	874.01	441.23 (N1-PROC)	952.63 (H1N2F1-PROC)	1317.67 (H2N3F1-PROC)	1948.79 (H4N3F1G1-PROC)	528.04 (H2N1)	997.63 (H3N1G1)	1524.63 (H5N2G1)
														587.20 (N1F1-PROC)	968.48 (H2N2-PROC)	1333.75 (H3N3-PROC)	308.02 (G1)	673.18 (H1N1G1)	1055.88 (H4N2)	1727.63 (H5N3G1)
														644.75 (N2-PROC)	1114.61 (H2N2F1-PROC)	1495.56 (H4N3-PROC)	325.05 (H2)	835.33 (H2N1G1)	1159.63 (H4N1G1)	
														790.45 (N2F1-PROC)	1130.48 (H3N2-PROC)	1641.69 (H4N3F1-PROC)	366.11 (H1N1)	852.38 (H4N1)	1200.38 (H3N2G1)	
														806.40 (H1N2-PROC)	1276.61 (H3N2F1-PROC)	1802.75 (H4N3G1-PROC)	487.88 (H3)	893.29 (H3N2)	1362.68 (H4N2G1)	

Table S4.5 N-glycans composition of immunoprecipitated L1CAM from SW620 membrane proteins identified by MS^n fragmentation analysis with identified Y- and B-ion fragments. N-glycans from IP L1CAM were released, labelled, and analysed by LC-ESI-MS/MS. Mass spectrometry data were analysed using the Bruker Compass DataAnalysis 4.1 software. LC-ESI-MS/MS chromatogram analysis was performed using Bruker Compass DataAnalysis 4.4 and GlycoWorkbench software. Structures were identified by comparing LC, MS, and MS/MS data. Structures for N-glycans are depicted with the following notation: PROC: procainamide; blue square: N-acetylglucosamine; green circle: Mannose; yellow circle: Galactose; red triangle: Fucose; purple diamond: N-acetylneuraminic acid; white diamond: N-glycolylneuraminic acid. Identified Y- and B-ion fragments, noted respectively in black and blue, are given in terms of the number of hexose (H), N-acetylhexosamine (N), deoxyhexose (F), N-acetylneuraminic acid (S) and N-glycolylneuraminic acid (G). Abbreviations: LC-ESI-MS/MS, liquid chromatography electrospray ionisation tandem mass spectrometry; Hex, hexose; HexNAc, N-acetylhexosamine; Fuc, Fucose; Neu5Ac, N-acetylneuraminic acid; Neu5Gc, N-glycolylneuraminic acid; Cmpd, compound; n.d., not detectable.

Peak ID	Retention time (min)	Structure	Composition					LC-ESI-MS						
			Hex (H)	HexNAc (N)	Fuc (F)	Neu5Ac (S)	Neu5Gc (G)	$[M/Z]^+$ calculated	$[M/Z]^{2+}$ calculated	$[M/Z]^{3+}$ calculated	$[M/Z]^+$ registered	$[M/Z]^{2+}$ registered	$[M/Z]^{3+}$ registered	[M/Z] characteristic fragment ions (composition)
1	11.0 (Cmpd 625)		2	2	1	0	0	1114.51	557.76	372.18	1114.55	557.78	n.d.	441.08 (N1-PROC) 952.51 (H1N2F1-PROC) 587.31 (N1F1-PROC) 968.46 (H2N2-PROC) 644.44 (N2-PROC) 325.13 (H2) 790.43 (N2F1-PROC) 528.38 (H2N1) 806.42 (H1N2-PROC)
2	13.3 (Cmpd 752)	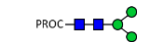	3	2	0	0	0	1130.51	565.76	377.51	1129.50	565.27	n.d.	441.26 (N1-PROC) 487.25 (H3) 644.41 (N2-PROC) 528.25 (H2N1) 806.44 (H1N2-PROC) 968.49 (H2N2-PROC) 325.11 (H2)
3	15.1 (Cmpd 859)		3	2	1	0	0	1276.57	638.79	426.19	1276.52	638.82	n.d.	441.24 (N1-PROC) 968.59 (H2N2-PROC) 528.15 (H2N1) 587.32 (N1F1-PROC) 1114.38 (H2N2F1-PROC) 690.17 (H3N1) 644.34 (N2-PROC) 203.93 (N1) 806.35 (H1N2-PROC) 324.97 (H2) 952.75 (H1N2F1-PROC) 366.08 (H1N1)
4	17.7 (Cmpd 1005)	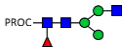	3	3	1	0	0	1479.65	740.33	493.89	1479.58	740.35	n.d.	441.27 (N1-PROC) 968.54 (H2N2-PROC) 325.13 (H2) 731.38 (H2N2) 587.23 (N1F1-PROC) 1114.56 (H2N2F1-PROC) 366.38 (H1N1) 893.41 (H3N2) 644.38 (N2-PROC) 1130.88 (H3N2-PROC) 487.30 (H3) 790.38 (N2F1-PROC) 1276.60 (H3N2F1-PROC) 528.20 (H2N1) 806.51 (H1N2-PROC) 203.87 (N1) 690.15 (H3N1)
5	18.2 (Cmpd 1035)		3	4	0	0	0	1536.67	768.84	512.89	1536.67	768.87	512.92	441.29 (N1-PROC) 1171.52 (H2N3-PROC) 690.25 (H3N1) 644.41 (N2-PROC) 1333.64 (H3N3-PROC) 731.66 (H2N2) 806.39 (H1N2-PROC) 325.00 (H2) 893.36 (H3N2) 968.58 (H2N2-PROC) 366.05 (H1N1) 1096.37 (H3N3) 1130.49 (H3N2-PROC) 528.13 (H2N1)
6	19.7 (Cmpd 1126)	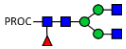	3	4	1	0	0	1682.72	841.87	561.58	1682.72	841.90	561.59	441.32 (N1-PROC) 952.40 (H1N2F1-PROC) 1276.60 (H3N2F1-PROC) 366.18 (H1N1) 1096.44 (H3N3) 587.35 (N1F1-PROC) 968.44 (H2N2-PROC) 1317.73 (H2N3F1-PROC) 528.24 (H2N1) 644.47 (N2-PROC) 1114.61 (H2N2F1-PROC) 1333.44 (H3N3-PROC) 690.16 (H3N1) 790.52 (N2F1-PROC) 1130.68 (H3N2-PROC) 1479.71 (H3N3F1-PROC) 731.75 (H2N2) 806.50 (H1N2-PROC) 1171.55 (H2N3-PRPC) 325.06 (H2) 893.32 (H3N2)
7	20.0 (Cmpd 1143)	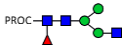	3	3	1	0	0	1479.65	740.33	493.89	1479.66	740.33	n.d.	441.27 (N1-PROC) 952.50 (H1N2F1-PROC) 203.8 (N1) 731.50 (H2N2) 587.39 (N1F1-PROC) 968.46 (H2N2-PROC) 325.13 (H2) 893.28 (H3N2) 644.25 (N2-PROC) 1114.40 (H2N2F1-PROC) 366.24 (H1N1) 790.38 (N2F1-PROC) 1130.57 (H3N2-PROC) 528.08 (H2N1) 806.26 (H1N2-PROC) 1276.60 (H3N2F1-PROC) 690.24 (H3N1)
8	21.2 (Cmpd 1211)		5	2	0	0	0	1454.61	727.81	485.54	1454.56	727.85	n.d.	441.27 (N1-PROC) 325.13 (H2) 690.23 (H3N1) 644.35 (N2-PROC) 366.15 (H1N1) 852.32 (H4N1) 806.49 (H1N2-PROC) 487.04 (H3) 1014.40 (H5N1) 968.75 (H2N2-PROC) 528.18 (H2N1) 203.97 (N1) 649.63 (H4)
9	21.3 (Cmpd 1220)	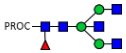	3	5	1	0	0	1885.80	943.41	629.27	n.d.	943.43	629.29	587.30 (N1F1-PROC) 1155.56 (H1N3F1-PROC) 1520.69 (H2N4F1-PROC) 569.16 (H1N2) 1299.53 (H3N4) 644.38 (N2-PROC) 1171.70 (H2N3-PROC) 1536.75 (H3N4-PROC) 690.13 (H3N1) 790.44 (N2F1-PROC) 1317.67 (H2N3F1-PROC) 1682.78 (H3N4F1-PROC) 731.01 (H2N2) 806.51 (H1N2-PROC) 1333.58 (H3N3-PROC) 366.13 (H1N1) 893.00 (H3N2) 1114.38 (H2N2F1-PROC) 1479.69 (H3N3F1-PROC) 528.13 (H2N1) 1096.50 (H3N3)
10	21.5 (Cmpd 1230)	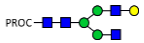	4	4	0	0	0	1698.72	849.86	566.91	n.d.	849.88	566.93	441.34 (N1-PROC) 1171.50 (H2N3-PROC) 690.14 (H3N1) 644.29 (N2-PROC) 1333.64 (H3N3-PROC) 731.63 (H2N2) 806.50 (H1N2-PROC) 1495.67 (H4N3-PROC) 893.25 (H3N2) 968.45 (H2N2-PROC) 366.14 (H1N1) 1055.31 (H4N2) 1130.58 (H3N2-PROC) 528.08 (H2N1) 1258.74 (H4N3)
11	21.9 (Cmpd 1253)	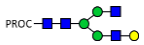	4	4	0	0	0	1698.72	849.86	566.91	n.d.	849.86	566.93	441.24 (N1-PROC) 1495.60 (H4N3-PROC) 731.01 (H2N2) 968.42 (H2N2-PROC) 325.25 (H2) 893.50 (H3N2) 1130.59 (H3N2-PROC) 366.15 (H1N1) 1055.50 (H4N2) 1171.56 (H2N3-PROC) 528.33 (H2N1) 1096.51 (H3N3) 1333.61 (H3N3-PROC) 690.51 (H3N1) 1258.37 (H4N3)
12	23.2 (Cmpd 1328)	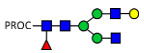	4	4	1	0	0	1844.78	922.89	615.60	n.d.	922.91	615.61	441.28 (N1-PROC) 952.45 (H1N2F1-PROC) 1276.59 (H3N2F1-PROC) 1641.74 (H4N3F1-PROC) 731.28 (H2N2) 1258.68 (H4N3) 587.32 (N1F1-PROC) 968.49 (H2N2-PROC) 1317.61 (H2N3F1-PROC) 325.13 (H2) 851.81 (H4N1) 644.37 (N2-PROC) 1114.55 (H2N2F1-PROC) 1333.63 (H3N3-PROC) 366.10 (H1N1) 893.25 (H3N2) 790.38 (N2F1-PROC) 1130.38 (H3N2-PROC) 1479.73 (H3N3F1-PROC) 528.12 (H2N1) 1055.34 (H4N2) 806.38 (H1N2-PROC) 1171.57 (H2N3-PROC) 1495.77 (H4N3-PROC) 690.17 (H3N1) 1096.61 (H3N3)

Table S4.5 (continued)

Peak ID	Retention time (min)	Structure	Composition					LC-ESI-MS								
			Hex (H)	HexNAc (N)	Fuc (F)	Neu5Ac (S)	Neu5Gc (G)	$[M/Z]^+$ calculated	$[M/Z]^{2+}$ calculated	$[M/Z]^{3+}$ calculated	$[M/Z]^+$ registered	$[M/Z]^{2+}$ registered	$[M/Z]^{3+}$ registered	[M/Z] characteristic fragment ions (composition)						
13	23.7 (Cmpd 1361)		4	4	1	0	0	1844.78	922.89	615.60	n.d.	922.92	615.61	441.28 (N1-PROC)	952.50 (H1N2F1-PROC)	1276.65 (H3N2F1-PROC)	1641.72 (H4N3F1-PROC)	690.27 (H3N1)	1258.53 (H4N3)	
														587.34 (N1F1-PROC)	968.53 (H2N2-PROC)	1317.62 (H2N3F1-PROC)	1682.25 (H3N4F1-PROC)	731.16 (H2N2)		
														644.50 (N2-PROC)	1114.55 (H2N2F1-PROC)	1333.69 (H3N3-PROC)	325.18 (H2)	852.50 (H4N1)		
														790.43 (N2F1-PROC)	1130.60 (H3N2-PROC)	1479.70 (H3N3F1-PROC)	366.12 (H1N1)	893.28 (H3N2)		
														806.26 (H1N2-PROC)	1171.63 (H2N3-PROC)	1495.67 (H4N3-PROC)	528.17 (H2N1)	1055.34 (H4N2)		
14	24.0 (Cmpd 1379)	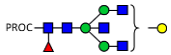	4	5	1	0	0	2047.86	1024.43	683.29	n.d.	1024.46	683.67	441.45 (N1-PROC)	968.88 (H2N2-PROC)	1479.67 (H3N3F1-PROC)	1682.71 (H3N4F1-PROC)	569.13(H1N2)	1299.38 (H3N4)	
														587.31 (N1F1-PROC)	1155.75 (H1N3F1-PROC)	1495.25 (H4N3-PROC)	1844.81 (H4N4F1-PROC)	690.30 (H3N1)	1461.61 (H4N4)	
														790.52 (N2F1-PROC)	1171.88 (H2N3-PROC)	1520.69 (H2N4F1-PROC)	325.38 (H2)	731.19 (H2N2)		
														806.38 (H1N2-PROC)	1317.60 (H2N3F1-PROC)	1536.75 (H3N4-PROC)	366.11 (H1N1)	1096.14 (H3N3)		
														952.38 (H1N2F1-PROC)	1333.57 (H3N3-PROC)	1641.63 (H4N3F1-PROC)	528.30 (H2N1)	1258.42 (H4N3)		
15	24.6 (Cmpd 1416)		6	2	0	0	0	1616.67	808.84	539.56	n.d.	808.86	n.d.	441.29 (N1-PROC)	366.21 (H1N1)	852.30 (H4N1)				
														644.37 (N2-PROC)	487.13 (H3)	1014.43 (H5N1)				
														968.50 (H2N2-PROC)	528.26 (H2N1)	1176.50 (H6N1)				
														1130.38 (H3N2-PROC)	648.89 (H4)					
														325.16 (H2)	690.25 (H3N1)					
16	25.2 (Cmpd 1449)		5	4	0	0	0	1860.77	930.89	620.93	n.d.	930.89	620.95	441.30 (N1-PROC)	1333.60 (H3N3-PROC)	731.25 (H2N2)				
														806.27 (H1N2-PROC)	1495.67 (H4N3-PROC)	893.73 (H3N2)				
														968.38 (H2N2-PROC)	325.16 (H2)	1055.38 (H4N2)				
														1130.63 (H3N2-PROC)	366.14 (H1N1)	1420.60 (H5N3)				
														1171.13 (H2N3-PROC)	528.22 (H2N1)					
17	26.3 (Cmpd 1511)	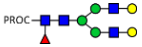	5	4	1	0	0	2006.83	1003.92	669.62	n.d.	1003.94	669.63	441.30 (N1-PROC)	968.76 (H2N2-PROC)	1333.57 (H3N3-PROC)	487.38 (H3)	893.38 (H3N2)		
														587.36 (N1F1-PROC)	1114.03 (H2N2F1-PROC)	1479.69 (H3N3F1-PROC)	528.19 (H2N1)	1055.29 (H4N2)		
														644.25 (N2-PROC)	1130.50 (H3N2-PROC)	1495.63 (H4N3-PROC)	690.01 (H3N1)	1217.50 (H5N2)		
														806.88 (H1N2-PROC)	1276.56 (H3N2F1-PROC)	1641.72 (H4N3F1-PROC)	731.13 (H2N2)	1258.53 (H4N3)		
														952.38 (H1N2F1-PROC)	1317.75 (H2N3F1-PROC)	366.14 (H1N1)	852.75 (H4N1)	1420.44 (H5N3)		
18	27.1 (Cmpd 1559)	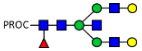	5	5	1	0	0	2209.91	1105.46	737.31	n.d.	1105.49	737.33	441.27 (N1-PROC)	952.46 (H1N2F1-PROC)	1333.59 (H3N3-PROC)	325.11 (H2)	893.32 (H3N2)		
														587.33 (N1F1-PROC)	1009.48 (H1N3-PROC)	1479.64 (H3N3F1-PROC)	366.14 (H1N1)	1096.40 (H3N3)		
														644.35 (N2-PROC)	1130.51 (H3N2-PROC)	1495.64 (H4N3-PROC)	528.19 (H2N1)	1258.46 (H4N3)		
														790.41 (N2F1-PROC)	1171.53 (H2N3-PROC)	1641.70 (H4N3F1-PROC)	569.22 (H1N2)	1461.54 (H4N4)		
														806.40 (H1N2-PROC)	1317.59 (H2N3F1-PROC)	204.09 (N1)	690.24 (H3N1)			
19	28.1 (Cmpd 1619)	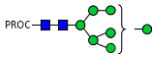	7	2	0	0	0	1778.72	889.86	593.58	n.d.	889.86	n.d.	441.27 (N1-PROC)	366.02 (H1N1)	1176.47 (H6N1)				
														644.36 (N2-PROC)	528.12 (H2N1)	1338.54 (H7N1)				
														806.54 (H1N2-PROC)	690.12 (H3N1)					
														968.44 (H2N2-PROC)	852.25 (H4N1)					
														1130.57 (H3N2-PROC)	1014.31 (H5N1)					
20	29.0 (Cmpd 1672)	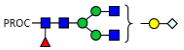	4	4	0	1	1	2151.87	1076.44	717.96	n.d.	1076.47	717.98	441.28 (N1-PROC)	968.50 (H2N2-PROC)	1317.58 (H2N3F1-PROC)	203.99 (N1)	673.18 (H1N1G1)	893.24 (H3N2)	1200.38 (H3N2G1)
														587.31 (N1F1-PROC)	1114.55 (H2N2F1-PROC)	1333.60 (H3N3-PROC)	325.12 (H2)	690.25 (H3N1)	997.38 (H3N1G1)	1258.46 (H4N3)
														644.39 (N2-PROC)	1130.55 (H3N2-PROC)	1479.70 (H3N3F1-PROC)	366.09 (H1N1)	731.23 (H2N2)	1055.26 (H4N2)	1362.52 (H4N2G1)
														806.44 (H1N2-PROC)	1171.44 (H2N3-PROC)	1495.66 (H4N3-PROC)	470.15 (H1G1)	835.29 (H2N1G1)	1096.34 (H3N3)	
														952.39 (H1N2F1-PROC)	1276.61 (H3N2F1-PROC)	1641.77 (H4N3F1-PROC)	528.18 (H2N1)	852.25 (H4N1)	1159.38 (H4N1G1)	
21	29.4 (Cmpd 1699)	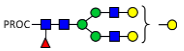	6	4	1	0	0	2168.88	1084.95	723.63	n.d.	1084.97	723.65	441.32 (N1-PROC)	952.55 (H1N2F1-PROC)	1333.50 (H3N3-PROC)	487.63 (H3)			
														587.42 (N1F1-PROC)	968.41 (H2N2-PROC)	1479.63 (H3N3F1-PROC)	528.17 (H2N1)			
														644.75 (N2-PROC)	1114.55 (H2N2F1-PROC)	1495.71 (H4N3-PROC)	690.36 (H3N1)			
														790.25 (N2F1-PROC)	1130.54 (H3N2-PROC)	203.88 (N1)	852.13 (H4N1)			
														806.29 (H1N2-PROC)	1276.59 (H3N2F1-PROC)	366.12 (H1N1)	1055.40 (H4N2)			
22	30.2 (Cmpd 1743)	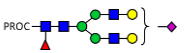	5	4	1	1	0	2297.93	1149.47	766.65	n.d.	1149.44	766.67	441.30 (N1-PROC)	952.51 (H1N2F1-PROC)	1317.75 (H2N3F1-PROC)	291.88 (S1)	819.26 (H2N1S1)	1258.50 (H4N3)	
														587.30 (N1F1-PROC)	968.40 (H2N2-PROC)	1333.63 (H3N3-PROC)	366.08 (H1N1)	852.25 (H4N1)	1346.63 (H4N2S1)	
														644.66 (N2-PROC)	1114.64 (H2N2F1-PROC)	1479.63 (H3N3F1-PROC)	528.32 (H2N1)	893.95 (H3N2)	1420.75 (H5N3)	
														790.50 (N2F1-PROC)	1130.56 (H3N2-PROC)	1495.72 (H4N3-PROC)	657.22 (H1N1S1)	1055.33 (H4N2)		
														806.63 (H1N2-PROC)	1276.64 (H3N2F1-PROC)	1641.80 (H4N3F1-PROC)	731.29 (H2N2)	1184.38 (H3N2S1)		
23	30.3 (Cmpd 1752)	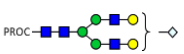	5	4	0	0	1	2167.86	1084.43	723.29	n.d.	1084.47	723.30	441.27 (N1-PROC)	1333.57 (H3N3-PROC)	366.09 (H1N1)	835.19 (H2N1G1)	1362.50 (H4N2G1)		
														644.43 (N2-PROC)	1495.71 (H4N3-PROC)	470.04 (H1G1)	893.25 (H3N2)			
														806.52 (H1N2-PROC)	204.04 (N1)	528.17 (H2N1)	1055.31 (H4N2)			
														968.54 (H2N2-PROC)	308.00 (G1)	673.23 (H1N1G1)	1159.50 (H3N1G1)			
														1130.57 (H3N2-PROC)	325.04 (H2)	690.13 (H3N1)	1200.88 (H3N2G1)			
24	30.9 (Cmpd 1784)	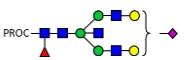	5	5	1	1	0	2501.01	1251.01	834.34	n.d.	n.d.	834.37	441.27 (N1-PROC)	952.63 (H1N2F1-PROC)	13333.60 (H3N3-PROC)	454.25 (H1S1)	819.17 (H2N1S1)	1549.38 (H4N3S1)	
														587.32 (N1F1-PROC)	968.38 (H2N2-PROC)	1479.79 (H3N3F1-PROC)	528.01 (H2N1)	893.13 (H3N2)		
														644.46 (N2-PROC)	1155.38 (H1N3F1-PROC)	1786.72 (H4N3S1-PROC)	657.23 (H1N1S1)	1096.39 (H3N3)		
														790.28 (N2F1-PROC)	1276.75 (H3N2F1-PROC)	1844.79 (H4N4F1-PROC)	690.27 (H3N1)	1258.13 (H4N3)		
														806.38 (H1N2-PROC)	1317.64 (H2N3F1-PROC)	366.14 (H1N1)	731.75 (H2N2)	1461.63 (H4N4)		
25	30.9 (Cmpd 1786)	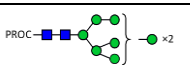	8	2	0	0	0	1940.77	970.89	647.60	n.d.	970.89	n.d.	441.28 (N1-PROC)	325.15 (H2)	690.33 (H3N1)	1297.50 (H8)			
														644.36 (N2-PROC)	366.12 (H1N1)	811.25 (H5)	1338.45 (H7N1)			
														806.47 (H1N2-PROC)	486.77 (H3)	852.26 (H4N1)	1500.54 (H8N1)			
														1130.75 (H3N2-PROC)	528.27 (H2N1)	1014.45 (H5N1)				
														1292.52 (H4N2-PROC)	649.15 (H4)	1176.72 (H6N1)				
26	31.0 (Cmpd 1789)		5	4	0	2	0	2442.96	1221.99	814.99	n.d.	1221.93	815.02	441.15 (N1-PROC)	1333.59 (H3N3-PROC)	454.13 (H1S1)	1346.38 (H4N2S1)			
														644.38 (N2-PROC)	1495.68 (H4N3-PROC)	528.14 (H2N1)	1420.50 (H5N3)			
														806.47 (H1N2-PROC)	1786.80 (H4N3S1-PROC)	657.19 (H1N1S1)	1549.51 (H4N3S1)			
														968.52 (H2N2-PROC)	292.05 (S1)	893.81 (H3N2)				
														1130.57 (H3N2-PROC)	366.08 (H1N1)	1055.38 (H4N2)				
27	31.6 (Cmpd 1826)	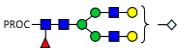	5	4	1	0	1	2313.92	1157.46	771.98	n.d.	1157.43	771.99	441.30 (N1-PROC)	952.38 (H1N2F1-PROC)	1276.60 (H3N2F1-PROC)	1641.72 (H4N3F1-PROC)	528.15 (H2N1)	852.23 (H4N1)	1200.41 (H3N2G1)
														587.32 (N1F1-PROC)	968.50 (H2N2-PROC)	1317.88 (H2N3F1-PROC)	308.05 (G1)	673.21 (H1N1G1)	893.85 (H3N2)	1217.26 (H5N2)
														644.30 (N2-PROC)	1114.56 (H2N2F1-PROC)	1333.50 (H3N3-PROC)	324.98 (H2)	690.19 (H3N1)	1055.42 (H4N2)	1362.58 (H4N2G1)
														790.15 (N2F1-PROC)	1130.60 (H3N2-PROC)	1479.75 (H3N3F1-PROC)	366.12 (H1N1)	731.27 (H2N2)	1096.50 (H3N3)	1420.55 (H5N3)
														806.32 (H1N2-PROC)	1171.75 (H2N3-PROC)	1495.68 (H4N3-PROC)	470.04 (H1G1)	835.24 (H2N1G1)	1159.63 (H4N1G1)	

Table S4.5 (continued)

Peak ID	Retention time (min)	Structure	Composition					[M/Z]$^{+}$ calculated	[M/Z]$^{2+}$ calculated	[M/Z]$^{3+}$ calculated	[M/Z]$^{+}$ registered	[M/Z]$^{2+}$ registered	[M/Z]$^{3+}$ registered	LC-ESI-MS [M/Z] characteristic fragment ions (composition)					
			Hex (H)	HexNAc (N)	Fuc (F)	Neu5Ac (S)	Neu5Gc (G)												
28	32.1 (Cmpd 1853)		5	4	1	2	0	2589.02	1295.01	863.68	n.d.	n.d.	864.04	587.31 (N1F1-PROC)	1130.76 (H3N2-PROC)	1641.65 (H4N3F1-PROC)	657.18 (H1N1S1)		
														644.69 (N2-PROC)	1276.69 (H3N2F1-PROC)	1932.79 (H4N3S1F1-PROC)	818.94 (H2N1S1)		
														790.26 (N2F1-PROC)	1333.67 (H3N3-PROC)	292.05 (S1)	852.13 (H4N1)		
														952.50 (H1N2F1-PROC)	1495.75 (H4N3-PROC)	366.14 (H1N1)	1055.5 (H4N2)		
														1114.63 (H2N2F1-PROC)	1508.75 (H5N2S1-PROC)	454.08 (H1S1)	1096.00 (H3N3)		
29	32.3 (Cmpd 1868)	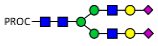	5	4	2	1	0	2442.96	1221.99	814.99	n.d.	1221.96	815.02	441.27 (N1-PROC)	1171.38 (H2N3-PROC)	325.13 (H2)	893.86 (H3N2)	1711.51 (H5N3S1)	
														644.38 (N2-PROC)	1333.63 (H3N3-PROC)	366.11 (H1N1)	981.50 (H3N1S1)	1799.88 (H5N2S2)	
														806.40 (H1N2-PROC)	1495.67 (H4N3-PROC)	454.25 (H1S1)	1055.50 (H4N2)		
														968.56 (H2N2-PROC)	1786.51 (H4N3S1-PROC)	657.18 (H1N1S1)	1346.59 (H4N2S1)		
														1130.54 (H3N2-PROC)	292.22 (S1)	731.75 (H2N2)	1549.71 (H4N3S1)		
30	33.2 (Cmpd 1922)		9	2	0	0	0	2102.82	1051.92	701.61	n.d.	1051.89	701.15	441.25 (N1-PROC)	1292.59 (H4N2-PROC)	649.13 (H4)	1176.47 (H6N1)		
														644.34 (N2-PROC)	325.09 (H2)	690.18 (H3N1)	1338.41 (H7N1)		
														806.37 (H1N2-PROC)	366.25 (H1N1)	852.28 (H4N1)	1500.31 (H8N1)		
														968.38 (H2N2-PROC)	487.13 (H3)	1014.50 (H5N1)	1662.27 (H9N1)		
														1130.61 (H3N2-PROC)	528.13 (H2N1)	1135.38 (H7)			
31	33.5 (Cmpd 1937)		5	4	1	2	0	2589.02	1295.01	863.68	n.d.	n.d.	863.70	441.38 (N1-PROC)	1114.38 (H2N2F1-PROC)	1641.79 (H4N3F1-PROC)	366.08 (H1N1)	852.39 (H4N1)	
														587.41 (N1F1-PROC)	1130.49 (H3N2-PROC)	1786.75 (H4N3S1-PROC)	528.00 (H2N1)	1184.60 (H3N2S1)	
														644.76 (N2-PROC)	1276.73 (H3N2F1-PROC)	1932.76 (H4N3S1F1-PROC)	657.23 (H1N1S1)	1258.02 (H4N3)	
														806.45 (H1N2-PROC)	1479.74 (H3N3F1-PROC)	292.03 (S1)	690.50 (H3N1)	1346.49 (H4N2S1)	
														968.39 (H2N2-PROC)	1495.50 (H4N3-PROC)	325.09 (H2)	819.37 (H2N1S1)	1711.63 (H5N3S1)	
32	33.8 (Cmpd 1959)		5	4	1	0	2	2621.01	1311.01	874.34	n.d.	n.d.	874.33	441.25 (N1-PROC)	952.75 (H1N2F1-PROC)	1276.55 (H3N2F1-PROC)	308.00 (G1)	835.00 (H2N1G1)	
														587.28 (N1F1-PROC)	968.52 (H2N2-PROC)	1479.80 (H3N3F1-PROC)	366.13 (H1N1)	852.88 (H4N1)	
														644.49 (N2-PROC)	1114.56 (H2N2F1-PROC)	1495.50 (H4N3-PROC)	470.25 (H1G1)	893.88 (H3N2)	
														790.31 (N2F1-PROC)	1130.50 (H3N2-PROC)	1641.71 (H4N3F1-PROC)	673.22 (H1N1G1)	1055.50 (H4N2)	
														806.51 (H1N2-PROC)	1171.63 (H2N3-PROC)	1948.76 (H4N3F1G1-PROC)	731.50 (H2N2)		
33	34.1 (Cmpd 1973)	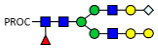	6	4	1	0	1	2475.97	1238.49	826.00	n.d.	1238.46	826.01	441.29 (N1-PROC)	952.47 (H1N2F1-PROC)	1276.59 (H3N2F1-PROC)	1803.75 (H5N3F1-PROC)	673.21 (H1N1G1)	893.54 (H3N2)	1362.45 (H4N2G1)
														587.30 (N1F1-PROC)	968.51 (H2N2-PROC)	1479.71 (H3N3F1-PROC)	308.02 (G1)	690.19 (H3N1)	997.37 (H3N1G1)	1524.44 (H5N2G1)
														644.67 (N2-PROC)	1114.57 (H2N2F1-PROC)	1495.70 (H4N3-PROC)	325.25 (H2)	731.13 (H2N2)	1055.36 (H4N2)	1686.75 (H6N2G1)
														790.44 (N2F1-PROC)	1130.53 (H3N2-PROC)	1641.87 (H4N3F1-PROC)	366.11 (H1N1)	835.27 (H2N1G1)	1200.41 (H3N2G1)	
														806.50 (H1N2-PROC)	1171.38 (H2N3-PROC)	1802.75 (H4N3G1-PROC)	528.18 (H2N1)	852.25 (H4N1)	1217.38 (H5N2)	
34	34.4 (Cmpd 1991)	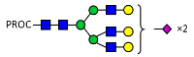	6	5	0	0	2	2808.10	1404.55	936.70	n.d.	n.d.	936.70	441.23 (N1-PROC)	1495.70 (H4N3-PROC)	292.13 (S1)	731.50 (H2N2)	1258.88 (H4N3-PROC)	2076.75 (H6N4S1)	
														806.47 (H1N2-PROC)	1624.73 (H3N3S1-PROC)	366.15 (H1N1)	819.25 (H2N1S1)	1420.75 (H5N3-PROC)		
														968.47 (H2N2-PROC)	1786.71 (H4N3S1-PROC)	454.20 (H1S1)	981.38 (H3N1S1)	1549.38 (H4N3S1)		
														1171.50 (H2N3-PROC)	1860.85 (H5N4-PROC)	528.38 (H2N1)	1022.38 (H2N2S1)	1711.75 (H5N3S1)		
														1333.54 (H3N3-PROC)	2151.88 (H5N4S1-PROC)	657.20 (H1N1S1)	1184.43 (H3N2S1)	1752.38 (H4N4S1)		
35	34.9 (Cmpd 2022)		5	4	1	0	2	2621.01	1311.01	874.34	n.d.	1311.47	874.36	441.17 (N1-PROC)	952.63 (H1N2F1-PROC)	1276.58 (H3N2F1-PROC)	1948.63 (H4N3F1G1-PROC)	673.20 (H1N1G1)	1055.47 (H4N2)	
														587.27 (N1F1-PROC)	968.42 (H2N2-PROC)	1333.50 (H3N3-PROC)	325.13 (H2)	731.49 (H2N2)	1159.63 (H4N1G1)	
														644.50 (N2-PROC)	1114.63 (H2N2F1-PROC)	1479.68 (H3N3F1-PROC)	366.15 (H1N1)	835.41 (H2N1G1)	1200.13 (H3N2G1)	
														790.38 (N2F1-PROC)	1130.65 (H3N2-PROC)	1495.88 (H4N3-PROC)	469.76 (H1G1)	893.84 (H3N2)	1362.50 (H4N2G1)	
														806.38 (H1N2-PROC)	1171.63 (H2N3-PROC)	1641.73 (H4N3F1-PROC)	528.15 (H2N1)	997.50 (H3N1G1)	1564.75 (H4N3G1)	
36	35.0 (Cmpd 2029)		6	4	1	0	1	2475.97	1238.49	826.00	n.d.	1238.48	826.12	441.30 (N1-PROC)	1333.75 (H3N3-PROC)	366.09 (H1N1)	1055.25 (H4N2)		
														790.63 (N2F1-PROC)	1495.68 (H4N3-PROC)	528.00 (H2N1)	1159.51 (H4N1G1)		
														806.58 (H1N2-PROC)	1802.73 (H4N3G1-PROC)	673.26 (H1N1G1)	1362.61 (H4N2G1)		
														968.34 (H2N2-PROC)	1803.69 (H5N3F1-PROC)	835.30 (H2N1G1)			
														1130.52 (H3N2-PROC)	325.00 (H2)	893.25 (H3N2)			
37	35.1 (Cmpd 2031)		5	4	0	0	2	2474.95	1237.98	825.66	n.d.	n.d.	825.68	441.29 (N1-PROC)	1333.70 (H3N3-PROC)	528.13 (H2N1)	1362.69 (H4N2G1)		
														644.38 (N2-PROC)	1495.81 (H4N3-PROC)	673.22 (H1N1G1)	1420.50 (H5N3)		
														806.15 (H1N2-PROC)	1802.71 (H4N3G1-PROC)	835.29 (H2N1G1)	1727.77 (H5N3G1)		
														968.41 (H2N2-PROC)	308.17 (G1)	893.38 (H3N2)			
														1130.56 (H3N2-PROC)	366.15 (H1N1)	1055.25 (H4N2)			
38	35.9 (Cmpd 2081)	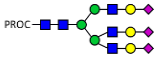	6	5	0	3	0	3099.19	1550.10	1033.74	n.d.	n.d.	1033.71	441.38 (N1-PROC)	1624.57 (H3N3S1-PROC)	2151.91 (H5N4S1-PROC)	893.13 (H3N2)	2002.87 (H5N3S2)	
														968.38 (H2N2-PROC)	1698.80 (H4N4-PROC)	2442.88 (H5N4S2-PROC)	934.80 (H2N3)	2077.00 (H6N4S1)	
														1130.63 (H3N2-PROC)	1786.83 (H4N3S1-PROC)	366.22 (H1N1)	1184.48 (H3N2S1)		
														1333.38 (H3N3-PROC)	1861.00 (H5N4-PROC)	657.23 (H1N1S1)	1475.71 (H3N2S2)		
														1495.56 (H4N3-PROC)	1989.80 (H4N4S1-PROC)	819.34 (H2N1S1)	1711.53 (H5N3S1)		
39	36.0 (Cmpd 2083)	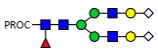	5	4	1	0	2	2621.01	1311.01	874.34	n.d.	1310.99	874.35	441.27 (N1-PROC)	952.53 (H1N2F1-PROC)	1276.57 (H3N2F1-PROC)	1786.38 (H3N3F1G1-PROC)	366.12 (H1N1)	690.38 (H3N1)	1200.55 (H3N2G1)
														587.39 (N1F1-PROC)	968.41 (H2N2-PROC)	1317.75 (H2N3F1-PROC)	1802.69 (H4N3G1-PROC)	470.13 (H1G1)	835.35 (H2N1G1)	1362.38 (H4N2G1)
														644.22 (N2-PROC)	1114.56 (H2N2F1-PROC)	1479.70 (H3N3F1-PROC)	1948.71 (H4N3F1G1-PROC)	487.63 (H3)	893.38 (H3N2)	1420.51 (H5N3)
														790.25 (N2F1-PROC)	1130.53 (H3N2-PROC)	1495.13 (H4N3-PROC)	307.99 (G1)	528.22 (H2N1)	997.38 (H3N1G1)	1727.38 (H5N3G1)
														806.39 (H1N2-PROC)	1171.38 (H2N3-PROC)	1641.76 (H4N3F1-PROC)	325.13 (H2)	673.21 (H1N1G1)	1055.14 (H4N2)	1831.38 (H5N2G2)
40	37.2 (Cmpd 2149)	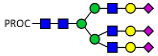	6	5	0	3	0	3099.19	1550.10	1033.74	n.d.	n.d.	1033.74	441.21 (N1-PROC)	1171.63 (H2N3-PROC)	1786.79 (H4N3S1-PROC)	366.13 (H1N1)	1184.38 (H3N2S1)		
														644.26 (N2-PROC)	1333.50 (H3N3-PROC)	1861.00 (H5N4-PROC)	528.76 (H2N1)	1475.35 (H3N2S2)		
														806.61 (H1N2-PROC)	1495.65 (H4N3-PROC)	2151.96 (H5N4S1-PROC)	657.21 (H1N1S1)	2002.62 (H5N3S2)		
														968.46 (H2N2-PROC)	1624.88 (H3N3S1-PROC)	2646.76 (H5N5S2-PROC)	818.75 (H2N1S1)	2205.63 (H5N4S2)		
														1130.50 (H3N2-PROC)	1698.75 (H4N4-PROC)	325.13 (H2)	934.72 (H2N3)			

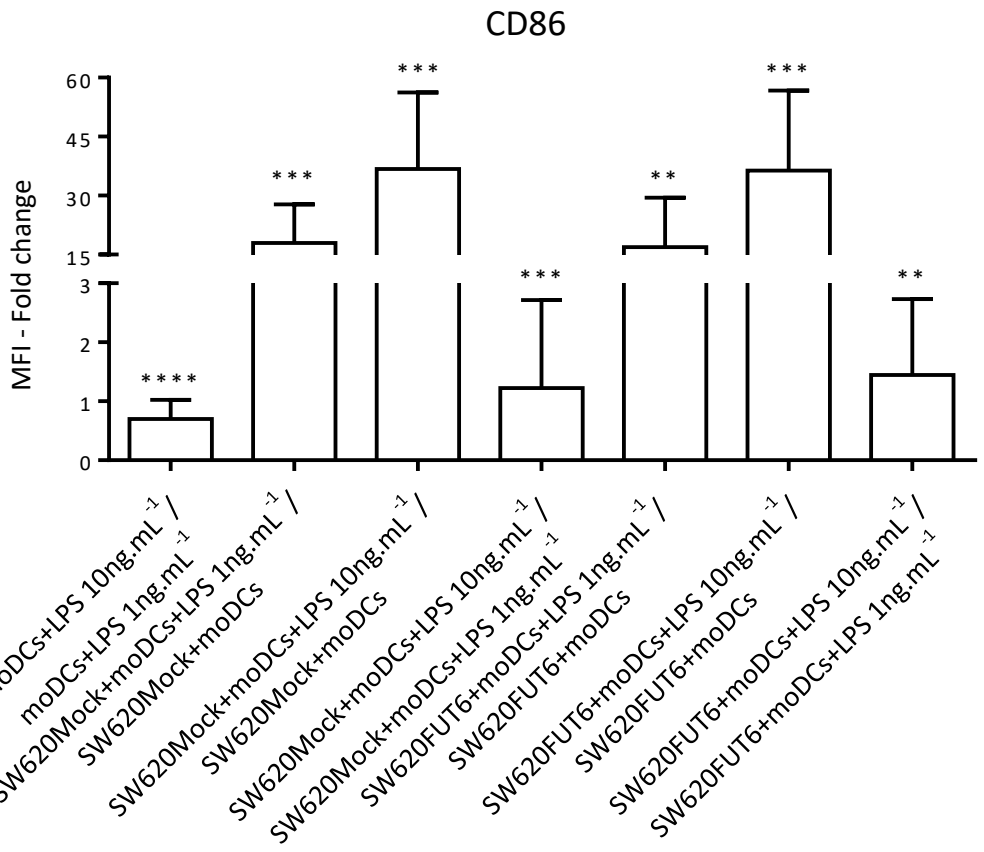

Figure S4.16 CD86 expression by moDCs increases with the supplementation of LPS in a dose-dependent manner. MoDCs were co-cultured with SW620 cell lines, supplemented or not at 6 hours with LPS 1ng.mL^{-1} or 10ng.mL^{-1}, and after 24 hours incubation, non-adherent moDCs were washed and co-cultured cells were harvested to assess CD86 expression by flow cytometry. MFI fold changes of CD86 expression by moDCs for 8 independent experiments were determined as described in materials and methods, p<0.0001 (****) for moDCs with LPS 10ng.mL^{-1}/moDCs with LPS 1ng.mL^{-1}, p=0.0001 (***) for moDCs with SW620Mock cells challenged with LPS 1ng.mL^{-1}/moDCs with SW620Mock cells, p=0.0001 (***) for moDCs with SW620Mock cells challenged with LPS 10ng.mL^{-1}/moDCs with SW620Mock cells, p=0.0002 (***) for moDCs with SW620Mock cells challenged with LPS 10ng.mL^{-1}/moDCs with SW620Mock cells challenged with LPS 1ng.mL^{-1}, p=0.0019 (**) for moDCs with SW620FUT6 cells challenged with LPS 1ng.mL^{-1}/moDCs with SW620FUT6 cells, p=0.0002 (***) for moDCs with SW620FUT6 cells challenged with LPS 10ng.mL^{-1}/moDCs with SW620FUT6 cells, p=0.0067 (**) for moDCs with SW620FUT6 cells challenged with LPS 10ng.mL^{-1}/moDCs with SW620FUT6 cells challenged with LPS 1ng.mL^{-1}.

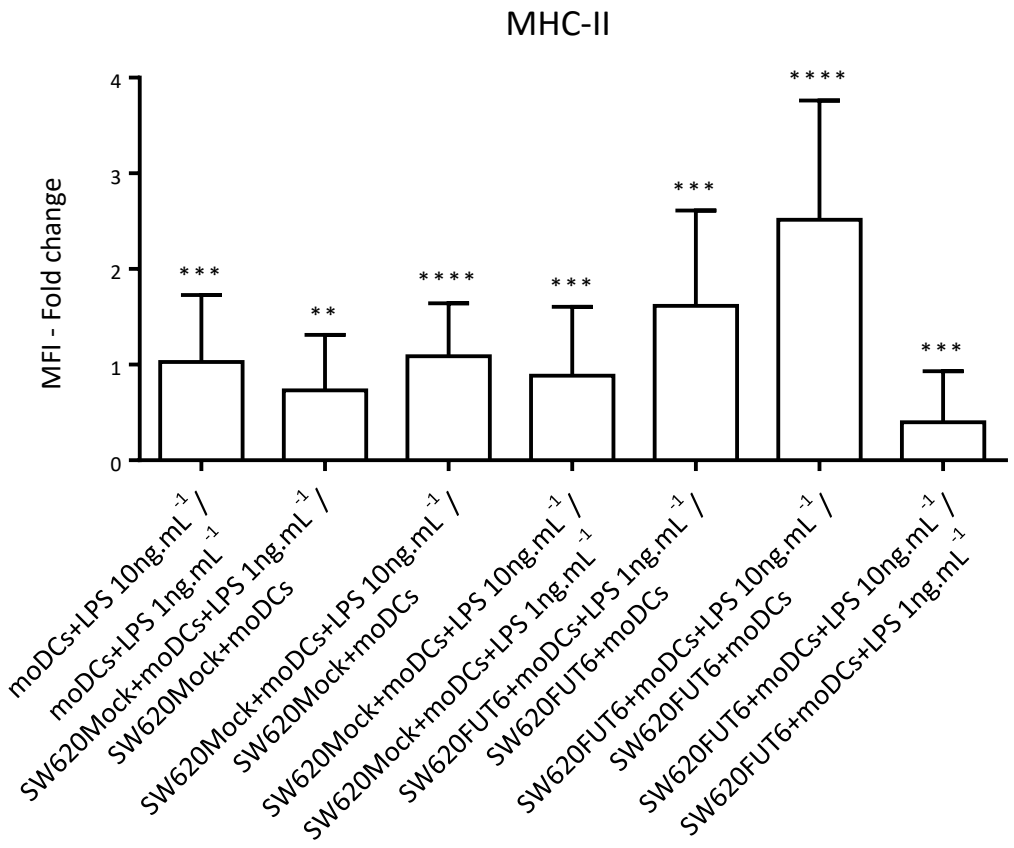

Figure S4.17 MHC-II expression by moDCs increases with the supplementation of LPS in a dose-dependent manner. MoDCs were co-cultured with SW620 cell lines, supplemented or not at 6 hours with LPS 1ng.mL^{-1} or 10ng.mL^{-1}, and after 24 hours incubation, non-adherent moDCs were washed and co-cultured cells were harvested to assess MHC-II expression by flow cytometry. MFI fold changes of MHC-II expression by moDCs for 8 independent experiments were determined as described in materials and methods, p=0.0009 (***) for moDCs with LPS 10ng.mL^{-1}/moDCs with LPS 1ng.mL^{-1}, p=0.003 (**) for moDCs with SW620Mock cells challenged with LPS 1ng.mL^{-1}/moDCs with SW620Mock cells, p<0.0001 (****) for moDCs with SW620Mock cells challenged with LPS 10ng.mL^{-1}/moDCs with SW620Mock cells, p=0.0002 (***) for moDCs with SW620Mock cells challenged with LPS 10ng.mL^{-1}/moDCs with SW620Mock cells challenged with LPS 1ng.mL^{-1}, p=0.0002 (***) for moDCs with SW620FUT6 cells challenged with LPS 1ng.mL^{-1}/moDCs with SW620FUT6 cells, p<0.0001 (****) for moDCs with SW620FUT6 cells challenged with LPS 10ng.mL^{-1}/moDCs with SW620FUT6 cells, p=0.0002 (***) for moDCs with SW620FUT6 cells challenged with LPS 10ng.mL^{-1}/moDCs with SW620FUT6 cells challenged with LPS 1ng.mL^{-1}.

Chapter 5 – Discussion

The importance of proteins and lipids modification by glycosylation is dramatically highlighted by genetic defects of this process observed in patients with congenital disorders of glycosylation (CDG). In regard of these diseases and their heavy consequences on human health (*e.g.*, severe psychomotor developmental delay, multiple organ malfunctions), the importance of glycosylation acquires real meaning. Glycan decoys are involved in essential biological processes from protein folding to cellular differentiation or even immune response, among others (Ohtsubo and Marth 2006). It is not surprising then that altered biological mechanisms, such as cell adhesion or signal transduction, observed in cancer development and progression can find their sources in glycosylation changes. Indeed, cell surface glycosylation is altered in cancer, aberrant glycans, truncated structures or specific increase of glycan antigens expression have been observed and contribute to cancer cell survival and spread (Drake 2015). Thus, glycosylation alterations in colorectal cancer (CRC) have been extensively studied and reviewed by Holst, Wuhrer, and Rombouts in 2015. Strong increase of sialylation and fucosylation was highlighted, leading to the high expression of sialyl Lewis X (sLe^X) and sialyl Lewis A (sLe^A) antigens. These two tetrasaccharides are particularly interesting since $sLe^{X/A}$ antigens are the minimal binding determinant for the lectin family of selectins (St Hill 2011). Indeed, as an example, E-selectin is involved in cancer metastasis formation process in CRC (Köhler et al. 2010; Kobayashi et al. 2000). Engagement of circulating tumour cells (CTCs) to endothelial cell adhesion molecules is supported by E-selectin essentially, allowing tumour cells to firmly adhere on endothelium and invade a new organ, developing thus metastasis (Baldawa et al. 2017; Valastyan and Weinberg 2011).

5.1. Characterisation of sialyl Lewis X expressing cell lines

5.1.1. Characterisation of colon cancer cell lines overexpressing *FUT6*

The sLe^x antigen expression has been highlighted in CRC and correlated with tumour metastasis and aggressiveness and with poorer prognosis and higher recurrence (Fukasawa et al. 2013; Yamadera et al. 2018). Therefore, part of this thesis depicts the characterisation of two cell lines transfected with *FUT6*. Trinchera et al. demonstrated that *FUT6* gene transfection in SW620 and HT29 cell lines increases the sLe^X expression and the FucTs activity (Trinchera et al. 2011). Thus, the transfection of *FUT6* in SW620 cell line increases the mRNA level expression, and sLe^X and E-selectin ligands expression increases as well as observed by the results in sections **4.1.1** and **4.2.1** with two different staining techniques, flow cytometry (**Figure 4.3**) and WB (**Figure 4.2** and **Figure 4.6**). However, some discrepancies between the techniques appeared. Indeed, in the Mock transfected cell line, the $sLe^{X/A}$ and E-selectin ligands expression is null by WB while flow cytometry assays show expression of both. Consistently, *FUT6* transfected cell line overexpresses sLe^X and E-selectin ligands compared to Mock cell line, as expected. The differences of expression observed between the flow cytometry and WB

staining techniques seem due to a sensitivity difference of the mAb when used in different applications (Acharya, Quinlan, and Neumeister 2017). Surprisingly, sLe^A antigen staining was found diminished by flow cytometry in *FUT6* transfected cell lines compared to control. Since sLe^A and sLe^X biosynthesis required different chain types, and FucT-VI can act only on type 2 chains, substrate competition cannot be considered. Interestingly, *FUT3* mRNA expression was significantly reduced in *FUT6* transfected cells, and FucT-III is the only FucT with an α1,4FucT activity, essential for sLe^A biosynthesis. Thus, the reduction of sLe^A antigen expression could be attributed to the lower expression of *FUT3*. When the expression of a glycosyltransferase is modulated, expression of others can be affected as Guo et al. (2004) showed with the effect of GlcNAcT-V expression on fucosyltransferases, sialyltransferases and core 2 O-glycans GlcNAcTs mRNA expression. Therefore, it is reasonable to suggest that overexpressing *FUT6* can affect *FUT3* expression. However, both *FUT3* mRNA expression and sLe^A immunostaining were detected at extremely low levels for Mock and *FUT6* transfected cell lines. These observations lead to the conclusion that the strong increase of E-selectin ligands expression in *FUT6* transfected cell lines can be imputed to the sLe^X overexpression, without an influence from sLe^A antigen expression.

Another *FUT* gene expression was reduced in *FUT6* overexpressing cell line, *FUT5*. FucT-V is involved in the same antigen synthesis than FucT-VI. According to the flow cytometry and WB staining, the low level of *FUT5* mRNA obviously does not affect the increase of sLe^X and E-selectin ligands expression in *FUT6* transfected cells, but it may have an impact on $Le^{X/Y}$ antigens expression which was not evaluated.

As for SW620, transfection of *FUT6* increases the mRNA level expression in HT29 colon cancer cell line and more $sLe^{X/A}$ antigens were found by WB in HT29FUT6 transfected cells rather than HT29Mock cells. Nevertheless, flow cytometry analysis presented contradictory results. Indeed, while HECA-452, *i.e.*, $sLe^{X/A}$ antigen staining, and E-selectin ligands staining remained unchanged, CD15s (sLe^X) and CA19-9 (sLe^A) staining was both diminished after *FUT6* transfection. Otherwise, *FUT3* mRNA was not significantly affected, but as in SW620, reduction of *FUT5* mRNA level was observed in *FUT6* transfected cells. Taken together, these results do not explain the aberrant observation in flow cytometry. The differences observed between WB and flow cytometry staining by HECA-452 can have various origins. To begin, the materials used for the two techniques are different, total cell lysate proteins were used for WB staining. Therefore $sLe^{X/A}$ carriers, in *FUT6* transfected cell lines, may be cytosolic proteins or membrane proteins from organelles or plasma membrane proteins with $sLe^{X/A}$ antigens oriented towards cytosolic compartment and not extracellularly, thus *FUT6* transfection increased the amount of these proteins which could not be detected by flow cytometry. Yet, this theory does not explain the flow cytometry results. Against logic, separate staining of sLe^X and sLe^A antigens showed reduction in *FUT6* transfected cells, but not of E-selectin ligands and HECA-452,

sensitivity or specificity of the mAb or recombinant Ab could be advanced to explain this discrepancy, however, without strong conviction especially since nothing similar has been observed in SW620 cell line characterisation. Therefore, the inconsistence of the results obtained from HT29FUT6 and HT29Mock cells leads to focus further experiments on SW620 cell lines.

5.1.2. N-glycan profiles of Mock vs. *FUT6* transfected SW620 cells

To deepen the characterisation of SW620Mock and FUT6 transfected cells, the N-glycan structures of the two cell lines membrane proteins were determined by LC-ESI-MS/MS. Taking into consideration that physiological conditions are not represented in cultured established cell lines, differences with N-glycan structures expressed by tumour could be observed. Indeed, the tumour microenvironment includes many different cell types such as immune cells, or fibroblasts, tumour vascularisation, signalling molecules expression, cell-cell and cell-extracellular matrix interactions represent a dynamic system which is not reproduced in cell cultures (Nishida-Aoki and Gujral 2019). Yet, despite this lack of physiological environment conditions, CRC cell lines retain similar genetic profiles and functional characteristics to tumour tissues (Pastor et al. 2010). Moreover, Holst et al. (2016) and Chik et al. (2014) established by MS approaches N-glycan profiles for several CRC cell lines which showed minor differences with CRC tumour tissues. On SW620Mock cells N-glycan analysis, our results are consistent with previously established N-glycosylation profiling of SW620WT cell line. Indeed, similar N-glycans such as high mannose type, hybrid, and complex sialylated and/or fucosylated structures were highlighted in our analysis of SW620Mock N-glycans.

Our N-glycan profiles revealed typical pauci-/high-mannose structures identified in SW620Mock and SW620FUT6 cells, which are found elevated in other CRC cell lines and tissues (section **1.3.1**). Interestingly, we observed core-fucosylated pauci- and high-mannosidic type structures in both cell lines: $Man_2GlcNAc_2Fuc_1$ (#2), $Man_3GlcNAc_2Fuc_1$ (#4), $Man_4GlcNAc_2Fuc_1$ (#8), $Man_5GlcNAc_2Fuc_1$ (#17 in SW620FUT6 cells only) and $Man_6GlcNAc_2Fuc_1$ (#24 for SW620Mock and #28 for SW620FUT6 cells). Such structures were reported to be up-regulated in CRC tumour tissues (Balog et al. 2012). The presence of core-fucosylated paucimannosidic type structure is likely to be due to trimmed hybrid or complex structures by lysosomal exoglycosidases. Indeed, the activity of such enzymes (*e.g.* α-mannosidase, β-galactosidase, β-N-acetyl-hexosaminidase) has been reported increased in CRC and proposed as a potential CRC biomarker for diagnosis (Świderska et al. 2014). Nevertheless, few authors reported the description of such structures in cancer and, of our knowledge, no functional role in cancer development has been studied for those. The core-fucosylated high-mannosidic type structure identified in our study contain 5- or 6-Man residues, therefore these structures can also be issued from hybrid type glycans trimmed by lysosomal exoglycosidases. The presence of these unusual

core-fucosylated structures in CRC cell lines and tissues depicts perfectly how the glycosylation process can be disturbed in cancer cells and reinforces the importance of the field in the study of malignant tumour arise and development.

Other identified structures presented hybrid type and mono- to penta-antennae branched complex type N-glycans. Among these structures, several blood group antigens were identified in both cell lines; one structure with H antigen (SW620Mock: #34, SW620FUT6: #37), four structures with $Le^{A/X}$ antigens (Mock: #36, #44, #60, #66; FUT6: #40, #47, #64, #68), three structures with $sLe^{A/X}$ antigens (Mock: #57, #60, #66; FUT6: #65, #64, #68) and one structure with two fucoses carried on the antenna of a tri-antennae core-fucosylated N-glycan without specific identified B-ion fragments to determine the type of antigen (Mock: #51, FUT6: #58). These structures are typically found elevated in CRC tissues especially sialylated or non sialylated Lewis type antigens (section **1.3.5**). As expected, more structures with sLe^{X} antigen were identified in *FUT6* transfected SW620 cells compare to Mock cells, no less than ten supplementary structures containing this antigen have been characterised (#34 #48 #49 #53 #59 #73 #74 #76 #77 #78). Thus, the N-glycan analysis showed for the first time the new structures carrying sLe^{X} antigen in SW620 cells transfected *FUT6*, and the abundance of the antigen is in accordance to the different immunostaining techniques and previous report (Trinchera et al. 2011). Few other structures with different blood group and Lewis type antigens were distinguished between the SW620Mock and FUT6 cells such as one structure with type A antigen (#27) and two structures with $Le^{A/X}$ antigen (#48 and #50) in SW620Mock N-glycan and three structures with $Le^{A/X}$ antigen (#49 #57 #70) and one structure with $Le^{B/Y}$ antigen (#50). Nevertheless, these differences concern a small number of structure and are probably not related to *FUT6* overexpression but to biological variation.

Bisecting N-GlcNAc structures have been described to be decreased in CRC tissues with higher stage and to have a preventive role in metastasis formation (D. Zhang et al. 2019; Balog et al. 2012; Khare et al. 2014; Gu et al. 2009). Despite that SW620 cell line is derived from metastatic lymph node site, we identify eight common structures with a bisecting GlcNAc for both SW620Mock and FUT6 cells. The studies of Holst et al. (2016) and Chik et al. (2014) also characterised N-glycan structures with bisecting GlcNAc in SW620WT cell line. As described in the introduction (section **1.2.1.2.3.1**), bisecting GlcNAc addition is mediated by the enzyme GlcNAcT-III, the expression of the gene *MGAT3*, encoding this glycosyltransferase, was found at very low level by Holst et al. (2016). Thus, they hypothesised that the N-glycan structures potentially carrying a bisecting GlcNAc were more susceptible to have a HexNAc located in terminal position of the antenna. In contrast Chik et al. (2014) study, where the mRNA level of *MGAT3* was also evaluated in SW620WT cells, affirmed that the *MGAT3* expression correlates with the amount of bisecting GlcNAc N-glycan structures. Moreover, Sethi et al. (2014) showed high levels of bisecting GlcNAc N-glycan structures together with high *MGAT3* mRNA level in CRC cell line derived

from omental metastasis. Therefore, it is not surprising to identify different bisecting GlcNAc N-glycan structures in our study.

Interestingly, when comparing N-glycan profiles of the two cell lines, SW620Mock cells presented seven additional bisected N-glycan structures against only two for SW620FUT6 cells. Furthermore, in SW620FUT6 cells, highly branched N-glycan structures with tetra- and penta-antenna were more abundant comparing to N-glycans from SW620Mock cells. Presence of bisecting GlcNAc has been shown to reduce the formation of branched N-glycan structures (Sasai et al. 2002) by preventing the action of branching GlcNAcTs, especially GlcNAcT-V. Moreover, reduced bisecting GlcNAc and increased branched N-glycans structures are typical glycosylation changes observed in CRC, correlating with tumour progression and metastasis formation. With the transfection of *FUT6*, SW620 cells acquires more aggressive and survival properties, with enhanced migration and immunomodulation abilities. In addition, more mono-sialylated N-glycans are observed in SW620FUT6 cells than Mock, and increase of sialylation is observed in CRC and associated with cancer progression, metastasis and poor prognosis (Sethi et al. 2014; Bresalier et al. 1996).

Taken together, *FUT6* overexpression in SW620 cells has a first direct and expected consequence by elevating the amount of sLe^X antigen but seems also to have an indirect influence on the expression of other N-glycan structures associated with tumour progression. Consequently, manipulating the glycosylation in cell lines by overexpressing glycosyltransferase genes seems to have unpredicted impact on the total glycan expression and requires deeper characterisation of glycan structures.

5.1.3. *FUT6* overexpression increases migration ability in SW620 cells

In this study, we showed that *FUT6* transfection increases sLe^X antigen and E-selectin ligands expression in CRC SW620 cell line. Therefore, this model was used to better understand the role of sLe^X antigen and E-selectin ligands in tumour progression. In **4.1.3**, we evaluated the migration capability of SW620FUT6 cells and compared it to Mock cells. Thus, SW620FUT6 cells possessed improved migration ability compared to control transfected cells. This result proves that increased sLe^X antigen and E-selectin ligands expression contributes to tumour cell migration. Similar observations were made in other cancer types. Indeed, *FUT6* transduced prostate cancer cells showed successful conversion of CD44 to an E-selectin ligand and higher migration capability than control transduced cells (J. Li et al. 2013). Enhanced expression of sLe^X and increased E-selectin binding lead to greater migration ability (Pérez-Garay et al. 2013). In primary invasive ductal carcinoma cell line, inhibition of fucosylation inhibited sle^X antigen and E-selectin ligands expression leading to lower migration capacity (Carrascal et al. 2018). Furthermore, *FUT6* silencing reduced TGF-β-mediated EMT and inhibited migration in CRC cancer cells (Hirakawa et al. 2014). In summary, we found that *FUT6* promotes cell

migration likely through increased expression of in CRC cells. Moreover, increased *FUT6* expression is associated to similar roles in other cancer types, suggesting that *FUT6*, sLe^X antigen and E-selectin ligands are potentially promising therapeutic targets for patients with cancer.

5.2. Selectin ligands

In **4.2.1**, we demonstrated that SW620FUT6 cell line expresses high level of E-selectin ligands using E-selectin chimera in different staining techniques. We detected the E-selectin ligands on cell surface and proteins presented high molecular weight (between 100 and 245 kDa). To identify the E-selectin ligands of SW620FUT6 cell lines, we first isolated these proteins and then used mass spectrometry for identification (**4.2.2**). This allowed us to identify 13 candidates, some of them were already known E-selectin ligand such as LAMP-2. Indeed, LAMP-1 and LAMP-2 have been identified in Colo-205 cell lines as E-selectin ligands and their expression levels mediated colon cancer cells adhesion to E-selectin (Tomlinson et al. 2000; Sawada, Lowe, and Fukuda 1993). Among the identified potential E-selectin ligands, we found integrins α-6 and β-1 which form the very late antigen 6 (VLA-6), receptor for laminin involved in leukocyte binding under physiological shear flow condition (Kitayama et al. 2000). In CRC cells, the two integrins are targeted by the microRNA miR-30e-5p, which expression is regulated by the tumour suppressor P53, modulating tumour cell adhesion, migration, invasion and proliferation (Laudato et al. 2017). Another identified E-selectin ligand candidate was the receptor-type tyrosine-protein phosphatase eta (PTPRJ). Different studies reported a role of *PTPRJ* gene due to the loss of heterozygosity of this tumour suppressor gene early in colon neoplasia (X.-F. Zhang et al. 2017; Luo et al. 2006; Ruivenkamp et al. 2003). Nevertheless, the staining of PTPRJ in SW620FUT6 failed in flow cytometry so we decided to not investigate further this protein (**4.2.3**).

We also demonstrated that the neural cell adhesion molecule L1 (L1CAM) is an E-selectin ligand in colon cancer cells, when carrying the tetrasaccharide determinant sLe^X antigen (**4.2.4**). L1CAM has been first identified in rat and was called NGF (Nerve Growth Factor)-inducible large external glycoprotein (McGuire, Greene, and Furano 1978). Subsequently, the human L1CAM was identify, showing similarity to mouse, rat and chick homologs (Wolff et al. 1988). L1CAM is a type 1 membrane glycoprotein belonging to the immunoglobulin superfamily, composed of six immunoglobulin-like domains and five fibronectin type III domains, and owning 21 potential N-glycosylation sites found on the extracellular portion. The protein is heavily glycosylated and migrates at ∼220 kDa in SDS-PAGE. Mainly found in the nervous system, L1CAM is involved in several processes such as neuronal migration, neurite fasciculation, synaptic plasticity, and its mutations cause severe neurological disorders (Schultheis, Diestel, and Schmitz 2007; Yamasaki, Thompson, and Lemmon 1997; Bateman et al. 1996). Surprisingly, L1CAM expression has been highlighted in several types of cancer. Indeed,

its expression correlates with aggressiveness of tumour and metastasis in endometrial adenocarcinoma (Klat et al. 2019), in breast cancer (J. Zhang et al. 2015), in non-small cell lung cancer (X. Liu et al. 2019) and in melanoma (Ernst et al. 2018), with reduce overall survival in oesophageal squamous cell carcinoma (J.-C. Guo et al. 2017), with nerve invasion of pancreatic ductal adenocarcinoma (Na'ara, Amit, and Gil 2019) and with chemoresistance in clear cell renal cell carcinoma (Doberstein et al. 2011) among others. Besides, chimeric antigen receptor (CAR)-T cell based immunotherapy using L1CAM as a target has been proposed, especially for neuroblastoma which presents high expression of the L1CAM CE7 epitope (Künkele et al. 2017; Hong et al. 2014). In colorectal cancer patients, L1CAM expression has been associated with invasion, tumour progression, poor survival and metastasis (Fang et al. 2010; Boo et al. 2007; Kaifi et al. 2007). Expression of L1CAM has been highlighted at the invasive front of CRC tumours and would contribute to invasion and liver metastasis formation (Kajiwara et al. 2011; Gavert et al. 2007; 2005). Different mutations of L1CAM showed that the full-length protein enhances proliferation, cell motility and *in vivo* liver metastasis formation (Haase et al. 2017).

So, E-selectin ligands expression is directly involved in metastasis development as it is showed in Brodt et al. (1997) study, modulation of E-selectin expression in the liver promotes metastasis formation *in vivo*. On the other hand, L1CAM expression in CRC is also linked to metastasis, by immunohistochemistry staining it has been shown that L1CAM expression is associated with lymph node and bone marrow metastasis (Kaifi et al. 2007). Furthermore, blocking L1CAM decreases adherence and migration of tumour cells from colon adenocarcinoma to nervous system showing involvement of L1CAM in perineural invasion in CRC (Duchalais et al. 2018). In our study, we showed an increase of sLe^X leading to high E-selectin ligands expression and, curiously, resulting in increased L1CAM in SW620FUT6. The role of L1CAM in CRC has been studied before but not as an E-selectin ligand. L1CAM is also expressed on leukocytes (Ebeling et al. 1996) and endothelial cells (Magrini et al. 2014). L1CAM can interact in homophilic binding but also heterophilic binding with integrins (Hall et al. 2004). Nevertheless, even if interaction with E-selectin has never been demonstrate so far, our findings show that being an E-selectin ligand can also contribute to metastasis and invasion role of L1CAM via improvement of endothelial cell interaction with CTCs. Another study reported a link between L1CAM expression and glycosylation, L1CAM overexpression improved cell migration in Chinese hamster ovary (CHO) cells through increase of cell surface sialylation and fucosylation (G. Shi et al. 2017).

In the scope of gathering more information on the glycosylation status of L1CAM, the protein was immunoprecipitated (IP) from membrane proteins of SW620FUT6 cells, N-glycans were released and analysed by LC-ESI-MS/MS (**4.2.5**). The use of mAb for the immunoprecipitation introduced a source

of contamination, therefore, identified N-glycan structures from L1CAM mAb were excluded to those identified in IP L1CAM. Among the identified N-glycans, pauci-/high-mannosidic and complex type structures were characterised. Complex structures presented multi-sialylated di-/tri-antenna with or without core-fucose. Regrettably, N-glycan structures did not present sLe^X structure, however, the antigen can also be present on O-glycan, which is, according to the previous several evidence, the most probable assumption.

Thus, this work provides new insight on the L1CAM involvement in colon cancer metastasis mediated by glycan-specific interaction with E-selectin. Thus, with the new role of L1CAM as E-selectin ligand, it is getting more interesting to use this glycoprotein as a therapeutic target in CRC.

5.3. Immunomodulation

Since the 1980's, the sLe^X antigen has been studied in human carcinomas due to its expression in serum and tumour tissue of patients with cancer. Therefore, sLe^X was reported as a tumour-associated carbohydrate antigen and its expression was found significantly correlated with tumour stage, invasion and recurrence, metastasis formation, and overall survival in diverse cancer types such as CRC, lung cancer, gastric cancer, breast cancer, head and neck squamous cell carcinoma, or oesophageal squamous cell carcinoma (Liang, Liang, and Gao 2016). In CRC cancer, sLe^X antigen expression is a valuable prognostic factor and has been associated with liver metastasis recurrence (Yamadera et al. 2018). Well known to be the ligand of selectin family, the role of sLe^X antigen in cancer has been studied regarding its capability to interact with endothelial cells through E-selectin binding. Many studies describe the inhibition of metastasis formation by targeting E-selectin ligands expression. However, potential relationship between sLe^X expression and anti-tumour immune responses has been less investigated, while immune cells express wide range of lectins including L-selectin which also has sLe^X as ligand. Knowing this, it is conceivable that sLe^X antigen, in addition to its role in metastasis and invasion, could as well influence immunologically tumour microenvironment by interacting with infiltrated immune cells, affecting pro-/anti-inflammatory molecules expression, contributing to immune evasion.

In section **4.3**, we addressed the influence of sLe^X antigen in the immunomodulation of DCs. DCs possess crucial functions in the immune responses and have a critical role in anti-tumour immunity. Briefly, DCs can induce innate immune responses by production of cytokines such as interferon (IFN) α in response to pattern recognition receptors (PRRs) activation through expressed tumour cells pathogen/damage-associated molecular patterns (PAMPs/DAMPs) recognition, leading to anti-tumoral cytotoxic action of stimulated Natural Killer (NK) cells, NK-T cells, and macrophages (Banchereau et al. 2000). Adaptive immunity can also be engaged by DCs, immature DCs capture

tumour antigens delivered by the cancer cells leading to their maturation and migration to lymphatic organs where mature DCs present the antigens to lymphocytes. Successfully activated lymphocytes can therefore trigger anti-tumour immune elimination (Banchereau et al. 2000). However, cancer cells can escape immune system responses by using DCs to induce tumour antigens tolerance. In our study, SW620FUT6 CRC cells, with increased sLe^X antigen expression, were co-cultured with DCs derived from monocytes (moDCs), in parallel SW620Mock control cells undergo identical procedure. In response to sLe^X antigen overexpressing cells, DCs showed less mature profile, translated by a reduced expression of antigen presenting MHC-II and co-stimulatory CD86 molecules, when compared to DCs maturation profile in Mock cells co-cultures. MHC-II and CD86 are essential to favourably induce T cell activation and downstream effective adaptive immune response. Therefore, the influence of the sLe^X antigen expression is likely to induce tolerant profile of DCs by maintaining their immature status. For our knowledges, this is the first report showing immunomodulation feature of DCs by sLe^X antigen expressing cancer cells. Another aspect of DCs maturation was evaluated, the expression of cytokines genes. *IL-1β*, *IL-6*, *IL-10*, *IL-12B*, *TGF-β1* and *TNFα* expression by DCs did not present differences between the co-cultures with cancer sLe^X antigen overexpressing cells and the co-cultures with control cancer cells.

Following these remarkable results, our goal was to evaluate the immunosuppressive properties towards DCs of sLe^X antigen expressing cancer cells with stimulus challenges. Thus, LPS, well-known DCs maturation inducer already used for mature DCs control evaluation, was added during the co-cultures of cancer cells with moDCs. The same lower expression of MHC-II and CD86 molecules by DCs has been measured when sLe^X antigen expressing CRC cells were in contact with moDCs, compared to Mock control CRC cells and moDCs co-cultures. The persistence of the resistance to DCs maturation with two different doses of LPS maturation stimuli confirmed and reinforced the fact that sLe^X antigen expressing cells possessed improved immunomodulation power.

With its wide high expression in multiple cancer types, another approach can also consider sLe^X antigen carriers, E-selectin ligands, as a target to develop anti-sLe^X/E-selectin ligands-based therapeutics. Indeed, it is largely accepted that classic chemotherapeutic, radiotherapeutic based treatments of cancer patients are extremely aggressive and even if results are achieved the side effects are extremely difficult for patients. Targeted and personalised medicine is the future of cancer treatment and we can already see the efficiency of such approaches with successful CAR-T and TCR-T cell-based treatments (Zhao and Cao 2019). Therefore, the importance of new target discovery for cancer immunotherapy-based treatment is essential and E-selectin ligands can represent promising targets for such therapeutic approaches.

5.4. Conclusions

In conclusion, we studied the roles of sLe^X antigen and E-selectin ligands in CRC. The precise characterisation of glycoengineered CRC cells establishment gave important insights on the influence of *FUT6* overexpression in CRC cells. Thus, sLe^X antigen overexpressing CRC cells induced improved cell migration ability, feature contributing to tumour spread and progression. Furthermore, we showed that sLe^X antigen expression by CRC cells modulated maturation profile of DCs, which resulted in reducing DCs ability to activate appropriate immune response against tumour cells. Therefore, the sLe^X antigen expression can contribute to the tumour immune system escape strategy. By MS-based identification technique, E-selectin ligands were identified in sLe^X antigen overexpressing CRC cells. Several E-selectin ligand candidates were evaluated, leading to the identification of L1CAM. This glycoprotein is elevated in many cancer types and can be considered as a promising therapeutic target. This study described L1CAM as an E-selectin ligand for the first time, opening new approaches to uncover the role of L1CAM in metastasis formation and cancer progression. Overall, these findings contribute to elucidate the role of sLe^X antigen and E-selectin ligands in CRC and to propose new targets for immunotherapeutic treatments.

References

Acharya, Poulomi, Anna Quinlan, and Veronique Neumeister. 2017. 'The ABCs of Finding a Good Antibody: How to Find a Good Antibody, Validate It, and Publish Meaningful Data'. *F1000Research* 6 (June). https://doi.org/10.12688/f1000research.11774.1.

Aebi, Markus. 2013. 'N-Linked Protein Glycosylation in the ER'. *Biochimica Et Biophysica Acta* 1833 (11): 2430–37. https://doi.org/10.1016/j.bbamcr.2013.04.001.

Agache, Alexandra, Petronel Mustăţea, Octavian Mihalache, Florin Teodor Bobîrca, Dragoş Eugen Georgescu, Cristina Mihaela Jauca, Andra Bîrligea, Horia Doran, and Traian Pătraşcu. 2018. 'Diabetes Mellitus as a Risk-Factor for Colorectal Cancer Literature Review - Current Situation and Future Perspectives'. *Chirurgia (Bucharest, Romania: 1990)* 113 (5): 603–10. https://doi.org/10.21614/chirurgia.113.5.603.

Alexander, Dominik D., John Waterbor, Timothy Hughes, Ellen Funkhouser, William Grizzle, and Upender Manne. 2007. 'African-American and Caucasian Disparities in Colorectal Cancer Mortality and Survival by Data Source: An Epidemiologic Review'. *Cancer Biomarkers: Section A of Disease Markers* 3 (6): 301–13.

American Joint Committee on Cancer. 2010. 'Chapter 14. Colon and Rectum'. In *AJCC Cancer Staging Manual*, Seventh Edition, 143–59. Stephen B. Edge, David R. Byrd, Carolyn C. Compton, April G. Fritz, Frederick L. Greene, Andy Trotti.

An, Guangyu, Bo Wei, Baoyun Xia, J. Michael McDaniel, Tongzhong Ju, Richard D. Cummings, Jonathan Braun, and Lijun Xia. 2007. 'Increased Susceptibility to Colitis and Colorectal Tumors in Mice Lacking Core 3-Derived O-Glycans'. *The Journal of Experimental Medicine* 204 (6): 1417–29. https://doi.org/10.1084/jem.20061929.

Anderson, Ana C., Nicole Joller, and Vijay K. Kuchroo. 2016. 'Lag-3, Tim-3, and TIGIT: Co-Inhibitory Receptors with Specialized Functions in Immune Regulation'. *Immunity* 44 (5): 989–1004. https://doi.org/10.1016/j.immuni.2016.05.001.

André, Thierry, Kai-Keen Shiu, Tae Won Kim, Benny Vittrup Jensen, Lars Henrik Jensen, Cornelis Punt, Denis Smith, et al. 2020. 'Pembrolizumab in Microsatellite-Instability-High Advanced Colorectal Cancer'. *The New England Journal of Medicine* 383 (23): 2207–18. https://doi.org/10.1056/NEJMoa2017699.

Aronica, Adele, Laura Avagliano, Anna Caretti, Delfina Tosi, Gaetano Pietro Bulfamante, and Marco Trinchera. 2017. 'Unexpected Distribution of CA19.9 and Other Type 1 Chain Lewis Antigens in Normal and Cancer Tissues of Colon and Pancreas: Importance of the Detection Method and Role of Glycosyltransferase Regulation'. *Biochimica Et Biophysica Acta. General Subjects* 1861 (1 Pt A): 3210–20. https://doi.org/10.1016/j.bbagen.2016.08.005.

Arteta, Beatriz, Nerea Lasuen, Aritz Lopategi, Baldur Sveinbjörnsson, Bård Smedsrød, and Fernando Vidal-Vanaclocha. 2010. 'Colon Carcinoma Cell Interaction with Liver Sinusoidal Endothelium Inhibits Organ-Specific Antitumor Immunity through Interleukin-1-Induced Mannose Receptor in Mice'. *Hepatology (Baltimore, Md.)* 51 (6): 2172–82. https://doi.org/10.1002/hep.23590.

Bae, Jeong Mo, Jung Ho Kim, Yoonjin Kwak, Dae-Won Lee, Yongjun Cha, Xianyu Wen, Tae Hun Lee, et al. 2017. 'Distinct Clinical Outcomes of Two CIMP-Positive Colorectal Cancer Subtypes Based on a Revised CIMP Classification System'. *British Journal of Cancer* 116 (8): 1012–20. https://doi.org/10.1038/bjc.2017.52.

Balcik-Ercin, Pelin, Metin Cetin, Irem Yalim-Camci, Gorkem Odabas, Nurettin Tokay, A. Emre Sayan, and Tamer Yagci. 2018. 'Genome-Wide Analysis of Endogenously Expressed ZEB2 Binding Sites Reveals Inverse Correlations between ZEB2 and GalNAc-Transferase GALNT3 in Human Tumors'. *Cellular Oncology (Dordrecht)* 41 (4): 379–93. https://doi.org/10.1007/s13402-018-0375-7.

Baldawa, Prachi, Pallavi Shirol, Jyoti Alur, and Venkatesh V. Kulkarni. 2017. 'Metastasis: To and Fro'. *Journal of Oral and Maxillofacial Pathology: JOMFP* 21 (3): 463–64. https://doi.org/10.4103/jomfp.JOMFP_158_17.

Baldus, S. E., S. P. Mönig, T. K. Zirbes, J. Thakran, D. Köthe, M. Köppel, F.-G. Hanisch, et al. 2006. 'Lewis(y) Antigen (CD174) and Apoptosis in Gastric and Colorectal Carcinomas: Correlations

with Clinical and Prognostic Parameters'. *Histology and Histopathology* 21 (5): 503–10. https://doi.org/10.14670/HH-21.503.

Balog, Crina I. A., Kathrin Stavenhagen, Wesley L. J. Fung, Carolien A. Koeleman, Liam A. McDonnell, Aswin Verhoeven, Wilma E. Mesker, Rob A. E. M. Tollenaar, André M. Deelder, and Manfred Wuhrer. 2012. 'N-Glycosylation of Colorectal Cancer Tissues: A Liquid Chromatography and Mass Spectrometry-Based Investigation'. *Molecular & Cellular Proteomics: MCP* 11 (9): 571–85. https://doi.org/10.1074/mcp.M111.011601.

Banchereau, J., F. Briere, C. Caux, J. Davoust, S. Lebecque, Y. J. Liu, B. Pulendran, and K. Palucka. 2000. 'Immunobiology of Dendritic Cells'. *Annual Review of Immunology* 18: 767–811. https://doi.org/10.1146/annurev.immunol.18.1.767.

Bandala-Sanchez, Esther, Yuxia Zhang, Simone Reinwald, James A. Dromey, Bo-Han Lee, Junyan Qian, Ralph M. Böhmer, and Leonard C. Harrison. 2013. 'T Cell Regulation Mediated by Interaction of Soluble CD52 with the Inhibitory Receptor Siglec-10'. *Nature Immunology* 14 (7): 741–48. https://doi.org/10.1038/ni.2610.

Barrow, Hannah, Benjamin Tam, Carrie A. Duckworth, Jonathan M. Rhodes, and Lu-Gang Yu. 2013. 'Suppression of Core 1 Gal-Transferase Is Associated with Reduction of TF and Reciprocal Increase of Tn, Sialyl-Tn and Core 3 Glycans in Human Colon Cancer Cells'. *PloS One* 8 (3): e59792. https://doi.org/10.1371/journal.pone.0059792.

Basile, Debora, Silvio Ken Garattini, Marta Bonotto, Elena Ongaro, Mariaelena Casagrande, Monica Cattaneo, Valentina Fanotto, et al. 2017. 'Immunotherapy for Colorectal Cancer: Where Are We Heading?' *Expert Opinion on Biological Therapy* 17 (6): 709–21. https://doi.org/10.1080/14712598.2017.1315405.

Bateman, A., M. Jouet, J. MacFarlane, J. S. Du, S. Kenwrick, and C. Chothia. 1996. 'Outline Structure of the Human L1 Cell Adhesion Molecule and the Sites Where Mutations Cause Neurological Disorders'. *The EMBO Journal* 15 (22): 6050–59.

Bause, E. 1983. 'Structural Requirements of N-Glycosylation of Proteins. Studies with Proline Peptides as Conformational Probes'. *The Biochemical Journal* 209 (2): 331–36. https://doi.org/10.1042/bj2090331.

Bause, E., E. Bieberich, A. Rolfs, C. Völker, and B. Schmidt. 1993. 'Molecular Cloning and Primary Structure of Man9-Mannosidase from Human Kidney'. *European Journal of Biochemistry* 217 (2): 535–40. https://doi.org/10.1111/j.1432-1033.1993.tb18274.x.

Berg, E. L., M. K. Robinson, O. Mansson, E. C. Butcher, and J. L. Magnani. 1991. 'A Carbohydrate Domain Common to Both Sialyl Le(a) and Sialyl Le(X) Is Recognized by the Endothelial Cell Leukocyte Adhesion Molecule ELAM-1'. *The Journal of Biological Chemistry* 266 (23): 14869–72.

Berg, E. L., T. Yoshino, L. S. Rott, M. K. Robinson, R. A. Warnock, T. K. Kishimoto, L. J. Picker, and E. C. Butcher. 1991. 'The Cutaneous Lymphocyte Antigen Is a Skin Lymphocyte Homing Receptor for the Vascular Lectin Endothelial Cell-Leukocyte Adhesion Molecule 1'. *The Journal of Experimental Medicine* 174 (6): 1461–66. https://doi.org/10.1084/jem.174.6.1461.

Blanas, Athanasios, Lenneke A. M. Cornelissen, Maximilianos Kotsias, Joost C. van der Horst, Henri J. van de Vrugt, Hakan Kalay, Daniel I. R. Spencer, Rad P. Kozak, and Sandra J. van Vliet. 2019. 'Transcriptional Activation of Fucosyltransferase (FUT) Genes Using the CRISPR-DCas9-VPR Technology Reveals Potent N-Glycome Alterations in Colorectal Cancer Cells'. *Glycobiology* 29 (2): 137–50. https://doi.org/10.1093/glycob/cwy096.

Blottière, H. M., R. Zennadi, M. Grégoire, G. Aillet, M. G. Denis, K. Meflah, and J. Le Pendu. 1993. 'Analysis of the Relationship between Stage of Differentiation and NK/LAK Susceptibility of Colon Carcinoma Cells'. *International Journal of Cancer* 53 (3): 409–17.

Boland, C. R., and F. J. Troncale. 1984. 'Familial Colonic Cancer without Antecedent Polyposis'. *Annals of Internal Medicine* 100 (5): 700–701.

Boo, Yoon-Jung, Joong-Min Park, Jin Kim, Yang-Seok Chae, Byung-Wook Min, Jun-Won Um, and Hong-Young Moon. 2007. 'L1 Expression as a Marker for Poor Prognosis, Tumor Progression,

and Short Survival in Patients with Colorectal Cancer'. *Annals of Surgical Oncology* 14 (5): 1703–11. https://doi.org/10.1245/s10434-006-9281-8.

Borsig, Lubor, Richard Wong, Richard O. Hynes, Nissi M. Varki, and Ajit Varki. 2002. 'Synergistic Effects of L- and P-Selectin in Facilitating Tumor Metastasis Can Involve Non-Mucin Ligands and Implicate Leukocytes as Enhancers of Metastasis'. *Proceedings of the National Academy of Sciences of the United States of America* 99 (4): 2193–98. https://doi.org/10.1073/pnas.261704098.

Bresalier, R. S., S. B. Ho, H. L. Schoeppner, Y. S. Kim, M. H. Sleisenger, P. Brodt, and J. C. Byrd. 1996. 'Enhanced Sialylation of Mucin-Associated Carbohydrate Structures in Human Colon Cancer Metastasis'. *Gastroenterology* 110 (5): 1354–67.

Brockhausen, Inka, and Pamela Stanley. 2015. 'O-GalNAc Glycans'. In *Essentials of Glycobiology*, edited by Ajit Varki, Richard D. Cummings, Jeffrey D. Esko, Pamela Stanley, Gerald W. Hart, Markus Aebi, Alan G. Darvill, et al., 3rd ed. Cold Spring Harbor (NY): Cold Spring Harbor Laboratory Press. http://www.ncbi.nlm.nih.gov/books/NBK453030/.

Brodt, P., L. Fallavollita, R. S. Bresalier, S. Meterissian, C. R. Norton, and B. A. Wolitzky. 1997. 'Liver Endothelial E-Selectin Mediates Carcinoma Cell Adhesion and Promotes Liver Metastasis'. *International Journal of Cancer* 71 (4): 612–19.

Burdick, Monica M., Julia T. Chu, Samuel Godar, and Robert Sackstein. 2006. 'HCELL Is the Major E- and L-Selectin Ligand Expressed on LS174T Colon Carcinoma Cells'. *The Journal of Biological Chemistry* 281 (20): 13899–905. https://doi.org/10.1074/jbc.M513617200.

Carrascal, Mylène A., Mariana Silva, José S. Ramalho, Cláudia Pen, Manuela Martins, Carlota Pascoal, Constança Amaral, et al. 2018. 'Inhibition of Fucosylation in Human Invasive Ductal Carcinoma Reduces E-selectin Ligand Expression, Cell Proliferation, and ERK1/2 and P38 MAPK Activation'. *Molecular Oncology* 12 (5): 579–93. https://doi.org/10.1002/1878-0261.12163.

Carroll, Magdalen R. R., Helen E. Seaman, and Stephen P. Halloran. 2014. 'Tests and Investigations for Colorectal Cancer Screening'. *Clinical Biochemistry* 47 (10–11): 921–39. https://doi.org/10.1016/j.clinbiochem.2014.04.019.

Carvalho, A. S., A. Harduin-Lepers, A. Magalhães, E. Machado, N. Mendes, L. T. Costa, R. Matthiesen, R. Almeida, J. Costa, and C. A. Reis. 2010. 'Differential Expression of Alpha-2,3-Sialyltransferases and Alpha-1,3/4-Fucosyltransferases Regulates the Levels of Sialyl Lewis a and Sialyl Lewis x in Gastrointestinal Carcinoma Cells'. *The International Journal of Biochemistry & Cell Biology* 42 (1): 80–89. https://doi.org/10.1016/j.biocel.2009.09.010.

'CFG Nomenclature'. n.d. Accessed 16 February 2021. http://www.functionalglycomics.org/static/consortium/Nomenclature.shtml.

Chen, Chia-Hua, Shui-Hua Wang, Chiung-Hui Liu, Yi-Ling Wu, Wei-Jen Wang, John Huang, Ji-Shiang Hung, I.-Rue Lai, Jin-Tung Liang, and Min-Chuan Huang. 2014. 'β-1,4-Galactosyltransferase III Suppresses B1 Integrin-Mediated Invasive Phenotypes and Negatively Correlates with Metastasis in Colorectal Cancer'. *Carcinogenesis* 35 (6): 1258–66. https://doi.org/10.1093/carcin/bgu007.

Chen, Wei-Shone, Hong-Yi Chang, Chung-Pin Li, Jacqueline Ming Liu, and Tze-Sing Huang. 2005. 'Tumor Beta-1,4-Galactosyltransferase IV Overexpression Is Closely Associated with Colorectal Cancer Metastasis and Poor Prognosis'. *Clinical Cancer Research: An Official Journal of the American Association for Cancer Research* 11 (24 Pt 1): 8615–22. https://doi.org/10.1158/1078-0432.CCR-05-1006.

Cheng, Jiemin, Yi Chen, Xiaolin Wang, Jianhua Wang, Zhiping Yan, Gaoquan Gong, Guoping Li, and Changyu Li. 2015. 'Meta-Analysis of Prospective Cohort Studies of Cigarette Smoking and the Incidence of Colon and Rectal Cancers'. *European Journal of Cancer Prevention: The Official Journal of the European Cancer Prevention Organisation (ECP)* 24 (1): 6–15. https://doi.org/10.1097/CEJ.0000000000000011.

Chik, Jenny H. L., Jerry Zhou, Edward S. X. Moh, Richard Christopherson, Stephen J. Clarke, Mark P. Molloy, and Nicolle H. Packer. 2014. 'Comprehensive Glycomics Comparison between Colon

Cancer Cell Cultures and Tumours: Implications for Biomarker Studies'. *Journal of Proteomics* 108 (August): 146–62. https://doi.org/10.1016/j.jprot.2014.05.002.

Clarke, Erica, Roger C. Green, Jane S. Green, Krista Mahoney, Patrick S. Parfrey, H. Banfield Younghusband, and Michael O. Woods. 2012. 'Inherited Deleterious Variants in GALNT12 Are Associated with CRC Susceptibility'. *Human Mutation* 33 (7): 1056–58. https://doi.org/10.1002/humu.22088.

Cleary, Sean P., Michelle Cotterchio, Mark A. Jenkins, Hyeja Kim, Robert Bristow, Roger Green, Robert Haile, et al. 2009. 'Germline MutY Human Homologue Mutations and Colorectal Cancer: A Multisite Case-Control Study'. *Gastroenterology* 136 (4): 1251–60. https://doi.org/10.1053/j.gastro.2008.12.050.

Corfield, Anthony. 2017. 'Eukaryotic Protein Glycosylation: A Primer for Histochemists and Cell Biologists'. *Histochemistry and Cell Biology* 147 (2): 119–47. https://doi.org/10.1007/s00418-016-1526-4.

Cross, Amanda J., Michael F. Leitzmann, Mitchell H. Gail, Albert R. Hollenbeck, Arthur Schatzkin, and Rashmi Sinha. 2007. 'A Prospective Study of Red and Processed Meat Intake in Relation to Cancer Risk'. *PLoS Medicine* 4 (12): e325. https://doi.org/10.1371/journal.pmed.0040325.

Cui, H., S. Yang, Y. Jiang, C. Li, Y. Zhao, Y. Shi, Y. Hao, F. Qian, B. Tang, and P. Yu. 2018. 'The Glycosyltransferase ST6Gal-I Is Enriched in Cancer Stem-like Cells in Colorectal Carcinoma and Contributes to Their Chemo-Resistance'. *Clinical & Translational Oncology: Official Publication of the Federation of Spanish Oncology Societies and of the National Cancer Institute of Mexico* 20 (9): 1175–84. https://doi.org/10.1007/s12094-018-1840-5.

Dall'Olio, Fabio, Nadia Malagolini, Marco Trinchera, and Mariella Chiricolo. 2014. 'Sialosignaling: Sialyltransferases as Engines of Self-Fueling Loops in Cancer Progression'. *Biochimica Et Biophysica Acta* 1840 (9): 2752–64. https://doi.org/10.1016/j.bbagen.2014.06.006.

De' Angelis, Gian Luigi, Lorena Bottarelli, Cinzia Azzoni, Nicola De' Angelis, Gioacchino Leandro, Francesco Di Mario, Federica Gaiani, and Francesca Negri. 2018. 'Microsatellite Instability in Colorectal Cancer'. *Acta Bio-Medica: Atenei Parmensis* 89 (9-S): 97–101. https://doi.org/10.23750/abm.v89i9-S.7960.

Di Carlo, E., G. Forni, P. Lollini, M. P. Colombo, A. Modesti, and P. Musiani. 2001. 'The Intriguing Role of Polymorphonuclear Neutrophils in Antitumor Reactions'. *Blood* 97 (2): 339–45. https://doi.org/10.1182/blood.v97.2.339.

Doberstein, Kai, Anja Wieland, Sophia B. Boyoung Lee, Roman A. Alexander Blaheta, Steffen Wedel, Holger Moch, Peter Schraml, Josef Pfeilschifter, Glen Kristiansen, and Paul Gutwein. 2011. 'L1-CAM Expression in CcRCC Correlates with Shorter Patients Survival Times and Confers Chemoresistance in Renal Cell Carcinoma Cells'. *Carcinogenesis* 32 (3): 262–70. https://doi.org/10.1093/carcin/bgq249.

Doherty, Margaret, Evropi Theodoratou, Ian Walsh, Barbara Adamczyk, Henning Stöckmann, Felix Agakov, Maria Timofeeva, et al. 2018. 'Plasma N-Glycans in Colorectal Cancer Risk'. *Scientific Reports* 8 (1): 8655. https://doi.org/10.1038/s41598-018-26805-7.

Dong, Xichen, Yuliang Jiang, Jian Liu, Zhe Liu, Tianbo Gao, Guangyu An, and Tao Wen. 2018. 'T-Synthase Deficiency Enhances Oncogenic Features in Human Colorectal Cancer Cells via Activation of Epithelial-Mesenchymal Transition'. *BioMed Research International* 2018: 9532389. https://doi.org/10.1155/2018/9532389.

Drake, Richard R. 2015. 'Glycosylation and Cancer: Moving Glycomics to the Forefront'. *Advances in Cancer Research* 126: 1–10. https://doi.org/10.1016/bs.acr.2014.12.002.

Duan, Jing, Lin Chen, Huabin Gao, Tiantian Zhen, Hui Li, Jiangtao Liang, Fenfen Zhang, Huijuan Shi, and Anjia Han. 2018. 'GALNT6 Suppresses Progression of Colorectal Cancer'. *American Journal of Cancer Research* 8 (12): 2419–35.

Duchalais, Emilie, Christophe Guilluy, Steven Nedellec, Melissa Touvron, Anne Bessard, Yann Touchefeu, Céline Bossard, et al. 2018. 'Colorectal Cancer Cells Adhere to and Migrate Along the Neurons of the Enteric Nervous System'. *Cellular and Molecular Gastroenterology and Hepatology* 5 (1): 31–49. https://doi.org/10.1016/j.jcmgh.2017.10.002.

Duffy, M. J., R. Lamerz, C. Haglund, A. Nicolini, M. Kalousová, L. Holubec, and C. Sturgeon. 2014. 'Tumor Markers in Colorectal Cancer, Gastric Cancer and Gastrointestinal Stromal Cancers: European Group on Tumor Markers 2014 Guidelines Update'. *International Journal of Cancer* 134 (11): 2513–22. https://doi.org/10.1002/ijc.28384.

Duijnhoven, Fränzel J. B. van, H. Bas Bueno-De-Mesquita, Pietro Ferrari, Mazda Jenab, Hendriek C. Boshuizen, Martine M. Ros, Corinne Casagrande, et al. 2009. 'Fruit, Vegetables, and Colorectal Cancer Risk: The European Prospective Investigation into Cancer and Nutrition'. *The American Journal of Clinical Nutrition* 89 (5): 1441–52. https://doi.org/10.3945/ajcn.2008.27120.

Dunn, Gavin P., Allen T. Bruce, Hiroaki Ikeda, Lloyd J. Old, and Robert D. Schreiber. 2002. 'Cancer Immunoediting: From Immunosurveillance to Tumor Escape'. *Nature Immunology* 3 (11): 991–98. https://doi.org/10.1038/ni1102-991.

Ebeling, O., A. Duczmal, S. Aigner, C. Geiger, S. Schöllhammer, J. T. Kemshead, P. Möller, R. Schwartz-Albiez, and P. Altevogt. 1996. 'L1 Adhesion Molecule on Human Lymphocytes and Monocytes: Expression and Involvement in Binding to Alpha v Beta 3 Integrin'. *European Journal of Immunology* 26 (10): 2508–16. https://doi.org/10.1002/eji.1830261035.

Ehrlich, Paul. 1909. 'Ueber den jetzigen Stand der Karzinomforschung'. *Ned Tijdschr Geneeskd* 5: 273–90.

Ernst, Ann-Kathrin, Annika Putscher, Timur R. Samatov, Anna Suling, Vladimir V. Galatenko, Maxim Yu Shkurnikov, Evgeny N. Knyazev, et al. 2018. 'Knockdown of L1CAM Significantly Reduces Metastasis in a Xenograft Model of Human Melanoma: L1CAM Is a Potential Target for Anti-Melanoma Therapy'. *PloS One* 13 (2): e0192525. https://doi.org/10.1371/journal.pone.0192525.

Evans, Daniel R., Srividya Venkitachalam, Leslie Revoredo, Amanda T. Dohey, Erica Clarke, Julia J. Pennell, Amy E. Powell, et al. 2018. 'Evidence for GALNT12 as a Moderate Penetrance Gene for Colorectal Cancer'. *Human Mutation* 39 (8): 1092–1101. https://doi.org/10.1002/humu.23549.

Fadok, V. A., D. L. Bratton, A. Konowal, P. W. Freed, J. Y. Westcott, and P. M. Henson. 1998. 'Macrophages That Have Ingested Apoptotic Cells in Vitro Inhibit Proinflammatory Cytokine Production through Autocrine/Paracrine Mechanisms Involving TGF-Beta, PGE2, and PAF'. *The Journal of Clinical Investigation* 101 (4): 890–98. https://doi.org/10.1172/JCI1112.

Fang, Qing-Xia, Liang-Zhong Lü, Bo Yang, Zhong-Sheng Zhao, Yue Wu, and Xiao-Chun Zheng. 2010. 'L1, β-Catenin, and E-Cadherin Expression in Patients with Colorectal Cancer: Correlation with Clinicopathologic Features and Its Prognostic Significance'. *Journal of Surgical Oncology* 102 (5): 433–42. https://doi.org/10.1002/jso.21537.

Fearon, E. R., K. R. Cho, J. M. Nigro, S. E. Kern, J. W. Simons, J. M. Ruppert, S. R. Hamilton, A. C. Preisinger, G. Thomas, and K. W. Kinzler. 1990. 'Identification of a Chromosome 18q Gene That Is Altered in Colorectal Cancers'. *Science (New York, N.Y.)* 247 (4938): 49–56.

Fernández, Lara P., Ruth Sánchez-Martínez, Teodoro Vargas, Jesús Herranz, Roberto Martín-Hernández, Marta Mendiola, David Hardisson, et al. 2018. 'The Role of Glycosyltransferase Enzyme GCNT3 in Colon and Ovarian Cancer Prognosis and Chemoresistance'. *Scientific Reports* 8 (1): 8485. https://doi.org/10.1038/s41598-018-26468-4.

Fogh, Jorgen, and Germain Trempe. 1975. 'New Human Tumor Cell Lines'. In *Human Tumor Cells in Vitro*, 115–59. J. Fogh, editor.

Forcella, Matilde, Alessandra Mozzi, Federico M. Stefanini, Alice Riva, Samantha Epistolio, Francesca Molinari, Elisabetta Merlo, Eugenio Monti, Paola Fusi, and Milo Frattini. 2018. 'Deregulation of Sialidases in Human Normal and Tumor Tissues'. *Cancer Biomarkers: Section A of Disease Markers* 21 (3): 591–601. https://doi.org/10.3233/CBM-170548.

Fukasawa, Takaharu, Takayuki Asao, Hayato Yamauchi, Munenori Ide, Yuichi Tabe, Takaaki Fujii, Satoru Yamaguchi, Soichi Tsutsumi, Shin Yazawa, and Hiroyuki Kuwano. 2013. 'Associated Expression of A2,3sialylated Type 2 Chain Structures with Lymph Node Metastasis in Distal

Colorectal Cancer'. *Surgery Today* 43 (2): 155–62. https://doi.org/10.1007/s00595-012-0141-9.

Galizia, Gennaro, Michele Orditura, Ciro Romano, Eva Lieto, Paolo Castellano, Luigi Pelosio, Vincenzo Imperatore, Giuseppe Catalano, Carlo Pignatelli, and Ferdinando De Vita. 2002. 'Prognostic Significance of Circulating IL-10 and IL-6 Serum Levels in Colon Cancer Patients Undergoing Surgery'. *Clinical Immunology (Orlando, Fla.)* 102 (2): 169–78. https://doi.org/10.1006/clim.2001.5163.

Gao, Liping, Li Shen, Meiyun Yu, Jianlong Ni, Xiaoxia Dong, Yinghui Zhou, and Shiliang Wu. 2014. 'Colon Cancer Cells Treated with 5-fluorouracil Exhibit Changes in Polylactosamine-type N-glycans'. *Molecular Medicine Reports* 9 (5): 1697–1702. https://doi.org/10.3892/mmr.2014.2008.

Gavert, Nancy, Maralice Conacci-Sorrell, Daniela Gast, Annette Schneider, Peter Altevogt, Thomas Brabletz, and Avri Ben-Ze'ev. 2005. 'L1, a Novel Target of β-Catenin Signaling, Transforms Cells and Is Expressed at the Invasive Front of Colon Cancers'. *The Journal of Cell Biology* 168 (4): 633–42. https://doi.org/10.1083/jcb.200408051.

Gavert, Nancy, Michal Sheffer, Shani Raveh, Simone Spaderna, Michael Shtutman, Thomas Brabletz, Francis Barany, et al. 2007. 'Expression of L1-CAM and ADAM10 in Human Colon Cancer Cells Induces Metastasis'. *Cancer Research* 67 (16): 7703–12. https://doi.org/10.1158/0008-5472.CAN-07-0991.

Geest, Lydia G. M. van der, Jorine't Lam-Boer, Miriam Koopman, Cees Verhoef, Marloes A. G. Elferink, and Johannes H. W. de Wilt. 2015. 'Nationwide Trends in Incidence, Treatment and Survival of Colorectal Cancer Patients with Synchronous Metastases'. *Clinical & Experimental Metastasis* 32 (5): 457–65. https://doi.org/10.1007/s10585-015-9719-0.

Gessner, P., S. Riedl, A. Quentmaier, and W. Kemmner. 1993. 'Enhanced Activity of CMP-NeuAc:Gal Beta 1-4GlcNAc:Alpha 2,6-Sialyltransferase in Metastasizing Human Colorectal Tumor Tissue and Serum of Tumor Patients'. *Cancer Letters* 75 (3): 143–49.

Giordano, Guido, Antonio Febbraro, Eugenio Tomaselli, Maria Lucia Sarnicola, Pietro Parcesepe, Domenico Parente, Nicola Forte, et al. 2015. 'Cancer-Related CD15/FUT4 Overexpression Decreases Benefit to Agents Targeting EGFR or VEGF Acting as a Novel RAF-MEK-ERK Kinase Downstream Regulator in Metastatic Colorectal Cancer'. *Journal of Experimental & Clinical Cancer Research: CR* 34 (October): 108. https://doi.org/10.1186/s13046-015-0225-7.

Gisbergen, Klaas P. J. M. van, Corlien A. Aarnoudse, Gerrit A. Meijer, Teunis B. H. Geijtenbeek, and Yvette van Kooyk. 2005. 'Dendritic Cells Recognize Tumor-Specific Glycosylation of Carcinoembryonic Antigen on Colorectal Cancer Cells through Dendritic Cell-Specific Intercellular Adhesion Molecule-3-Grabbing Nonintegrin'. *Cancer Research* 65 (13): 5935–44. https://doi.org/10.1158/0008-5472.CAN-04-4140.

Globocan. 2018. 'Globocan 2018 Portugal'. 2018. http://gco.iarc.fr/today/data/factsheets/populations/620-portugal-fact-sheets.pdf.

Gonzalez, D. S., K. Karaveg, A. S. Vandersall-Nairn, A. Lal, and K. W. Moremen. 1999. 'Identification, Expression, and Characterization of a CDNA Encoding Human Endoplasmic Reticulum Mannosidase I, the Enzyme That Catalyzes the First Mannose Trimming Step in Mammalian Asn-Linked Oligosaccharide Biosynthesis'. *The Journal of Biological Chemistry* 274 (30): 21375–86. https://doi.org/10.1074/jbc.274.30.21375.

González-Vallinas, Margarita, Teodoro Vargas, Juan Moreno-Rubio, Susana Molina, Jesús Herranz, Paloma Cejas, Emilio Burgos, et al. 2015. 'Clinical Relevance of the Differential Expression of the Glycosyltransferase Gene GCNT3 in Colon Cancer'. *European Journal of Cancer (Oxford, England: 1990)* 51 (1): 1–8. https://doi.org/10.1016/j.ejca.2014.10.021.

Gu, Jianguo, Yuya Sato, Yoshinobu Kariya, Tomoya Isaji, Naoyuki Taniguchi, and Tomohiko Fukuda. 2009. 'A Mutual Regulation between Cell-Cell Adhesion and N-Glycosylation: Implication of the Bisecting GlcNAc for Biological Functions'. *Journal of Proteome Research* 8 (2): 431–35. https://doi.org/10.1021/pr800674g.

Guda, Kishore, Helen Moinova, Jian He, Oliver Jamison, Lakshmeswari Ravi, Leanna Natale, James Lutterbaugh, et al. 2009. 'Inactivating Germ-Line and Somatic Mutations in Polypeptide N-Acetylgalactosaminyltransferase 12 in Human Colon Cancers'. *Proceedings of the National Academy of Sciences of the United States of America* 106 (31): 12921–25. https://doi.org/10.1073/pnas.0901454106.

Guile, G R, P M Rudd, D R Wing, S B Prime, and R A Dwek. 1996. 'A Rapid High-Resolution High-Performance Liquid Chromatographic Method for Separating Glycan Mixtures and Analyzing Oligosaccharide Profiles.' *Analytical Biochemistry* 240 (2): 210–26. https://doi.org/10.1006/abio.1996.0351.

Guinney, Justin, Rodrigo Dienstmann, Xin Wang, Aurélien de Reyniès, Andreas Schlicker, Charlotte Soneson, Laetitia Marisa, et al. 2015. 'The Consensus Molecular Subtypes of Colorectal Cancer'. *Nature Medicine* 21 (11): 1350–56. https://doi.org/10.1038/nm.3967.

Guo, Jian-Ming, Hui-Li Chen, Guo-Min Wang, Yong-Kang Zhang, and Hisashi Narimatsu. 2004. 'Expression of UDP-GalNAc:Polypeptide N-Acetylgalactosaminyltransferase-12 in Gastric and Colonic Cancer Cell Lines and in Human Colorectal Cancer'. *Oncology* 67 (3–4): 271–76. https://doi.org/10.1159/000081328.

Guo, Jin-Cheng, Yang-Min Xie, Li-Qiang Ran, Hui-Hui Cao, Chun Sun, Jian-Yi Wu, Zhi-Yong Wu, et al. 2017. 'L1CAM Drives Oncogenicity in Esophageal Squamous Cell Carcinoma by Stimulation of Ezrin Transcription'. *Journal of Molecular Medicine (Berlin, Germany)* 95 (12): 1355–68. https://doi.org/10.1007/s00109-017-1595-4.

Guo, Peng, Ying Zhang, Zong-hou Shen, Xia-ying Zhang, and Hui-li Chen. 2004. 'Effect of N-Acetylglucosaminyltransferase V on the Expressions of Other Glycosyltransferases'. *FEBS Letters* 562 (1–3): 93–98. https://doi.org/10.1016/S0014-5793(04)00188-7.

Haase, G., N. Gavert, T. Brabletz, and A. Ben-Ze'ev. 2017. 'A Point Mutation in the Extracellular Domain of L1 Blocks Its Capacity to Confer Metastasis in Colon Cancer Cells via CD10'. *Oncogene* 36 (11): 1597–1606. https://doi.org/10.1038/onc.2016.329.

Hägerbäumer, Pia, Michael Vieth, Mario Anders, and Udo Schumacher. 2015. 'Lectin Histochemistry Shows WGA, PHA-L and HPA Binding Increases During Progression of Human Colorectal Cancer'. *Anticancer Research* 35 (10): 5333–39.

Hall, Heike, Valentin Djonov, Martin Ehrbar, Matthias Hoechli, and Jeffrey A. Hubbell. 2004. 'Heterophilic Interactions between Cell Adhesion Molecule L1 and Alphavbeta3-Integrin Induce HUVEC Process Extension in Vitro and Angiogenesis in Vivo'. *Angiogenesis* 7 (3): 213–23. https://doi.org/10.1007/s10456-004-1328-5.

Hanley, William D., Monica M. Burdick, Konstantinos Konstantopoulos, and Robert Sackstein. 2005. 'CD44 on LS174T Colon Carcinoma Cells Possesses E-Selectin Ligand Activity'. *Cancer Research* 65 (13): 5812–17. https://doi.org/10.1158/0008-5472.CAN-04-4557.

Hanley, William D., Susan L. Napier, Monica M. Burdick, Ronald L. Schnaar, Robert Sackstein, and Konstantinos Konstantopoulos. 2006. 'Variant Isoforms of CD44 Are P- and L-Selectin Ligands on Colon Carcinoma Cells'. *FASEB Journal: Official Publication of the Federation of American Societies for Experimental Biology* 20 (2): 337–39. https://doi.org/10.1096/fj.05-4574fje.

He, Li-Zhen, Venky Ramakrishna, John E. Connolly, Xi-Tao Wang, Patricia A. Smith, Charles L. Jones, Maria Valkova-Valchanova, et al. 2004. 'A Novel Human Cancer Vaccine Elicits Cellular Responses to the Tumor-Associated Antigen, Human Chorionic Gonadotropin Beta'. *Clinical Cancer Research: An Official Journal of the American Association for Cancer Research* 10 (6): 1920–27.

Herbeuval, Jean-Philippe, Eric Lelievre, Claude Lambert, Michel Dy, and Christian Genin. 2004. 'Recruitment of STAT3 for Production of IL-10 by Colon Carcinoma Cells Induced by Macrophage-Derived IL-6'. *Journal of Immunology (Baltimore, Md.: 1950)* 172 (7): 4630–36. https://doi.org/10.4049/jimmunol.172.7.4630.

Hiller, K. M., J. P. Mayben, K. M. Bendt, G. A. Manousos, K. Senger, H. S. Cameron, and B. W. Weston. 2000. 'Transfection of Alpha(1,3)Fucosyltransferase Antisense Sequences Impairs the

Proliferative and Tumorigenic Ability of Human Colon Carcinoma Cells'. *Molecular Carcinogenesis* 27 (4): 280–88.

Hirakawa, M., R. Takimoto, F. Tamura, M. Yoshida, M. Ono, K. Murase, Y. Sato, et al. 2014. 'Fucosylated TGF-β Receptors Transduces a Signal for Epithelial-Mesenchymal Transition in Colorectal Cancer Cells'. *British Journal of Cancer* 110 (1): 156–63. https://doi.org/10.1038/bjc.2013.699.

Höchst, Bastian, Frank A. Schildberg, Jan Böttcher, Christina Metzger, Sebastian Huss, Andreas Türler, Markus Overhaus, et al. 2012. 'Liver Sinusoidal Endothelial Cells Contribute to CD8 T Cell Tolerance toward Circulating Carcinoembryonic Antigen in Mice'. *Hepatology (Baltimore, Md.)* 56 (5): 1924–33. https://doi.org/10.1002/hep.25844.

Holst, Stephanie, Anna J. M. Deuss, Gabi W. van Pelt, Sandra J. van Vliet, Juan J. Garcia-Vallejo, Carolien A. M. Koeleman, André M. Deelder, et al. 2016. 'N-Glycosylation Profiling of Colorectal Cancer Cell Lines Reveals Association of Fucosylation with Differentiation and Caudal Type Homebox 1 (CDX1)/Villin MRNA Expression'. *Molecular & Cellular Proteomics: MCP* 15 (1): 124–40. https://doi.org/10.1074/mcp.M115.051235.

Holst, Stephanie, Manfred Wuhrer, and Yoann Rombouts. 2015. 'Glycosylation Characteristics of Colorectal Cancer'. *Advances in Cancer Research* 126: 203–56. https://doi.org/10.1016/bs.acr.2014.11.004.

Hong, Hao, Michael Stastny, Christine Brown, Wen-Chung Chang, Julie R. Ostberg, Stephen J. Forman, and Michael C. Jensen. 2014. 'Diverse Solid Tumors Expressing a Restricted Epitope of L1-CAM Can Be Targeted by Chimeric Antigen Receptor Redirected T Lymphocytes'. *Journal of Immunotherapy (Hagerstown, Md.: 1997)* 37 (2): 93–104. https://doi.org/10.1097/CJI.0000000000000018.

Hu, Jialei, Yujia Shan, Jia Ma, Yue Pan, Huimin Zhou, Liqun Jiang, and Li Jia. 2019. 'LncRNA ST3Gal6-AS1/ST3Gal6 Axis Mediates Colorectal Cancer Progression by Regulating α-2,3 Sialylation via PI3K/Akt Signaling'. *International Journal of Cancer* 145 (2): 450–60. https://doi.org/10.1002/ijc.32103.

Huang, M.-C., H.-Y. Chen, H.-C. Huang, J. Huang, J.-T. Liang, T.-L. Shen, N.-Y. Lin, C.-C. Ho, I.-M. Cho, and S.-M. Hsu. 2006. 'C2GnT-M Is Downregulated in Colorectal Cancer and Its Re-Expression Causes Growth Inhibition of Colon Cancer Cells'. *Oncogene* 25 (23): 3267–76. https://doi.org/10.1038/sj.onc.1209350.

Hung, Ji-Shiang, John Huang, Yo-Chuen Lin, Miao-Juei Huang, Po-Huang Lee, Hong-Shiee Lai, Jin-Tung Liang, and Min-Chuan Huang. 2014. 'C1GALT1 Overexpression Promotes the Invasive Behavior of Colon Cancer Cells through Modifying O-Glycosylation of FGFR2'. *Oncotarget* 5 (8): 2096–2106. https://doi.org/10.18632/oncotarget.1815.

Ichikawa, T., J. Nakayama, N. Sakura, T. Hashimoto, M. Fukuda, M. N. Fukuda, and T. Taki. 1999. 'Expression of N-Acetyllactosamine and Beta1,4-Galactosyltransferase (Beta4GalT-I) during Adenoma-Carcinoma Sequence in the Human Colorectum'. *The Journal of Histochemistry and Cytochemistry: Official Journal of the Histochemistry Society* 47 (12): 1593–1602. https://doi.org/10.1177/002215549904701211.

Ishida, Akiko, Mariko Ohta, Munetoyo Toda, Takeomi Murata, Taichi Usui, Kaoru Akita, Mizue Inoue, and Hiroshi Nakada. 2008. 'Mucin-Induced Apoptosis of Monocyte-Derived Dendritic Cells during Maturation'. *Proteomics* 8 (16): 3342–49. https://doi.org/10.1002/pmic.200800039.

Ishida, Hiroyasu, Akira Togayachi, Tokiko Sakai, Toshie Iwai, Toru Hiruma, Takashi Sato, Reiko Okubo, et al. 2005. 'A Novel Beta1,3-N-Acetylglucosaminyltransferase (Beta3Gn-T8), Which Synthesizes Poly-N-Acetyllactosamine, Is Dramatically Upregulated in Colon Cancer'. *FEBS Letters* 579 (1): 71–78. https://doi.org/10.1016/j.febslet.2004.11.037.

Ishikawa, M., Y. Koga, M. Hosokawa, and H. Kobayashi. 1986. 'Augmentation of B16 Melanoma Lung Colony Formation in C57BL/6 Mice Having Marked Granulocytosis'. *International Journal of Cancer* 37 (6): 919–24. https://doi.org/10.1002/ijc.2910370619.

Isshiki, S., A. Togayachi, T. Kudo, S. Nishihara, M. Watanabe, T. Kubota, M. Kitajima, et al. 1999. 'Cloning, Expression, and Characterization of a Novel UDP-Galactose:Beta-N-

Acetylglucosamine Beta1,3-Galactosyltransferase (Beta3Gal-T5) Responsible for Synthesis of Type 1 Chain in Colorectal and Pancreatic Epithelia and Tumor Cells Derived Therefrom'. *The Journal of Biological Chemistry* 274 (18): 12499–507. https://doi.org/10.1074/jbc.274.18.12499.

Isshiki, Soichiro, Takashi Kudo, Shoko Nishihara, Yuzuru Ikehara, Akira Togayachi, Akiko Furuya, Kenya Shitara, et al. 2003. 'Lewis Type 1 Antigen Synthase (Beta3Gal-T5) Is Transcriptionally Regulated by Homeoproteins'. *The Journal of Biological Chemistry* 278 (38): 36611–20. https://doi.org/10.1074/jbc.M302681200.

Ito, H., N. Hiraiwa, M. Sawada-Kasugai, S. Akamatsu, T. Tachikawa, Y. Kasai, S. Akiyama, K. Ito, H. Takagi, and R. Kannagi. 1997. 'Altered MRNA Expression of Specific Molecular Species of Fucosyl- and Sialyl-Transferases in Human Colorectal Cancer Tissues'. *International Journal of Cancer* 71 (4): 556–64.

Itzkowitz, S. H., M. Yuan, Y. Fukushi, H. Lee, Z. R. Shi, V. Zurawski, S. Hakomori, and Y. S. Kim. 1988. 'Immunohistochemical Comparison of Lea, Monosialosyl Lea (CA 19-9), and Disialosyl Lea Antigens in Human Colorectal and Pancreatic Tissues'. *Cancer Research* 48 (13): 3834–42.

Iwai, Toshie, Takashi Kudo, Risa Kawamoto, Tomomi Kubota, Akira Togayachi, Toru Hiruma, Tomoko Okada, Toru Kawamoto, Kyoei Morozumi, and Hisashi Narimatsu. 2005. 'Core 3 Synthase Is Down-Regulated in Colon Carcinoma and Profoundly Suppresses the Metastatic Potential of Carcinoma Cells'. *Proceedings of the National Academy of Sciences of the United States of America* 102 (12): 4572–77. https://doi.org/10.1073/pnas.0407983102.

Jacobs, Pieter P., and Robert Sackstein. 2011. 'CD44 and HCELL: Preventing Hematogenous Metastasis at Step 1'. *FEBS Letters* 585 (20): 3148–58. https://doi.org/10.1016/j.febslet.2011.07.039.

Jadhav, S., B. S. Bochner, and K. Konstantopoulos. 2001. 'Hydrodynamic Shear Regulates the Kinetics and Receptor Specificity of Polymorphonuclear Leukocyte-Colon Carcinoma Cell Adhesive Interactions'. *Journal of Immunology (Baltimore, Md.: 1950)* 167 (10): 5986–93. https://doi.org/10.4049/jimmunol.167.10.5986.

Jadhav, Sameer, and Konstantinos Konstantopoulos. 2002. 'Fluid Shear- and Time-Dependent Modulation of Molecular Interactions between PMNs and Colon Carcinomas'. *American Journal of Physiology. Cell Physiology* 283 (4): C1133-1143. https://doi.org/10.1152/ajpcell.00104.2002.

Jiang, Yanmei, Changfu Zhang, Kai Chen, Zhe Chen, Zhigang Sun, Zhuqing Zhang, Dongbing Ding, Shuangyi Ren, and Yunfei Zuo. 2014. 'The Clinical Significance of DC-SIGN and DC-SIGNR, Which Are Novel Markers Expressed in Human Colon Cancer'. *PloS One* 9 (12): e114748. https://doi.org/10.1371/journal.pone.0114748.

Jiang, Yuliang, Zhe Liu, Feng Xu, Xichen Dong, Yurong Cheng, Yizhang Hu, Tianbo Gao, et al. 2018. 'Aberrant O-Glycosylation Contributes to Tumorigenesis in Human Colorectal Cancer'. *Journal of Cellular and Molecular Medicine* 22 (10): 4875–85. https://doi.org/10.1111/jcmm.13752.

Jiang, Zhi, Huan Zhang, Chunliang Liu, Jun Yin, Shan Tong, Junxing Lv, Shaohua Wei, and Shiliang Wu. 2018. 'B3GnT8 Promotes Colorectal Cancer Cells Invasion via CD147/MMP2/Galectin3 Axis'. *Frontiers in Physiology* 9: 588. https://doi.org/10.3389/fphys.2018.00588.

Johnson, Constance M., Caimiao Wei, Joe E. Ensor, Derek J. Smolenski, Christopher I. Amos, Bernard Levin, and Donald A. Berry. 2013. 'Meta-Analyses of Colorectal Cancer Risk Factors'. *Cancer Causes & Control: CCC* 24 (6): 1207–22. https://doi.org/10.1007/s10552-013-0201-5.

Ju, Tongzhong, and Richard D. Cummings. 2002. 'A Unique Molecular Chaperone Cosmc Required for Activity of the Mammalian Core 1 Beta 3-Galactosyltransferase'. *Proceedings of the National Academy of Sciences of the United States of America* 99 (26): 16613–18. https://doi.org/10.1073/pnas.262438199.

Kaifi, Jussuf T., Uta Reichelt, Alexander Quaas, Paulus G. Schurr, Robin Wachowiak, Emre F. Yekebas, Tim Strate, et al. 2007. 'L1 Is Associated with Micrometastatic Spread and Poor Outcome in

Colorectal Cancer'. *Modern Pathology: An Official Journal of the United States and Canadian Academy of Pathology, Inc* 20 (11): 1183–90. https://doi.org/10.1038/modpathol.3800955.

Kajiwara, Yoshiki, Hideki Ueno, Yojiro Hashiguchi, Eiji Shinto, Hideyuki Shimazaki, Hidetaka Mochizuki, and Kazuo Hase. 2011. 'Expression of L1 Cell Adhesion Molecule and Morphologic Features at the Invasive Front of Colorectal Cancer'. *American Journal of Clinical Pathology* 136 (1): 138–44. https://doi.org/10.1309/AJCP63NRBNGCTXVF.

Kakugawa, Yoichiro, Tadashi Wada, Kazunori Yamaguchi, Hideaki Yamanami, Kiyoaki Ouchi, Ikuro Sato, and Taeko Miyagi. 2002. 'Up-Regulation of Plasma Membrane-Associated Ganglioside Sialidase (Neu3) in Human Colon Cancer and Its Involvement in Apoptosis Suppression'. *Proceedings of the National Academy of Sciences of the United States of America* 99 (16): 10718–23. https://doi.org/10.1073/pnas.152597199.

Kamińska, J., M. M. Kowalska, M. P. Nowacki, M. G. Chwaliński, A. Rysińska, and M. Fuksiewicz. 2000. 'CRP, TNF-Alpha, IL-1ra, IL-6, IL-8 and IL-10 in Blood Serum of Colorectal Cancer Patients'. *Pathology Oncology Research: POR* 6 (1): 38–41.

Kaprio, Tuomas, Tero Satomaa, Annamari Heiskanen, Cornelis H. Hokke, André M. Deelder, Harri Mustonen, Jaana Hagström, Olli Carpen, Juhani Saarinen, and Caj Haglund. 2015. 'N-Glycomic Profiling as a Tool to Separate Rectal Adenomas from Carcinomas'. *Molecular & Cellular Proteomics: MCP* 14 (2): 277–88. https://doi.org/10.1074/mcp.M114.041632.

Kato, Kengo, Kiyoto Shiga, Kazunori Yamaguchi, Keiko Hata, Toshimitsu Kobayashi, Kaoru Miyazaki, Shigeru Saijo, and Taeko Miyagi. 2006. 'Plasma-Membrane-Associated Sialidase (NEU3) Differentially Regulates Integrin-Mediated Cell Proliferation through Laminin- and Fibronectin-Derived Signalling'. *The Biochemical Journal* 394 (Pt 3): 647–56. https://doi.org/10.1042/BJ20050737.

Khare, Vineeta, Michaela Lang, Kyle Dammann, Christoph Campregher, Alex Lyakhovich, and Christoph Gasche. 2014. 'Modulation of N-Glycosylation by Mesalamine Facilitates Membranous E-Cadherin Expression in Colon Epithelial Cells'. *Biochemical Pharmacology* 87 (2): 312–20. https://doi.org/10.1016/j.bcp.2013.10.021.

Kim, Yong-Sam, Yeong Hee Ahn, Kyoung Jin Song, Jeong Gu Kang, Ju Hee Lee, Seong Kook Jeon, Hyoung-Chin Kim, Jong Shin Yoo, and Jeong-Heon Ko. 2012. 'Overexpression and β-1,6-N-Acetylglucosaminylation-Initiated Aberrant Glycosylation of TIMP-1: A "Double Whammy" Strategy in Colon Cancer Progression'. *The Journal of Biological Chemistry* 287 (39): 32467–78. https://doi.org/10.1074/jbc.M112.370064.

Kitayama, J., S. Ikeda, K. Kumagai, H. Saito, and H. Nagawa. 2000. 'Alpha 6 Beta 1 Integrin (VLA-6) Mediates Leukocyte Tether and Arrest on Laminin under Physiological Shear Flow'. *Cellular Immunology* 199 (2): 97–103. https://doi.org/10.1006/cimm.1999.1596.

Klat, Jaroslav, Ales Mladenka, Jana Dvorackova, Sylva Bajsova, and Ondrej Simetka. 2019. 'L1CAM as a Negative Prognostic Factor in Endometrioid Endometrial Adenocarcinoma FIGO Stage IA-IB'. *Anticancer Research* 39 (1): 421–24. https://doi.org/10.21873/anticanres.13128.

Kobayashi, K., S. Matsumoto, T. Morishima, T. Kawabe, and T. Okamoto. 2000. 'Cimetidine Inhibits Cancer Cell Adhesion to Endothelial Cells and Prevents Metastasis by Blocking E-Selectin Expression'. *Cancer Research* 60 (14): 3978–84.

Köhler, S., S. Ullrich, U. Richter, and U. Schumacher. 2010. 'E-/P-Selectins and Colon Carcinoma Metastasis: First in Vivo Evidence for Their Crucial Role in a Clinically Relevant Model of Spontaneous Metastasis Formation in the Lung'. *British Journal of Cancer* 102 (3): 602–9. https://doi.org/10.1038/sj.bjc.6605492.

Kohsaki, T., I. Nishimori, H. Nakayama, E. Miyazaki, H. Enzan, M. Nomoto, M. A. Hollingsworth, and S. Onishi. 2000. 'Expression of UDP-GalNAc: Polypeptide N-Acetylgalactosaminyltransferase Isozymes T1 and T2 in Human Colorectal Cancer'. *Journal of Gastroenterology* 35 (11): 840–48.

Koseki, Koichi, Tadashi Wada, Masahiro Hosono, Keiko Hata, Kazunori Yamaguchi, Kazuo Nitta, and Taeko Miyagi. 2012. 'Human Cytosolic Sialidase NEU2-Low General Tissue Expression but

Involvement in PC-3 Prostate Cancer Cell Survival'. *Biochemical and Biophysical Research Communications* 428 (1): 142–49. https://doi.org/10.1016/j.bbrc.2012.10.028.

Kozak, Radoslaw P., Concepcion Badia Tortosa, Daryl L. Fernandes, and Daniel I. R. Spencer. 2015. 'Comparison of Procainamide and 2-Aminobenzamide Labeling for Profiling and Identification of Glycans by Liquid Chromatography with Fluorescence Detection Coupled to Electrospray Ionization-Mass Spectrometry'. *Analytical Biochemistry* 486 (October): 38–40. https://doi.org/10.1016/j.ab.2015.06.006.

Kumar, Vinay, Stanley L Robbins, and Ramzi S Cotran. 2005. *Robbins and Cotran Pathologic Basis of Disease*. Philadelphia, Pa.: Elsevier Saunders.

Künkele, Annette, Agne Taraseviciute, Laura S. Finn, Adam J. Johnson, Carolina Berger, Olivia Finney, Cindy A. Chang, et al. 2017. 'Preclinical Assessment of CD171-Directed CAR T-Cell Adoptive Therapy for Childhood Neuroblastoma: CE7 Epitope Target Safety and Product Manufacturing Feasibility'. *Clinical Cancer Research: An Official Journal of the American Association for Cancer Research* 23 (2): 466–77. https://doi.org/10.1158/1078-0432.CCR-16-0354.

Labianca, R., B. Nordlinger, G. D. Beretta, S. Mosconi, M. Mandalà, A. Cervantes, D. Arnold, and ESMO Guidelines Working Group. 2013. 'Early Colon Cancer: ESMO Clinical Practice Guidelines for Diagnosis, Treatment and Follow-Up'. *Annals of Oncology: Official Journal of the European Society for Medical Oncology* 24 Suppl 6 (October): vi64-72. https://doi.org/10.1093/annonc/mdt354.

Läubli, Heinz, Frederico Alisson-Silva, Michal A. Stanczak, Shoib S. Siddiqui, Liwen Deng, Andrea Verhagen, Nissi Varki, and Ajit Varki. 2014. 'Lectin Galactoside-Binding Soluble 3 Binding Protein (LGALS3BP) Is a Tumor-Associated Immunomodulatory Ligand for CD33-Related Siglecs'. *The Journal of Biological Chemistry* 289 (48): 33481–91. https://doi.org/10.1074/jbc.M114.593129.

Laudato, Sara, Nitin Patil, Mohammed L. Abba, Joerg H. Leupold, Axel Benner, Timo Gaiser, Alexander Marx, and Heike Allgayer. 2017. 'P53-Induced MiR-30e-5p Inhibits Colorectal Cancer Invasion and Metastasis by Targeting ITGA6 and ITGB1'. *International Journal of Cancer* 141 (9): 1879–90. https://doi.org/10.1002/ijc.30854.

Lavrsen, Kirstine, Sally Dabelsteen, Sergey Y. Vakhrushev, Asha M. R. Levann, Amalie Dahl Haue, August Dylander, Ulla Mandel, et al. 2018. 'De Novo Expression of Human Polypeptide N-Acetylgalactosaminyltransferase 6 (GalNAc-T6) in Colon Adenocarcinoma Inhibits the Differentiation of Colonic Epithelium'. *The Journal of Biological Chemistry* 293 (4): 1298–1314. https://doi.org/10.1074/jbc.M117.812826.

Le, Dung T., Tae Won Kim, Eric Van Cutsem, Ravit Geva, Dirk Jäger, Hiroki Hara, Matthew Burge, et al. 2020. 'Phase II Open-Label Study of Pembrolizumab in Treatment-Refractory, Microsatellite Instability-High/Mismatch Repair-Deficient Metastatic Colorectal Cancer: KEYNOTE-164'. *Journal of Clinical Oncology: Official Journal of the American Society of Clinical Oncology* 38 (1): 11–19. https://doi.org/10.1200/JCO.19.02107.

Lee, Albert, Joel M. Chick, Daniel Kolarich, Paul A. Haynes, Graham R. Robertson, Maria Tsoli, Lucy Jankova, Stephen J. Clarke, Nicolle H. Packer, and Mark S. Baker. 2011. 'Liver Membrane Proteome Glycosylation Changes in Mice Bearing an Extra-Hepatic Tumor'. *Molecular & Cellular Proteomics: MCP* 10 (9): M900538MCP200. https://doi.org/10.1074/mcp.M900538-MCP200.

Lee, Minyoung, Hae-June Lee, Woo Duck Seo, Ki Hun Park, and Yun-Sil Lee. 2010. 'Sialylation of Integrin Beta1 Is Involved in Radiation-Induced Adhesion and Migration in Human Colon Cancer Cells'. *International Journal of Radiation Oncology, Biology, Physics* 76 (5): 1528–36. https://doi.org/10.1016/j.ijrobp.2009.11.022.

Leibovitz, A., J. C. Stinson, W. B. McCombs, C. E. McCoy, K. C. Mazur, and N. D. Mabry. 1976. 'Classification of Human Colorectal Adenocarcinoma Cell Lines'. *Cancer Research* 36 (12): 4562–69.

Li, J., A. D. Guillebon, J.-w Hsu, S. R. Barthel, C. J. Dimitroff, Y.-F. Lee, and M. R. King. 2013. 'Human Fucosyltransferase 6 Enables Prostate Cancer Metastasis to Bone'. *British Journal of Cancer* 109 (12): 3014–22. https://doi.org/10.1038/bjc.2013.690.

Li, Rj Eveline, Sandra J. van Vliet, and Y. van Kooyk. 2018. 'Using the Glycan Toolbox for Pathogenic Interventions and Glycan Immunotherapy'. *Current Opinion in Biotechnology* 51: 24–31. https://doi.org/10.1016/j.copbio.2017.11.003.

Li, Yang, Changqian Zeng, Jialei Hu, Yue Pan, Yujia Shan, Bing Liu, and Li Jia. 2018. 'Long Non-Coding RNA-SNHG7 Acts as a Target of MiR-34a to Increase GALNT7 Level and Regulate PI3K/Akt/MTOR Pathway in Colorectal Cancer Progression'. *Journal of Hematology & Oncology* 11 (1): 89. https://doi.org/10.1186/s13045-018-0632-2.

Liang, Jin-xiao, Yong Liang, and Wei Gao. 2016. 'Clinicopathological and Prognostic Significance of Sialyl Lewis X Overexpression in Patients with Cancer: A Meta-Analysis'. *OncoTargets and Therapy* 9 (May): 3113–25. https://doi.org/10.2147/OTT.S102389.

Lier, M. G. F. van, A. Wagner, E. M. H. Mathus-Vliegen, E. J. Kuipers, E. W. Steyerberg, and M. E. van Leerdam. 2010. 'High Cancer Risk in Peutz-Jeghers Syndrome: A Systematic Review and Surveillance Recommendations'. *The American Journal of Gastroenterology* 105 (6): 1258–64; author reply 1265. https://doi.org/10.1038/ajg.2009.725.

Liu, Bing, Shimeng Pan, Yang Xiao, Qianqian Liu, Jingchao Xu, and Li Jia. 2018. 'LINC01296/MiR-26a/GALNT3 Axis Contributes to Colorectal Cancer Progression by Regulating O-Glycosylated MUC1 via PI3K/AKT Pathway'. *Journal of Experimental & Clinical Cancer Research: CR* 37 (1): 316. https://doi.org/10.1186/s13046-018-0994-x.

Liu, Xincheng, Shengping Min, Nan Wu, Hongli Liu, Tao Wang, Wei Li, Yuanbing Shen, et al. 2019. 'MiR-193a-3p Inhibition of the Slug Activator PAK4 Suppresses Non-Small Cell Lung Cancer Aggressiveness via the P53/Slug/L1CAM Pathway'. *Cancer Letters* 447 (April): 56–65. https://doi.org/10.1016/j.canlet.2019.01.027.

Liu, Zhe, Jian Liu, Xichen Dong, Xin Hu, Yuliang Jiang, Lina Li, Tan Du, et al. 2019. 'Tn Antigen Promotes Human Colorectal Cancer Metastasis via H-Ras Mediated Epithelial-Mesenchymal Transition Activation'. *Journal of Cellular and Molecular Medicine* 23 (3): 2083–92. https://doi.org/10.1111/jcmm.14117.

Loureiro, Liliana R., Diana P. Sousa, Dylan Ferreira, Wengang Chai, Luís Lima, Carina Pereira, Carla B. Lopes, et al. 2018. 'Novel Monoclonal Antibody L2A5 Specifically Targeting Sialyl-Tn and Short Glycans Terminated by Alpha-2-6 Sialic Acids'. *Scientific Reports* 8 (1): 12196. https://doi.org/10.1038/s41598-018-30421-w.

Luo, Liping, Gong-Qing Shen, Karen A. Stiffler, Qing K. Wang, Thomas G. Pretlow, and Theresa P. Pretlow. 2006. 'Loss of Heterozygosity in Human Aberrant Crypt Foci (ACF), a Putative Precursor of Colon Cancer'. *Carcinogenesis* 27 (6): 1153–59. https://doi.org/10.1093/carcin/bgi354.

Lynch, Henry T., Wendy S. Rubinstein, and Gershon Y. Locker. 2004. 'Cancer in Jews: Introduction and Overview'. *Familial Cancer* 3 (3–4): 177–92. https://doi.org/10.1007/s10689-004-9538-y.

Maciejewski, Ryszard, Sebastian Radej, Jacek Furmaga, Andrzej Chrościcki, Sławomir Rudzki, Jacek Roliński, and Grzegorz Wallner. 2013. 'Evaluation of Immature Monocyte-Derived Dendritic Cells Generated from Patients with Colorectal Cancer'. *Polski Przeglad Chirurgiczny* 85 (12): 714–20. https://doi.org/10.2478/pjs-2013-0109.

Magrini, Elena, Alessandra Villa, Francesca Angiolini, Andrea Doni, Giovanni Mazzarol, Noemi Rudini, Luigi Maddaluno, et al. 2014. 'Endothelial Deficiency of L1 Reduces Tumor Angiogenesis and Promotes Vessel Normalization'. *The Journal of Clinical Investigation* 124 (10): 4335–50. https://doi.org/10.1172/JCI70683.

Majuri, M. L., R. Niemelä, S. Tiisala, O. Renkonen, and R. Renkonen. 1995. 'Expression and Function of Alpha 2,3-Sialyl- and Alpha 1,3/1,4-Fucosyltransferases in Colon Adenocarcinoma Cell Lines: Role in Synthesis of E-Selectin Counter-Receptors'. *International Journal of Cancer* 63 (4): 551–59.

Mannori, G., P. Crottet, O. Cecconi, K. Hanasaki, A. Aruffo, R. M. Nelson, A. Varki, and M. P. Bevilacqua. 1995. 'Differential Colon Cancer Cell Adhesion to E-, P-, and L-Selectin: Role of Mucin-Type Glycoproteins'. *Cancer Research* 55 (19): 4425–31.

Marcos, Nuno T., Sandra Pinho, Catarina Grandela, Andrea Cruz, Bénédicte Samyn-Petit, Anne Harduin-Lepers, Raquel Almeida, et al. 2004. 'Role of the Human ST6GalNAc-I and ST6GalNAc-II in the Synthesis of the Cancer-Associated Sialyl-Tn Antigen'. *Cancer Research* 64 (19): 7050–57. https://doi.org/10.1158/0008-5472.CAN-04-1921.

Mare, Lydia, Anna Caretti, Riccardo Albertini, and Marco Trinchera. 2013. 'CA19.9 Antigen Circulating in the Serum of Colon Cancer Patients: Where Is It From?' *The International Journal of Biochemistry & Cell Biology* 45 (4): 792–97. https://doi.org/10.1016/j.biocel.2013.01.004.

Mare, Lydia, and Marco Trinchera. 2004. 'Suppression of Beta 1,3galactosyltransferase Beta 3Gal-T5 in Cancer Cells Reduces Sialyl-Lewis a and Enhances Poly N-Acetyllactosamines and Sialyl-Lewis x on O-Glycans'. *European Journal of Biochemistry* 271 (1): 186–94. https://doi.org/10.1046/j.1432-1033.2003.03919.x.

McGuire, J. C., L. A. Greene, and A. V. Furano. 1978. 'NGF Stimulates Incorporation of Fucose or Glucosamine into an External Glycoprotein in Cultured Rat PC12 Pheochromocytoma Cells'. *Cell* 15 (2): 357–65.

McNabb, Sarah, Tabitha A. Harrison, Demetrius Albanes, Sonja I. Berndt, Hermann Brenner, Bette J. Caan, Peter T. Campbell, et al. 2019. 'Meta-Analysis of 16 Studies of the Association of Alcohol with Colorectal Cancer'. *International Journal of Cancer*, April. https://doi.org/10.1002/ijc.32377.

Melero, Ignacio, Izaskun Gabari, Angel L. Corbí, Miguel Relloso, Guillermo Mazzolini, Volker Schmitz, Mercedes Rodriguez-Calvillo, et al. 2002. 'An Anti-ICAM-2 (CD102) Monoclonal Antibody Induces Immune-Mediated Regressions of Transplanted ICAM-2-Negative Colon Carcinomas'. *Cancer Research* 62 (11): 3167–74.

Mihalache, Adriana, Jean-François Delplanque, Bélinda Ringot-Destrez, Cindy Wavelet, Pierre Gosset, Bertrand Nunes, Sophie Groux-Degroote, Renaud Léonard, and Catherine Robbe-Masselot. 2015. 'Structural Characterization of Mucin O-Glycosylation May Provide Important Information to Help Prevent Colorectal Tumor Recurrence'. *Frontiers in Oncology* 5: 217. https://doi.org/10.3389/fonc.2015.00217.

Misago, M., Y. F. Liao, S. Kudo, S. Eto, M. G. Mattei, K. W. Moremen, and M. N. Fukuda. 1995. 'Molecular Cloning and Expression of CDNAs Encoding Human Alpha-Mannosidase II and a Previously Unrecognized Alpha-Mannosidase IIx Isozyme'. *Proceedings of the National Academy of Sciences of the United States of America* 92 (25): 11766–70. https://doi.org/10.1073/pnas.92.25.11766.

Miwa, H. 1984. 'Identification and Prognostic Implications of Tumor Infiltrating Lymphocytes--a Review'. *Acta Medica Okayama* 38 (3): 215–18. https://doi.org/10.18926/AMO/30357.

Miyagi, Taeko, Tadashi Wada, Kazunori Yamaguchi, Kazuhiro Shiozaki, Ikuro Sato, Yoichiro Kakugawa, Hideaki Yamanami, and Tsuneaki Fujiya. 2008. 'Human Sialidase as a Cancer Marker'. *Proteomics* 8 (16): 3303–11. https://doi.org/10.1002/pmic.200800248.

Miyata, R., K. Iwabuchi, S. Watanabe, N. Sato, and I. Nagaoka. 1999. 'Short Exposure of Intestinal Epithelial Cells to TNF-Alpha and Histamine Induces Mac-1-Mediated Neutrophil Adhesion Independent of Protein Synthesis'. *Journal of Leukocyte Biology* 66 (3): 437–46. https://doi.org/10.1002/jlb.66.3.437.

Miyazaki, Keiko, Katsuyuki Ohmori, Mineko Izawa, Tetsufumi Koike, Kensuke Kumamoto, Koichi Furukawa, Takayuki Ando, et al. 2004. 'Loss of Disialyl Lewis(a), the Ligand for Lymphocyte Inhibitory Receptor Sialic Acid-Binding Immunoglobulin-like Lectin-7 (Siglec-7) Associated with Increased Sialyl Lewis(a) Expression on Human Colon Cancers'. *Cancer Research* 64 (13): 4498–4505. https://doi.org/10.1158/0008-5472.CAN-03-3614.

Miyazaki, Keiko, Keiichiro Sakuma, Yuki I. Kawamura, Mineko Izawa, Katsuyuki Ohmori, Motoaki Mitsuki, Toshiyuki Yamaji, et al. 2012. 'Colonic Epithelial Cells Express Specific Ligands for

Mucosal Macrophage Immunosuppressive Receptors Siglec-7 and -9'. *Journal of Immunology (Baltimore, Md.: 1950)* 188 (9): 4690–4700. https://doi.org/10.4049/jimmunol.1100605.

Moehler, Thomas M., Sandra Sauer, Maximilian Witzel, Mindaugas Andrulis, Juan J. Garcia-Vallejo, Rainer Grobholz, Martina Willhauck-Fleckenstein, Axel Greiner, Hartmut Goldschmidt, and Reinhard Schwartz-Albiez. 2008. 'Involvement of Alpha 1-2-Fucosyltransferase I (FUT1) and Surface-Expressed Lewis(y) (CD174) in First Endothelial Cell-Cell Contacts during Angiogenesis'. *Journal of Cellular Physiology* 215 (1): 27–36. https://doi.org/10.1002/jcp.21285.

Mondal, Nandini, Brad Dykstra, Jungmin Lee, David J. Ashline, Vernon N. Reinhold, Derrick J. Rossi, and Robert Sackstein. 2018. 'Distinct Human α(1,3)-Fucosyltransferases Drive Lewis-X/Sialyl Lewis-X Assembly in Human Cells'. *The Journal of Biological Chemistry* 293 (19): 7300–7314. https://doi.org/10.1074/jbc.RA117.000775.

Morichika, Hiroshi, Yuichiro Hamanaka, Tadashi Tai, and Ineo Ishizuka. 1996. 'Sulfatides as a Predictive Factor of Lymph Node Metastasis in Patients with Colorectal Adenocarcinoma' 78 (1): 43–47. https://doi.org/10.1002/(SICI)1097-0142(19960701)78:1<43::AID-CNCR8>3.0.CO;2-I.

Muinelo-Romay, L., S. Villar-Portela, E. Cuevas Alvarez, E. Gil-Martín, and Almudena Fernández-Briera. 2011. 'α(1,6)Fucosyltransferase Expression Is an Independent Prognostic Factor for Disease-Free Survival in Colorectal Carcinoma'. *Human Pathology* 42 (11): 1740–50. https://doi.org/10.1016/j.humpath.2011.01.021.

Munkley, Jennifer. 2016. 'The Role of Sialyl-Tn in Cancer'. *International Journal of Molecular Sciences* 17 (3): 275. https://doi.org/10.3390/ijms17030275.

Murata, K., E. Miyoshi, M. Kameyama, O. Ishikawa, T. Kabuto, Y. Sasaki, M. Hiratsuka, et al. 2000. 'Expression of N-Acetylglucosaminyltransferase V in Colorectal Cancer Correlates with Metastasis and Poor Prognosis'. *Clinical Cancer Research: An Official Journal of the American Association for Cancer Research* 6 (5): 1772–77.

Mytar, Bozenna, Maria Woloszyn, Anna Macura-Biegun, Barbara Hajto, Irena Ruggiero, Barbara Piekarska, and Marek Zembala. 2004. 'Involvement of Pattern Recognition Receptors in the Induction of Cytokines and Reactive Oxygen Intermediates Production by Human Monocytes/Macrophages Stimulated with Tumour Cells'. *Anticancer Research* 24 (4): 2287–93.

Na'ara, Shorook, Moran Amit, and Ziv Gil. 2019. 'L1CAM Induces Perineural Invasion of Pancreas Cancer Cells by Upregulation of Metalloproteinase Expression'. *Oncogene* 38 (4): 596–608. https://doi.org/10.1038/s41388-018-0458-y.

Neves, Manuel, Rita Azevedo, Luís Lima, Marta I. Oliveira, Andreia Peixoto, Dylan Ferreira, Janine Soares, et al. 2019. 'Exploring Sialyl-Tn Expression in Microfluidic-Isolated Circulating Tumour Cells: A Novel Biomarker and an Analytical Tool for Precision Oncology Applications'. *New Biotechnology* 49 (March): 77–87. https://doi.org/10.1016/j.nbt.2018.09.004.

Neville, A. M. 1974. 'Clinical Value of Tumour-Associated Antigens'. *Journal of Clinical Pathology. Supplement (Royal College of Pathologists)* 7: 119–26.

Ni, Jianlong, Zhi Jiang, Li Shen, Liping Gao, Meiyun Yu, Xu Xu, Shitao Zou, Dong Hua, and Shiliang Wu. 2014. 'B3GnT8 Regulates the Metastatic Potential of Colorectal Carcinoma Cells by Altering the Glycosylation of CD147'. *Oncology Reports* 31 (4): 1795–1801. https://doi.org/10.3892/or.2014.3042.

Nishida-Aoki, Nao, and Taranjit S. Gujral. 2019. 'Emerging Approaches to Study Cell–Cell Interactions in Tumor Microenvironment'. *Oncotarget* 10 (7): 785–97. https://doi.org/10.18632/oncotarget.26585.

Nishihara, S., T. Hiraga, Y. Ikehara, T. Kudo, H. Iwasaki, K. Morozumi, S. Akamatsu, T. Tachikawa, and H. Narimatsu. 1999. 'Molecular Mechanisms of Expression of Lewis b Antigen and Other Type I Lewis Antigens in Human Colorectal Cancer'. *Glycobiology* 9 (6): 607–16. https://doi.org/10.1093/glycob/9.6.607.

Noda, Masaru, Hirokazu Okayama, Kazunoshin Tachibana, Wataru Sakamoto, Katsuharu Saito, Aung Kyi Thar Min, Mai Ashizawa, et al. 2018. 'Glycosyltransferase Gene Expression Identifies a Poor Prognostic Colorectal Cancer Subtype Associated with Mismatch Repair Deficiency and Incomplete Glycan Synthesis'. *Clinical Cancer Research: An Official Journal of the American Association for Cancer Research* 24 (18): 4468–81. https://doi.org/10.1158/1078-0432.CCR-17-3533.

Nonaka, Motohiro, Hirotsugu Imaeda, Shogo Matsumoto, Bruce Yong Ma, Nobuko Kawasaki, Eiji Mekata, Akira Andoh, et al. 2014. 'Mannan-Binding Protein, a C-Type Serum Lectin, Recognizes Primary Colorectal Carcinomas through Tumor-Associated Lewis Glycans'. *Journal of Immunology (Baltimore, Md.: 1950)* 192 (3): 1294–1301. https://doi.org/10.4049/jimmunol.1203023.

Nonaka, Motohiro, Bruce Yong Ma, Hirotsugu Imaeda, Keiko Kawabe, Nobuko Kawasaki, Keiko Hodohara, Nana Kawasaki, Akira Andoh, Yoshihide Fujiyama, and Toshisuke Kawasaki. 2011. 'Dendritic Cell-Specific Intercellular Adhesion Molecule 3-Grabbing Non-Integrin (DC-SIGN) Recognizes a Novel Ligand, Mac-2-Binding Protein, Characteristically Expressed on Human Colorectal Carcinomas'. *The Journal of Biological Chemistry* 286 (25): 22403–13. https://doi.org/10.1074/jbc.M110.215301.

Nonaka, Motohiro, Bruce Yong Ma, Ryuuya Murai, Natsuko Nakamura, Makoto Baba, Nobuko Kawasaki, Keiko Hodohara, Shinji Asano, and Toshisuke Kawasaki. 2008. 'Glycosylation-Dependent Interactions of C-Type Lectin DC-SIGN with Colorectal Tumor-Associated Lewis Glycans Impair the Function and Differentiation of Monocyte-Derived Dendritic Cells'. *Journal of Immunology (Baltimore, Md.: 1950)* 180 (5): 3347–56. https://doi.org/10.4049/jimmunol.180.5.3347.

Odegard, Jared M., Brenna Kelley-Clarke, Semih U. Tareen, David J. Campbell, Patrick A. Flynn, Christopher J. Nicolai, Megan M. Slough, et al. 2015. 'Virological and Preclinical Characterization of a Dendritic Cell Targeting, Integration-Deficient Lentiviral Vector for Cancer Immunotherapy'. *Journal of Immunotherapy (Hagerstown, Md.: 1997)* 38 (2): 41–53. https://doi.org/10.1097/CJI.0000000000000067.

Ogawa, Tadashi, Yoshihiko Hirohashi, Aiko Murai, Toshihiko Nishidate, Kenji Okita, Liming Wang, Yuzuru Ikehara, et al. 2017. 'ST6GALNAC1 Plays Important Roles in Enhancing Cancer Stem Phenotypes of Colorectal Cancer via the Akt Pathway'. *Oncotarget* 8 (68): 112550–64. https://doi.org/10.18632/oncotarget.22545.

Ohnishi, Koji, Yoshihiro Komohara, Yoichi Saito, Yuji Miyamoto, Masayuki Watanabe, Hideo Baba, and Motohiro Takeya. 2013. 'CD169-Positive Macrophages in Regional Lymph Nodes Are Associated with a Favorable Prognosis in Patients with Colorectal Carcinoma'. *Cancer Science* 104 (9): 1237–44. https://doi.org/10.1111/cas.12212.

Ohtsubo, Kazuaki, and Jamey D. Marth. 2006. 'Glycosylation in Cellular Mechanisms of Health and Disease'. *Cell* 126 (5): 855–67. https://doi.org/10.1016/j.cell.2006.08.019.

Orr, F. W., and S. Mokashi. 1985. 'Effect of Leukocyte Activation on the Formation of Heterotypic Tumor-Cell Aggregates in Vitro'. *International Journal of Cancer* 35 (1): 101–6. https://doi.org/10.1002/ijc.2910350116.

Overman, Michael J., Ray McDermott, Joseph L. Leach, Sara Lonardi, Heinz-Josef Lenz, Michael A. Morse, Jayesh Desai, et al. 2017. 'Nivolumab in Patients with Metastatic DNA Mismatch Repair-Deficient or Microsatellite Instability-High Colorectal Cancer (CheckMate 142): An Open-Label, Multicentre, Phase 2 Study'. *The Lancet. Oncology* 18 (9): 1182–91. https://doi.org/10.1016/S1470-2045(17)30422-9.

Pastor, Danielle M, Lisa S Poritz, Thomas L Olson, Christina L Kline, Leonard R Harris, Walter A Koltun, Vernon M Chinchilli, and Rosalyn B Irby. 2010. 'Primary Cell Lines: False Representation or Model System? A Comparison of Four Human Colorectal Tumors and Their Coordinately Established Cell Lines'. *International Journal of Clinical and Experimental Medicine* 3 (1): 69–83.

Pérez-Garay, Marta, Beatriz Arteta, Esther Llop, Lara Cobler, Lluís Pagès, Rosa Ortiz, María José Ferri, et al. 2013. 'A2,3-Sialyltransferase ST3Gal IV Promotes Migration and Metastasis in Pancreatic Adenocarcinoma Cells and Tends to Be Highly Expressed in Pancreatic Adenocarcinoma Tissues'. *The International Journal of Biochemistry & Cell Biology* 45 (8): 1748–57. https://doi.org/10.1016/j.biocel.2013.05.015.

Petersen, G. M., J. Slack, and Y. Nakamura. 1991. 'Screening Guidelines and Premorbid Diagnosis of Familial Adenomatous Polyposis Using Linkage'. *Gastroenterology* 100 (6): 1658–64.

Petretti, T., W. Kemmner, B. Schulze, and P. M. Schlag. 2000. 'Altered MRNA Expression of Glycosyltransferases in Human Colorectal Carcinomas and Liver Metastases'. *Gut* 46 (3): 359–66. https://doi.org/10.1136/gut.46.3.359.

Platt, N., H. Suzuki, Y. Kurihara, T. Kodama, and S. Gordon. 1996. 'Role for the Class A Macrophage Scavenger Receptor in the Phagocytosis of Apoptotic Thymocytes in Vitro'. *Proceedings of the National Academy of Sciences of the United States of America* 93 (22): 12456–60. https://doi.org/10.1073/pnas.93.22.12456.

Popovic, Zoran V., Roger Sandhoff, Tjeerd P. Sijmonsma, Sylvia Kaden, Richard Jennemann, Eva Kiss, Edgar Tone, et al. 2007. 'Sulfated Glycosphingolipid as Mediator of Phagocytosis: SM4s Enhances Apoptotic Cell Clearance and Modulates Macrophage Activity'. *Journal of Immunology (Baltimore, Md.: 1950)* 179 (10): 6770–82. https://doi.org/10.4049/jimmunol.179.10.6770.

Prendergast, Jillian M., Ana Paula Galvao da Silva, David A. Eavarone, Darius Ghaderi, Mai Zhang, Dane Brady, Joan Wicks, Julie DeSander, Jeff Behrens, and Bo R. Rueda. 2017. 'Novel Anti-Sialyl-Tn Monoclonal Antibodies and Antibody-Drug Conjugates Demonstrate Tumor Specificity and Anti-Tumor Activity'. *MAbs* 9 (4): 615–27. https://doi.org/10.1080/19420862.2017.1290752.

Qiu, Miaozhen, Jianming Hu, Dajun Yang, David Peter Cosgrove, and Ruihua Xu. 2015. 'Pattern of Distant Metastases in Colorectal Cancer: A SEER Based Study'. *Oncotarget* 6 (36): 38658–66.

Qu, Jian-Jun, Xiang-Yang Qu, and De-Zhen Zhou. 2017. 'MiR-4262 Inhibits Colon Cancer Cell Proliferation via Targeting of GALNT4'. *Molecular Medicine Reports* 16 (4): 3731–36. https://doi.org/10.3892/mmr.2017.7057.

Ramirez-Ortiz, Zaida G., William F. Pendergraft, Amit Prasad, Michael H. Byrne, Tal Iram, Christopher J. Blanchette, Andrew D. Luster, Nir Hacohen, Joseph El Khoury, and Terry K. Means. 2013. 'The Scavenger Receptor SCARF1 Mediates the Clearance of Apoptotic Cells and Prevents Autoimmunity'. *Nature Immunology* 14 (9): 917–26. https://doi.org/10.1038/ni.2670.

Rodríguez, Ernesto, Sjoerd T. T. Schetters, and Yvette van Kooyk. 2018. 'The Tumour Glyco-Code as a Novel Immune Checkpoint for Immunotherapy'. *Nature Reviews. Immunology* 18 (3): 204–11. https://doi.org/10.1038/nri.2018.3.

Ruivenkamp, Claudia, Mario Hermsen, Cindy Postma, Anita Klous, Jan Baak, Gerrit Meijer, and Peter Demant. 2003. 'LOH of PTPRJ Occurs Early in Colorectal Cancer and Is Associated with Chromosomal Loss of 18q12-21'. *Oncogene* 22 (22): 3472–74. https://doi.org/10.1038/sj.onc.1206246.

Saeland, Eirikur, Ana I. Belo, Sandra Mongera, Irma van Die, Gerrit A. Meijer, and Yvette van Kooyk. 2012. 'Differential Glycosylation of MUC1 and CEACAM5 between Normal Mucosa and Tumour Tissue of Colon Cancer Patients'. *International Journal of Cancer* 131 (1): 117–28. https://doi.org/10.1002/ijc.26354.

Sahasrabudhe, Neha M., Kristiaan Lenos, Joost C. van der Horst, Ernesto Rodríguez, and Sandra J. van Vliet. 2018. 'Oncogenic BRAFV600E Drives Expression of MGL Ligands in the Colorectal Cancer Cell Line HT29 through N-Acetylgalactosamine-Transferase 3'. *Biological Chemistry* 399 (7): 649–59. https://doi.org/10.1515/hsz-2018-0120.

Sakuma, Keiichiro, Masahiro Aoki, and Reiji Kannagi. 2012. 'Transcription Factors C-Myc and CDX2 Mediate E-Selectin Ligand Expression in Colon Cancer Cells Undergoing EGF/BFGF-Induced Epithelial-Mesenchymal Transition'. *Proceedings of the National Academy of Sciences of the United States of America* 109 (20): 7776–81. https://doi.org/10.1073/pnas.1111135109.

Salvini, R., A. Bardoni, M. Valli, and M. Trinchera. 2001. 'Beta 1,3-Galactosyltransferase Beta 3Gal-T5 Acts on the GlcNAcbeta 1-->3Galbeta 1-->4GlcNAcbeta 1-->R Sugar Chains of Carcinoembryonic Antigen and Other N-Linked Glycoproteins and Is down-Regulated in Colon Adenocarcinomas'. *The Journal of Biological Chemistry* 276 (5): 3564–73. https://doi.org/10.1074/jbc.M006662200.

Samsen, Alexandra, Valentina Bogoevska, Birgit Klampe, Ana-Maria Bamberger, Lothar Lucka, Andrea K. Horst, Peter Nollau, and Christoph Wagener. 2010. 'DC-SIGN and SRCL Bind Glycans of Carcinoembryonic Antigen (CEA) and CEA-Related Cell Adhesion Molecule 1 (CEACAM1): Recombinant Human Glycan-Binding Receptors as Analytical Tools'. *European Journal of Cell Biology* 89 (1): 87–94. https://doi.org/10.1016/j.ejcb.2009.11.018.

Sasai, Ken, Yoshitaka Ikeda, Hironobu Eguchi, Takeo Tsuda, Koichi Honke, and Naoyuki Taniguchi. 2002. 'The Action of N-Acetylglucosaminyltransferase-V Is Prevented by the Bisecting GlcNAc Residue at the Catalytic Step'. *FEBS Letters* 522 (1–3): 151–55.

Sauer, Sandra, Tobias Meissner, and Thomas Moehler. 2015. 'A Furan-Based Lewis-Y-(CD174)-Saccharide Mimetic Inhibits Endothelial Functions and In Vitro Angiogenesis'. *Advances in Clinical and Experimental Medicine: Official Organ Wroclaw Medical University* 24 (5): 759–68. https://doi.org/10.17219/acem/38562.

Sawada, R., J. B. Lowe, and M. Fukuda. 1993. 'E-Selectin-Dependent Adhesion Efficiency of Colonic Carcinoma Cells Is Increased by Genetic Manipulation of Their Cell Surface Lysosomal Membrane Glycoprotein-1 Expression Levels'. *The Journal of Biological Chemistry* 268 (17): 12675–81.

Schmielau, J., and O. J. Finn. 2001. 'Activated Granulocytes and Granulocyte-Derived Hydrogen Peroxide Are the Underlying Mechanism of Suppression of t-Cell Function in Advanced Cancer Patients'. *Cancer Research* 61 (12): 4756–60.

Schneider, F., W. Kemmner, W. Haensch, G. Franke, S. Gretschel, U. Karsten, and P. M. Schlag. 2001. 'Overexpression of Sialyltransferase CMP-Sialic Acid:Galbeta1,3GalNAc-R Alpha6-Sialyltransferase Is Related to Poor Patient Survival in Human Colorectal Carcinomas'. *Cancer Research* 61 (11): 4605–11.

Schoen, Robert E., Anthony Razzak, Kelly J. Yu, Sonja I. Berndt, Kevin Firl, Thomas L. Riley, and Paul F. Pinsky. 2015. 'Incidence and Mortality of Colorectal Cancer in Individuals with a Family History of Colorectal Cancer'. *Gastroenterology* 149 (6): 1438-1445.e1. https://doi.org/10.1053/j.gastro.2015.07.055.

Schultheis, M., S. Diestel, and B. Schmitz. 2007. 'The Role of Cytoplasmic Serine Residues of the Cell Adhesion Molecule L1 in Neurite Outgrowth, Endocytosis, and Cell Migration'. *Cellular and Molecular Neurobiology* 27 (1): 11–31. https://doi.org/10.1007/s10571-006-9113-1.

Sethi, Manveen K., Hoguen Kim, Cheol Keun Park, Mark S. Baker, Young-Ki Paik, Nicolle H. Packer, William S. Hancock, Susan Fanayan, and Morten Thaysen-Andersen. 2015. 'In-Depth N-Glycome Profiling of Paired Colorectal Cancer and Non-Tumorigenic Tissues Reveals Cancer-, Stage- and EGFR-Specific Protein N-Glycosylation'. *Glycobiology* 25 (10): 1064–78. https://doi.org/10.1093/glycob/cwv042.

Sethi, Manveen K., Morten Thaysen-Andersen, Joshua T. Smith, Mark S. Baker, Nicolle H. Packer, William S. Hancock, and Susan Fanayan. 2014. 'Comparative N-Glycan Profiling of Colorectal Cancer Cell Lines Reveals Unique Bisecting GlcNAc and α-2,3-Linked Sialic Acid Determinants Are Associated with Membrane Proteins of the More Metastatic/Aggressive Cell Lines'. *Journal of Proteome Research* 13 (1): 277–88. https://doi.org/10.1021/pr400861m.

Shan, Yujia, Jia Ma, Yue Pan, Jialei Hu, Bing Liu, and Li Jia. 2018. 'LncRNA SNHG7 Sponges MiR-216b to Promote Proliferation and Liver Metastasis of Colorectal Cancer through Upregulating GALNT1'. *Cell Death & Disease* 9 (7): 722. https://doi.org/10.1038/s41419-018-0759-7.

Shen, Feng, Junhui Cui, Xia Hong, Feng Yu, and Xiangdong Bao. 2019. 'Preoperative Serum Carcinoembryonic Antigen Elevation in Stage I Colon Cancer: Improved Risk of Mortality in Stage T1 than in Stage T2'. *International Journal of Colorectal Disease* 34 (6): 1095–1104. https://doi.org/10.1007/s00384-019-03298-y.

Shen, Li, Xiaoxia Dong, Yingying Wang, Li Qiu, Feng Peng, and Zhiguo Luo. 2018. 'B3GnT8 Regulates Oxaliplatin Resistance by Altering Integrin B1 Glycosylation in Colon Cancer Cells'. *Oncology Reports* 39 (4): 2006–14. https://doi.org/10.3892/or.2018.6243.

Shen, Li, Meiyun Yu, Xu Xu, Liping Gao, Jianlong Ni, Zhiguo Luo, and Shiliang Wu. 2014. 'Knockdown of B3GnT8 Reverses 5-Fluorouracil Resistance in Human Colorectal Cancer Cells via Inhibition the Biosynthesis of Polylactosamine-Type N-Glycans'. *International Journal of Oncology* 45 (6): 2560–68. https://doi.org/10.3892/ijo.2014.2672.

Shi, Gang, Yue Du, Yali Li, Yue An, Zhenwei He, Yingwei Lin, Rui Zhang, et al. 2017. 'Cell Recognition Molecule L1 Regulates Cell Surface Glycosylation to Modulate Cell Survival and Migration'. *International Journal of Medical Sciences* 14 (12): 1276–83. https://doi.org/10.7150/ijms.20479.

Shi, Lewis Zhichang, Tihui Fu, Baoxiang Guan, Jianfeng Chen, Jorge M. Blando, James P. Allison, Liangwen Xiong, Sumit K. Subudhi, Jianjun Gao, and Padmanee Sharma. 2016. 'Interdependent IL-7 and IFN-γ Signalling in T-Cell Controls Tumour Eradication by Combined α-CTLA-4+α-PD-1 Therapy'. *Nature Communications* 7: 12335. https://doi.org/10.1038/ncomms12335.

Shibao, Kazunori, Hiroto Izumi, Yoshifumi Nakayama, Ryo Ohta, Naoki Nagata, Minoru Nomoto, Ken-ichi Matsuo, et al. 2002. 'Expression of UDP-N-Acetyl-Alpha-D-Galactosamine-Polypeptide GalNAc N-Acetylgalactosaminyl Transferase-3 in Relation to Differentiation and Prognosis in Patients with Colorectal Carcinoma'. *Cancer* 94 (7): 1939–46.

Shida, Dai, Yukihide Kanemitsu, Tetsuya Hamaguchi, and Yasuhiro Shimada. 2019. 'Introducing the Eighth Edition of the Tumor-Node-Metastasis Classification as Relevant to Colorectal Cancer, Anal Cancer and Appendiceal Cancer: A Comparison Study with the Seventh Edition of the Tumor-Node-Metastasis and the Japanese Classification of Colorectal, Appendiceal, and Anal Carcinoma'. *Japanese Journal of Clinical Oncology* 49 (4): 321–28. https://doi.org/10.1093/jjco/hyy198.

Shiozaki, Kazuhiro, Kazunori Yamaguchi, Kohta Takahashi, Setsuko Moriya, and Taeko Miyagi. 2011. 'Regulation of Sialyl Lewis Antigen Expression in Colon Cancer Cells by Sialidase NEU4'. *The Journal of Biological Chemistry* 286 (24): 21052–61. https://doi.org/10.1074/jbc.M111.231191.

Shrimal, Shiteshu, Natalia A. Cherepanova, and Reid Gilmore. 2015. 'Cotranslational and Posttranslocational N-Glycosylation of Proteins in the Endoplasmic Reticulum'. *Seminars in Cell & Developmental Biology* 41 (May): 71–78. https://doi.org/10.1016/j.semcdb.2014.11.005.

Siddiqui, B., J. S. Whitehead, and Y. S. Kim. 1978. 'Glycosphingolipids in Human Colonic Adenocarcinoma'. *The Journal of Biological Chemistry* 253 (7): 2168–75.

Siegel, Rebecca L., Kimberly D. Miller, Stacey A. Fedewa, Dennis J. Ahnen, Reinier G. S. Meester, Afsaneh Barzi, and Ahmedin Jemal. 2017. 'Colorectal Cancer Statistics, 2017'. *CA: A Cancer Journal for Clinicians* 67 (3): 177–93. https://doi.org/10.3322/caac.21395.

Smith, Kortnye Maureen, and Jayesh Desai. 2018. 'Nivolumab for the Treatment of Colorectal Cancer'. *Expert Review of Anticancer Therapy* 18 (7): 611–18. https://doi.org/10.1080/14737140.2018.1480942.

Sperandio, Markus, Christian A. Gleissner, and Klaus Ley. 2009. 'Glycosylation in Immune Cell Trafficking'. *Immunological Reviews* 230 (1): 97–113. https://doi.org/10.1111/j.1600-065X.2009.00795.x.

St Hill, Catherine A. 2011. 'Interactions between Endothelial Selectins and Cancer Cells Regulate Metastasis'. *Frontiers in Bioscience (Landmark Edition)* 16 (June): 3233–51. https://doi.org/10.2741/3909.

Stanley, Pamela, and Richard D. Cummings. 2009. 'Structures Common to Different Glycans'. In *Essentials of Glycobiology*, edited by Ajit Varki, Richard D. Cummings, Jeffrey D. Esko, Hudson H. Freeze, Pamela Stanley, Carolyn R. Bertozzi, Gerald W. Hart, and Marilynn E. Etzler, 2nd

ed. Cold Spring Harbor (NY): Cold Spring Harbor Laboratory Press. http://www.ncbi.nlm.nih.gov/books/NBK1892/.

———. 2015. 'Structures Common to Different Glycans'. In *Essentials of Glycobiology*, edited by Ajit Varki, Richard D. Cummings, Jeffrey D. Esko, Pamela Stanley, Gerald W. Hart, Markus Aebi, Alan G. Darvill, et al., 3rd ed. Cold Spring Harbor (NY): Cold Spring Harbor Laboratory Press. http://www.ncbi.nlm.nih.gov/books/NBK453042/.

Stanley, Pamela, Harry Schachter, and Naoyuki Taniguchi. 2009. 'N-Glycans'. In *Essentials of Glycobiology*, edited by Ajit Varki, Richard D. Cummings, Jeffrey D. Esko, Hudson H. Freeze, Pamela Stanley, Carolyn R. Bertozzi, Gerald W. Hart, and Marilynn E. Etzler, 2nd ed. Cold Spring Harbor (NY): Cold Spring Harbor Laboratory Press. http://www.ncbi.nlm.nih.gov/books/NBK1917/.

Starkey, J. R., H. D. Liggitt, W. Jones, and H. L. Hosick. 1984. 'Influence of Migratory Blood Cells on the Attachment of Tumor Cells to Vascular Endothelium'. *International Journal of Cancer* 34 (4): 535–43. https://doi.org/10.1002/ijc.2910340417.

Stern, Howard M., Mary Padilla, Klaus Wagner, Lukas Amler, and Avi Ashkenazi. 2010. 'Development of Immunohistochemistry Assays to Assess GALNT14 and FUT3/6 in Clinical Trials of Dulanermin and Drozitumab'. *Clinical Cancer Research: An Official Journal of the American Association for Cancer Research* 16 (5): 1587–96. https://doi.org/10.1158/1078-0432.CCR-09-3108.

Stiegelbauer, Verena, Petra Vychytilova-Faltejskova, Michael Karbiener, Anna-Maria Pehserl, Andreas Reicher, Margit Resel, Ellen Heitzer, et al. 2017. 'MiR-196b-5p Regulates Colorectal Cancer Cell Migration and Metastases through Interaction with HOXB7 and GALNT5'. *Clinical Cancer Research: An Official Journal of the American Association for Cancer Research* 23 (17): 5255–66. https://doi.org/10.1158/1078-0432.CCR-17-0023.

Sun, J., J. Thurin, H. S. Cooper, P. Wang, M. Mackiewicz, Z. Steplewski, and M. Blaszczyk-Thurin. 1995. 'Elevated Expression of H Type GDP-L-Fucose:Beta-D-Galactoside Alpha-2-L-Fucosyltransferase Is Associated with Human Colon Adenocarcinoma Progression'. *Proceedings of the National Academy of Sciences of the United States of America* 92 (12): 5724–28. https://doi.org/10.1073/pnas.92.12.5724.

Sun, Xiaodong, Tongzhong Ju, and Richard D. Cummings. 2018. 'Differential Expression of Cosmc, T-Synthase and Mucins in Tn-Positive Colorectal Cancers'. *BMC Cancer* 18 (1): 827. https://doi.org/10.1186/s12885-018-4708-8.

Sun, Zhenqiang, Fuqi Wang, Quanbo Zhou, Shuaixi Yang, Xiantao Sun, Guixian Wang, Zhen Li, et al. 2017. 'Pre-Operative to Post-Operative Serum Carcinoembryonic Antigen Ratio Is a Prognostic Indicator in Colorectal Cancer'. *Oncotarget* 8 (33): 54672–82. https://doi.org/10.18632/oncotarget.17931.

Świderska, Magdalena, Barbara Choromańska, Ewelina Dąbrowska, Emilia Konarzewska-Duchnowska, Katarzyna Choromańska, Grzegorz Szczurko, Piotr Myśliwiec, Jacek Dadan, Jerzy Robert Ładny, and Krzysztof Zwierz. 2014. 'The Diagnostics of Colorectal Cancer'. *Contemporary Oncology* 18 (1): 1–6. https://doi.org/10.5114/wo.2013.39995.

Swindall, Amanda F., Angelina I. Londoño-Joshi, Matthew J. Schultz, Naomi Fineberg, Donald J. Buchsbaum, and Susan L. Bellis. 2013. 'ST6Gal-I Protein Expression Is Upregulated in Human Epithelial Tumors and Correlates with Stem Cell Markers in Normal Tissues and Colon Cancer Cell Lines'. *Cancer Research* 73 (7): 2368–78. https://doi.org/10.1158/0008-5472.CAN-12-3424.

Takahashi, Shiro, Taiki Sugiyama, Mayuka Shimomura, Yoshihiro Kamada, Kazutoshi Fujita, Norio Nonomura, Eiji Miyoshi, and Miyako Nakano. 2016. 'Site-Specific and Linkage Analyses of Fucosylated N-Glycans on Haptoglobin in Sera of Patients with Various Types of Cancer: Possible Implication for the Differential Diagnosis of Cancer'. *Glycoconjugate Journal* 33 (3): 471–82. https://doi.org/10.1007/s10719-016-9653-7.

Thirunavukarasu, Pragatheeshwar, Shyamsunder Sukumar, Magesh Sathaiah, Meredith Mahan, Kothai Divya Pragatheeshwar, James F. Pingpank, Herbert Zeh, Christopher J. Bartels,

Kenneth K. W. Lee, and David L. Bartlett. 2011. 'C-Stage in Colon Cancer: Implications of Carcinoembryonic Antigen Biomarker in Staging, Prognosis, and Management'. *Journal of the National Cancer Institute* 103 (8): 689–97. https://doi.org/10.1093/jnci/djr078.

Thomas, Susan N., Fei Zhu, Ronald L. Schnaar, Christina S. Alves, and Konstantinos Konstantopoulos. 2008. 'Carcinoembryonic Antigen and CD44 Variant Isoforms Cooperate to Mediate Colon Carcinoma Cell Adhesion to E- and L-Selectin in Shear Flow'. *The Journal of Biological Chemistry* 283 (23): 15647–55. https://doi.org/10.1074/jbc.M800543200.

Tomlinson, J., J. L. Wang, S. H. Barsky, M. C. Lee, J. Bischoff, and M. Nguyen. 2000. 'Human Colon Cancer Cells Express Multiple Glycoprotein Ligands for E-Selectin'. *International Journal of Oncology* 16 (2): 347–53.

Tremblay, L. O., N. Campbell Dyke, and A. Herscovics. 1998. 'Molecular Cloning, Chromosomal Mapping and Tissue-Specific Expression of a Novel Human Alpha1,2-Mannosidase Gene Involved in N-Glycan Maturation'. *Glycobiology* 8 (6): 585–95. https://doi.org/10.1093/glycob/8.6.585.

Tremblay, L. O., and A. Herscovics. 2000. 'Characterization of a CDNA Encoding a Novel Human Golgi Alpha 1, 2-Mannosidase (IC) Involved in N-Glycan Biosynthesis'. *The Journal of Biological Chemistry* 275 (41): 31655–60. https://doi.org/10.1074/jbc.M004935200.

Trinchera, Marco, Nadia Malagolini, Mariella Chiricolo, Donatella Santini, Francesco Minni, Anna Caretti, and Fabio Dall'olio. 2011. 'The Biosynthesis of the Selectin-Ligand Sialyl Lewis x in Colorectal Cancer Tissues Is Regulated by Fucosyltransferase VI and Can Be Inhibited by an RNA Interference-Based Approach'. *The International Journal of Biochemistry & Cell Biology* 43 (1): 130–39. https://doi.org/10.1016/j.biocel.2010.10.004.

Trombetta, E. Sergio, and Armando J. Parodi. 2005. 'Glycoprotein Reglucosylation'. *Methods (San Diego, Calif.)* 35 (4): 328–37. https://doi.org/10.1016/j.ymeth.2004.10.004.

Tsuchida, Akiko, Tetsuya Okajima, Keiko Furukawa, Takayuki Ando, Hideharu Ishida, Aruto Yoshida, Yoko Nakamura, Reiji Kannagi, Makoto Kiso, and Koichi Furukawa. 2003. 'Synthesis of Disialyl Lewis a (Le(a)) Structure in Colon Cancer Cell Lines by a Sialyltransferase, ST6GalNAc VI, Responsible for the Synthesis of Alpha-Series Gangliosides'. *The Journal of Biological Chemistry* 278 (25): 22787–94. https://doi.org/10.1074/jbc.M211034200.

Ubillos, Luis, Edgardo Berriel, Daniel Mazal, Sabina Victoria, Enrique Barrios, Eduardo Osinaga, and Nora Berois. 2018. 'Polypeptide-GalNAc-T6 Expression Predicts Better Overall Survival in Patients with Colon Cancer'. *Oncology Letters* 16 (1): 225–34. https://doi.org/10.3892/ol.2018.8686.

Uemura, T., K. Shiozaki, K. Yamaguchi, S. Miyazaki, S. Satomi, K. Kato, H. Sakuraba, and T. Miyagi. 2009. 'Contribution of Sialidase NEU1 to Suppression of Metastasis of Human Colon Cancer Cells through Desialylation of Integrin Beta4'. *Oncogene* 28 (9): 1218–29. https://doi.org/10.1038/onc.2008.471.

Vacante, Marco, Antonio Maria Borzì, Francesco Basile, and Antonio Biondi. 2018. 'Biomarkers in Colorectal Cancer: Current Clinical Utility and Future Perspectives'. *World Journal of Clinical Cases* 6 (15): 869–81. https://doi.org/10.12998/wjcc.v6.i15.869.

Valastyan, Scott, and Robert A. Weinberg. 2011. 'Tumor Metastasis: Molecular Insights and Evolving Paradigms'. *Cell* 147 (2): 275–92. https://doi.org/10.1016/j.cell.2011.09.024.

Videira, Paula A, Manuela Correia, Nadia Malagolini, Hélio J Crespo, Dário Ligeiro, Fernando M Calais, Helder Trindade, and Fabio Dall'Olio. 2009. 'ST3Gal.I Sialyltransferase Relevance in Bladder Cancer Tissues and Cell Lines'. *BMC Cancer* 9 (October): 357. https://doi.org/10.1186/1471-2407-9-357.

Vroome, Stefan W. de, Stephanie Holst, Mar Rodriguez Girondo, Yuri E. M. van der Burgt, Wilma E. Mesker, Rob A. E. M. Tollenaar, and Manfred Wuhrer. 2018. 'Serum N-Glycome Alterations in Colorectal Cancer Associate with Survival'. *Oncotarget* 9 (55): 30610–23. https://doi.org/10.18632/oncotarget.25753.

Wada, T., K. Hata, K. Yamaguchi, K. Shiozaki, K. Koseki, S. Moriya, and T. Miyagi. 2007. 'A Crucial Role of Plasma Membrane-Associated Sialidase in the Survival of Human Cancer Cells'. *Oncogene* 26 (17): 2483–90. https://doi.org/10.1038/sj.onc.1210341.

Weng, Li, Jun Ma, Yi-Ping Jia, Shao-Qiu Wu, Bin-Yan Liu, Yan Cao, Xiang Yin, Ming-Yi Shang, and Ai-Wu Mao. 2018. 'MiR-4262 Promotes Cell Apoptosis and Inhibits Proliferation of Colon Cancer Cells: Involvement of GALNT4'. *American Journal of Translational Research* 10 (12): 3969–77.

Weston, B. W., K. M. Hiller, J. P. Mayben, G. A. Manousos, K. M. Bendt, R. Liu, and J. C. Cusack. 1999. 'Expression of Human Alpha(1,3)Fucosyltransferase Antisense Sequences Inhibits Selectin-Mediated Adhesion and Liver Metastasis of Colon Carcinoma Cells'. *Cancer Research* 59 (9): 2127–35.

Westwood, Jennifer A., William K. Murray, Melanie Trivett, Nicole M. Haynes, Benjamin Solomon, Linda Mileshkin, David Ball, et al. 2009. 'The Lewis-Y Carbohydrate Antigen Is Expressed by Many Human Tumors and Can Serve as a Target for Genetically Redirected T Cells despite the Presence of Soluble Antigen in Serum'. *Journal of Immunotherapy (Hagerstown, Md.: 1997)* 32 (3): 292–301. https://doi.org/10.1097/CJI.0b013e31819b7c8e.

Wolff, J. M., R. Frank, K. Mujoo, R. C. Spiro, R. A. Reisfeld, and F. G. Rathjen. 1988. 'A Human Brain Glycoprotein Related to the Mouse Cell Adhesion Molecule L1'. *The Journal of Biological Chemistry* 263 (24): 11943–47.

World Health Organization. 2018. 'Cancer Key Facts'. 12 September 2018. https://www.who.int/news-room/fact-sheets/detail/cancer.

Wu, Q. D., J. H. Wang, C. Condron, D. Bouchier-Hayes, and H. P. Redmond. 2001. 'Human Neutrophils Facilitate Tumor Cell Transendothelial Migration'. *American Journal of Physiology. Cell Physiology* 280 (4): C814-822. https://doi.org/10.1152/ajpcell.2001.280.4.C814.

Xie, Jingjing, Haiyan Dong, Hongning Chen, Rongli Zhao, Patrick J. Sinko, Weiyu Shen, Jichuang Wang, et al. 2015. 'Exploring Cancer Metastasis Prevention Strategy: Interrupting Adhesion of Cancer Cells to Vascular Endothelia of Potential Metastatic Tissues by Antibody-Coated Nanomaterial'. *Journal of Nanobiotechnology* 13 (1): 9. https://doi.org/10.1186/s12951-015-0072-x.

Yamada, N., Y. S. Chung, S. Takatsuka, Y. Arimoto, T. Sawada, T. Dohi, and M. Sowa. 1997. 'Increased Sialyl Lewis A Expression and Fucosyltransferase Activity with Acquisition of a High Metastatic Capacity in a Colon Cancer Cell Line'. *British Journal of Cancer* 76 (5): 582–87. https://doi.org/10.1038/bjc.1997.429.

Yamadera, Masato, Eiji Shinto, Hitoshi Tsuda, Yoshiki Kajiwara, Yoshihisa Naito, Kazuo Hase, Junji Yamamoto, and Hideki Ueno. 2018. 'Sialyl Lewisx Expression at the Invasive Front as a Predictive Marker of Liver Recurrence in Stage II Colorectal Cancer'. *Oncology Letters* 15 (1): 221–28. https://doi.org/10.3892/ol.2017.7340.

Yamanami, Hideaki, Kazuhiro Shiozaki, Tadashi Wada, Kazunori Yamaguchi, Takuji Uemura, Yoichiro Kakugawa, Tsuneaki Hujiya, and Taeko Miyagi. 2007. 'Down-Regulation of Sialidase NEU4 May Contribute to Invasive Properties of Human Colon Cancers'. *Cancer Science* 98 (3): 299–307. https://doi.org/10.1111/j.1349-7006.2007.00403.x.

Yamasaki, M., P. Thompson, and V. Lemmon. 1997. 'CRASH Syndrome: Mutations in L1CAM Correlate with Severity of the Disease'. *Neuropediatrics* 28 (3): 175–78. https://doi.org/10.1055/s-2007-973696.

Yan, Xialin, Jishun Lu, Xia Zou, Sen Zhang, Yalu Cui, Leqi Zhou, Feng Liu, et al. 2018. 'The Polypeptide N-Acetylgalactosaminyltransferase 4 Exhibits Stage-Dependent Expression in Colorectal Cancer and Affects Tumorigenesis, Invasion and Differentiation'. *The FEBS Journal*, June. https://doi.org/10.1111/febs.14593.

Yang, J. M., J. C. Byrd, B. B. Siddiki, Y. S. Chung, M. Okuno, M. Sowa, Y. S. Kim, K. L. Matta, and I. Brockhausen. 1994. 'Alterations of O-Glycan Biosynthesis in Human Colon Cancer Tissues'. *Glycobiology* 4 (6): 873–84. https://doi.org/10.1093/glycob/4.6.873.

Yazawa, Shin, Toyo Nishimura, Munenori Ide, Takayuki Asao, Akihiko Okamura, Susumu Tanaka, Izumi Takai, Yuko Yagihashi, Abby R. Saniabadi, and Naohisa Kochibe. 2002. 'Tumor-Related

Expression of Alpha1,2fucosylated Antigens on Colorectal Carcinoma Cells and Its Suppression by Cell-Mediated Priming Using Sugar Acceptors for Alpha1,2fucosyltransferase'. *Glycobiology* 12 (9): 545–53. https://doi.org/10.1093/glycob/cwf070.

Yeung, Kay T., and Jing Yang. 2017. 'Epithelial-Mesenchymal Transition in Tumor Metastasis'. *Molecular Oncology* 11 (1): 28–39. https://doi.org/10.1002/1878-0261.12017.

Yokoigawa, Norio, Noriko Takeuchi, Munetoyo Toda, Mizue Inoue, Masaki Kaibori, Hidesuke Yanagida, Hironori Tanaka, et al. 2005. 'Enhanced Production of Interleukin 6 in Peripheral Blood Monocytes Stimulated with Mucins Secreted into the Bloodstream'. *Clinical Cancer Research: An Official Journal of the American Association for Cancer Research* 11 (17): 6127–32. https://doi.org/10.1158/1078-0432.CCR-05-0292.

Yoshiizumi, Kazuya, Fumio Nakajima, Rika Dobashi, Noriyasu Nishimura, and Shoji Ikeda. 2002. 'Studies on Scavenger Receptor Inhibitors. Part 1: Synthesis and Structure-Activity Relationships of Novel Derivatives of Sulfatides'. *Bioorganic & Medicinal Chemistry* 10 (8): 2445–60.

Yu, Ping, Mingyi Zhou, Jinglei Qu, Lingyu Fu, Xuedan Li, Ruimei Cai, Bo Jin, et al. 2018. 'The Dynamic Monitoring of CEA in Response to Chemotherapy and Prognosis of MCRC Patients'. *BMC Cancer* 18 (November). https://doi.org/10.1186/s12885-018-4987-0.

Zhang, Baojie, Ingrid A. M. van Roosmalen, Carlos R. Reis, Rita Setroikromo, and Wim J. Quax. 2019. 'Death Receptor 5 Is Activated by Fucosylation in Colon Cancer Cells'. *The FEBS Journal* 286 (3): 555–71. https://doi.org/10.1111/febs.14742.

Zhang, Dongmei, Qing Xie, Yanping Wang, Jinsheng Miao, Ling Li, Tong Zhang, Xiufeng Cao, and Yunsen Li. 2019. 'Mass Spectrometry Analysis Reveals Aberrant N-Glycans in Colorectal Cancer Tissues'. *Glycobiology*, January. https://doi.org/10.1093/glycob/cwz005.

Zhang, Jian, Fei Yang, Yong Ding, Linlin Zhen, Xuedong Han, Feng Jiao, and Jinhai Tang. 2015. 'Overexpression of L1 Cell Adhesion Molecule Correlates with Aggressive Tumor Progression of Patients with Breast Cancer and Promotes Motility of Breast Cancer Cells'. *International Journal of Clinical and Experimental Pathology* 8 (8): 9240–47.

Zhang, Sen, Jishun Lu, Zhijue Xu, Xia Zou, Xue Sun, Yingjiao Xu, Aidong Shan, et al. 2017. 'Differential Expression of ST6GAL1 in the Tumor Progression of Colorectal Cancer'. *Biochemical and Biophysical Research Communications* 486 (4): 1090–96. https://doi.org/10.1016/j.bbrc.2017.03.167.

Zhang, Ting, Fang Wang, Jing-Yi Wu, Zhi-Chao Qiu, Yan Wang, Fen Liu, Xiao-Song Ge, Xiao-Wei Qi, Yong Mao, and Dong Hua. 2018. 'Clinical Correlation of B7-H3 and B3GALT4 with the Prognosis of Colorectal Cancer'. *World Journal of Gastroenterology* 24 (31): 3538–46. https://doi.org/10.3748/wjg.v24.i31.3538.

Zhang, Xiao-Fei, Rongfu Tu, Keke Li, Pengxiang Ye, and Xiaofeng Cui. 2017. 'Tumor Suppressor PTPRJ Is a Target of MiR-155 in Colorectal Cancer'. *Journal of Cellular Biochemistry* 118 (10): 3391–3400. https://doi.org/10.1002/jcb.25995.

Zhao, Lijun, and Yu J. Cao. 2019. 'Engineered T Cell Therapy for Cancer in the Clinic'. *Frontiers in Immunology* 10: 2250. https://doi.org/10.3389/fimmu.2019.02250.

Zhu, Y., U. Srivatana, A. Ullah, H. Gagneja, C. S. Berenson, and P. Lance. 2001. 'Suppression of a Sialyltransferase by Antisense DNA Reduces Invasiveness of Human Colon Cancer Cells in Vitro'. *Biochimica Et Biophysica Acta* 1536 (2–3): 148–60. https://doi.org/10.1016/s0925-4439(01)00044-8.